Alma Mater Studiorum - Università di Bologna

DOTTORATO DI RICERCA IN GEOFISICA

Ciclo XXIX

Settore Concorsuale di afferenza: 04/A4
Settore Scientifico Disciplinare: GEO/10

Ionospheric plasma response to the anomalous minimum of the solar cycle 23/24: modeling and comparison with IRI-2012

Presentata da: Luigi Perna

Coordinatore Dottorato:
Prof. Nadia Pinardi

Supervisore:
Prof. Michele Dragoni

Relatore:
Dr. Michael Pezzopane (INGV)

Esame finale anno 2017

A chi è l'amore,
a chi è il sacrificio,
a chi è la pazienza,
a chi è la passione,
a chi è il sostegno,
a chi è il sorriso.

Contents

Introduction

The section of the terrestrial atmosphere included between the thermopause ($\sim$500 km) and the stratopause ($\sim$50 km) is identified with the term *ionosphere*. The ionosphere represents the portion of the Earth's atmosphere where the density of free electrons is high enough to influence the propagation of radio waves.

The first hypothesis about the existence of a conducting atmospheric layer was formulated at the beginning of the XIX century, when Carl Gauss and Balfour Stewart hypothesized the existence of atmospheric electric currents to explain the observed variations of the Geomagnetic Field (GF). The clear proof of the ionosphere existence was given on 12 December 1901, when Guglielmo Marconi established a radio link between the cities of Poldhu (UK) and St. John's (Canada).

The ionosphere can be considered a *minority plasma*, meaning that the ionized component (ions and free electrons) represents a smaller fraction than the neutral one. The GF interacts with the ionospheric plasma, therefore they talk about a *magnetoionic plasma* or simply a *magnetoplasma*. The study of the electromagnetic waves propagation through a magnetoplasma represents the *magnetoionic theory*, which became of great interest since the beginning of the XX century.

The observed pattern of the ionosphere is produced by the differential interaction between the neutral atmospheric species and the ionizing solar radiation, which produces a vertical electron density profile characterized by several relative maxima and minima. At every maximum, a specific frequency, called *critical frequency*, and an ionospheric layer are associated. The critical frequencies of the ionospheric layers are very important, representing the maximum frequencies at which a radio wave sent vertically towards the ionosphere is reflected towards the Earth. The absolute electronic density maximum (NmF2) of the vertical profile is associated to the diurnal F2 layer (or the nighttime F region) and the correspondent critical frequency is called *fo*F2. This is the most important ionospheric parameter, because it represents the maximum frequency vertically reflected by the ionosphere.

Besides considering *fo*F2, the ionospheric plasma is investigated by analyzing NmF2 and the corresponding height hmF2. *fo*F2 is strictly linked to NmF2, by virtue of the plasma frequency formula: $Nm\mathrm{F2}[\mathrm{m}^{-3}] = 1.24 \cdot 10^{10} (fo\mathrm{F2}[\mathrm{MHz}])^2$.

The climatological pattern of the aforementioned ionospheric parameters is strongly influenced by the latitude, longitude, geomagnetic activity and solar activity. However, the solar activity represents the most relevant cause of the ionospheric variability.

During the last decades, the interest in studying the ionosphere has strongly increased because: (1) the ionosphere swiftly reacts to variations of the Sun-Earth environment and it is then expected to be strictly linked to the Sun activity; (2) long- and short-time variations of the ionosphere significantly affect the communications Earth-Earth, Earth-satellite and satellite-satellite; (3) possible signatures of the greenhouse gases increase could be observed in the ionospheric parameters long-term trends.

The last solar minimum, between the solar cycle 23 and 24 (minimum 23/24), has shown unprecedented characteristics, being the longest and quietest period since the advent of space-based measurements. The minimum interested the years between 2007 and 2010, with 2008 and 2009 representing the deepest phase for which a very low solar activity occurred. For the minimum 21/22, 176 spotless days were registered for the two years 1986-1987; for the minimum 22/23 (years 1996-1997), the observed spotless days were 226; for the years 2008-2009 of the last minimum, 527 days without sunspots have been registered, revealing an extremely quiet solar activity period. In addition, the last solar minimum has been characterized by an uncommon long duration. As a first step, the beginning of the minimum has been set around March 2006 and many predictions of the start and length of solar cycle 24 were given thereafter. In 2007, the solar cycle 24 Prediction Panel anticipated that the solar minimum marking the onset of cycle 24 would occur in March 2008 (±6 months), but the date was then corrected to August 2008 and later to December 2008. Actually, the minimum was registered in the middle of 2009 and thus more than 2 years after the earliest prediction and with a whole 23 cycle length of 12 years and 6 months, that is 18 months longer than the "canonical" 11-year solar cycle.

The unique features that characterized the last minimum have been confirmed by numerous observations: (1) the magnetic field at solar poles was approximately 40% weaker than that of cycle 22/23; (2) a 20% drop in solar-wind pressure has been measured since the mid-1990s, touching the lowest point since the start of measurements in the 1960s; (3) solar-wind speed and radiation-belt flux were lower than those of previous minima; (4) the thermospheric densities at an altitude of 400 km were the lowest observed in the 43-year (1967-2010) database, and were anomalously lower, by 10-30%, than the climatologically expected levels; (5) for the latter half of 2008, the O^+/H^+ transition height, that represents a sensitive indicator of both the solar extreme ultra violet ionizing flux and the dynamics of the topside ionosphere, was much cooler and much closer to the planet than expected.

Because of the strong influence that ionospheric disturbances can have in particular in radio communications, there is an increasing interest in studying the ionospheric plasma response to extreme solar activity conditions, and the corresponding possible consequences on the near-Earth environment. Under the aforementioned unprecedented conditions, the minimum of the solar cycle 23/24 provides a perfect natural window to study the ionospheric plasma response under a very low and prolonged solar activity.

The main ionospheric ionization source is the radiation in the Ultra Violet band (120-400 nm) and in particular in the Extreme Ultra Violet band (EUV, 0.1-120 nm). The solar EUV irradiance explains around 90% of the variance of ionospheric parameters such as foF2 and hmF2, and solar indices which refer to wavelengths in the EUV band are theoretically the most appropriate to describe the ionospheric variability. Nevertheless, accurate measurements of EUV/UV irradiance are possible only from above the terrestrial atmosphere. Consequently, EUV continuous measurements started only with the launch of the Solar Heliospheric Observatory (SOHO), in the mid-1990s. Moreover, instruments used to perform measurements in these bands quickly degrade because of the intense UV and EUV exposure, and monitoring of this instrumental degradation is particularly difficult. Therefore, continuous and reliable EUV datasets are not common and, for ionospheric studies, it is necessary to use solar indices with longer datasets that can be considered good proxies for the solar activity in these wavelengths.

Among the numerous available indices, the solar radio flux at 10.7 cm, namely $F_{10.7}$, represents the most widely used solar activity proxy, being used by ionospheric and thermospheric models such as the *IRI* (*International Reference Ionosphere*) model and the *NRLMSISE-00* model. The solar radiation at 10.7 cm can be easily measured with ground-based instruments,

Introduction

and this is why $F_{10.7}$ has a long and continuous dataset starting since 1947. Nevertheless, the reliability of this index as a good proxy for both the general solar activity and the radiation in the EUV band has been questioned during the last solar minimum. It has been shown that the decrease of the solar EUV irradiance from the minimum 22/23 to the last minimum was much larger (15%) than the decrease of $F_{10.7}$ (5%). Furthermore, marked changes in the long-term relation between the EUV irradiance and $F_{10.7}$ have been observed since 2006, with EUV levels decreasing more than those of $F_{10.7}$. Therefore, it has been highlighted how $F_{10.7}$ can no more be considered both a good EUV proxy and a good solar activity proxy for ionospheric purposes.

In light of the very particular conditions observed for the last solar minimum and of the variations in the relation between the EUV radiation and the index $F_{10.7}$, a deeper analysis of the relations between parameters that characterize the ionospheric plasma and the most widely used solar indices is of primary importance. Focusing the attention on the main ionospheric parameter *fo*F2, which shows a marked dependence on solar activity variations, it is worth noting that the analysis of relationships (*fo*F2 vs *Solar Index*) results to be essential because: (1) every ionospheric model is based on these relations; (2) when accurate, these relations can be used to "clean" ionospheric time series from the solar activity influence, in order to extract possible ionospheric signatures of the greenhouse effect.

As mentioned before, the solar activity represents the main cause of the observed ionospheric variability. Therefore, the knowledge of relations that link *fo*F2 with solar activity indices is essential to improve the performances of ionospheric models.

Over the last four decades, long-term prediction models of the ionospheric conditions have represented an important tool for both applied science and theoretical studies. The systematic collection of regular observations and the evolution of computing systems allowed William B. Jones and Roger M. Gallet to produce, in 1965, the first global model for long-term mapping of *fo*F2 and the propagation factor for a distance of 3000 km, namely $M(3000)$F2.

In the last years, together with a long-term description of the ionospheric characteristics, the interest has increased in a short-term forecasting and nowcasting of the ionosphere. With the aim of short-time forecasting and nowcasting on a continental scale, numerous international projects have been developed, such as the *COST* (*Cooperation in Science and Technology*) actions, the European projects *DIAS* (*DIgital upper Atmosphere Server*; http://www.iono.noa.gr/DIAS/) and *ESPAS* (*Near-Earth Data Infrastructure for e-Science*; http://www.espas-fp7.eu/); also working programs has been opened, such as *IPS* (*Ionospheric Prediction Service*, Australia) and *NOAA* (*National Oceanic and Atmospheric Administration*, USA).

Recent advances in global and regional networks of real-time ionosondes and ground-based dual-frequency *GNSS* (*Global Navigation Satellite System*) receivers, together with data-driven ionospheric modeling, have brought new insights to ionospheric physics, with significant improvements of prediction and forecasting modeling.

A clear proof of this is the possibility to obtain from satellite "top-side" electron density profiles (above the electron density peak), which is not possible from ground-based ionosondes.

HF (High Frequency) radio communications are widely used in many fields like: emergency services, strategic implementations, in-flight information and communications, and general radio services. As mentioned before, the ionosphere represents the portion of the atmosphere that significantly influences the HF propagation. For example, disturbed conditions of the solar-terrestrial environment (such as those caused by geomagnetic storms) may seriously affect the trans-ionospheric transmissions used by navigational systems. Therefore, the ionospheric modeling, that can be global or regional/local, represents a primary goal.

Global ionospheric models usually use ground-based and in-situ data to provide empirically

a global mean description of the ionospheric parameters. Nevertheless, when an accurate and quick description of the ionospheric features for a limited sector is needed, regional/local models are preferable. The limit cases of regional/local models are the *Single-Station Models* (*SSMs*) that use data only from one station, providing a very accurate and simple description of the ionosphere around the corresponding site.

Nowadays, the most widely used global ionospheric model is the IRI model that represents the reference model for the ionospheric community. The IRI is an international project sponsored by the Committee on Space Research (COSPAR) and the International Union of Radio Science (URSI), based on an extensive database, and able to capture much of the repeatable characteristics of the ionosphere for quiet and storm-time periods, such as the electron density, the electron content, the plasma temperatures and the ion composition, as a function of height, location, and local time.

The *Simplified Ionospheric Regional Model* (*SIRM*) is a European regional model based on data from seven ionosondes. The model has been developed in the early 90s and provides an accurate description of the monthly median values of several ionospheric characteristics. SIRM is a very simple model that takes into account the dependence of the parameters from the solar activity, by means of linear regressions, and uses a Fourier analysis to characterize and forecast the variations of the ionospheric characteristics. Due to the longitudinally limited sector considered (40°), the model takes into account only latitudinal variations.

Both IRI and SIRM use solar activity indices as input parameters, and when using uncertain predicted values for them, significant discrepancies can be obtained by comparing the modeled output with the measured one. Therefore, by virtue of the unprecedented features observed for the last solar minimum, it is expected that ionospheric models have some problems in representing the ionosphere during the minimum 23/24, also because there were no previous data recorded under similar conditions. The present work is focused on the ionospheric plasma response to the anomalous minimum of the solar cycle 23/24, with a particular interest in the corresponding modeling and on the results given by the IRI model in its last version IRI-2012. The study carried out concerns also a partial implementation of the SIRM model, which gave useful guidelines for a future complete implementation of the model.

Chapter 1 concerns a general description of the main ionospheric features, with particular attention to the ones useful for the development of the work. After a brief introduction about the history of the development of ionospheric studies since the first observation in 1901, the formation and the vertical structure of the ionosphere are discussed. The *plasma frequency* and the *critical frequency* are defined. The formation of the ionosphere is described using the equation of the electronic equilibrium and discussing the mechanisms of electronic production, disappearing and transport. Moreover, the layers composing the ionospheric vertical structure are described with their most relevant features, along with a deep description of the ionospheric parameters used in the work (*fo*F2, *Nm*F2 and *hm*F2). The climatological pattern of the ionosphere is influenced by numerous phenomena linked to the solar and geomagnetic activity, seasons, hour of the day, latitude, and longitude. Hence, a brief description on the ionospheric variability is reported, focusing the attention on the solar activity dependence. In detail, the *saturation* and *hysteresis effects*, usually encountered in the study of the relationships between *fo*F2 and indices of solar activity, are introduced and discussed. The *winter* and *semi-annual anomalies* are also introduced, being strictly linked to solar activity changes and particularly specific at mid and low latitudes, respectively. A deep analysis of these two anomalies can provide key information about the influence of the low levels of solar activity on the ionospheric plasma during the solar minimum 23/24. The last section of the chapter focuses on a brief review

Introduction

of the ionospheric vertical sounding method, based on the radar technique. The main features of the *ionograms*, which represent the outputs of the ionospheric vertical soundings, are explained and it is reported how to obtain, when possible, the main ionospheric parameters. Concerning hmF2, the methodology of the target function for the ionogram inversion is described, along with two widely used analytical relations, namely *Shimazaki* and *D55*.

The work inspects the ionospheric plasma response during the minimum of solar activity between solar cycles 23 and 24. Based on analyses conducted with different instrumentations by several researchers, the main observed features of the last solar minimum 23/24 are reported in Chapter 2. This review allows to understand the unprecedented characteristics featuring the Sun-Earth environment. In this chapter the main fields of interest in studying the ionosphere under the particular conditions of the last minimum are also discussed. In particular, it is shown how, using as input forecasted values for the ionospheric index *IG12* (used by IRI to perform a global mapping of *fo*F2), the IRI model provides huge *fo*F2 overestimations for the deep phase of the last minimum (years 2008 and 2009). This result clearly shows (1) the difficult to reliably forecast the last minimum and (2) the strong influence that input parameters have on the output of ionospheric models.

The main core of the work is described in Chapter 3, 4 and 5.

Chapter 3 analyzes the relationships (*fo*F2 vs *Solar Index*). The study is based on the long, continuous and very reliable *fo*F2 dataset (hourly validated values) recorded at the Rome ionospheric station between the 1st January 1976 and the 31st December 2013, hence covering the whole solar cycles 21, 22, 23 and the ascending phase of cycle 24. It is important to underline that the continuous dataset provided by the Rome station is the key to carry out this study, because all over the world there are few ionosondes with a so long and continuous dataset. The study takes into account five widely used solar activity indices: $F_{10.7}$, Lym-α, $MgII$, the sunspots number R and the solar irradiance in the EUV band 0.1-50 nm ($EUV_{0.1-50}$). Every index is described in detail, along with the available dataset and the sources from which solar indices data have been downloaded. The study is accomplished by considering *fo*F2 values recorded at local noon (LT=UT+1h for Rome station). This choice was suggested by the fact that for every index only one daily value is available and measurements usually refer to local noon. Furthermore, studies of ionospheric long-term trends usually refer to local noon.
The main aim of this part of the work is to examine the *fo*F2 dependence on solar activity, trying to discuss and solve specific problematics in order to obtain simple analytical relations to be used for ionospheric modeling. In order to obtain these results, a 1-year running mean is applied for both *fo*F2 and solar indices. By using this methodology, it is possible to eliminate short-time ionospheric features, like those caused by geomagnetic disturbances, ionospheric seasonal and day-to-day variations, and (partially) reduce the saturation effect occurring at high solar activity. Furthermore, from "clean" (*fo*F2 vs *Solar Index*) plots it is easier to obtain accurate analytical formulae.
In the first part of the chapter the a priori supposed linear fit is tested to investigate whether it can still be considered as the best one. After that, the best fit is found using a residuals analysis. Then, the search for the best index, able to describe the variations of *fo*F2 both globally (for the complete dataset 1976-2013) and for the last solar minimum (time interval January 2008-December 2009), is reported. The analysis is carried out by comparing ionosonde values with opportune synthetic datasets obtained for every solar index. Moreover, by introducing the R-Solomon parameter, it has been possible to compare the *fo*F2 variations with the ones of indices for the whole cycle 23. This analysis gives the possibility to discuss another important issue: the search for the EUV solar radiation "best proxy", which means to search for an index

with a long available dataset that well approximates the variations of the solar radiation in EUV wavelengths. A section of the chapter is dedicated to additional analyses carried out during the work, providing some starting points for future studies. Specifically, the following issues are discussed: (1) systems of analytical relations; (2) foF2 (at 01 LT and 19 LT) vs *Solar Index* relationships for Rome station; (3) (NmF2 vs *Solar Index*) and (hmF2 vs *Solar Index*) relationships; (4) dependence of (foF2 vs *Solar Index*) relationships on the geomagnetic activity.

Chapter 4 is an outline about the update of the SIRM model: it can be interesting to discuss how and whether the SIRM model can be improved according to the findings reported in Chapter 3. First, the theoretical aspects of the SIRM model are reported. Then, SIRM outputs for foF2 are compared with ionosonde values for the low solar activity years 2008 and 2009 to test its reliability in such particular conditions. After this preliminary analysis, the updated model, called *SIRMPol*, is introduced. SIRMPol foF2 outputs are then compared with both values measured by the ionosonde and calculated by SIRM, for both low solar activity (2008 and 2009) and very high solar activity (year 1958). In fact, as it is discussed in depth in the chapter, passing from SIRM to SIRMPol, more pronounced improvements are expected for high solar activity levels, when the saturation effect is dominant.

However, the most accurate description of the ionospheric parameters for a single station can be obtained by the development of opportune SSMs. The accuracy of these models increase with the availability of a long and continuous dataset. As previously underlined, for the Rome station a very robust dataset is available. For this reason, a SSM, namely *Single Station Model for Rome* (*SSM-R*), has been developed. SSM-R outputs for foF2 are compared with the ones given as output by SIRM and SIRMPol and values measured by the ionosonde for the aforementioned years at low and high solar activity. A complete updating of the SIRM model falls outside the main objectives of the present work and further analyses need to be carried out. Nevertheless, the preliminary results described in this chapter give the possibility to list several useful guidelines for a future updating of the SIRM, which are reported at the end of the chapter.

Chapter 5 is about the analysis of the recent solar minima and the investigation of the IRI-2012 reliability, at mid- and low-latitude stations. In this part of the work, data from four ionospheric stations are used: Rome (41.8°N, 12.5°E, geomagnetic latitude 41.7°N, Italy), Gibilmanna (37.9°N, 14.0°E, geomagnetic latitude 37.6°N, Italy), São José dos Campos (23.1°S, 314.5°E, geomagnetic latitude 19.8°S, Brazil), and Tucumán (26.9°S, 294.6°E, geomagnetic latitude 17.2°S, Argentina). Rome and Gibilmanna are descriptive of the mid-latitude ionosphere, while São José dos Campos and Tucumán represent low-latitude stations located in an ionospherically critical position, being close to the south crest of the *Equatorial Ionization Anomaly*. Rome, Gibilmanna, and Tucumán stations are all equipped with an *AIS-INGV* (*Advanced Ionospheric Sounder-INGV*) ionosonde, the São Josè dos Campos station is equipped with a *CADI* (*Canadian Advanced Digital Ionosonde*) ionosonde, and corresponding data related to recent minima have been all validated, which has generated a very reliable dataset. The analysis concerns the electron density peak NmF2 and the height hmF2 at which it is reached. NmF2 has been obtained from validated foF2 values, using the plasma frequency formula; hmF2 has been obtained using Shimazaki and D55 analytical relations. However, for hmF2 a preliminary study has been carried out, comparing values from analytical relations with those from ionogram inversions, in order to understand which is the relation that gives the most reliable values for a definite period.

The particularity of the last solar minimum is emphasized by an inter-minima comparison for

Introduction

both NmF2 and hmF2. Moreover, the reliability of the outputs given by the IRI-2012 model is tested for both parameters, for low solar activity, by comparing them with measured ones. A comparison between the results obtained at mid latitudes with the ones inferred at low latitudes for both the inter-minima comparison and the IRI-2012 reliability is also carried out.

The most important goals of this work can be summarized as follows:

1. To use the long and continuous dataset recorded at the ionospheric station of Rome to study the relations (foF2 vs *Solar Index*):

   - To observe whether the a priori supposed linear relation is valid or there have been changes owing to the last solar minimum;
   - To find the best fit and index to describe the foF2 variations;

2. To obtain useful guidelines for a future complete update of the regional SIRM model and to develop a reliable SSM for the Rome station;

3. To evaluate the main behaviors of the ionosphere for the last solar minimum, making a comparison with the previous minima, for NmF2 and hmF2;

4. To evaluate the IRI outputs for the last solar minimum, making a comparison with the previous minima.

The results obtained and possible future analyses related to the present work are the subject of the "Conclusions and future developments" section.

Two papers have been extracted from the present work and accepted for publication in international journals. The first paper is based on the work described in Chapter 3:

Perna, L., Pezzopane, M., 2016. foF2 vs solar indices for the Rome station: Looking for the best general relation which is able to describe the anomalous minimum between cycles 23 and 24. Journal of Atmospheric Solar-Terrestrial Physics 148, 13-21, http://dx.doi.org/10.1016/j.jastp.2016.08.003.

The second paper (in press) is based on the work reported in Chapter 5:

Perna, L., Pezzopane, M., Ezquer, R., Cabrera, M., Baskaradas, J. A., 2016. NmF2 trends at low and mid latitudes for the recent solar minima and comparison with IRI-2012 model. Advances in Space Research, http://dx.doi.org/10.1016/j.asr.2016.09.025.

The front pages of both papers are attached after the "Conclusions and future developments" section.

The Acknowledgements and Bibliography are reported at the end of the thesis.

Chapter 1

The Terrestrial Ionosphere

Introduction

The term *ionosphere* usually identifies the part of the terrestrial atmosphere included between 50 and 500 km of height, that is between the stratopause and the termopause. The main feature of the ionosphere is the presence of free electrons and ions in a quantity that strongly influences the radio wave propagation.

The first hypothesis about the existence of the ionosphere can be found at the beginning of the XIX century, when Carl Gauss and Balfour Stewart hypothesized the existence of atmospheric electric currents in order to explain the observed variations of the terrestrial magnetic field. The definitive proof of the existence of the ionosphere was given on 12 December 1901, when Guglielmo Marconi established a radio link between the city of Poldhu (in the UK) and the Canadian city of St. John's. At that time, the theory considered only a straight-line propagation, so the Marconi's experiment could be explained only considering the possibility of a reflection in the atmosphere. In 1902, A. E. Kennelly and O. Heaviside suggested the existence of an ionized layer in the atmosphere, able to deviate and reflect waves in radio wavelength ranges. Lee de Forest and L. F. Fuller, members of the *Federal Telegraph Company* of San Francisco, between 1912 and 1914, made the first measures about the height of this layer, but unfortunately the corresponding results are not well known. The first available measures are the ones of E. V. Appleton and M. A. F. Barnett (UK, 1924), who with an interferometric methodology found a reflection height of ∼92 km.

R. A. Watson-Watt suggested the name *'ionosphere'* for the first time in a letter sent to the *United Kingdom Radio Research Board* on 8 November 1926. At the same time, Appleton started using the same term when writing a letter to J. A. Ratcliffe on 2 November 1926:

> *'For the ionised part of the upper atmosphere I think the terms ionosphere or electrosphere might be useful. Which do you prefer?'*

Nevertheless, the term ionosphere does not appear in literature until the 1929, when Watson-Watt at the Symond Memorial Lecture of the Royal Meteorological Society said:

> *'It might be permissible to call it the Belfour-Stewart-Fitzgerald-Heaviside-Kennelly-Zenneck-Schuster- Eccles-Larmor-Appleton space, but something less direct is desirable. I have suggested the name ionosphere to make a systematic group troposphere, stratosphere, ionosphere, but meanwhile the term 'upper conducting layers' seems to hold the field'.*

After the 1932, the term proposed by Watson-Watt started to be used frequently in literature, stopping a long discussion about the name of this layer that, in the previous years, had also been called *upper reflection surface*, *conducting layer*, *Heaviside layer*, *day* (or *night*) *effect* from Marconi experiment, *Kennelly-Heaviside layer* and so on. A series of curiosities and anecdotes about the born of the name ionosphere can be found in Gillmor (1976).

The *magnetoionic theory*, the study of the propagation of electromagnetic waves in an ionized mean immersed in the terrestrial magnetic field, started being of great interest in particular since the beginning of the XX century. The most relevant results were obtained by Appleton that won the Nobel prize in 1947 for the discovery of the ionospheric layers and for his contribute to the magnetoionic theory.

The importance of the study of the ionosphere can be found in a series of aspects, the most important of which is that it significantly influences the communications Earth-Earth, Earth-satellite and satellite-satellite. Moreover, the ionosphere is strongly affected by the solar activity variations, and it is then strictly connected to the interactions between the Sun and the Earth.

This first chapter focuses on a general description and introduction of the main ionospheric features, with particular attention to the ones useful for the development of this work.

In the first section of this chapter, a description of the formation and vertical structure of the ionosphere will be reported. The second section will be instead devoted to the ionospheric variability, with a focus on the strong influence that the solar activity has on the ionospheric plasma. A brief review of the vertical ionospheric sounding technique is carried out in the last section.

1.1   Formation and vertical structure of the ionosphere

The ionosphere can be considered a low-density plasma, with an ionized component (ions and free electrons) representing a smaller fraction than the neutral one, so we can consider it a *minority plasma*. This kind of plasma, immersed into the terrestrial magnetic field, is called *magnetoplasma*.

The ionosphere forms due to the interaction between the radiation coming from the Sun and the high layers of the terrestrial atmosphere. The differential interaction of the radiation with the different atmospheric chemical species is responsible for the typical stratification of the ionosphere.

The main parameter characterizing a plasma is its *plasma frequency*, that represents the oscillation frequency of the electrons with respect to the fixed ions, when moved from a stable state position.
Considering a unidimensional configuration in which the electrons move a distance x from the fixed ions, neglecting the thermal agitation and considering an infinite layer, under the action of a disturbing electric field $\mathbf{E}$, the restoring force due to the induced electric field $\mathbf{E}_i$ has the intensity:

$$e\mathbf{E}_i = e\frac{\sigma}{\epsilon_0}\hat{\mathbf{x}} = e\frac{Nex}{\epsilon_0}\hat{\mathbf{x}}, \qquad (1.1)$$

where $\mathbf{E}_i = \sigma/\epsilon_0$ is the electric field of an electrical double layer, $\sigma = Nex$ is the superficial charge density, ϵ_0 is the permittivity of free space, N is the electron density, and e is the charge

of the electron. The momentum equation for the electron of mass m is then:

$$\frac{d^2\mathbf{x}}{dt^2} + \frac{Ne^2}{m\epsilon_0}\mathbf{x} = 0, \tag{1.2}$$

which is the equation of an harmonic oscillator of which the angular frequency is:

$$\omega_N = \sqrt{\frac{Ne^2}{m\epsilon_0}}. \tag{1.3}$$

Considering that $\omega_N = 2\pi f_N$, the plasma frequency is then:

$$f_N = \sqrt{\frac{Ne^2}{4\pi^2 m\epsilon_0}}. \tag{1.4}$$

The value of f_N is crucial to determine the frequency usable for a radio communication.

The vertical structure of the ionosphere is caused by the counterpoised trend between the ionizing solar radiation (increasing outward) and the atmospheric density (increasing inward). Moreover, the differential interaction of the various chemical species with the solar radiation causes the formation of relative maxima of electron density in the profile. These maxima individuate the ionospheric layers. Figure 1.1 shows typical daytime and nighttime electron density profiles at mid latitude and for low solar activity (sunspot number $R=0$), where the F, E and D regions are pointed out.

The most important parameter characterizing an ionospheric layer is its critical frequency. If in the equation (1.4) we substitute the electron density N with an electron density relative maximum N_{mi}, we obtain $f_{N\mathrm{mi}}$ that represents the maximum frequency vertically reflected by the ionospheric layer i. At each ionospheric layer is associated a critical frequency, with a simple notation; for example foE represents the critical frequency of the E region, foF2 the critical frequency of the F2 region and so on. The critical frequency foF2 is the most important ionospheric parameter and represents the maximum frequency vertically reflected by the ionosphere.

1.1.1 Processes involved in the formation of the ionosphere

The free electrons represent the main cause for the ionospheric reflection of radio waves, so the electron density value and its variations are of primary importance. The variation of N with the time can be expressed using the *electronic equilibrium equation*:

$$\frac{dN}{dt} = q(t, \mathbf{X}) - l(t, \mathbf{X}) + d(t, \mathbf{X}). \tag{1.5}$$

The parameters q, l and d represent the *production rate*, *disappearing rate* and *transport rate* for electrons in the unity of time and volume, respectively. As equation (1.5) shows, the rate dN/dt depends also on the position $\mathbf{X}$.

The main mechanism causing the production of free electrons is the *photoionization* due to the solar radiation. At mid and low latitudes the photoionization can be considered the only mechanism responsible for the formation of the ionosphere, meanwhile at polar zones other mechanisms such as the transport cannot be neglected.

The photoionization can be schematized as $A + h\nu \rightarrow A^+ + e^-$, where A is a generic neutral
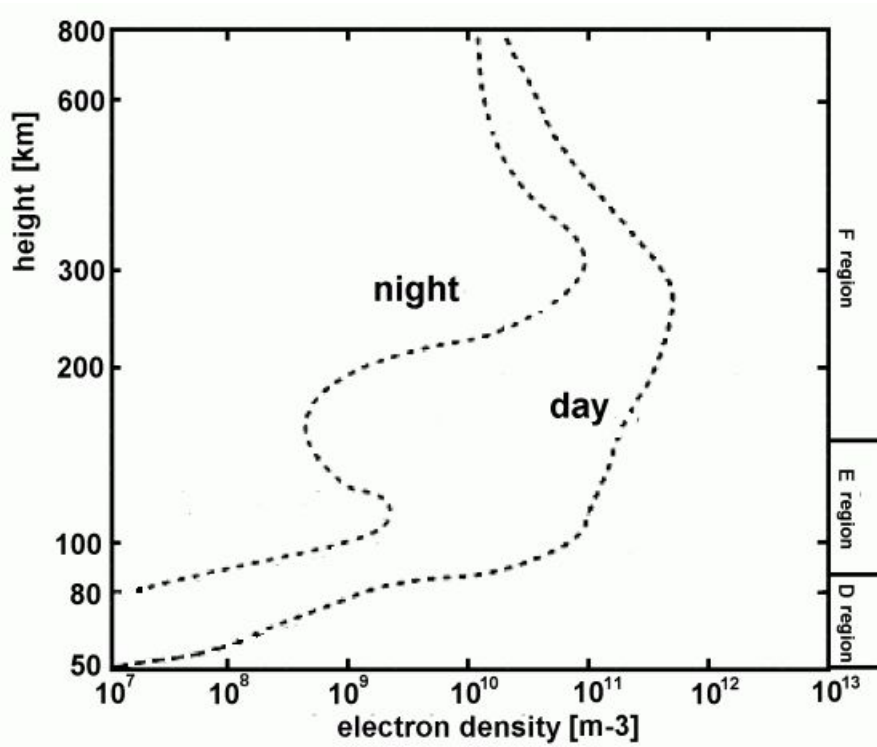
Figure 1.1: Typical day- and night-time electron density profile at mid latitude, for low solar activity. The ionospheric D, E and F regions are highlighted on the right.

species, h is the Planck constant, and ν the wave frequency of the Sun radiation; the ionization is possible only if $h\nu \geq E_i$, where E_i is the energy of ionization for the generic species i.

The *photoionization cross section* σ is introduced to consider the stochastic character of the process, depending on the wavelength λ of the incident radiation and on the particular species A_i. If I is the intensity of the radiation and n the density of a specific atomic species, we can write the production rate q as:

$$q = \sigma(\lambda, A_i)nI. \tag{1.6}$$

The main ionizing radiations coming from the Sun are those falling in the Ultra Violet wavelength range of 10-400 nm, and in the X-ray wavelength range of 0.1-10 nm.

The loss of electrons is due to two main mechanisms: *recombination* and *attachment.* The recombination consists in the interaction between positive ions and electrons, to form neutral atoms and release energy $(A^+ + e^- \rightarrow A + Energy)$. Introducing the *coefficient of recombination* γ (expressed in [m^3/sec]), the probability of recombination will be:

$$l_{\mathrm{r}} = \gamma N A^+. \tag{1.7}$$

The attachment consists in the interaction between neutral atoms and electrons, to form negative ions and release energy $(A + e^- \rightarrow A^- + Energy)$. Introducing the *coefficient of attachment* δ (expressed in [m^3/sec]), the probability of the attachment will be:

$$l_{\mathrm{a}} = \delta N A. \tag{1.8}$$

In this simple treatise, we consider δ and γ constants and do not take into account the dissociative recombination phenomenon.

Local variations of N that cannot be ascribed to photoionization or recombination are due to *transport mechanisms*, such as *diffusion*, *thermal transport* and *turbulence*.
The transport rate can be then expressed as:

$$d = \frac{\partial D}{\partial h}\left(\frac{\partial N}{\partial h} + \frac{N}{T}\frac{\partial T}{\partial h} + G\frac{N}{H}\right) - div(N\mathbf{V}), \qquad (1.9)$$

where D is the *diffusive transport coefficient*, G is the *gravitational transport coefficient*, T the *absolute temperature*, H the *scale height*, h the *height* and $\mathbf{V}$ the velocity field.

Introducing equations (1.6)-(1.9) in equation (1.5), we obtain

$$\frac{dN}{dt} = \sum_i \sigma(\lambda, A_i)n_i I - \sum_i \gamma_i N[A_i^+] - \sum_i \delta_i N[A_i] + d. \qquad (1.10)$$

Introducing into the (1.10) the *effective recombination coefficient* ($\alpha = \Sigma_i\gamma_i$), the *effective attachment coefficient* ($\beta = \Sigma_i\delta_i[A_i]$), and assuming $[A_i^+] = N^+$, the final version of the electronic equilibrium equation can be written as:

$$\frac{dN}{dt} = q - \alpha N N^+ - \beta N + d. \qquad (1.11)$$

1.1.2 Ionospheric layers and main parameters

As shown in Figure 1.1, the electronic density varies with the height being characterized by relative maxima. Every relative maximum identifies and characterizes a specific ionospheric region:

- D region;

- E region;

- F region.

The D region is the lowest one and extends from 50 to 90 km, with an electron density peak of $\sim10^9$ m^{-3} at ~80 km. Sometimes a lower layer, called *C layer*, can be visible at heights of 65-70 km. The D region is not useful for radio communication because of the very low electron density; instead it represents the most absorbing layer, because of the highest value of the quantity $N\upsilon$, where υ is the *collisional frequency*. The D and C regions are only visible during daytime hours.

The E region, characterized by heavy ions (O_2^+ and NO^+), extends from 90 to 150 km, with an electron density peak of $\sim10^{11}$ m^{-3} at ~120 km. A peculiar feature of this layer is the appearance of random and fast stratifications (0.2-2 km thick) with $N > 10^{12}$ m^{-3}, called *sporadic E layers*. The E region is mainly a typical daytime region, even though a light nighttime stratification ($N \sim 5 \cdot 10^9$ m^{-3}) is observed.

The region between 150 and 500 km, dominated by light ions (O^+, H^+, He^+, N^+), represents the F region, of which the electron density maximum of $N \sim 5 \cdot 10^{12}$ m^{-3} is reached at ~300 km. During daytime hours, the F region can be split in two different layers: the F_1 layer and the F_2 layer. The F_1 layer is characterized by an electron density maximum of $\sim10^{11}$ m^{-3} at ~180 km, with a predominance of ions O^+, and it is a layer typically diurnal. The F_2 layer, formed for the 95% of ions O^+, is the most important layer for radio communication purposes, with an electron density peak of $\sim10^{12}$ m^{-3} at ~300 km.

During the nighttime it is visible a unique *F region* with an electron density peak of $\sim 7 \cdot 10^{10}$ m^{-3} at ~ 300 km.

D, E and F$_1$ layers can be considered α-*Chapman* layers, that means diurnal layers with maximum electron density at midday and in summer; the F2 layer instead can be considered a *Bradbury layer*, with the electron density monotonically decreasing with the height, after reaching its maximum (Dominici, 1971).

As mentioned, the F region is the most important for radio communication purposes. Therefore, the critical frequency *fo*F2 represents the most important ionospheric parameter. It represents the maximum frequency reflected by the ionosphere for a radio wave transmitted vertically.

*fo*F2 is linked to the maximum electron density *Nm*F2 of the vertical profile, in fact from equation (1.4) we obtain that *Nm*F2 [m^{-3}]= $1.24 \cdot 10^{10}(fo$F2 [MHz]$)^2$. The height at which *Nm*F2 is reached is indicated as *hm*F2. *fo*F2 is easily deducted, manually or automatically, directly from an ionogram. To calculate *hm*F2 the situation is quite different and complex. Only in the last years, the calculation of this value has become a routine operation for automatic scaling systems which perform an inversion of the ionogram[1], a necessary step to obtain *hm*F2. Alternatively, as it will be explained in more detail in Section 1.3.2, it is possible to use analytical relations that include other ionospheric parameters such as *fo*E or the *Maximum Usable Frequency MUF*(3000)F2, which represents the maximum frequency usable for a radio communication between two points at a distance of 3000 km. Also *fo*E and *MUF*(3000)F2 can be easily deducted from an ionogram.

1.2   Variability of the ionosphere

The ionosphere is a very variable system. It is strongly influenced by a great number of phenomena linked to the solar and geomagnetic activity, the seasons, the hour of the day, the latitude, and the longitude. A complete discussion on the ionospheric variability is out of the scope of this work, nevertheless in this section ionospheric features that will be useful to the comprehension of the next chapters will be discussed and introduced.

As mentioned, the ionosphere forms owing to the interaction between the solar radiation and the terrestrial atmosphere. By virtue of this, the solar activity represents the main controller of the ionospheric variability. Consequently, the ionospheric parameters show trends that follow quite well the indices representing the solar activity level. In Figure 1.2 are plotted the 1-year running mean of the index $F_{10.7}$ (representing the solar flux at 10.7 cm and described in detail in Section 3.1), that represents a widely used indicator of solar activity, and the 1-year running mean of validated values of *fo*F2, observed at 12 LT at the ionospheric station of Rome, from the 1 January 1976 to the 31 December 2014, a period of time covering partially the solar cycle 24 and completely the solar cycles 21, 22 and 23. It is visible the similar trend of the two parameters, which means that there is a strong correlation between the solar activity variations and the response of the ionosphere. In fact, the parameter *fo*F2 follows the increase/decrease of the solar activity, with higher/lower values for high/low solar activity. Furthermore, Figure 1.2 suggests a quasi-linear relation between $F_{10.7}$ and *fo*F2. This will be the object of the study described in Chapter 3.

An important ionospheric feature, linked to the dependence of the ionosphere on the solar activity, is the *saturation effect* observed for high solar activity (Liu et al., 2003, 2006, 2011b;

---

[1]Inverting an ionogram means to pass from the typical ionogram trace to the vertical electron density profile.
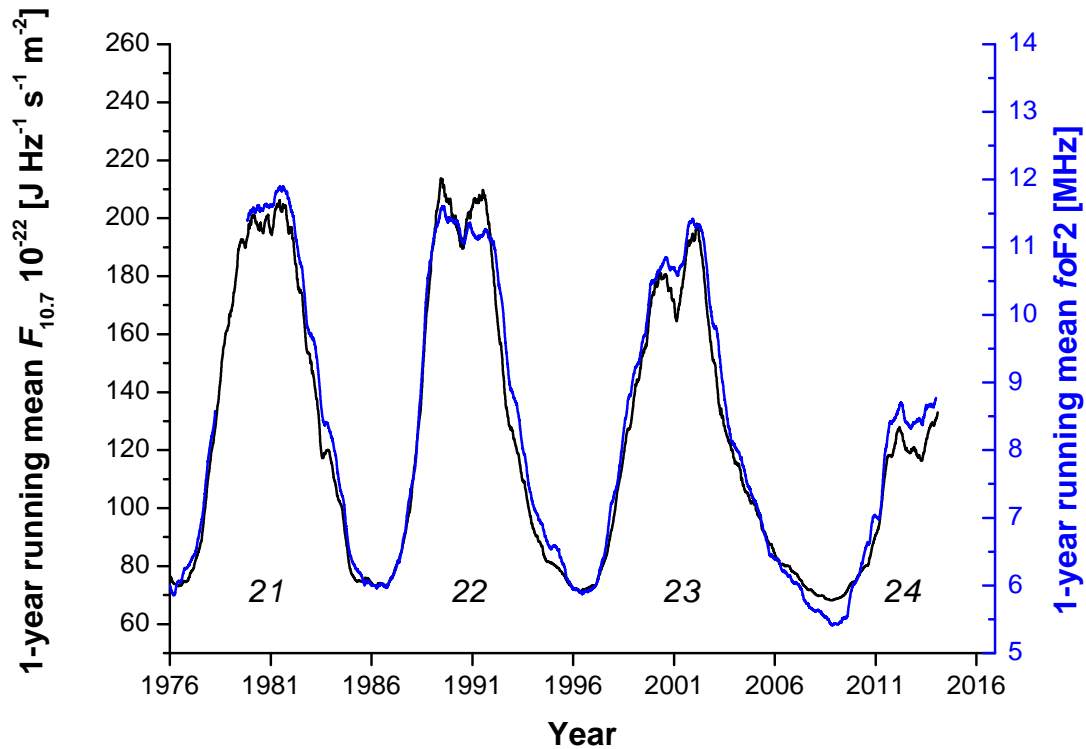
Figure 1.2: 1-year running mean of the solar index $F_{10.7}$ (black line) and foF2 (12 LT in Rome, blue line), from 1 January 1976 to 31 December 2013.

Ma et al., 2009), for which after a definite level of solar activity, the parameter foF2 does not increase anymore as the solar activity increases. This effect is particularly visible when using mean or median values for both the ionospheric parameter and the solar activity index, and shows a seasonal dependence, with a more pronounced saturation from April to September in the North hemisphere, at all the hours of the day.

Figure 1.3 shows the monthly median values of foF2 (at local noon in Rome) as a function of the 12-month running mean of the monthly mean sunspots number R_{12}, for May, from 1958 to 2007. The red dashed circle highlights the values affected by the saturation. For the trend foF2 vs R_{12}, the saturation is visible after a level of $\sim$150 for R_{12}.

The trends between foF2 and solar activity indices can be subjected to another important phenomenon, linked most probably to the geomagnetic activity level, the *hysteresis effect* (Kane, 1992; Mikhailov and Mikhailov, 1995; Liu et al., 2006; Rao and Rao, 1969; Triskova and Chum, 1996).

The hysteresis effect causes two different values of foF2 for the ascending and descending phase of the same solar cycle, in correspondence of the same level of solar activity. Mikhailov and Mikhailov (1995) postulated that the hysteresis is associated with differences in the geomagnetic activity during the ascending and descending phases of a solar cycle. Nevertheless, there is not yet an accepted explanation for the hysteresis effect (Liu et al., 2011b). In Figure 1.4 is shown the clear hysteresis effect observed in the trend foF2 (12 LT) vs Lym-α (see Section 3.1 for a detailed description of this solar index), for the solar cycle 23.

The vertical arrows stress the hysteresis for foF2. It is important to note that this effect is
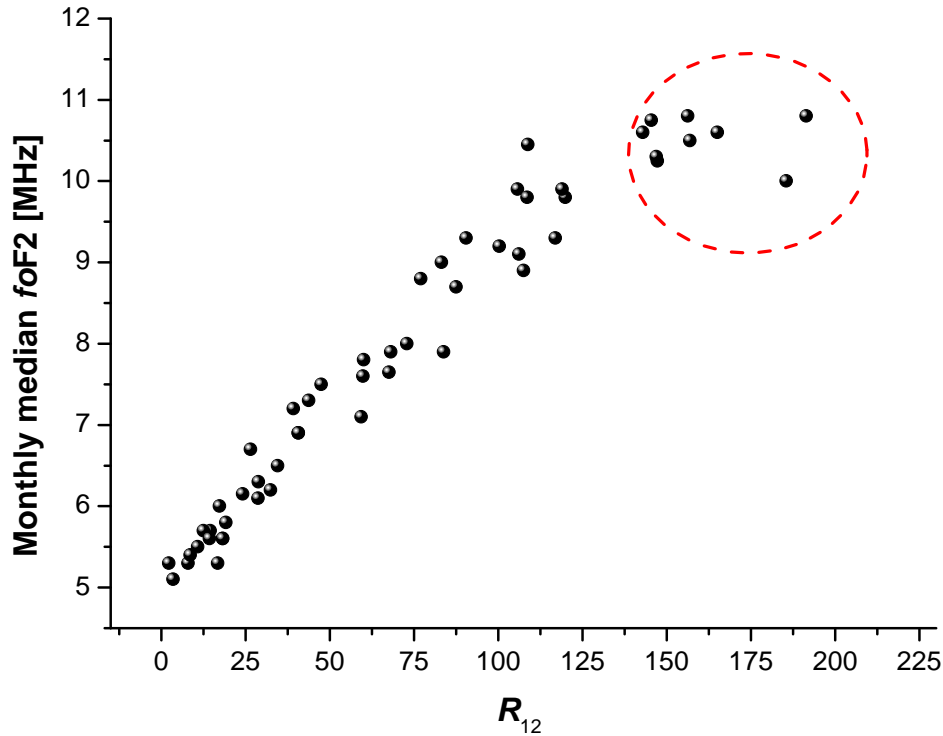
Figure 1.3: Monthly median values of *fo*F2 as recorded at Rome in May, at local noon, from 1958 to 2007 as a function of R_{12}. The red dashed circle highlights data affected by the saturation effect.

visible only for mid solar activity, and not for low and high solar activity.

Both the saturation and the hysteresis effect have a great influence on the relation between the ionospheric parameter *fo*F2 and the indices of solar activity. As it will be discussed in Chapter 3, the research of the best index to describe the variations of *fo*F2 has to take into account these two effects.

Very important is the seasonal ionospheric variation, linked to the Sun-Earth interaction. In particular, for this study, we will consider the *winter anomaly* and the *semiannual anomaly* (Ezquer et al., 2014; Dominici, 1971; Chen and Liu, 2010; Liu et al., 2012; Rishbeth and Setty, 1961; Rishbeth et al., 2000; Yu et al., 2004; Rishbeth and Garriot, 1969; Yonezawa and Arima, 1959; Yonezawa, 1967, 1971; Torr and Torr, 1973).

The winter anomaly consists in the observation of values of the electron density peak $NmF2$ (or analogously of the critical frequency *fo*F2) at local noon that are lower in summer than in winter.

It has been proposed that this anomaly is related to changes in the neutral composition of the atmosphere, generated by heating in the summer hemisphere and a subsequent convection of lighter neutral elements towards the winter sector, which causes changes in the ratio of [O]/[N2] in both hemispheres (Rishbeth and Setty, 1961; Johnson, 1964; Torr and Torr, 1973). In Figure 1.5 the effect is clearly visible, with values of $NmF2$ around the local noon that are significantly lower in June (in red) than in December (in blue). The latitude and the solar activity influence the winter anomaly, which is less visible at low latitude, in the South hemisphere and for low solar activity.

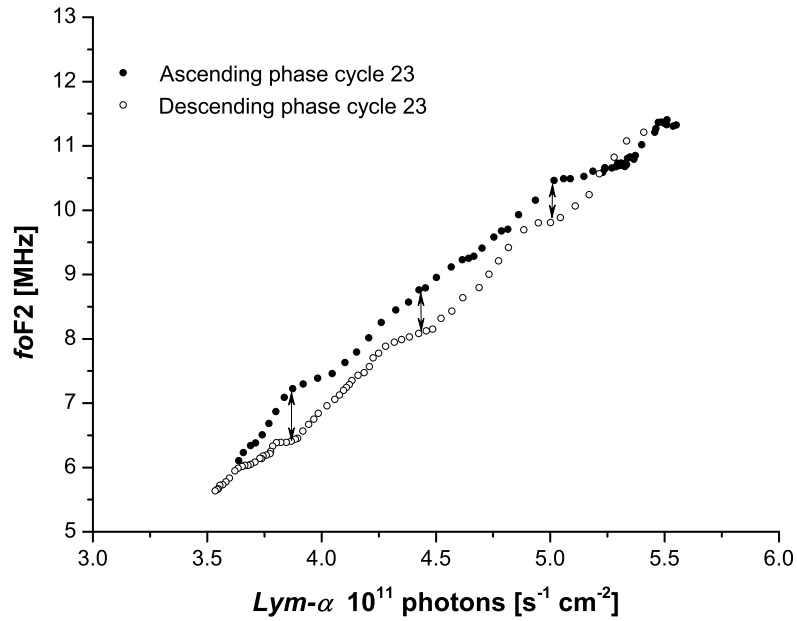**Figure 1.4:** *fo*F2 vs *Lym-α* for the ascending phase (full circles) and descending phase (empty circles) of the solar cycle 23. The vertical arrows highlight the hysteresis effect.
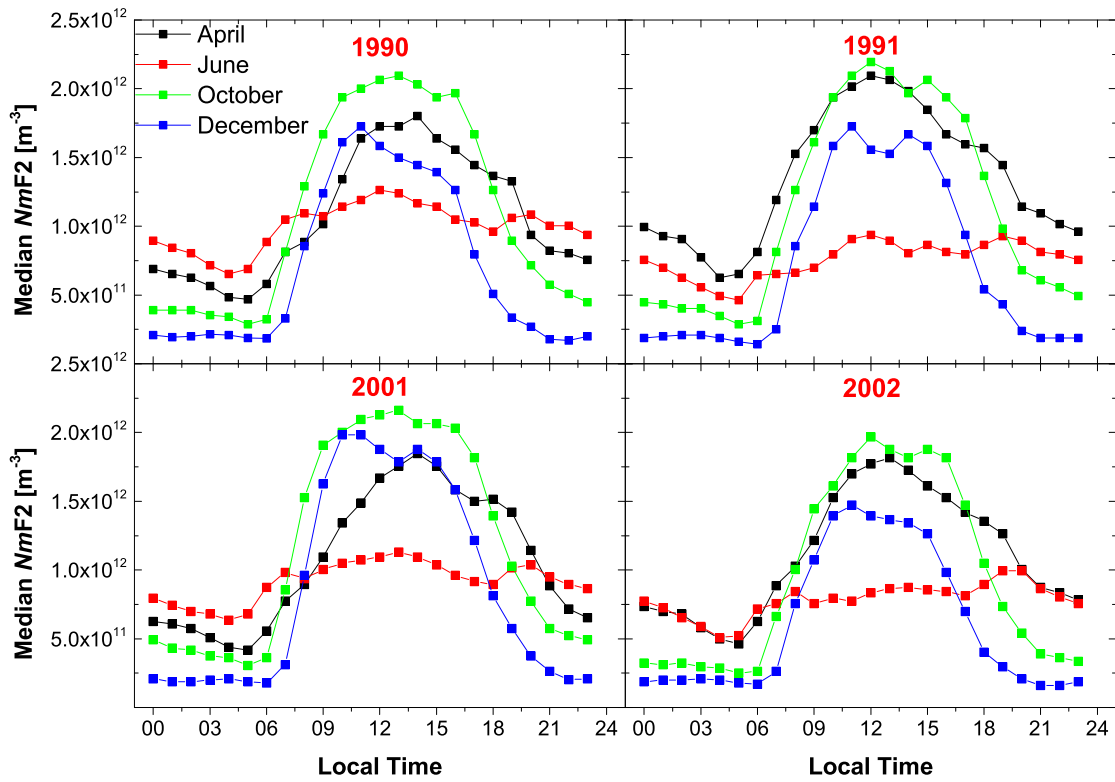

Figure 1.5: Monthly median values of *Nm*F2 as recorded at Rome in April, June, October and December for the years of maximum activity 1990-1991 (max of solar cycle 22) and 2001-2002 (max of solar cycle 23).

Another important feature visible in Figure 1.5 is the *semiannual anomaly* for which values of NmF2 are greater around equinoxes (April and October) than around solstices (June and December). Also this effect depends on the latitude, being more visible at low latitudes (Rishbeth and Garriot, 1969; Ezquer et al., 2014). Furthermore, the amplitude of the semiannual anomaly is larger in years of solar maximum than in years of solar minimum (Ma et al., 2003). Several mechanisms have been proposed to explain this anomaly. Yonezawa (1971) proposed that it is related with the variation of the upper atmosphere temperature. Torr and Torr (1973) suggested that it is caused by the semi-annual variation of neutral densities associated with the geomagnetic and aurora activity. Mayr and Mahajan (1971) showed that the anomaly requires significant variation in the neutral composition at lower height. Ma et al. (2003) suggested that the semi-annual variation of the diurnal tide in the lower thermosphere induces the semi-annual variation of the amplitude of the equatorial electrojet, thus causing the semi-annual anomaly at low latitude.

All the phenomena introduced in this section will be considered in the development of the work, and will be recalled in the next chapters. In particular, the saturation and hysteresis effects strongly affect the research of the best solar index to describe the variations of foF2. The winter and semiannual anomalies will be instead considered in the inter-minima comparison, owing to their dependence on solar activity level.

1.3   Ionospheric vertical sounding: a brief review

In order to determine the parameters characterizing the ionosphere, different typologies of ionospheric sounding can be used. The ionospheric soundings can be divided in three main branches: active, passive and perturbative. The active methodologies are the most widely used and are: the vertical and oblique sounding, the ground scatter radar and the incoherent scatter radar. Passive measures are those performed by riometers, and those exploiting the GPS constellation. Examples of measures performed with a perturbative methodology are the HF heating and the cross modulation. In this section we will treat the most used technique: the *vertical ionospheric sounding*. In Section 1.3.1 an introduction about the radar technique will be reported, while Section 1.3.2 will be devoted to the description of the main features of an ionogram.

1.3.1   Radar technique

The vertical sounding is based on the *Radar Theory* (*Radio Detection and Ranging*). Considering the ionosphere as an infinite and perfectly reflecting layer, it is possible to record the travel time of a radio wave (in the High Frequency (HF)[2] band) sent vertically and reflected by the ionosphere. Assuming the wave travelling at the speed of light c, measuring the travel time t it is possible to obtain the *virtual height of reflection h'*, that is $h' = ct/2$. As a consequence, the result of an ionospheric vertical sounding will be a plot of h' as a function of the frequency f. This plot is called *ionogram* and from it the most important ionospheric parameters can be inferred, as it will be described in the next section.

To understand the meaning of an ionogram, we need to obtain the *radar equation* and adapt it to the special case of the ionosphere.

---

[2]3 to 30 MHz.

In the simple case of a bi-static radar, with gain of the antennas G_T (transmitter TX) and G_R (receiver RX) at a distance r, from the TX antenna the target will receive a power flux

$$\phi_i = \frac{P_{rad}G_T}{4\pi r^2}, \tag{1.12}$$

where P_{rad} is the emitted power.

Owing to the power diffusion of the target $\sigma\phi_i$, being σ the *radar cross section*, the flux turning back to the radar is:

$$\frac{\sigma\phi_i}{4\pi r^2} = \frac{P_{rad}G_T\sigma}{(4\pi r^2)^2}. \tag{1.13}$$

If A_{eff} is the effective surface of the receiver RX, the corresponding captured power can be expressed as:

$$P_r = \frac{P_{rad}G_T\sigma A_{eff}}{(4\pi r^2)^2}. \tag{1.14}$$

Using the relation $A_{eff} = (\lambda G_R)/(4\pi)$, the relation (1.14) becomes:

$$P_r = \frac{\lambda^2 G_T G_R \sigma P_{rad}}{(4\pi)^3 r^4}, \tag{1.15}$$

that represents the explicit form of the radar equation.

The vertical ionospheric sounding can be understood considering a particular case of the equation (1.15), which for the ionosphere can be expressed as:

$$P_r = \frac{(\lambda G)^2 P_{rad}}{(4\pi r)^2 L}, \tag{1.16}$$

with L attenuation of the signal, and considering the ionosphere as an infinite reflecting layer, which means $G = G_T = G_R$.

The sounding depends on the variations of the electron density N with the height. By neglecting both the magnetic field and collisions, the reflection occurs at heights where the emitted frequency f equalizes the plasma frequency f_N. The plasma frequency depends on N and consequently on the real height h and according to (1.4) is expressed as:

$$f_N(h) = \sqrt{\frac{N(h)e^2}{4\pi^2 m\epsilon_0}}. \tag{1.17}$$

By virtue of the equation (1.17), different frequencies will be reflected at different heights and so will turn back to the Earth with different delay times. From the delay time (or travel time) measured it is possible to obtain h' and then the ionogram trace that, as mentioned, is a plot of h' as a function of the emitted frequency.

For a vertical sounding, usually the frequency range is between 1 and 20 MHz, depending on the latitude of the ionospheric station, with a frequency step of 25, 50 or 100 kHz. The height resolution is less than 5 km, with minimum and maximum heights of about 90 and 600 km respectively, covering all the ionospheric regions of interest.
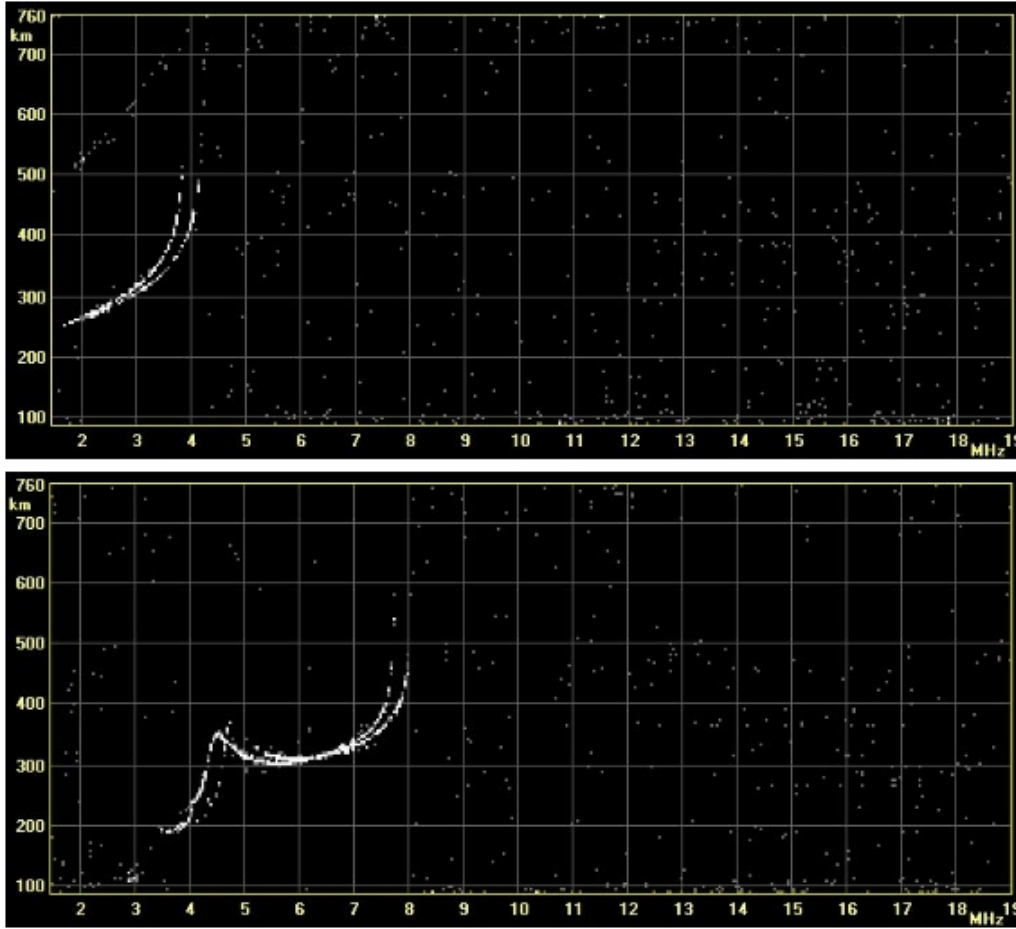
Figure 1.6: Example of ionograms recorded at Tucumán, Argentina, (top) on 9 August 2010 at 22:05 LT, and (bottom) on 9 September 2010 at 10:25 LT.

1.3.2   Main ionogram features

As previously said, an ionogram is the output of a vertical ionospheric sounding.

Figure 1.6 shows two typical ionogram traces for nighttime and daytime hours. The ionograms have been recorded at the ionospheric station of Tucumán (Argentina) on 9 August 2010 at 22:05 LT and on 9 September 2010 at 10:25 LT, respectively, and give us the possibility to make a comparison between the daytime and nighttime ionosphere. In the top ionogram, it is possible to distinguish only one cusp that individuates the nighttime F region. Instead, in the bottom ionogram are visible three cusps that individuate, as the frequency increases, the E, F_1 and F_2 layers.

At every cusp corresponds a critical frequency of an ionospheric layer. In fact, for a vertical travelling wave at constant velocity c, the equivalent height of reflection h' can be expressed as:

$$h' = \frac{cT}{2} \int_0^T \frac{c}{2} \mathrm{d}t, \tag{1.18}$$

where T is the delay time of the measured eco. The group velocity of the travelling wave is

$v_{\text{gr}} = c/n_{\text{gr}}$ where n_{gr} is the *refraction group index*, and if we introduce it in equation (1.18) we obtain:

$$h' = \int_0^T \frac{n_{\text{gr}} \cdot v_{\text{g}}}{2} \mathrm{d}t. \qquad (1.19)$$

If $\mathrm{d}h$ is the infinitesimal height variation, considering $v_{\text{gr}} = 2\mathrm{d}h/\mathrm{d}t$, the equation (1.19) becomes:

$$h' = \int_0^{h_{\text{r}}} n_{\text{gr}} \mathrm{d}h, \qquad (1.20)$$

where h_{r} is the real reflection height. By taking a unitary refraction index under a height of h_0, considered as the lower limit of the ionosphere, equation (1.20) can be rewritten as:

$$h' = h_0 + \int_{h_0}^{h_{\text{r}}} n_{\text{gr}} \mathrm{d}h, \qquad (1.21)$$

In the simplest case of no collisions and no magnetic field, the *phase refraction index* n can be written as:

$$n^2 = 1 - X = 1 - \frac{f_N^2}{f^2}, \qquad (1.22)$$

and the relationship $n_{\text{gr}} \cdot n = 1$ is valid (for more details see Ratcliffe (1959)). So, equation (1.21) can be also written as:

$$h' = h_0 + \int_{h_0}^{h_{\text{r}}} n_{\text{gr}} \mathrm{d}h = h_0 + \int_{f_N=0}^{f_N=f} n_{\text{gr}}(f_N) \left(\frac{\mathrm{d}h}{\mathrm{d}f_N} \right) \mathrm{d}f_N. \qquad (1.23)$$

The equation (1.23) shows that for h' there will be an infinite value when the ratio $\mathrm{d}f_N/\mathrm{d}h$ goes to zero. This situation is verified only when a relative maximum of the electron density N occurs, and this explains why a cusp is observed in the ionogram in correspondence of a relative maximum of the electron density in the vertical profile, that is in correspondence of a critical frequency.

It is quite simple now to understand how the critical frequencies of the different ionospheric layers can be easily obtained from an ionogram.

With reference to Figure 1.7, it is possible to see how at every cusp corresponds the critical frequency of an ionospheric layer; in fact, the vertical asymptotes occur exactly in correspondence of critical frequencies. At the same time, the horizontal asymptotes individuate the virtual heights of reflection of the base of the different ionospheric layers.

So, it is clear now how the main ionospheric parameters can be validated from an ionogram, in particular the critical frequency of the F2 layer, foF2. As it was already said, foF2 is related to the maximum electron density of the vertical profile, NmF2.

An important parameter that cannot be directly calculated from an ionogram is the height of the maximum electron density, hmF2. To obtain this ionospheric parameter it is necessary to perform an inversion of the ionogram, passing from the ionogram trace $h'(f)$ to the vertical electron density profile $N(h)$. This passage is also called *reduction to the real heights*. Usually, to invert ionograms methodologies based on *Target functions* or *polynomial inversion* are used.

A Target Function is defined as follow:

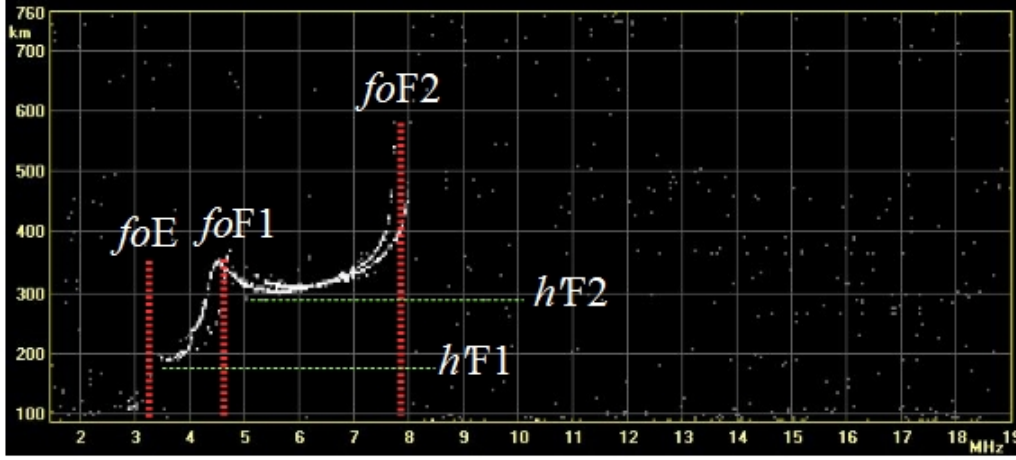$$\Gamma = \int (h'(f) - h'_{\text{a}}(f))^2 \mathrm{d}f, \qquad (1.24)$$

Figure 1.7: Critical frequencies and virtual reflection heights of the base of different ionospheric layers as obtained from an ionogram. The vertical asymptotes (in red) individuate the critical frequencies, while the horizontal asymptotes (in green) individuate the equivalent reflection heights of the base of layers. The ionogram was recorded in Gibilmanna on 19 May 2011 at 15:30 LT.

with $h'_a(f)$ representing a synthetic ionogram constructed "ad hoc", starting from a specific vertical electron density profile $N(h)$. $h'_a(f)$ can be expressed as:

$$h'_a(f) - h_0 = \int_{h_0}^{h_r} n_{gr} dh = \int_{h_0}^{h_r} \frac{dh}{n} = \int_{h_0}^{h_r} \frac{dh}{\sqrt{1 - \frac{e^2 N(h)}{4\pi^2 \epsilon_0 m f^2}}}. \tag{1.25}$$

Varying $N(h)$, it is possible to minimize the value of the target function given by the equation (1.24). The synthetic profile for which the function is minimum will be the electron density profile associated to the ionogram.

Concerning the polynomial inversion, the most widely used program is *POLAN*, developed by John Titheridge. Detailed information about this program can be found in Titheridge (1985). Nevertheless, the use of POLAN requires an accurate ionogram validation, fixing various points on the trace that will be used for the inversion. It is clear that for long ionogram time series this methodology requires a long validation procedure and "clean" ionograms that are not always available.

However, in the years, analytical formulations to obtain an approximate value for hmF2 have been developed (see Ulich (2000) for a very good summary of them). Among them, in this work, we are mostly interested in the *Shimazaki formula* (Shimazaki, 1955) and the *Dudeney formula D55* (Dudeney, 1974).

The Shimazaki formula is expressed by the following equation,

$$hm\text{F2[km]} = \frac{1490 \cdot fo\text{F2[MHz]}}{MUF(3000)\text{F2}} - 176. \tag{1.26}$$

The formula (1.26) is very simple and is calculable for every given time of the day, because only the ionospheric parameters foF2 and MUF are required.

The $D55$ formula is expressed by the following system of equations,

$$
\begin{cases}
hm\text{F2} = \dfrac{1490}{M + \Delta M} - 176, \\[2ex]
\Delta M = \dfrac{0.280 \pm 0.009}{\frac{fo\text{F2}}{fo\text{E}} - 1.200} - (0.028 \pm 0.010).
\end{cases}
\tag{1.27}
$$

The D55 formula requires to know foF2 and foE, so its use is limited to daytime hours when foE is available.

In our study, before obtaining hmF2 for very long time periods by using (1.26) and (1.27), a preliminary phase to test their reliability was performed by comparing the corresponding values with those calculated by inversion methodologies of automatic scaling programs. As will be reported in Chapter 5, we found a good reliability of the Shimazaki formula for nighttime hours and for all the months, meanwhile the D55 formula is reliable during daytime hours, in particular for winter/autumn months, with bigger uncertainties for summer months.

Chapter 2

The particular minimum of the solar cycle 23/24

Introduction

This work is focused on the last solar minimum, the minimum between the solar cycle 23 and the solar cycle 24 (minimum 23/24).

The great interest in the last minimum is due to the fact that the solar activity has been unusually low for a very long period including the years 2008-2009, that represent the years with the lowest solar activity, and partially the years 2007 and 2010.

Using as a solar activity indicator the observed number of sunspot, 527 days without sunspots have been observed for the period 2008-2009, while a mean of ∼300 days without sunspots characterized the last 10 solar minima. Furthermore, the solar cycle 23 lasted 12 years and 6 months, against a mean solar cycle duration of ∼11 years. Therefore, we are talking about a minimum that has come later than we expected and characterized by a very low and prolonged solar activity.

In the study of the ionosphere there is always an increasing interest in the analyses of the ionospheric plasma response for extreme conditions of solar activity (very high or very low). The last solar minimum gives us a natural unique window to study the ionosphere under conditions of extreme low solar activity. It is also particularly interesting to evaluate the response of the most widely used ionospheric models in such extreme conditions.

In this short chapter we will report the most relevant and interesting characteristics observed for the last solar minimum, highlighting at the same time why it is so interesting for ionospheric studies.

2.1   Main observed features of the minimum 23/24

The last minimum of solar activity, the minimum 23/24, was characterized by a very low and prolonged solar activity. This situation is very uncommon and offers us a unique natural window to study the ionospheric plasma response in such very particular conditions.

The Figure 2.1 shows the 1-year running mean for the sunspots number R. The complete solar cycles 21, 22 and 23 are shown until December 2014, covering partially the solar cycle 24. The plot shows interesting characteristics that are useful to understand the particularity

of the last solar minimum. Focusing the attention on the sunspots number[1], 176 days without sunspots were observed for the years 1986-1987 that characterize the minimum of the solar cycle 21/22, with a duration of 10 years and 7 months for the cycle 21. For the years 1996-1997, which are the years of solar activity minimum of the cycle 22/23, 226 days without sunspots were observed, with a duration of 9 years and 8 months for the cycle 22. For the solar cycle 23, characterized by a duration of 12 years and 6 months, 527 days without sunspots were observed, only limiting the duration of the minimum to the years 2008-2009. Therefore, we are talking about a minimum that has come later than we expected and characterized by an extreme low and prolonged solar activity. As mentioned, it is important to note that the low solar activity can be considered particularly prolonged, because the period of uncommon low solar activity also interests partially the 2007 and the 2010. Nevertheless, the years 2008-2009 represent the deepest part of the minimum.

With reference to Chapter 1 and to the strong influence that the solar activity has on the ionospheric plasma, interesting and important responses are expected in the study of the main ionospheric parameters. In particular, it is very important to assess whether and how the relationships between the main ionospheric parameters and the most used solar indices are changed, being these relations essential to develop ionospheric models.
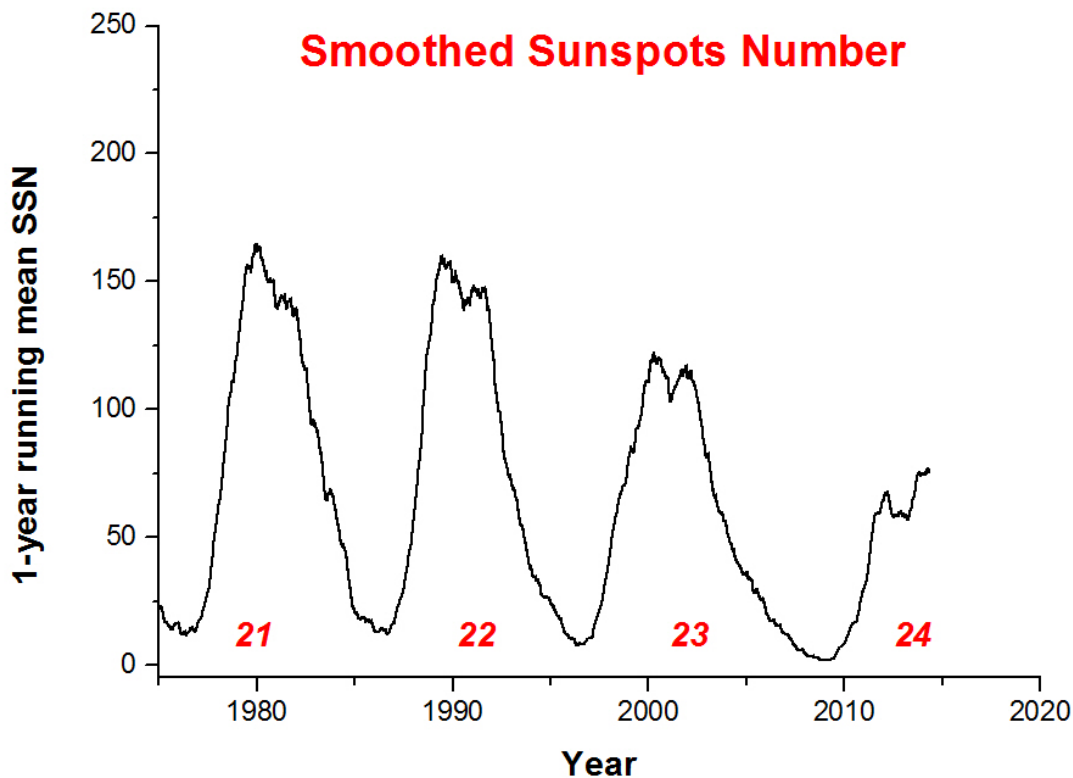

Figure 2.1: 1-year running mean of the sunspots number R for the last complete three solar cycles 21, 22 and 23. The solar cycle 24 is partially covered until December 2014.
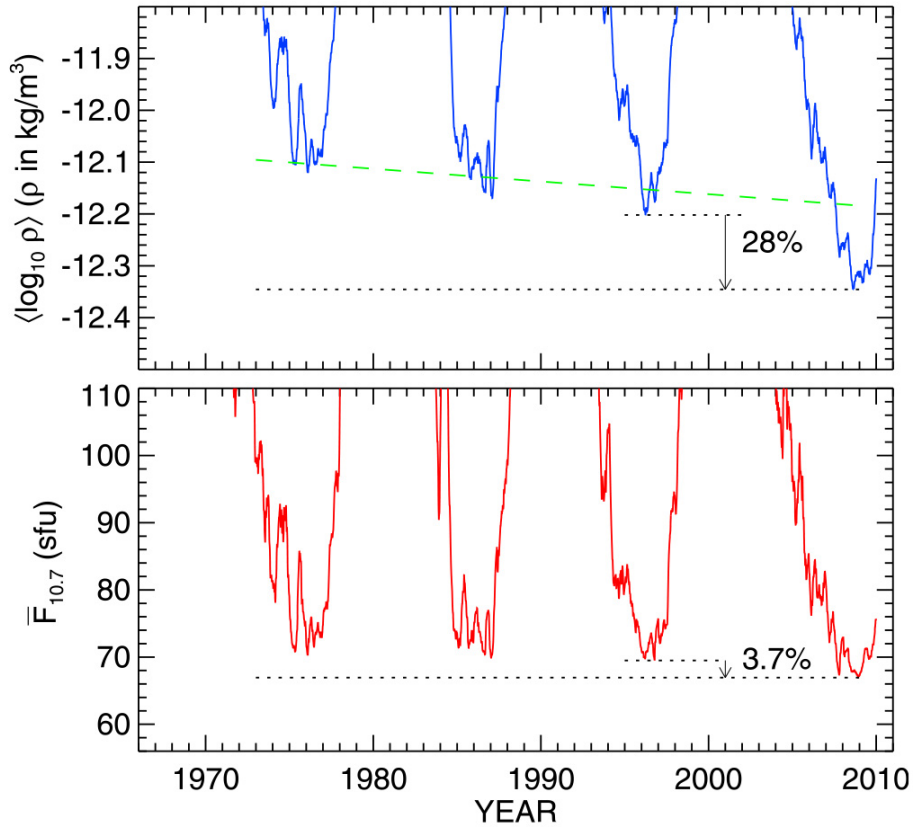

Figure 2.2: (top) 81-day average log-density at a fiducial altitude of 400 km, after removing seasonal and geomagnetic activity effects; (bottom) 81-day average for the solar index $F_{10.7}$. The horizontal black lines illustrate the differences between the cycle 23/24 and 22/23 minima (modified from Emmert et al. (2010)).

Emmert et al. (2010) used global-average thermospheric total mass density, derived from the drag effect on the orbits of many space objects, to study the behaviors of the thermosphere during the last solar minimum. They found that during the period 2007-2009 the thermospheric densities at an altitude of 400 km were the lowest observed in the 43-year (1967-2010) database, and were anomalously low, by 10-30%, compared with climatologically expected levels. They also found that the density anomalies appeared well before during the cycle 23/24 minimum, and are larger than what expected correspondingly to an enhanced thermospheric cooling caused by increasing concentrations of CO_2.

Figure 2.2 shows the 81-day averages for the log-density at 400 km and for the solar index $F_{10.7}$, for the last four solar cycles; a comparison for the last two solar minima shows a decrease of 28% in the log-density and of 3.7% in $F_{10.7}$. The green dashed line individuates the trend expected considering the previous solar minima, which can explains a decrease of 6% between the last two solar minima; so the observed decrease is much bigger than that expected, proofing the particularity of the last solar minimum.

Heelis et al. (2009) report results about the transition height O^+/H^+ for the year of minimum 2008 measured by the satellite *C/NOFS* (*Communications/Navigation Outage Forecasting System*) launched in April 2008. The O^+/H^+ transition height is a sensitive indicator of solar extreme ultra violet ionizing flux and the dynamics of the topside ionosphere (MacPherson et al., 1998). Usually, the transition height resides near 450 km at night and rises to 850 km during daytime. The results show that for the latter half of 2008 this surface is much closer

to the planet than expected, it is much cooler than expected and the ion concentration at the surface is lower than expected. All these parameters indicate that both the photoionization and extreme ultra violet heating rates are much lower than that it is indicated by the 10.7 cm radio flux (index $F_{10.7}$), usually used as a proxy for these rates. In addition, the distribution of ionization in latitude and local time suggests that the ionospheric dynamics might also have been significantly modified during this period (Heelis et al., 2009).

Figure 2.3 shows the transition height surface around the magnetic equator. The ion temperature (O^+) is illustrated on the top, while on the bottom the log-ion concentration is plotted. It is worth noting that in particular after sunset the transition height falls throughout the night, under the expected level of 450 km. Furthermore, at night the ion temperature falls to unprecedented low levels reaching values around 600 K by local midnight.
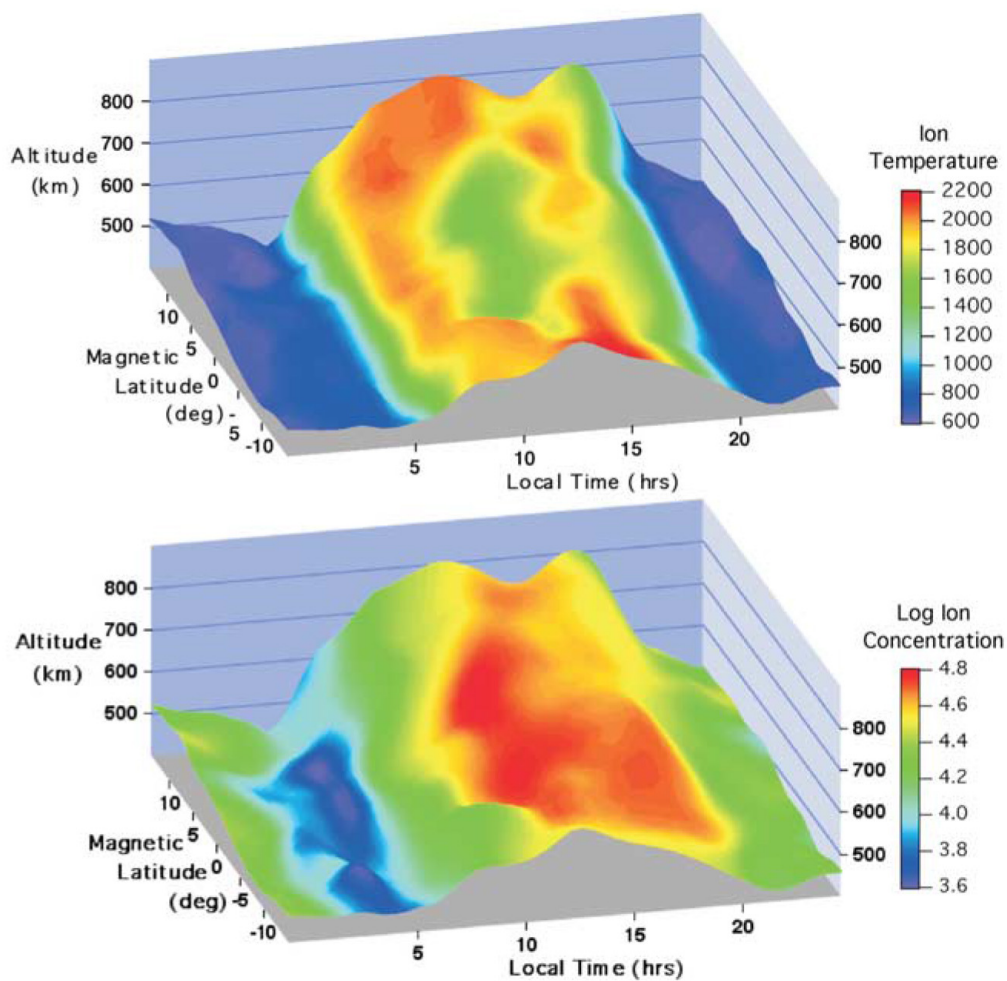
Figure 2.3: Altitude of the O^+/H^+ transition surface described by averaging the *CINDI* (*Coupled Ion Neutral Dynamics Investigation* mission) measurements over the period June-August 2008. Both (top) the temperature and (bottom) the log of the total ion concentration are described by the color shading of the surface (from Heelis et al. (2009)).

The extended solar minimum has already produced unprecedented conditions in the solar wind and in the Earth's magnetosphere, when compared against the records obtained since the beginning of the space age (Russell et al., 2010). The study of Russell et al. (2010) reports evidences for this in the solar wind velocity record and in the radiation belts monitored by the

Figure 2.4: (Top) Solar wind speed since 2007 and (bottom) the SAMPEX energetic electron count rate in the L value range of 1-7; SAMPEX is in a low altitude polar orbit. When the stream structure, as defined by the periodic oscillations of the solar wind speed, disappeared at the end of 2008, the radiation belts weakened considerably. The dashed line at 500 km/s shows the level at which in the past a fast solar wind stream was defined (from Russell et al. (2010)).

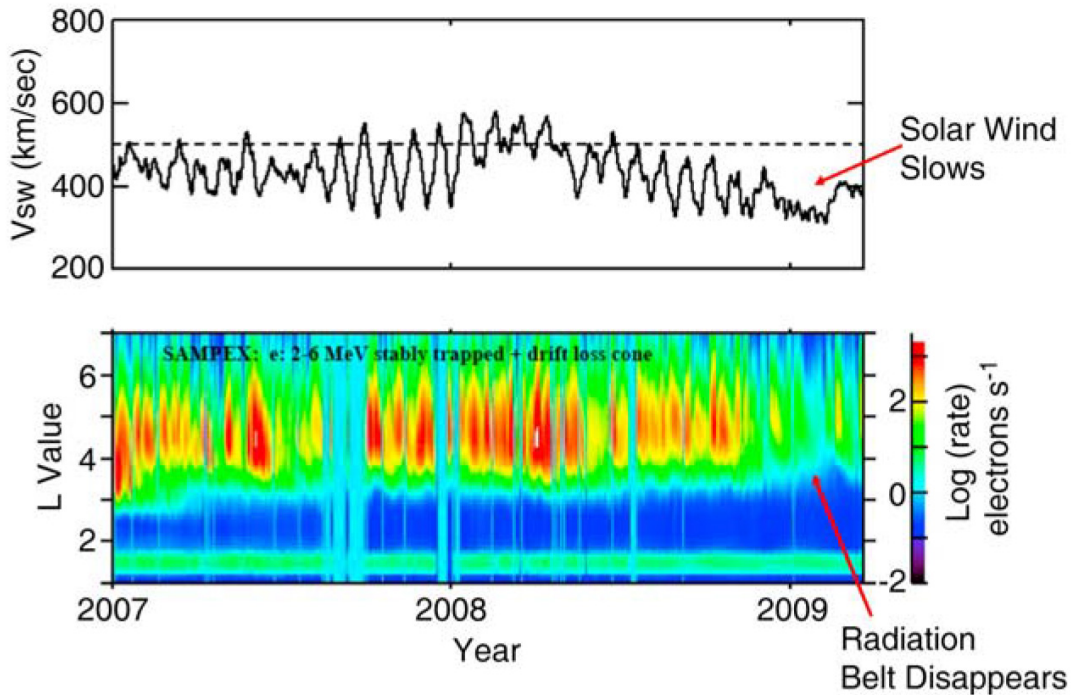*SAMPEX* satellite (*Solar Anomalous and Magnetospheric Particle Explorer*).

Figure 2.4 shows the variation of the solar wind velocity over a 2-year period during the minimum 23/24 and the corresponding radiation belt fluxes in the inner magnetosphere that are thought to be controlled by the solar wind speed. The L value measures the distance at which these particles traverse the equator. The deep blue region is the usual energetic particle void called "the slot". Typically, the median speed of the solar wind is 450 km/s and consists of fast streams which rise from about 350 km/s to about 600 km/s, and when these fast streams disappeared, the radiation belts measured by SAMPEX rapidly decreased in flux because the radiation belts depend on these high speed streams for their energization (Russell et al., 2010).

Another central discussion regarding the last solar minimum is the relationship between the parameters describing the ionosphere and the indices used to identify the level of solar activity (see Section 3.1 for a detailed description of the most widely used indices). In particular, it is very important to analyze if there have been changes in these relationships caused by the particular conditions characterizing the last solar minimum.

Chen et al. (2011a) found a consistent variation in the relation between the solar index $F_{10.7}$ and the solar radiation in the extreme ultra violet wavelengths (0.1-50 nm and 26-34 nm ranges) between the last two solar minima. This result is extremely important because some solar EUV irradiance models were constructed on the basis of the postulation that the relationship between the solar EUV radiation and $F_{10.7}$ is invariant over different solar cycles. Furthermore, $F_{10.7}$ is also usually used as the solar activity proxy to develop ionospheric and thermospheric models, such as the *IRI* (*International Reference Ionosphere*) model (Bilitza et al., 2014) and the *NRLMSISE-00* model (Picone et al., 2002).
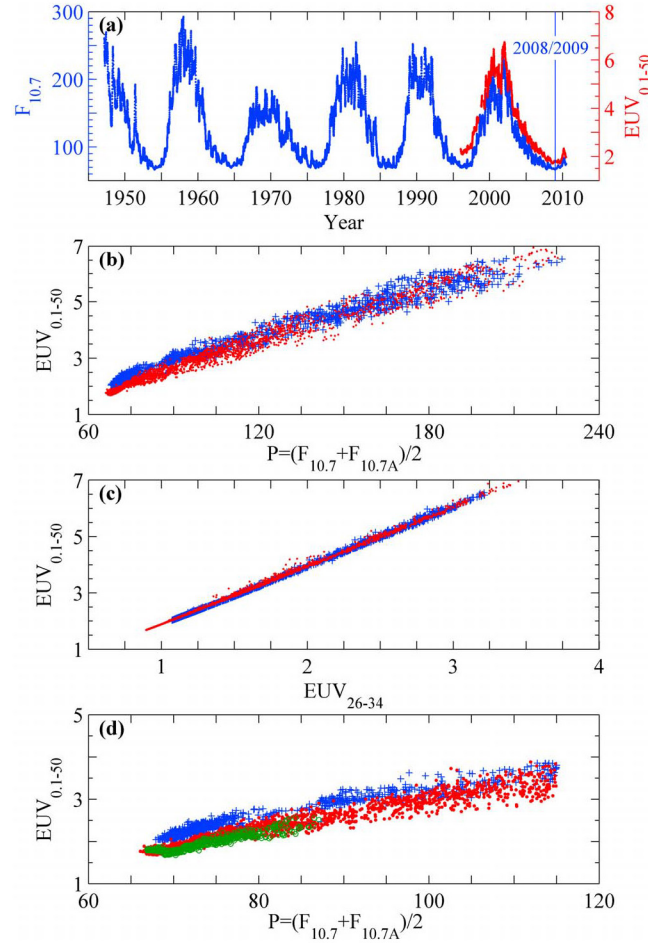
Figure 2.5: (a) The 27 day averages of daily $F_{10.7}$ values (in units of 10^{-22} [J s^{-1} m^{-2} Hz^{-1}]) and *SOHO/SEM* (*Solar and Heliospheric Observatory/Solar EUV Monitor*) 0.1-50 nm EUV flux (in units of 10^{14} photons [m^{-2} s^{-1}]). (b) SOHO/SEM 0.1-50 nm flux versus $P = (F_{10.7} + F_{10.7A})/2$ in SC 23; blue crosses show the ascending cycle, and red dots show the descending cycle till December 2008. (c) Same as (b) but for SOHO/SEM 0.1-50 nm flux versus 26-34 nm flux with red line representing the linear fit. (d) Same as (b) but with green dots showing the observations since 2009 (from Chen and Liu, 2010).

Figure 2.5 shows that $F_{10.7}$ and the solar EUV flux decrease from the minimum 22/23 to the recent one with different amplitudes. The decreases are $\sim 5\%$ in $F_{10.7}$ and $\sim 15\%$ in EUV flux. As a result, EUV flux is significantly lower in the recent minimum than in the previous one for the same level of $F_{10.7}$, while fluxes in the two wave EUV bands (0.1-50 nm and 26-34 nm) are still linearly correlated during the recent minimum, as it was during the previous one. Therefore, $F_{10.7}$ does not describe the EUV flux in the recent minimum as it did in the previous one (Chen et al., 2011a).

2.2 Interest in studying the ionosphere for the last solar minimum

In the previous section has been shown that the minimum 23/24 was characterized by very particular conditions in the near-Earth/Earth environment. However, why there is a so strong

interest in studying the last solar minimum and in particular the ionospheric plasma features and responses corresponding to these extreme conditions? Russell et al. (2010) reports a quite exhaustive explanation for which the minimum 23/24 can provide new key information about the entire near-Earth/Earth environment. Here is reported a brief extract from Russell et al. (2010) that starts from a discussion about the meaning of "*unprecedented minimum*" for the minimum 23/24:

> "*However, is it unprecedented over the period for which we have geomagnetic records, over the longer period for which we have sunspot records, or over the longer period for which we have proxy measurements of solar activity? Understanding how unprecedented is the solar minimum is not just an academic exercise. Deep solar minima have also been associated with atmospheric cooling. In particular, the Dalton minimum (1795-1830), the Maunder minimum (circa 1635-1705), and the Spörer minimum (circa 1450-1550) have been associated with significantly cooler climates (e.g., Eddy, 1981). These associations could be coincidental. For example, volcanic activity could lead to an increase in the Earth's albedo and a decrease in the heat received from the Sun. We now monitor volcanic activity closely and can calculate the effects of any dust and aerosols injected into the upper atmosphere. Moreover, the relative impact of anthropogenic sources of global warming, such as the increasing atmospheric content of carbon dioxide versus natural sources such as volcanic dust and solar variations, is under debate. A period in which solar activity decreased would be helpful in sorting out the sensitivity of Earth's climate to various forcing functions. A very long and deep solar minimum would be quite welcome in this regard. The historical record may be an aid in judging what to expect in the ensuing years. In the absence of guidance from history, a priori there are several equally possible outcomes. Nothing much might follow. Deep solar minima occur randomly and the Sun recovers quickly. Alternatively, the deep solar minimum could be a warning, like the sea level drop before a tsunami; all solar hell may be going to break loose momentarily. Or possibly, a Maunder minimum is on the way, accompanied perhaps by very cold winters. Finally, this could be one of the very deep solar minima that occur every century or so that are followed by one or more weak solar maxima. Until the Sun recovers from these weak maxima, space weather will become more benign, resulting in less risk to our power and information transmission systems and to our assets in space. This latter scenario could result in a significant change in direction for magnetospheric and heliospheric research and lead to a reduction in space weather preparedness in the space-based communication and monitoring sectors, as well as in power transmission companies. Finally, and possibly most importantly, the present solar minimum is making us question our basic understanding of the solar dynamo and its effects on the photosphere and the corona. We depend on sunspots and flares to define the solar cycle, but what really is a solar minimum or a solar maximum? What is the root cause deep below the photosphere? Could the dynamo process be continuing on its schedule but becoming weakly coupled to the photosphere? Is the dynamo currently reaching the phase that usually produces a solar maximum but not producing a strong enough magnetic field to energize active regions? If so, these are certainly interesting times for solar physicists!*"

Figure 2.6 shows the reconstructed time series of the annual mean sunspots number for

the period 1600-2007, where the historically prominent *Maunder minimum* (1645-1715) and *Dalton minimum* (1785-1825) are highlighted. It is worth noting that both minima were linked to particular conditions characterizing the Earth's environment, in particular a significant cooler climate. Unfortunately, the Maunder minimum occurred when there were few sunspot observers (Eddy, 1976). Thus, its beginning ($\sim$1645) and its end ($\sim$1715) result poorly defined. The more recent Dalton minimum is better defined and was characterized by very interesting features that can be found again in the minimum 23/24:

- The opening cycle of the Dalton minimum was long, lasting $\sim$15 years from about 1785 to 1800, similarly to the solar cycle 23;

- It was followed by two quite weak sunspot cycles with maxima near 50 and 40 sunspots numbers, similarly to the "gentle" current maximum of the cycle 24, if compared to the recent ones (see Figure 1.2 and Figure 2.1).

The similarities found between the onset of the Dalton minimum and the solar activity features observed during the last decades, justify the increasing interest in studying the near-Earth and Earth environments under extreme solar activity conditions. In particular, differently from the Maunder and Dalton minima, we now manage all the necessary technologies to provide a clear picture of the phenomenon. This is in fact the first time in the space age that similar extremely low and prolonged solar activity conditions are observed. Thanks to the development of new technologies and to the availability of satellite data, for both solar fluxes and atmospheric data, it is possible to determine the cause of extended solar minima analyzing the present solar irradiance measurements and, more important, it is possible to study carefully the resulting terrestrial response.

Another crucial point of interest in studying the ionospheric plasma under extreme and prolonged low solar activity is to test the output of the main ionospheric models in such particular conditions, in order to improve their reliability for the future. Therefore, it is very interesting to make a comparison between real data and results of models by considering the last solar minimum and the previous ones, using stations all around the world, in order to appreciate possible differences dependent on the geographic position. This kind of study can represent a key point to improve the ionospheric forecast models and let them to be updated for possible next very low solar activity periods.

In the last years the interest in this last solar minimum increased due to the preliminary discouraging results of models in predicting the observed values for the main ionospheric parameters such as foF2 or NmF2.

Among a great number of ionospheric models, the *International Reference Ionosphere* (*IRI*) represents the most widely used and a reference point in the ionospheric studies. IRI is an empirical standard for the representation of ionospheric densities and temperatures that was initiated in the late sixties by the Committee on Space Research (COSPAR) and the International Union of Radio Science (URSI)[2] (e.g. Bilitza et al., 1990; Bilitza, 2001; Bilitza and Reinisch, 2008; Bilitza et al., 2014).

Figure 2.7 and Figure 2.8 can help us to understand the problems affecting the ionospheric models for the last solar minimum.

Figure 2.7 shows the plot of three different updates of the ionospheric index *IG12*, that is an input parameter for the IRI-2012 model. For every curve, we plot observed values until the data of the update, which means that after the update dates the plotted values are forecasted values.

---

[2]See Section 5.3.1 for further details about the IRI model.
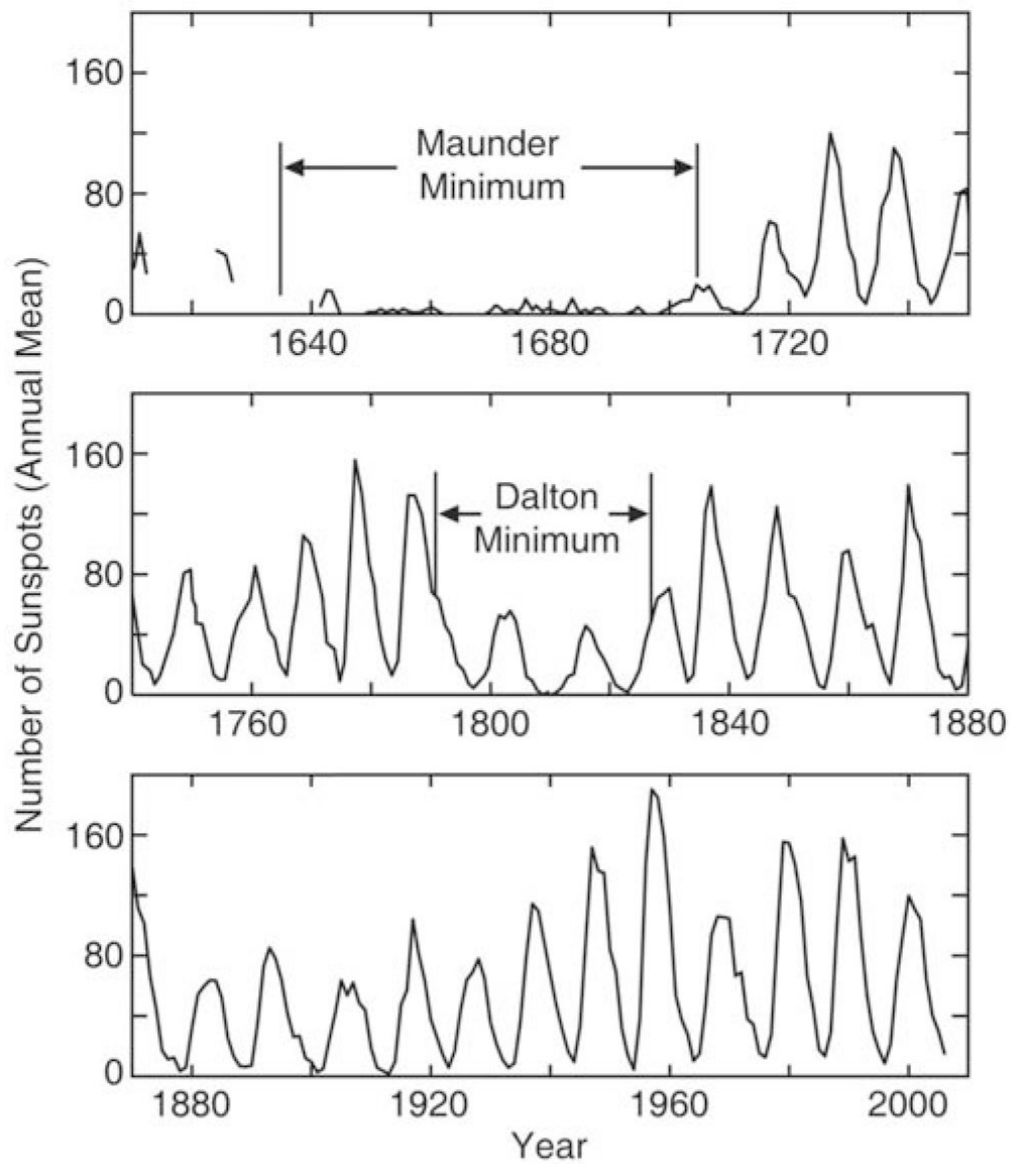
Figure 2.6: Reconstructed time series of annual mean sunspots number from 1600 to 2007. The Maunder minimum and Dalton minimum are emphasized (modified from Russell et al. (2010)).
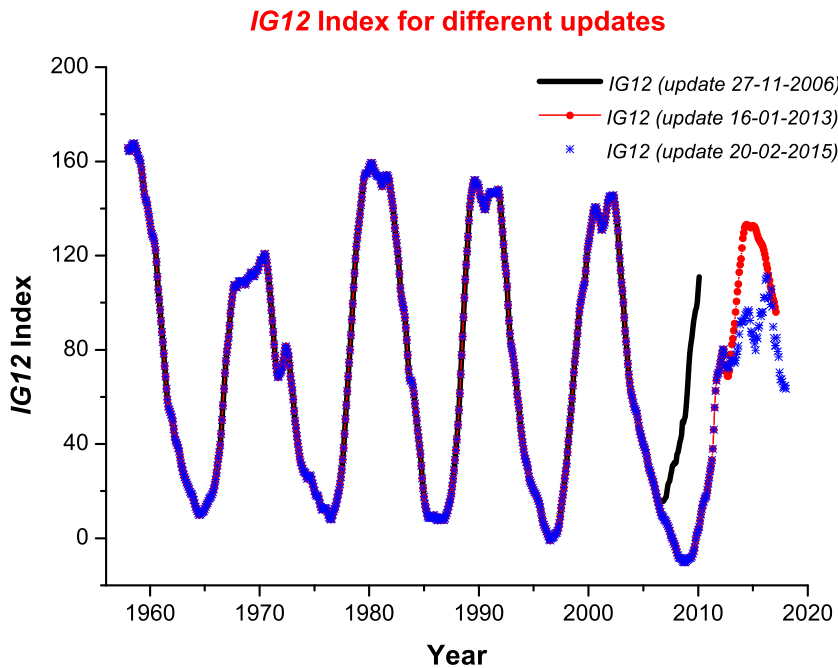
Figure 2.7: Three different updates for the ionospheric index *IG12*. The black line represents the update at 27/11/2006, the red line the update at 16/01/2013, the blue line the update at 20/02/2015.
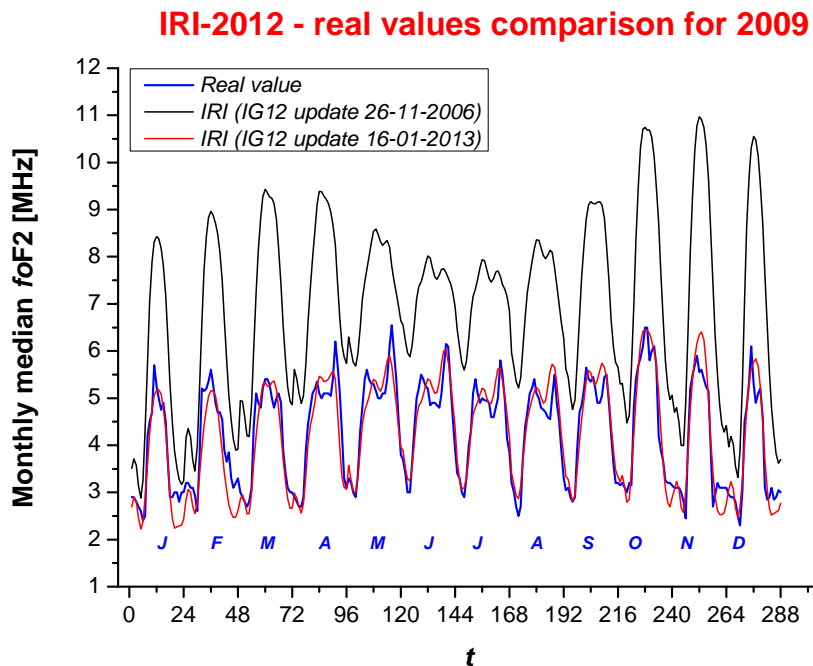
Figure 2.8: Comparison between IRI-2012 outputs and observed hourly monthly median values for Rome station for the year 2009. The blue line represents the observed values. The black line represents the IRI outputs using as input the update at 26/11/2006 for the index *IG12*; the red line represents the IRI outputs using as input the update at 16/01/2013 for the index *IG12*. The x scale spans from $t = 0$ (00:00 UT of January 2009) to $t = 288$ (23:00 UT of December 2009). The capital letters in blue identify the months from January (J) to December (D).
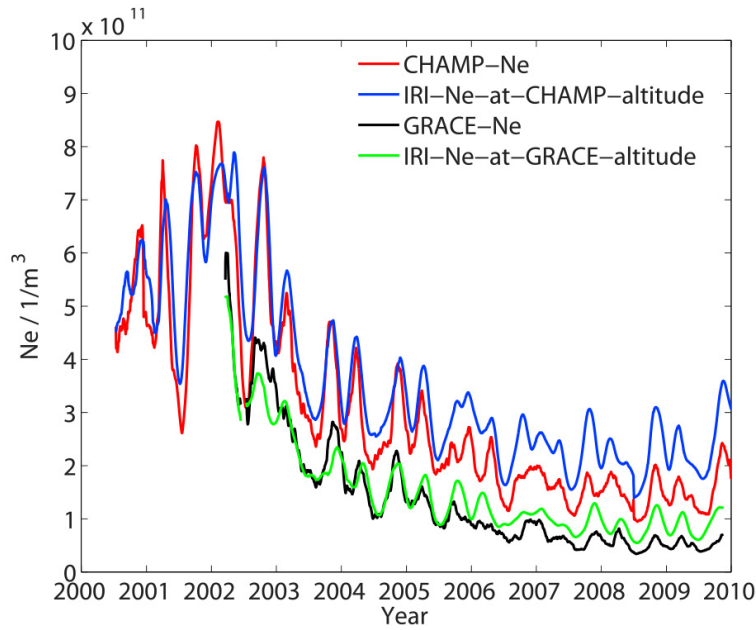
Figure 2.9: Comparison of *CHAMP* and *GRACE* electron density measurements with the predictions of the IRI model. Orbital averages are averaged over 31 days (modified from Lühr and Xiong (2010)).

The very particularity of the last minimum can be observed making a comparison between the black curve (updated on 27/11/2006) and the red or blue curve (updated on 16/01/2013 and on 20/02/2015 respectively). For the last solar minimum (2008-2009), the black curve forecasts values of *IG12*, meanwhile the red (or blue) curve shows measured values of the index. It is clear how the black line forecasts the last minimum before the effective observation, and with higher values than the measured ones for *IG12*.

By virtue of these results, it is interesting to evaluate the responses of the IRI-2012 model using different updates for *IG*12. Figure 2.8 shows the hourly monthly median values of f_0F2 for the Rome station, for the year 2009 of the last minimum, as measured (blue curve), as modeled by IRI-2012 using forecasted values of *IG12* (black curve), and as modeled by IRI-2012 using measured values of *IG12* (red curve). The x scale identifies the hour of the month from $t = 0$ (00:00 UT of January 2009) to $t = 288$ (23:00 UT of December 2009). The figure clearly shows how using forecasted values of *IG12*, the IRI-2012 model strongly overestimates the observed values. It is interesting to note also the huge differences between the IRI outputs using forecasted and observed values of *IG12*.

It is important to underline the key role that the input parameters have on the outputs of the ionospheric models. In particular, because of the main control of the solar activity level on the ionospheric plasma, the reliability of the solar activity indices dataset used as input for the ionospheric models is of primary importance. From this point of view, the study of the relationships between solar indices and the main ionospheric parameters carried out in Chapter 3 is crucial for the improvement of the "forecasting power" of the models.

Figure 2.9 shows the result obtained by Lühr and Xiong (2010) by comparing electron densities from the two satellites *CHAMP* and *GRACE* with the outputs of the IRI model[3] for the period 2000-2009. It is very interesting to note that during the first half of the period

---

[3]The IRI electron density outputs are referred to the heights of work of CHAMP (from a starting height of 456 km to ~310 km at the end of 2009) and GRACE (stable at ~490km)

(2000-2004) measurements and collocated model predictions track each other reasonably well at both sampling heights of CHAMP and GRACE. From 2005 onward the overestimation of the electron density by the model is progressively increasing. Annual averages show that IRI values are higher by 50% for 2008 and by more than 60% for 2009 (Lühr and Xiong, 2010). In the same study, an inspection of the latitudinal and local time distributions reveals that the IRI model strongly overestimated the equatorial ion fountain effect during the last deep solar minimum.

Heelis et al. (2009) found that the observed behavior of the transition height and plasma properties of the topside ionosphere are in significant contrast to those predicted using the IRI model.
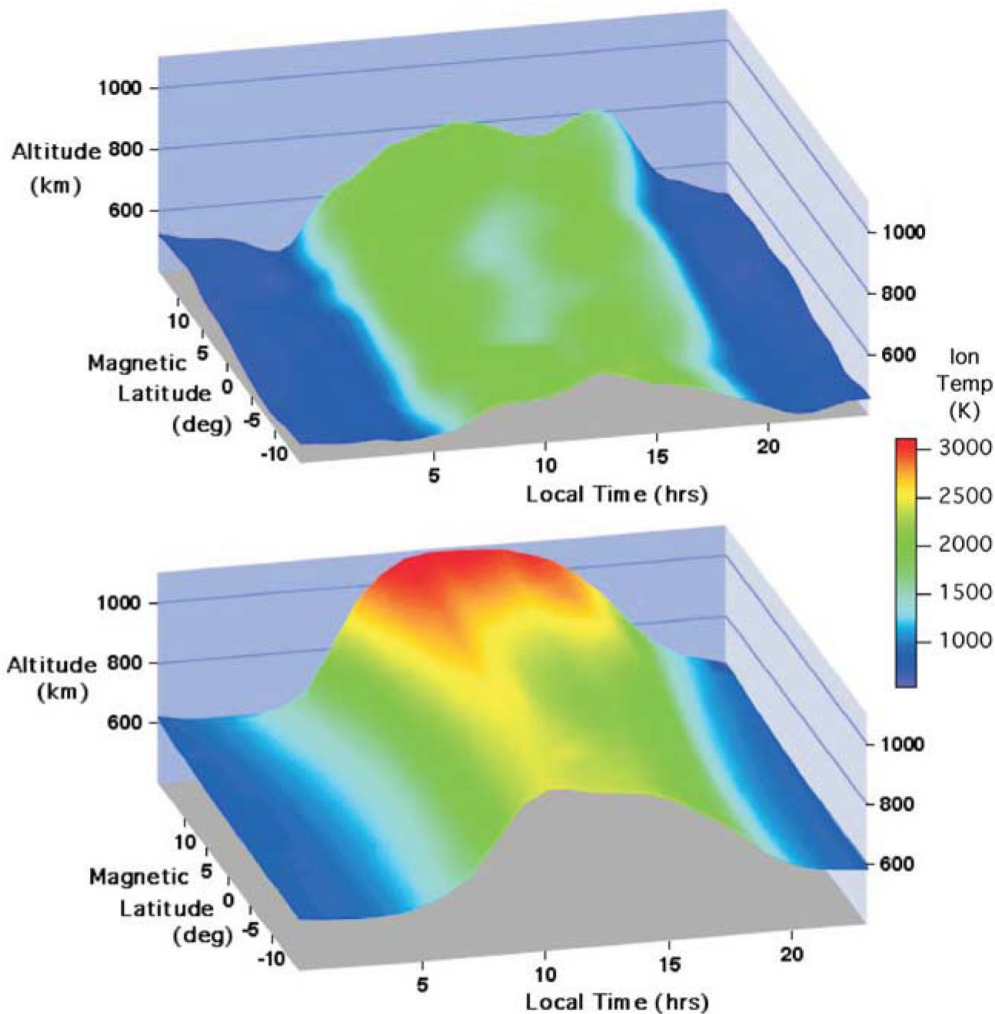
Figure 2.10: Comparison of (top) CINDI measurements and (bottom) predictions from the IRI model highlights the difference in the altitude of the transition surface and the ion temperature at the surface, showing that the surface is much lower and much cooler than expected (from Heelis et al. (2009)).

Figure 2.10 compares the height of the transition surface and the total ion concentration at that surface observed by the mission *CINDI* (*Coupled Ion Neutral Dynamics Investigation*) onboard the satellite C/NOFS with the IRI model results. By both day and night, the transition height is over 200 km lower than that predicted by the model and the peak daytime

ion concentration is over a factor of 5 lower than expected. While a well-formed equatorial anomaly is present in the model, it is largely absent in the observations, and the minimum ion concentration observed just before sunrise is almost a factor of 10 lower than expected (Heelis et al., 2009).

As mentioned, it is very important to study the characteristics of the ionosphere during the last solar minimum. The deficiencies shown by the IRI model suggest that there is not yet a complete knowledge of the ionospheric plasma responses to conditions of very low solar activity, so the years 2008-2009 give us the possibility to understand better the ionospheric response to these particular conditions, with the aim to improve the reliability of ionospheric models.

The present work focuses the attention on three crucial aspects: (1) the study of the relationships between the most important ionospheric parameter foF2 and five widely used solar indices; (2) the study of the ionospheric plasma response to the last minimum, with a comparison to the previous ones; (3) a comparison between the IRI-2012 model outputs and measurements obtained by ionosonde.

The study of the relationships (foF2 vs *Solar Index*) is important in order to improve the forecasting capability of the ionospheric models. An inter-minima comparison for stations located at mid and low latitudes can give us important information about the particularity of the last minimum, highlighting at the same time possible dependence on the latitude. The comparison of ionosonde data with the IRI model can confirm or not the results shown in this section, giving important information about the reliability of the most widely used ionospheric model for very low solar activity.

Chapter 3

Analysis of the relations *fo*F2 (12 LT) vs *Solar Indices* for the Rome station

Introduction

The terrestrial ionosphere is produced by the ionization of the neutral atmosphere caused by the solar radiation. The radiation in the Ultra Violet (UV, 120-400 nm) band, and in particular in the Extreme Ultra Violet (EUV, 0.1-120 nm) band, is ionospherically crucial because represents the main ionization source for the high atmospheric layers and can be considered the first cause for the formation of the ionosphere (e.g., Tobiska, 1996; Chen et al., 2012), explaining around 90% of the variance of characteristics such as *fo*F2 and *hm*F2 (e.g., Elias et al., 2014).

The solar activity variations represent the most influent cause of the ionospheric characteristics observed variability. This has been clearly shown in Figure 1.2 where the 1-year running means of the solar radio flux at 10.7 cm ($F_{10.7}$), and of the F2 layer critical frequency (*fo*F2), observed at local noon at the ionospheric station of Rome (41.8°N, 12.5°E; Italy), are plotted for the period from January 1976 to December 2013. $F_{10.7}$ is a widely used solar activity index and *fo*F2 represents the maximum frequency vertically reflected by the ionosphere. The similarity of the two trends suggests that the variability of the ionosphere is expected to follow the Sun's behavior and a quasi-linear constant relation is a priori expected between *fo*F2 and indices describing the solar activity (e.g., Araujo-Pradere et al., 2011; Hargreaves, 1995; Liu et al., 2006, 2011b; Solomon et al., 2010, 2013).

The study of ionospheric parameters trends have become a main subject of research since the beginning of nineties when they gained importance in the context of the global climatic change (Roble and Dickinson, 1989; Roble, 1995; Rishbeth, 1990; Rishbeth and Roble, 1992). Since then, a significant number of studies focused on ionospheric trends and on their possible link with the middle and upper atmosphere cooling due to an increase of greenhouse gases (e.g., Ulich and Turunen, 1997; Danilov, 2012; Laštovička et al., 2012; Laštovička, 2013; Danilov and Konstantinova, 2015; Danilov, 2015; Scott and Stamper, 2015; Upadhyay and Mahajan, 1998; Hall and Cannon, 2002; Bremer et al., 2012; Mielich and Bremer, 2013; Qian et al., 2014; Cnossen and Franzke, 2014; Roininen et al., 2015). To carry out these kind of studies a deep knowledge on solar activity dependence of the ionospheric parameters is necessary.

The study of the relations between the main ionospheric characteristics and the indices of solar activity has recently increased because of the more accurate measurements of solar radiation in the EUV wavelength band. For the most part, EUV radiation emerges from the solar transition region and corona while UV radiation originates in the transition region, chromosp-

here, and upper photosphere. Virtually, none of the solar EUV and UV irradiance below 300 nm reaches the Earth's surface, therefore accurate measurements of EUV/UV irradiance must be made from above the terrestrial atmosphere. For more than 20 years, experiments of various designs have measured the solar EUV and UV spectral irradiance from satellites, balloons, and rockets (Floyd et al., 2002; Rottman et al., 2004; Thuillier et al., 2004). Unfortunately, instruments used to perform measurements in these bands quickly degrade because of intense UV and EUV exposure, and monitoring of this instrumental degradation is particularly difficult. As a consequence, the spectral irradiances measured are often afflicted by large uncertainties relative to the corresponding solar variation (Woods et al., 1996; Cebula et al., 1998). EUV continuous measurements started with the launch of the *SOlar Heliospheric Observatory* (*SOHO*), only in late 1995 (Floyd et al., 2005). For these reasons, ionospheric models use different solar indices characterized by a longer dataset than the EUV one and that can be considered good proxy for the EUV radiation.

By virtue of the aforementioned considerations, the analysis of relations (foF2 vs *Solar Index*)[1] results to be essential for two main reasons: (1) to improve the ionospheric models performances, because every ionospheric model is based on these relations; (2) possible ionospheric signatures of the greenhouse effect can be found only after an accurate "cleaning" of the ionospheric parameters time series from solar activity dependence.

As described in Section 2.1, the last solar minimum (cycle 23/24, years 2008-2009) showed very interesting characteristics with clear changes in the long-term relations between the EUV irradiance and solar indices such as $F_{10.7}$ and R, as reported by Emmert et al. (2010), Chen et al. (2011a) and Elias et al. (2014). Under these particular conditions, the minimum of solar cycle 23/24 provides a perfect window to verify the relations between the main ionospheric parameter foF2 and the most widely used solar activity indices in order to detect if there have been changes in these long-term relations. Furthermore, in order to improve the efficiency of the ionospheric models, the research of a solar index that can approximate as reliably as possible the EUV radiation (research of the "best proxy" for the solar EUV radiation) represents a very interesting study to carry out.

This chapter is focused on the analysis of relations of foF2, measured at local noon in Rome, as a function of five widely used solar activity indices: $F_{10.7}$, Lym-α, $MgII$, sunspots number R, and the solar irradiance in the EUV band 0.1-50 nm ($EUV_{0.1-50}$). The study is based on the long, continuous and very reliable foF2 dataset (hourly validated values) recorded at the Rome ionospheric station between 1976 and 2013. It is important to underline that the continuous dataset provided by Rome ionosonde is the key to carry out this study, because all around the world there are not so many ionosondes with a so long and continuous dataset.

The aims for this part of the present work are: (1) to inspect the relations (foF2 vs *Index*) for the period January 1976-December 2013, looking for the best fit and to test if the a priori supposed linear fit can be still considered the best one; (2) to search for the best index able to describe the variations of foF2, both globally (for the complete dataset January 1976-December 2013) and for the last solar minimum (time interval January 2008-December 2009) and (3) to provide useful information about the "best proxy" index for the solar radiation in the EUV range. The datasets used for both foF2 and indices of solar activity are described in Section 3.1. Section 3.2 will report the analysis of the relations (foF2 vs *Index*) with the results for the best fit. Section 3.3 is focused on the research of the best index to describe the variations of foF2 and on the research of the best proxy for the EUV radiation. Section 3.4 briefly summarizes the results obtained for analyses correlated to the study of the relations (foF2 vs *Index*) and

---

[1]Hereafter (foF2 vs *Index*).

Section 3.5 reports the conclusions.

3.1 Data used

3.1.1 Dataset for *fo*F2

The critical frequency of the F2 layer is the most important and used ionospheric parameter, representing the maximum frequency that can be reflected by the ionosphere for an electromagnetic wave vertically transmitted. As reported in Section 1.3.2 and displayed in Figure 1.7, *fo*F2 can be easily retrieved directly from an ionogram using either manual validation or automatic ionogram interpretation applications.

In this work, the continuous and long dataset recorded at the Rome ionospheric station at local noon (12 LT; LT=UT+1h for Rome) is considered. The dataset is composed by hourly manually validated values recorded since the 1st January 1976 to the 31st December 2013, hence covering the whole solar cycles 21, 22, 23 and the ascending phase of cycle 24. The values were manually validated according to the International Union of Radio Science (URSI) standard (Wakai et al., 1987), and in this work all the corresponding numerical values were considered independently of the presence of qualifying and descriptive letters. The validation was performed from traces recorded by classical ionosondes, which cannot tag the different polarization characterizing the two different modes of propagation of the electromagnetic wave. A VOS-1 chirp ionosonde produced by the Barry Research Corporation, Palo Alto, CA, USA (Barry Research Corporation, 1975) sounded from January 1976 to November 2004, and then it was replaced by an AIS-INGV (Advanced Ionospheric Sounder-INGV) ionosonde (Zuccheretti et al., 2003), for which the ionograms were validated by using the Interpre software (Pezzopane, 2004). This means that the *fo*F2 validated time series considered in this study represent a very reliable and homogeneous dataset. Data for Rome station were downloaded from the *electronic Space Weather upper atmosphere* database (*eSWua*; http://www.eswua.ingv.it/) (Romano et al., 2008).

3.1.2 Datasets for solar activity indices

In this work, five widely used solar activity indices, namely $F_{10.7}$, *Lym-α*, *MgII*, the sunspot number R and the solar $EUV_{0.1-50}$ have been considered.

$F_{10.7}$ is a solar proxy that correlates quite well with the solar activity, in terms of EUV and X-ray emissions (Solomon et al., 2013). The Sun radiation at 10.7 cm can be easily measured with ground-based instruments, therefore a long dataset is available and for this reason it has been extensively used in solar and upper atmosphere empirical models, such as IRI (Bilitza et al., 1990; Bilitza, 2001; Bilitza et al., 2014) and NRLMSISE-00 (Picone et al., 2002). It is continuously available from measurements obtained in Penticton, Canada, from which data for this flux have been given as daily values measured at local noon (17:00 GMT) since 14 February 1947 (Covington and Medd, 1954). $F_{10.7}$ data have been downloaded from the database of the *National Oceanic and Atmospheric Administration* (*NOAA*) (http://www.ngdc.noaa.gov/stp/space-weather/solar-data/).

The hydrogen *Lyman-α* emission at 121.6 nm (hereafter *Lym-α*) represents the strongest single line in the UV band, and has been measured for decades by rockets, the Atmosphere Explorer (AE) series of satellites, the Solar Mesosphere Explorer (SME), the Upper Atmosphere Research Satellite (UARS), the Thermosphere Ionosphere Mesosphere Energetics and Dynamics

(TIMED), and the Solar Radiation and Climate Experiment (SORCE) missions (Solomon et al., 2013). A composite index, that was compiled by Woods et al. (2000), is based on a careful intercalibration of these measurements and the corresponding gaps are filled using correlation relations with $F_{10.7}$ and $MgII$ indices. It is worth noting that the wavelength of hydrogen *Lym-α* emission is near the upper boundary of the EUV wavelengths range, therefore good results should be expected in term of the "best proxy" for the EUV radiation. The dataset used in this work consists of a composite index that integrates data from different satellite missions since 1947 and was downloaded from the *Lasp Interactive Solar Irradiance Datacenter* (*LISIRD*) database. Detailed information about the composite dataset used and free downloadable data are available at the website http://lasp.colorado.edu/lisird/composite_timeseries.html.

The core-to-wing ratio of the magnesium ion h and k lines, at 279.56 and 280.27 nm respectively, is a good indicator of the solar chromospheric activity, and is a useful proxy for solar irradiance in the UV and EUV wavelengths as reported by Viereck et al. (2004, 2010). Called *MgII core-to-wing* index, it is calculated by taking the ratio between the highly variable chromospheric lines and the weakly varying photospheric wings (Solomon et al., 2013). As for the *Lym-α* index, the dataset is composite. *MgII* data for this work were downloaded from the database of Bremen University (http://www.iup.uni-bremen.de/gome/gomemgii.html), and start from 07 November 1978.

The sunspots number R represents the most common and widely used index to describe the activity of the Sun, because characterized by the longest dataset, with data available also before the 1900. The daily values provided from *SILSO* (*Sunspot Index and Long-term Solar Observations*, Royal Observatory of Belgium, Brussels) database were here considered and datasets are available online at http://www.sidc.be/silso/datafiles.

Concerning the *Solar EUV* index, corresponding space-based observations include among others the Solar EUV Monitor (SEM) on the SOlar Heliospheric Observatory (SOHO) (Judge et al., 1998), the Solar EUV Experiment (SEE) on TIMED satellite (Woods et al., 2005), and the EUV Variability Experiment (EVE) on the Solar Dynamics Observatory (Woods et al., 2012). Nevertheless, only SEM has made measurements throughout the solar cycle 23 and during the last two solar minima in 1996-1997 and 2008-2009. SEM provides the integrated solar EUV flux in the two bands 0.1-50 nm and 26-34 nm, which contain the prominent 30.4 nm HeII line and several coronal lines (Solomon et al., 2013). The two indices give comparable results. The one considered in this study is the $EUV_{0.1-50}$ index. Corresponding data are available as daily mean values from SOHO/SEM measurements since 01 January 1996, and were downloaded at the website http://www.usc.edu/dept/space_science/semdatafolder/semdownload.htm of the Space Sciences Center of the University of Southern California.

It is important to underline that for every index only one daily value is available and measurements usually refer to local noon. Therefore, the choice to carry out an analysis considering foF2 at local noon is the one providing the most reliable results. However, in Section 3.4 brief considerations on relationships between foF2 measured at 01 and 19 LT and solar indices are reported.

3.2   Analysis of the relations (foF2 vs $Index$)

The solar activity represents the main controller for the variability of ionospheric parameters. In this section, the strong relationship between solar activity and the parameter foF2 is examined. Therefore, the study is focused only on the dependence of foF2 on solar activity. However, other important phenomena have to be considered altering the trend of foF2, such as geomagnetic

activity and the climatological variations of the ionosphere for short and long periods.

In order to pay our attention only on the solar activity influence, before starting the analysis, a 1-year running mean for both *fo*F2 and solar indices was performed. As mentioned, this is done because we are interested in the study of the relation between *fo*F2 and solar activity indices, and the best way to accomplish this task is to "clean" the *fo*F2 time series from short-time ionospheric features, like those caused by geomagnetic disturbances, ionospheric seasonal and day-to-day variations (Liu et al., 2003, 2006, 2011a; Ma et al., 2009).

The data considered in the analysis are based on the *fo*F2 availability for Rome station at local noon starting from 1st January 1976. In order to study the recent solar cycles, data until the 31th December 2013 have been taken into account, covering the solar cycle 21, 22, 23 and partially the solar cycle 24. Due to the lack of data for consecutive months in the range hours 08:00-19:00 LT, the *fo*F2 1-year running mean cannot be considered reliable in the period April 1978-December 1979, consequently data for this period have been removed. It is worth noting that the analysis was done accordingly to Liu et al. (2011a), considering only the first smoothed (1-year running mean) value of each month, for both *fo*F2 and the solar index. Anyhow, a consistency test using the 15th smoothed value of each month has produced identical results.

In Figure 3.1 it is clearly shown how using a 1-year running mean and considering only the first smoothed value of the month it is possible to obtain "clean plots", useful to obtain simple and reliable relations.
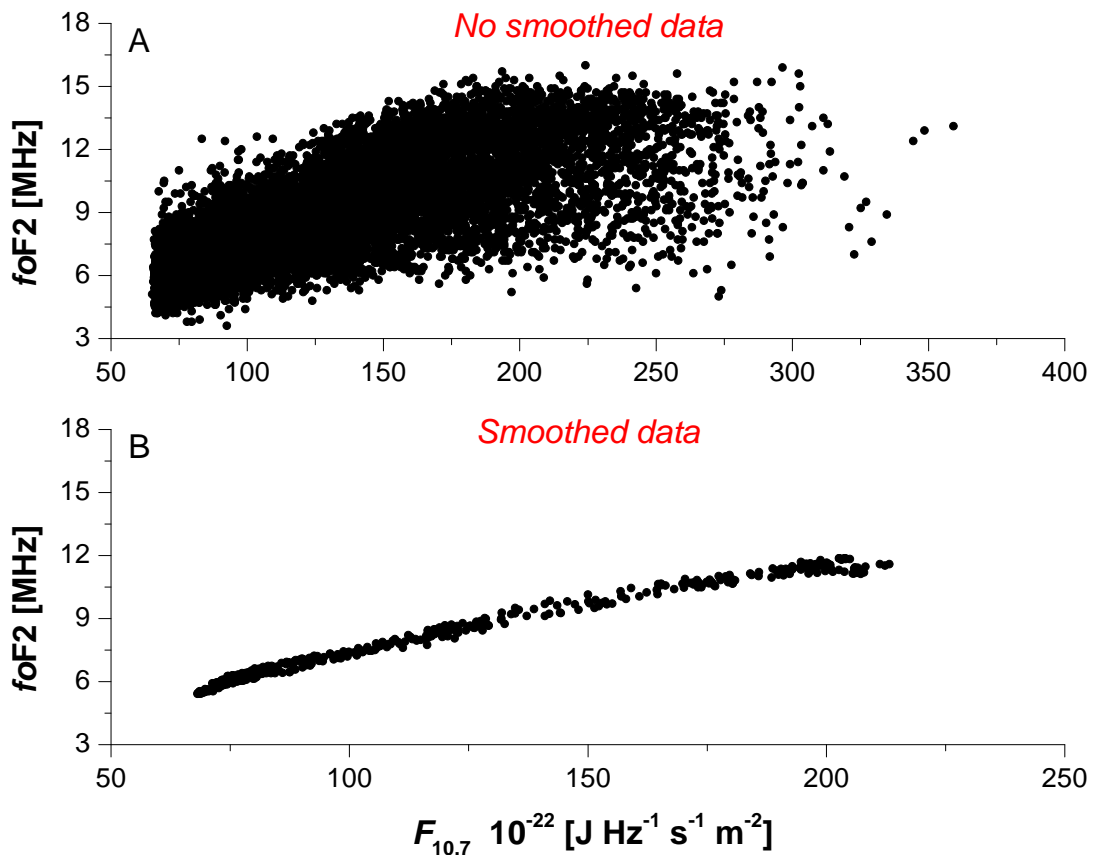

Figure 3.1: *fo*F2 (12 LT) vs $F_{10.7}$ for the period 1 January 1976-31 December 2013 for the Rome station: (A) daily non-smoothed values; (B) first smoothed values of each month.

Solar Index	Saturation level
$F_{10.7}$	$170 \cdot 10^{-22}$ [J Hz^{-1} s^{-1} m^{-2}]
Lym-α	$5 \cdot 10^{11}$ photons [s^{-1} cm^{-2}]
$MgII$	0.164
Sunspots number R	117
$EUV_{0.1-50}$	$2.6 \cdot 10^{10}$ photons [s^{-1} cm^{-2}]

Table 3.1: Levels of solar activity above which the foF2 saturation effect is visible.

Figure 3.1A reports daily non-smoothed values of foF2 (12 LT), measured at Rome station, and $F_{10.7}$, for the period January 1976-December 2013. Figure 3.1B reports for the same parameters and the same period the first smoothed values of each month. A comparison between Figure 3.1A and Figure 3.1B clearly highlights that the use of a 1-year running mean provides: (1) a less scattered plot that is suitable to make a fit and consequently obtain a reliable relation; (2) a reduction of both geomagnetic disturbances and ionospheric seasonal and day-to-day variations; (3) a strong reduction of the saturation effect, that is dominant above the solar activity level $F_{10.7} = 170 \cdot 10^{-22}$ [J Hz^{-1} s^{-1} m^{-2}].

It is important to underline that the saturation effect can be strongly reduced using a 1-year running mean but not completely and a small influence remains also after applying this filtering to the dataset. Moreover, as it will be shown in the next sections, the influence of saturation and hysteresis effects strongly depend on the chosen index; in particular, the hysteresis effect can strongly increase switching from one index to another. From the analyses carried out, it came out that the saturation effect is visible for all the indices above the levels reported in Table 3.1.

In Figure 3.2 the 1-year running mean for both the solar activity indices (in their own unit) and foF2 noon values in MHz recorded at Rome between January 1976 and December 2013 is plotted. The similarity between the foF2 curve and the solar indices ones is clear, with no a priori detectable variations among different solar cycles.

In light of these similarities, as a first step, it will be investigated whether a linear relation describes properly the relations (foF2 vs *Index*), that is if a linear fit is suitable to represent relationships as the one plotted in Figure 3.1B; a particular attention will be paid to the last anomalous and prolonged solar minimum occurred in the years 2008-2009. It was decided to investigate first a linear relation because, when looking for long-term trends, this relation often is the one used to eliminate the solar activity influence (e.g., Ulich and Turunen, 1997; Upadhyay and Mahajan, 1998; Laštovička et al., 2006; Bremer et al., 2012; Laštovička et al., 2012; Mielich and Bremer, 2013; Cnossen and Franzke, 2014; Roininen et al., 2015). According to this, a linear fit and the corresponding residuals analysis were performed for all the investigated relations (foF2 vs *Index*), and the results are reported in Section 3.2.1. The residuals analysis provides the simplest and better way to test the reliability of a linear fit. In particular, it gives the possibility to make interesting additional considerations by evaluating how much both saturation and hysteresis effects affect the relations (foF2 vs *Index*).

After the considerations about a linear fit, the results for the research of the best fit are reported in Section 3.2.2. To look for the best fit to describe, with a global unique relation, the foF2 dependence on solar activity, represents the most important task to be accomplished in order to improve the reliability of ionospheric models that, as mentioned, are significantly based on this kind of relations.
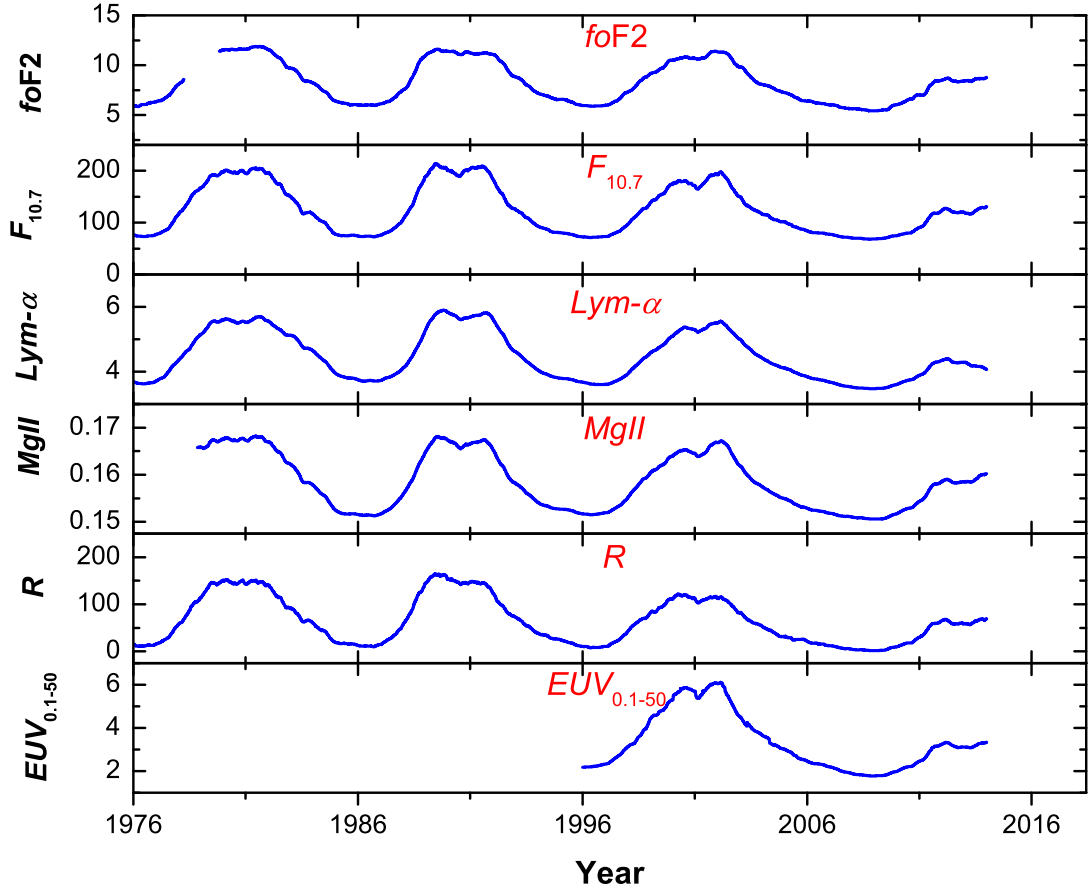
Figure 3.2: 1-year running mean over the period 1 January 1976-31 December 2013 for the ionospheric parameter *fo*F2 (in MHz) recorded at 12 LT in Rome and for the solar indices $F_{10.7}$ (in unit 10^{-22} [J Hz^{-1} s^{-1} m^{-2}]), *Lym-α* (in unit 10^{11} photons [s^{-1} cm^{-2}]), *MgII*, sunspots number *R* and solar $EUV_{0.1-50}$ (in unit 10^{10} photons [s^{-1} cm^{-2}]).

3.2.1 Residuals analysis and discussion about a linear fit for the relations (*fo*F2 vs *Index*)

Scatter plots between *fo*F2 and considered solar indices, with the corresponding linear regression, are shown in the left column of Figure 3.3. For every relation, the first smoothed value of the month is plotted for both *fo*F2 and solar index, from January 1976 to December 2013; the red line represents the linear fit of data whereas blue, green and red dots indicate the first smoothed value of each month for the minimum of solar cycle 21/22 (years 1986-1987), 22/23 (years 1996-1997), and 23/24 (years 2008-2009), respectively. The corresponding residuals analysis is shown in the right column of Figure 3.3, where the residuals are plotted as a function of fitted *fo*F2 values, so that the horizontal black line corresponds exactly with the values of the linear fit. Red and brown dots indicate respectively residuals for data related to the last solar minimum and for data influenced by the remaining saturation effect. The levels above which saturation of *fo*F2 is observed are reported in Table 3.1. Orange dots in the (*fo*F2 vs $EUV_{0.1-50}$) scatter plots identify data related to the ascending phase of solar cycle 24 (from December 2010 to December 2013). The linear correlation coefficient *r* and the statistical parameter *Adjusted*

R-square (*Adj. R-square*) are also displayed.

Both the linear correlation coefficient r and the parameter *Adj. R-square* are widely used statistical parameters to test the reliability of a fit, being r specific for a linear fit and *Adj. R-square* used also for non-linear fits. The introduced *Adj. R-square* parameter can be expressed as:

$$Adj.\ R - Square = 1 - \frac{\sum_{i=1}^{n} w_{i}(y_{i} - \tilde{y})^2}{\sum_{i=1}^{n} w_{i}(y_{i} - \bar{y})} \cdot \frac{n-1}{\nu},   \tag{3.1}$$

where ν represents the number of independent pieces of information involving the data points required to calculate the sum of squares (n), y_{i} represents the observed value, $\tilde{y}_{i}$ represents the synthetic value, $\bar{y}$ represents the average of the observed data and w_{i} is the weight applied to each data point (usually $w_{i} = 1$). The parameter can assume any value from 0 to 1, with values closer to 1 that indicate a better fit. The *Adj. R-square* parameter is very useful and reliable if compared to *R-square* that is expressed with (3.1) avoiding the correction factor $(n-1)/\nu$; in fact, the latter can increase just increasing the number of fitted coefficients, even without a real improve of the fit. This situation is avoided taking into account the degrees of freedom of the residuals.

Focusing on foF2 values recorded during the last solar minimum, Figure 3.3 shows that these deviate from a linear fit for every index. In particular, the deviation is quite significant for $F_{10.7}$, for which residuals are of the order of about 0.5 MHz, and less pronounced for Lym-α, $MgII$, R and $EUV_{0.1-50}$, for which residuals are of the order of about 0.25 MHz. Chen et al. (2011a), studying the relation between 12-month mean foF2 values (at 14:00 LT) and 12-month mean P values (where $P = (F_{10.7} + F_{10.7A})/2$ and $F_{10.7A}$ is the 81-days running mean of $F_{10.7}$), found that the deviation from a linear approximation characterizing the last solar minimum shows a strong dependence on latitude. Figure 3.4 reports the results obtained by Chen et al. (2011a) for stations at different latitudes at 14:00 LT: Wakkanai (lat. 45.4°N, lon. 141.7°E; mid latitude), Kokubunji (lat. 35.7°N, lon. 139.5°E; mid latitude), Okinawa (lat. 26.3°N, lon. 127.8°E; low latitude), Vanimo (lat. 2.7°S, lon. 141.3°E; equatorial), Townsville (lat. 19.6°S, lon. 146.9°E; low latitude) and Norfolk Islands (lat. 29.0°S, lon. 168.0°E; low latitude). It is observed that larger deviations characterize low-latitude stations (Okinawa, Vanimo and Townsville), in particular those close to the equatorial ionization anomaly, while very low deviations characterize mid-latitude stations. In particular, the deviation is less pronounced at Wakkanai, located at a latitude similar to that of Rome. Therefore, the low deviations observed in Rome are somewhat expected.

Figure 3.5 reports for the Rome station plots similar to that of Figure 3.4, for the indices $F_{10.7}$ (top) and $MgII$ (bottom). Black dots refer to data from January 1976 to April 2002, including the cycle 21, 22 and the ascending phase of cycle 23; blue triangles refer to the descending phase of solar cycle 23 (May 2002-December 2007); red dots refer to the minimum 23/24 (2008-2009). The red line is the linear fit of the black dots. It is observed how the results obtained in the present study agree with that reported by Chen et al. (2011a) for the Wakkanai station. Figure 3.5 confirms a more pronounced deviation from the linearity for the index $F_{10.7}$ than for the index $MgII$. However, all analyzed indices are affected by a deviation from the linearity for the very low values registered during the deep phase of the last solar minimum 23/24. Moreover, Figure 3.5 shows that for both $F_{10.7}$ and $MgII$ (but this result is true for all indices), there have been changes in the (foF2 vs *Index*) relation, with a linear fit that results to be good for the previous cycles, but cannot be considered a good fit for the descending phase of the cycle 23, owing to the very low solar activity of the last minimum. Therefore, a better
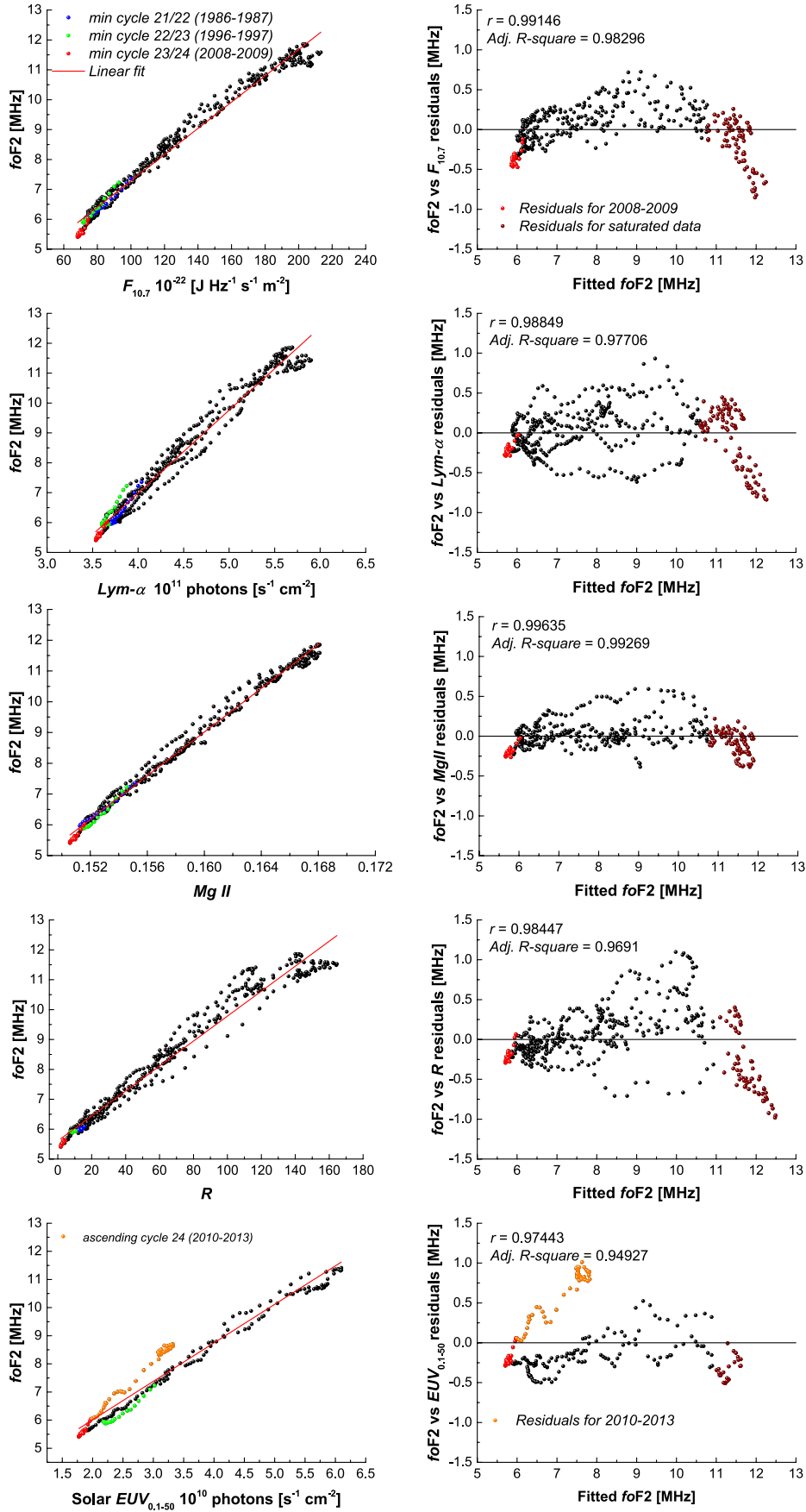
Figure 3.3: (left column) Scatter plots (*fo*F2 vs *Index*) for indices $F_{10.7}$, Lym-α, $MgII$, R and $EUV_{0.1-50}$. Blue, green and red dots represent values for minima of solar cycles 21/22, 22/23 and 23/24 respectively. The linear fit of the whole dataset is highlighted by the red line. (right column) Residuals analysis of the linear fits. Red and brown dots represent respectively the residuals related to the last solar minimum and for data influenced by the remaining saturation effect. Orange dots in the scatter plots (*fo*F2 vs $EUV_{0.1-50}$) highlight the ascending phase of solar cycle 24 (January 2010 to December 2013). The linear correlation coefficient r and the statistical parameter *Adj. R-square* are also displayed. For both *fo*F2 and solar indices only the first smoothed (1-year running mean) value of each month is considered.

Figure 3.4: Plots of *fo*F2 versus $P = (F_{10.7} + F_{10.7A})/2$ for (a) Northern Hemisphere stations and (b) Southern Hemisphere stations. Blue dots and red circles represent observations before and after the maximum of solar cycle 23; green triangles in K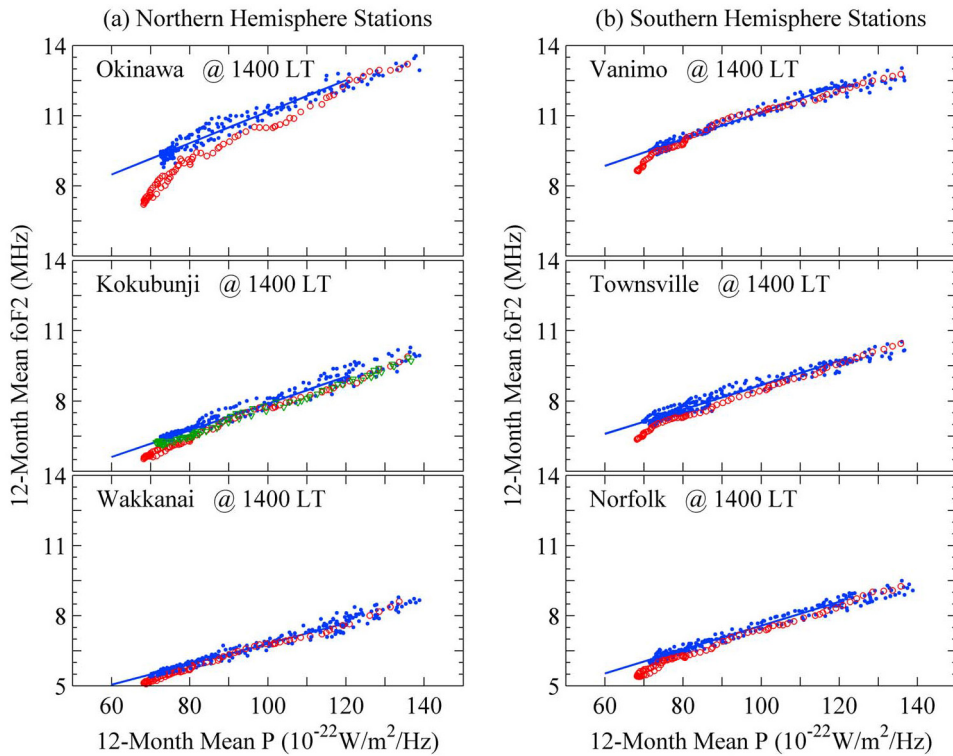okubunji represent observations during the minimum of solar cycle 22/23. The solid line is the linear fit of dots (only for $P < 120$), except for Kokubunji for which it is the linear fit of dots and triangles (from Chen et al. (2011a)).

fit relation should be found to describe, with a unique global equation, the relationship (*fo*F2 vs *Index*).

Some solar EUV irradiance models rely on the assumption that the relation between solar EUV indices and $F_{10.7}$ is invariant over different solar cycles (Chen et al., 2011a). Figure 3.3 and Figure 3.5 show that, for the last solar minimum, the relation (*fo*F2 vs $F_{10.7}$) shows a significant deviation from the linearity, while the values for the previous minima are still well represented using a linear fit. At the same time, a better-conserved linearity for the relation (*fo*F2 vs $EUV_{0.1-50}$) is obtained. These two results indicate a clear change in the relation between $F_{10.7}$ and $EUV_{0.1-50}$ for the last solar minimum. Moreover, Figure 3.3 shows a clear non-random arrangement of residuals for $F_{10.7}$, which proves that a linear fit is not appropriate for this relation. Accordingly to the results of Chen et al. (2011a) and Solomon et al. (2013), it is possible to claim that $F_{10.7}$ cannot more be considered a good proxy for the radiation in the EUV wavelengths. The research of the best proxy for the EUV radiation will be the focus of Section 3.3.3.

However, it is important to underline that if it is true that the linear fit of the (*fo*F2 vs $EUV_{0.1-50}$) relation is somewhat good for the last minimum, because of the short dataset characterizing $EUV_{0.1-50}$, a comparison with the previous minima cannot be done. Therefore, it is not possible to obtain information about possible changes of the relation (*fo*F2 vs $EUV_{0.1-50}$) for different solar cycles. Nevertheless, concerning the index $EUV_{0.1-50}$, Figure 3.3 shows a huge deviation from the linearity for the ascending phase of solar cycle 24, a feature that is
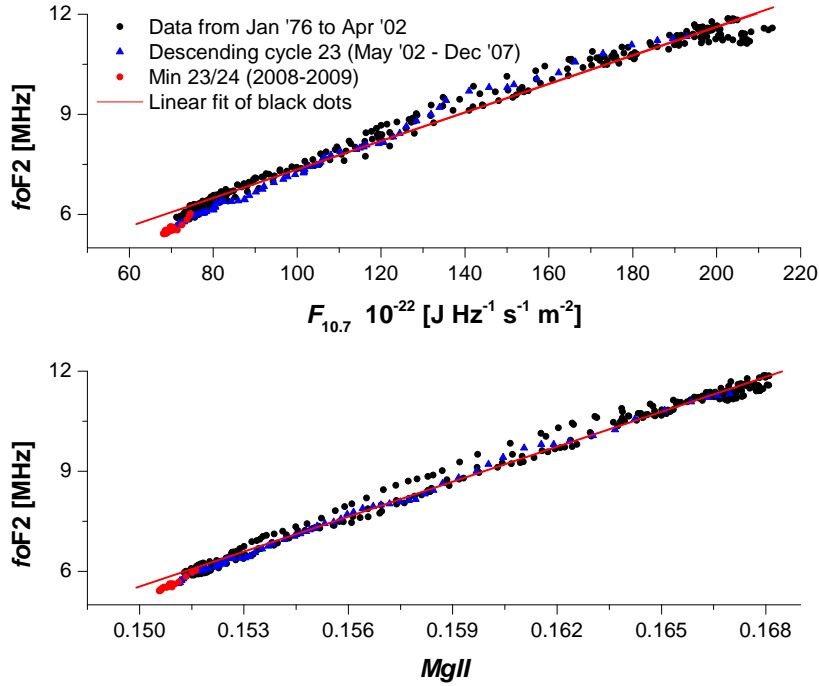
Figure 3.5: (foF2 vs $F_{10.7}$) (top) and (foF2 vs $MgII$) (bottom) for the period January 1976-December 2009. Black dots refer to data from January 1976 to April 2002 (cycles 21, 22 and ascending cycle 23), blue triangles refer to the period May 2002-December 2007 (descending cycle 23) and red dots refer to the solar minimum 23/24 (years 2008-2009). The red lines are linear fits of the black dots.

not observed for the other indices. This could be ascribed to a potential degradation of the SOHO/SEM instrument, which would cause a drift of solar measurements and a consequent overestimation of the $EUV_{0.1-50}$ irradiance (Chen et al., 2011a; Wieman et al., 2014), even though Didkovsky et al. (2009) and Solomon et al. (2010) suggested that this effect is not overriding. Hence, for $EUV_{0.1-50}$, the slightly deviation of the linear fit from values related to the last solar minimum could also be due to this potential degradation, taking into account how the linear regression is affected by the dataset from January 2010 to December 2013. In fact, a linear fit done only on data from January 1996 to December 2009 describes very well the observed values for the last solar minimum (plot not shown).

As it was already highlighted, the index $F_{10.7}$ is characterized by a quasi-parabolic feature of the residuals, which means a non-random pattern around the zero line, proofing that a linear fit cannot properly represent the relation (foF2 vs $F_{10.7}$). On the contrary, for the other indices a non-random distribution of the residuals is significantly observed only for high solar activity, because of the remaining saturation effect. This means that using a linear fit, foF2 is overestimated for high solar activity, and the overestimation becomes more evident when monthly means, median values or no-smoothed values for both foF2 and solar indices are considered. This was already shown in Figure 1.3 and in Figure 3.1, both of them showing a stronger saturation effect than respect to the use of smoothed data.

An important feature that can be studied using the residuals analysis is the spread of dots around the horizontal black line, which is particularly visible for medium solar activity (corresponding to foF2 values from about 6.3 to 11 MHz), more markedly for Lym-α and R than for $F_{10.7}$, $MgII$ and $EUV_{0.1-50}$. This spread is due to the hysteresis effect that causes two different
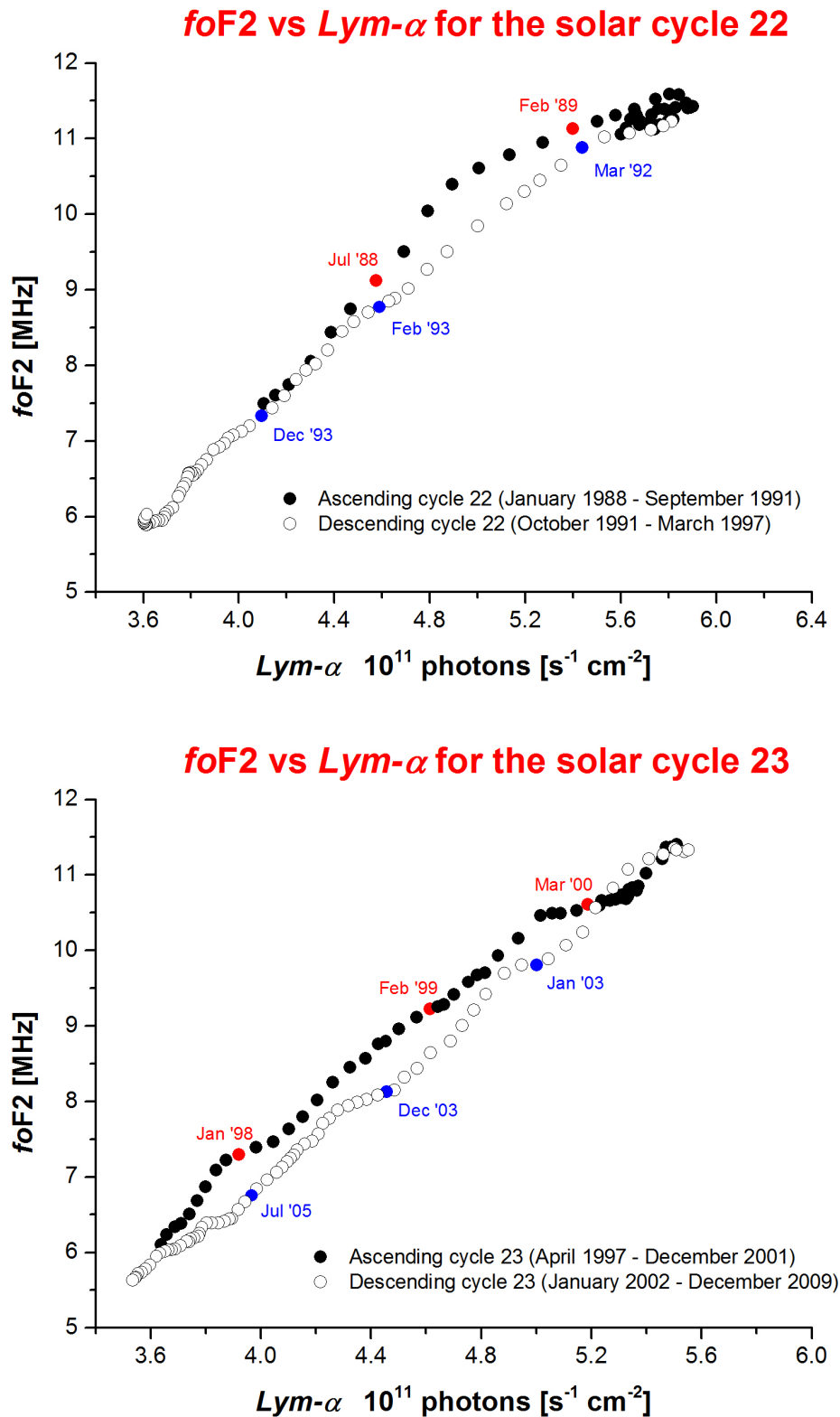
Figure 3.6: Scatter plots (foF2 vs Lym-α) for solar cycles 22 and 23. Full circles represent the ascending phase of the cycle whereas open circles represent the descending phase of the cycle. For both foF2 and Lym-α only the first smoothed (1-year running mean) value of each month is plotted.

Solar Index	Linear correlation coefficient r
$F_{10.7}$	0.99146
Lym-α	0.98849
$MgII$	0.99635
R	0.98447
$EUV_{0.1-50}$	0.97443

Table 3.2: Linear correlation coefficients r for the relations (foF2 vs $Index$) plotted on the left column of Figure 3.3.

values of foF2 for the ascending and descending phases of a solar cycle, in correspondence of the same level of solar activity.

To further describe this important effect, Figure 3.6 shows scatter plots (foF2 vs Lym-α) for the ascending (full circles) and descending (open circles) phases of solar cycles 22 (top) and 23 (bottom). Mikhailov and Mikhailov (1995) postulated that the hysteresis is associated with differences in the geomagnetic activity during the ascending and descending phases of a solar cycle. Nevertheless, there is not yet an accepted explanation for the hysteresis effect (Liu et al., 2011b).

The strong influence of the hysteresis effect and other considerations about the reliability of a linear fit for the relations reported in Figure 3.3 are noticeable looking at the linear correlation coefficient r values summarized in Table 3.2.

The r value results to be lower for Lym-α and R, that are characterized by a strong hysteresis effect, and closer to one for $MgII$ and $F_{10.7}$, characterized by a lower hysteresis effect. Nevertheless, looking at Figure 3.3, it is clear how the linearity is lost for the last minimum in particular for $F_{10.7}$ while it better holds for Lym-α, $MgII$ and R. Furthermore, as it was discussed, a linear fit is not a good choice to describe the global relation (foF2 vs $F_{10.7}$). These considerations show how the scatter of the residuals around the horizontal zero line, due to the hysteresis effect, plays a key role in determining the value of R; the saturation effect and the particular low values for the last solar minimum only marginally influence it. Consequently, the hysteresis effect characterizing the medium solar activity strongly influences the research for the best index to describe the variation of foF2. With regard to this, it is interesting to notice that the best linear correlation coefficient ($r \sim 0.996$) is observed for the index $MgII$, that results to be less affected by both hysteresis and remaining saturation effect than the other indices.

The saturation effect, visible for high solar activity level and indicated by brown dots in the residuals analysis of Figure 3.3, is visible as a "tail-like" feature of the residuals for all the considered indices. Lym-α, R and $F_{10.7}$ are characterized by a more pronounced saturation effect than $MgII$ and $EUV_{0.1-50}$. However, in every case, a linear fit would provide an overestimation of the observed values for high solar activity levels.

By virtue of the analyses and results found in this section, it is possible to claim that there have been changes in the relations (foF2 vs $Index$), due to the last minimum, and that the a priori supposed linear fit cannot be considered the best one to describe them. In particular, two main reasons suggest that a linear fit is not a good one: a linear fit provides (1) an overestimation for the very low solar activity level registered during the last solar minimum and (2) an overestimation for high solar activity level due to the remaining saturation effect. It is important to stress again that using no-smoothed values (such as mean or median values),

these two effects would be emphasized.

Therefore, it is very interesting and useful to find the best fit to describe, globally and with a unique simple equation, the relationships (*fo*F2 vs *Index*). The results of this analysis, reported in the next Section 3.2.2, have a strong importance for all the ionospheric models that are based on this kind of relations. Moreover, an accurate fit can help to "clean" more reliably the trends of ionospheric parameters from the predominant solar activity dependence.

3.2.2   Looking for the best fit

In order to find the best fit, polynomial regressions (quadratic, third- and fourth-degree fits) of the relations (*fo*F2 vs *Index*) were carried out by considering the whole dataset (January 1976-December 2013).

Table 3.3 reports the values of the parameter *Adj. R-square* for a linear, a quadratic, a third- and a fourth-degree polynomial fit, for each solar index. It is possible to notice that in every case, increasing the polynomial degree, there is an improvement of the fitting. However, the more conspicuous improvement is in the passage from a linear to a quadratic fit relation. This is essentially due to the fact that a quadratic fit can properly catch the deviation from the linearity due to both the remaining saturation effect and the very low solar activity of the last solar minimum. Higher-degree polynomial regressions were tested by virtue of what it was done by other authors (Danilov and Mikhailov, 1999, 2001; Mikhailov and Marin, 2000, 2001; Ouattara, 2012; Danilov and Konstantinova, 2015), but the obtained results were practically identical to those obtained with a quadratic polynomial regression, confirming the results obtained by Kouris et al. (1998) and Liu et al. (2011b) who found that a higher-order polynomial does not improve significantly the fitting.

Solar Index	Linear fit	Polynomial fit (2° order)	Polynomial fit (3° order)	Polynomial fit (4° order)
$F_{10.7}$	0.983	0.99258	0.99281	0.99336
$Lym\text{-}\alpha$	0.977	0.98113	0.98238	0.98339
$MgII$	0.993	0.99412	0.99413	0.99452
R	0.969	0.98078	0.98479	0.98497
$EUV_{0.1-50}$	0.949	0.96234	0.96255	0.96342

Table 3.3: *Adj. R-Square* parameter for a linear, quadratic, third-order and fourth-order fit of the relations (*fo*F2 vs *Index*) by considering the whole dataset (January 1976-December 2013).

Figure 3.7 reports the scatterplots *fo*F2 vs indices $F_{10.7}$ (left side) and $Lym\text{-}\alpha$ (right side), with superimposed a linear (red line) and a quadratic (blue curve) fit. As already mentioned, the most important improvements, using a quadratic fit, are visible for the very low solar activity of the last minimum and for high solar activity where the remaining saturation effect has to be considered. These results are particularly clear for the index $F_{10.7}$ for which both the saturation effect and the loss of linearity for the last minimum are more pronounced than respect to the other indices. In fact, Figure 3.7 also shows how, passing from a linear to a quadratic fit, the improvement for the $Lym\text{-}\alpha$ index is less pronounced.

The improvements obtained passing from a linear to a quadratic fit are clearly visible in the residuals analyses reported in Figure 3.8. The figure reports the residuals of the linear fit related to the scatterplots (*fo*F2 vs $F_{10.7}$) (panel A) and (*fo*F2 vs $Lym\text{-}\alpha$) (panel B), and the
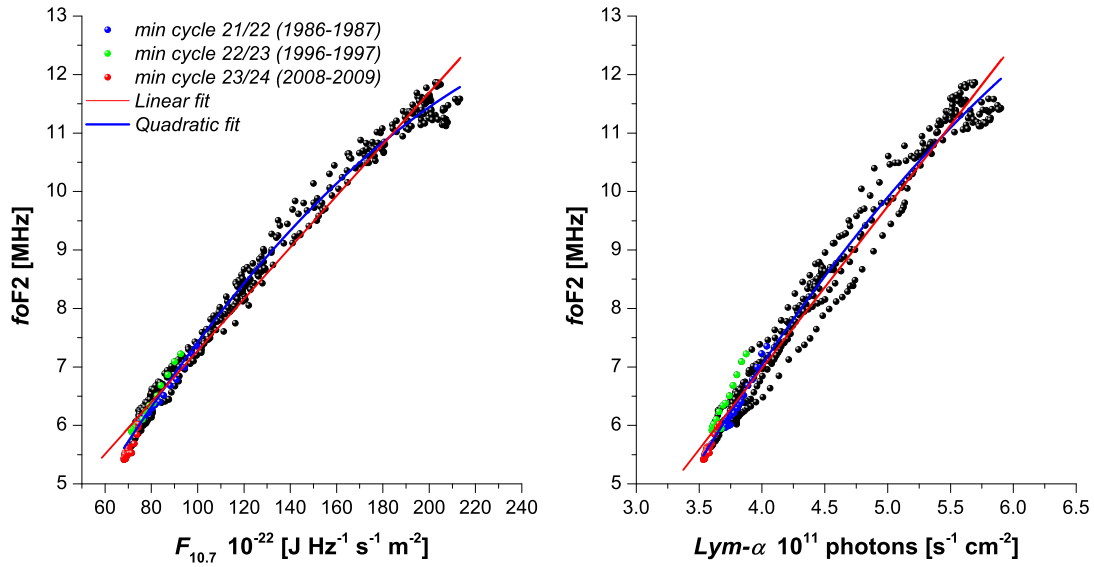
Figure 3.7: Linear (red line) and quadratic (blue curve) fit for the relations (*fo*F2 vs $F_{10.7}$) (left) and (*fo*F2 vs *Lym-α*) (right).
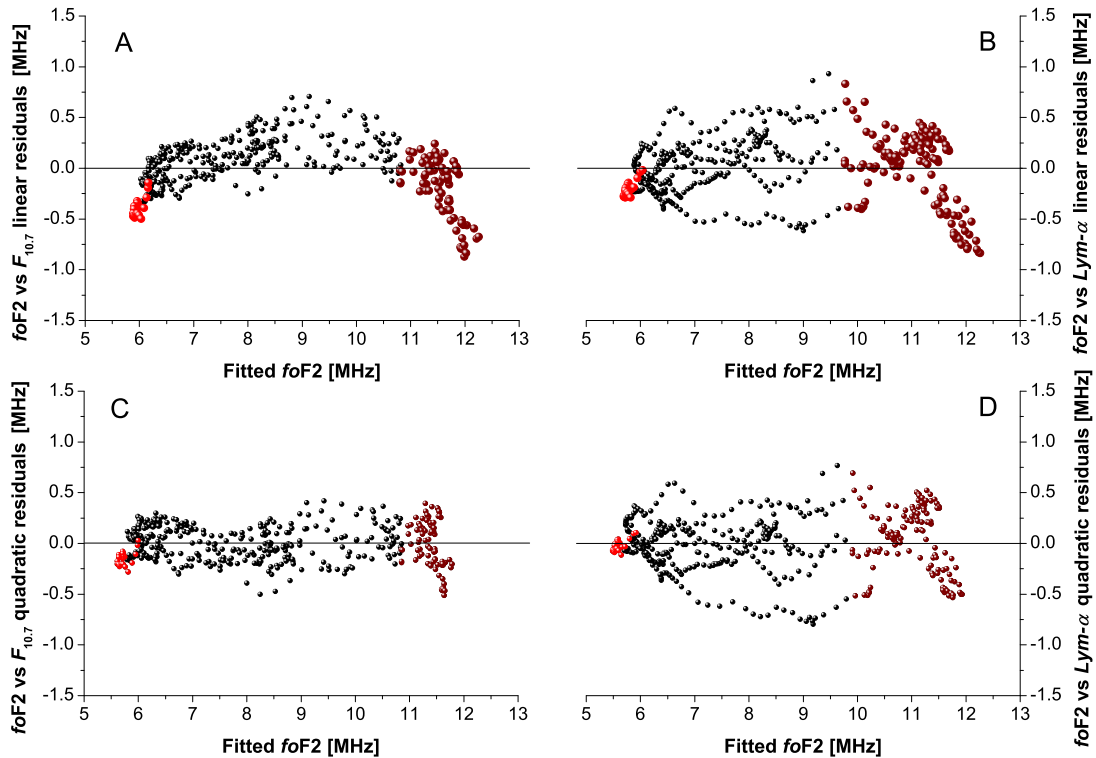
Figure 3.8: (A) Residuals for a linear fit applied to the scatterplot (*fo*F2 vs $F_{10.7}$). (B) Residuals for a linear fit applied to scatterplot (*fo*F2 vs *Lym-α*). (C) Residuals for a quadratic fit applied to the scatterplot (*fo*F2 vs $F_{10.7}$). (D) Residuals for a quadratic fit applied to the scatterplot (*fo*F2 vs *Lym-α*). Residuals are plotted as a function of fitted *fo*F2 values, so that the horizontal black line corresponds exactly with the values of the fit. Red and brown dots represent respectively the residuals related to the last solar minimum and to data influenced by the remaining saturation effect.

residuals of the corresponding quadratic fit (panel C and D for $F_{10.7}$ and *Lym-α* respectively). The plots confirm what it was previously observed, showing how the residuals for both the last solar minimum (red dots) and the remaining saturation effect (brown dots) are randomly distributed around the zero line only after the use of a quadratic fit. It is important to underline that, looking at panels B and D of Figure 3.8, the scatter of points around the zero line, due to the hysteresis effect, do not depend from the degree of the fit, so no improvements are obtained passing from a linear to a polynomial fit. The same situation is obtained using higher polynomial degree fits. This is a key aspect that we have to take into account searching for the best index to describe the variations of the parameter foF2. In particular, an index less affected by the hysteresis effect is preferable and further studies should consider the possibility to use two different relations, one for the ascending phase of a solar cycle and another one for the descending phase.

The key results obtained in this section can be summarized as follow:

- A linear fit is not appropriate to globally describe the (foF2 vs *Index*) relations;

- A quadratic (2° order polynomial) fit is the most appropriate to describe the (foF2 vs *Index*) relations;

- Using a quadratic fit both the very low solar activity values and the remaining saturation effect can be accurately described;

- It is not possible to reduce the hysteresis effect.

Starting from these partial results, the next step is the research of the best index to describe the variation of the ionospheric parameter foF2 at local noon at Rome station.

3.3   Looking for the best index to describe the variations of foF2

By virtue of the results obtained and reported in Section 3.2, the quadratic approximation has been chosen to represent the relations (foF2 vs *Index*). The following step consists in looking for the corresponding best solar index to describe the variations of foF2. In order to accomplish this task, two different approaches were considered and discussed, as it will be described in the Sections 3.3.1 and 3.3.2: (1) a comparison between observed and synthetic values of foF2; (2) the calculation of a particular parameter introduced by Solomon et al. (2013), hereafter called *R-Solomon*, for each of solar indices and foF2.

As it was previously said, continuous data for the solar radiation in EUV wavelengths are available only starting from 1996 with the launch of the SOHO/SEM mission. Moreover, in ionospheric and solar physics, the research of the "best proxy" for the EUV radiation is still an open problem. All these considerations bring to look for an index with a longer and more continuous dataset than that of solar EUV, but at the same time that is a good proxy for the variations of the solar radiation in these wavelengths. For many years, the sunspots number in solar physics and $F_{10.7}$ in ionospheric studies have been widely used as the best solar proxies for the EUV radiation, considering time-invariant relations. As reported by Chen et al. (2011a) and as it was previously shown, owing to the last solar minimum, there have been notable changes in the (*EUV* vs $F_{10.7}$) relationship, which demonstrated that $F_{10.7}$ can no more be considered a good proxy for EUV. In Section 3.3.3, brief considerations and results obtained in this work about this issue will be reported.

3.3.1   Comparison based on synthetic datasets

The first methodology used to find the best index to describe the variations of the parameter foF2, at local noon at the mid-latitude station of Rome, is a comparison between the 1-year running mean of foF2 obtained using validated values, and appropriate synthetic foF2 dataset obtained for every index.

The synthetic foF2 values were calculated for every index using analytical formulas that were obtained after fitting with a quadratic relation the scatterplot (foF2 vs $Index$), where only the first smoothed value of each month is used for both parameters. In order to test the forecasting power of every index, the fit is done by considering only data from January 1976 to June 2000 (dataset 1). The time period between July 2000 and December 2013 (dataset 2), including the descending phase of cycle 23, the anomalous minimum of solar cycle 23/24, and the ascending phase of cycle 24, was then considered as a validation window.

Figure 3.9 shows the two datasets and the quadratic fitting related to dataset 1 for the case (foF2 vs $F_{10.7}$). The fitting equation is also shown in the figure. The analytical formulas, obtained by fitting dataset 1 for every index, are reported in Table 3.4. Due to the short available dataset, it is not possible to obtain a reliable analytical formula for the $EUV_{0.1-50}$ index, and consequently this analysis is not carried out for this index and no corresponding synthetic foF2 values have been calculated.

Index	Quadratic regression (foF2 vs $Index$)$_{\text{Jan 76-Jun 00}}$
$F_{10.7}$	$fo\text{F2} = 1.161 + 0.075(F_{10.7}) - 1.175 \cdot 10^{-4}(F_{10.7})^2$
$Lym\text{-}\alpha$	$fo\text{F2} = -10.55 + 5.676(Lym\text{-}\alpha) + 0.318(Lym\text{-}\alpha)^2$
$MgII$	$fo\text{F2} = 1.439 \cdot 10^2 + 1.568 \cdot 10^3(MgII) - 3.819 \cdot 10^3(MgII)^2$
R	$fo\text{F2} = 5.273 + 0.055(R) - 8.946 \cdot 10^{-5}(R)^2$

Table 3.4: Analytical formulas found by fitting scatter plots (foF2 vs $Index$), from January 1976 to June 2000, with a 2° order polynomial. foF2 is expressed in [MHz], $F_{10.7}$ in [J Hz^{-1} s^{-1} m^{-2}], and $Lym\text{-}\alpha$ in [s^{-1} cm^{-2}].

Starting from these analytical relations, synthetic datasets of foF2 (one for each solar index) were then generated simply introducing in them smoothed (1-year running mean) daily measured values of the solar index. These synthetic values were then compared with the observed ones.

Figure 3.10 compares synthetic curves of foF2 with the observed ones at local noon in Rome. Looking at years of the last solar minimum, it is clear how the relation for $F_{10.7}$ gives an important overestimation of the observed values, while a better correspondence is found for $MgII$, $Lym\text{-}\alpha$ and R. In addition, it is interesting to notice also the following features: (1) a significant underestimation of the maximum of solar cycle 23 (years 2000-2001) made by the R synthetic dataset; (2) an overestimation of the minimum of solar cycle 21/22 (years 1986-1987) made by the $Lym\text{-}\alpha$ synthetic dataset; (3) a poor representation of the descending phase of solar cycle 21 and of maximum phases of solar cycles 21/22 and 22/23 made by the $Lym\text{-}\alpha$ synthetic dataset; (4) an underestimation of the maximum of solar cycle 21 (years 1979-1980) related to the synthetic dataset of indices $F_{10.7}$, $Lym\text{-}\alpha$ and R.

Figure 3.11 shows the results obtained focusing the attention on the validation window July 2000-December 2013 (left-side) and on the last solar minimum (right-side). On the right panel, synthetic foF2 values calculated by the analytical formula obtained after applying a linear fit on the (foF2 vs $F_{10.7}$) scatterplot, are also represented as an orange dashed curve. It is confirmed

$$fo\text{F2} = 1.161 + 0.075\,(F_{10.7}) - 1.175 \cdot 10^{-4}\,(F_{10.7})^2$$
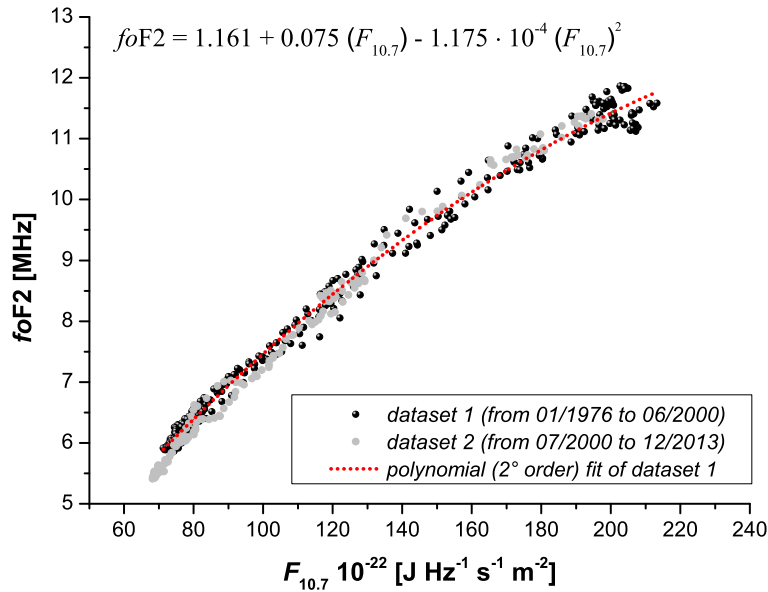
Figure 3.9: Scatterplot of (foF2 vs $F_{10.7}$). Black dots indicate data used for the fit (dataset 1, from January 1976 to June 2000), while grey dots indicate data excluded from the fit (dataset 2, from July 2000 to December 2013). The red dotted curve represents the quadratic fit of dataset 1. Only the first smoothed (1-year running mean) value of each month is plotted for both foF2 and $F_{10.7}$.
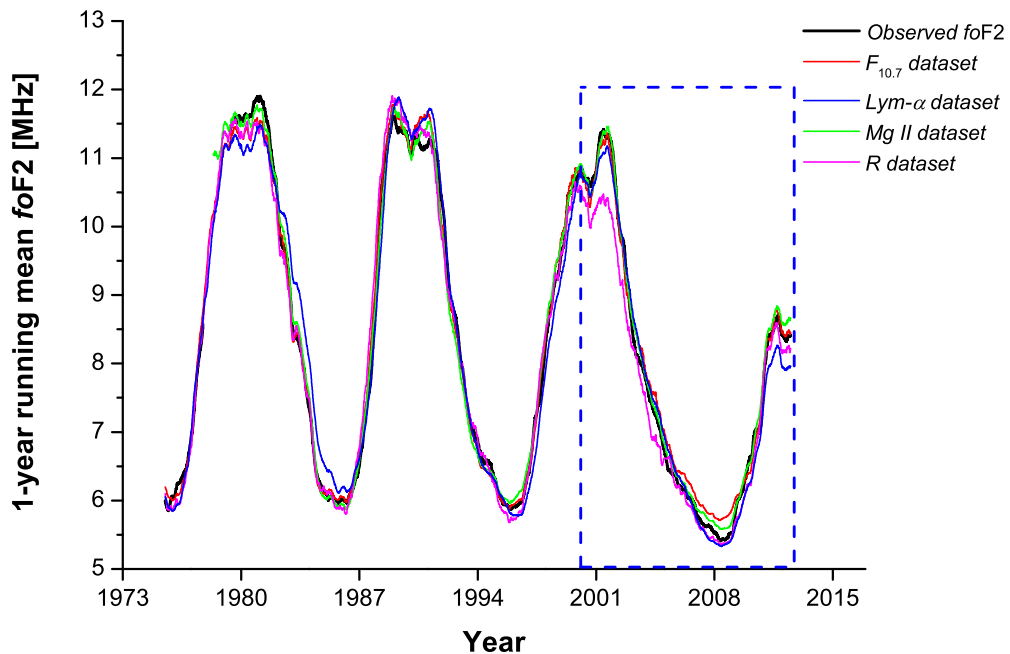
Figure 3.10: (black) 1-year running mean of the observed values of foF2 recorded at local noon at Rome compared with synthetic values of foF2 calculated using the quadratic relations shown in Table 3.4. The dashed blue box highlights the validation window between July 2000 and December 2013.

how, using a linear fit for the index $F_{10.7}$, huge overestimations are obtained, in particular for low solar activity. Contrariwise, for mid solar activity until the level of saturation, the results are similar to those related to the quadratic fit. In every case, it is interesting to underline that, even using a quadratic fit, the synthetic values provided by the index $F_{10.7}$ are higher than the observed ones. Therefore, $F_{10.7}$ seems to face a sort of saturation below a definite level of solar activity.

In general, Figure 3.10 and Figure 3.11 show how the goodness of a synthetic dataset is strongly linked to the solar activity level considered. As it was just discussed, the synthetic dataset provided by using the index $F_{10.7}$ is not appropriate for the very low solar activity of the last solar minimum, using both a linear and a quadratic fit. Contrariwise, good results are obtained for mid/high solar activity and for the minima 21/22 and 22/23, characterized by a higher activity than respect to the last one. The indices Lym-α and R show an opposite behavior with respect to $F_{10.7}$, providing very good results for low solar activity and less accurate correspondences for mid and high solar activity. The $MgII$ index seems to provide the best synthetic dataset for low, mid and high solar activity.
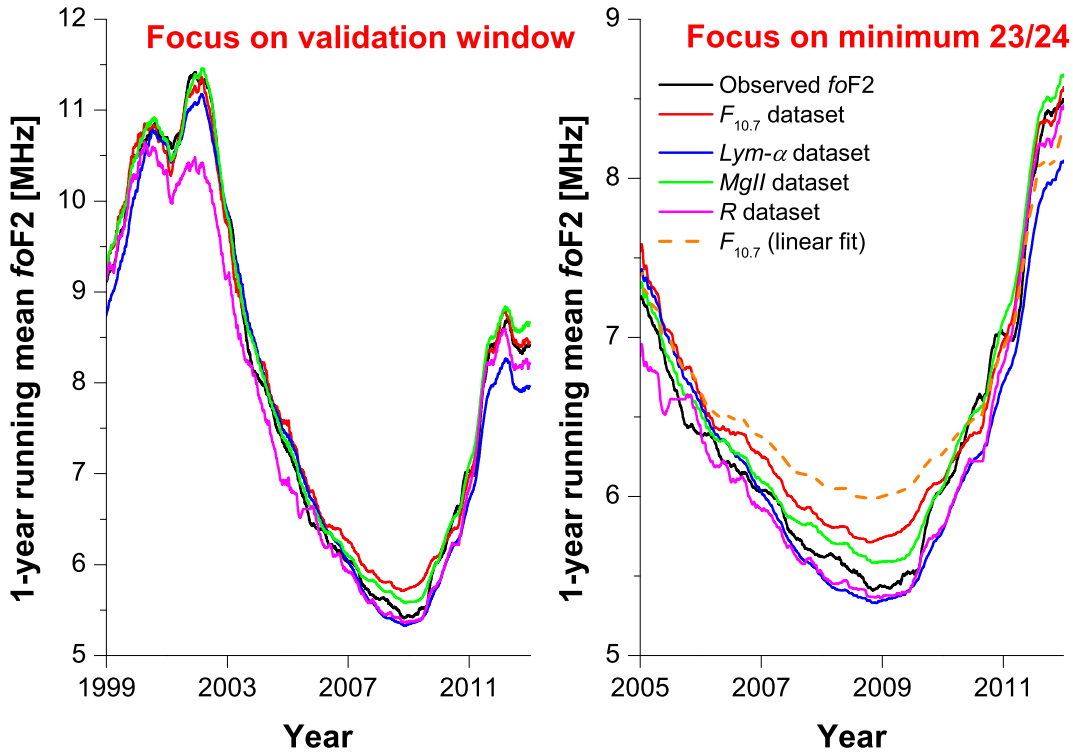
Figure 3.11: Same as Figure 3.10 but focused on validation window period July 2000-December 2013 (left) and on the last solar minimum (right). In the plot on the right-side, the dashed orange line represents the synthetic foF2 dataset obtained in the same manner of the other ones but using an analytical formula obtained after applying a linear fit on the (foF2 vs $F_{10.7}$) scatterplot.

To assess quantitatively the difference between synthetic and observed values of foF2, the corresponding absolute deviation was calculated. Hence, by averaging the daily deviations, mean deviations $\left(\sum_{i=1}^{n} |fo\mathrm{F2}_{\mathrm{syn}} - fo\mathrm{F2}_{\mathrm{obs}}|_i /n\right)_{\mathrm{SI}} = M_{\mathrm{SI}}$ (where n is the number of values and SI stands for Solar Index) were then calculated for the following periods: 1 January 2008-31

December 2009 (last solar minimum), 1 January 1976-31 December 2013 (complete dataset), and 1 July 2000-31 December 2013 (validation window). In this way, it is possible to find the best synthetic dataset and consequently the best solar index. The corresponding results are reported in Table 3.5, which shows that the good results characterizing the indices Lym-α and R for the last solar minimum, are not confirmed for the whole dataset. On the contrary, the acceptable result characterizing $F_{10.7}$ for the whole dataset is not confirmed for the last solar minimum. Specifically, $F_{10.7}$ seems to lose its sensibility, facing a saturation for variations of foF2 under a specific solar activity level of $\sim$82$\cdot$10^{-22} [J Hz^{-1} s^{-1} m^{-2}]. Overall, the best results are obtained for the $MgII$ index, which can satisfactorily represent the foF2 variations along all the considered solar cycles; at the same time, the $MgII$ index is characterized by a good representation of the last solar minimum. The mean deviation values related to the validation window, providing information about the "forecasting power" of the indices, further confirm that the $MgII$ is the best index to model the variations of foF2.

It is very important to underline how the mean absolute deviations for the time period 1976-2013 are strongly influenced by the hysteresis (in particular) and saturation (partially) effect. This explains the opposite results obtained in comparison with the period 2008-2009. In fact, low values of M_{SI} are observed for indices less afflicted in particular by the hysteresis effect ($F_{10.7}$ and $MgII$), while considerable higher values are obtained for indices characterized by a strong hysteresis (Lym-α and R). Therefore, the synthetic dataset provided by using the $MgII$ index is the best one, mainly because this is the index for which both the hysteresis effect and the saturation effect have the smallest impact.

Time period	$\mathbf{M}_{F_{10.7}}$	$\mathbf{M}_{Lym\text{-}\alpha}$	$\mathbf{M}_{MgII}$	$\mathbf{M}_R$
2008-2009	0.248	0.140	0.121	0.104
1976-2013	0.577	0.678	0.446	0.644
Validation window (Jul 2000-Dec 2013)	0.169	0.252	0.126	0.282

Table 3.5: Mean absolute deviations $\left(\sum_{i=1}^{n}|fo\mathrm{F2}_{\mathrm{syn}}-fo\mathrm{F2}_{\mathrm{obs}}|_i/n\right)_{\mathrm{SI}}=M_{\mathrm{SI}}$ in MHz between observed and synthetic foF2 values (where n is the number of values and SI stands for Solar Index), calculated by using analytical formulas shown in Table 3.4, for indices $F_{10.7}$, Lym-α, $MgII$ and R, for the very low solar activity of years 2008-2009, for the whole dataset (1 January 1976-31 December 2013), and for the validation window (1 July 2000-31 December 2013).

3.3.2   Comparison based on the R-Solomon parameter

In order to compare in a consistent way the variations of solar indices for the entire cycle 23, from minimum (22/23) to minimum (23/24), Solomon et al. (2013) introduced the following parameter:

$$R - \mathrm{Solomon} = \frac{i(2008) - i(2009)}{i(2001) - i(1996)}, \tag{3.2}$$

where $i(\cdot)$ represents the annual average of the generic solar index (or generic parameter) i for the year indicated in brackets. Hence, the difference of the annual average value of each index in 2008 and 1996, that identify respectively minima of solar cycles 23/24 and 22/23, is divided by the expected solar cycle range of the index, as estimated by the difference between the annual average in the solar maximum year of 2001 and in 1996. The values obtained for the

R-Solomon parameter for each of solar indices are: $R_{F_{10.7}}$=-0.028, R_R=-0.056, R_{MgII}=-0.058, $R_{Lym-\alpha}$=-0.071, and $R_{EUV_{0.1-50}}$=-0.123. A negative value of the R-Solomon parameter means a lower value of the physical characteristics for the last solar minimum than for the previous one. With the aim to compare solar indices variations to that of foF2, in addition to what was done by Solomon et al. (2013), the R-Solomon parameter was calculated also for foF2 at local noon, obtaining R_{foF2}=-0.074, which is a value well correlated with those of $MgII$ and $Lym-\alpha$. Specifically, Table 3.6 reports the values of the R-Solomon parameter for all the solar indices under investigation, and for foF2, with the corresponding averages for years 2008 (minimum 23/24), 1996 (minimum 22/23) and 2001 (maximum cycle 23) used to calculate it.

Physical characteristic	2008 avg (min cycle 23/24)	1996 avg (min cycle 22/23)	2001 avg (max solar cycle 23)	R-Solomon parameter
foF2	5.52	5.89	10.82	-0.074
$F_{10.7}$	69.06	72.27	181.10	-0.028
$Lym-\alpha$	3.49	3.61	5.34	-0.071
$MgII$	0.1508	0.1516	0.1648	-0.058
R	2.85	8.63	111.00	-0.056
$EUV_{0.1-50}$	1.82	2.22	5.78	-0.123

Table 3.6: 2008, 1996, 2001 yearly averages and R-Solomon parameter for all solar indices under investigation, and for foF2 as measured at local noon at Rome. foF2 is in MHz, $F_{10.7}$ is in 10^{-22} [J Hz^{-1} s^{-1} m^{-2}], $Lym-\alpha$ is in 10^{11} photons [s^{-1} cm^{-2}] and $EUV_{0.1-50}$ is in 10^{10} photons [s^{-1} cm^{-2}].

The most striking feature coming out from Table 3.6 is that the index $F_{10.7}$ confirms its poor ability to follow correctly the variations of foF2 for low solar activity, especially those characterizing the anomalous and prolonged last solar minimum. Surprisingly, the R-Solomon parameter for $EUV_{0.1-50}$ is quite higher than the one for foF2. The reason could be found again in the potential degradation of the SOHO/SEM instrument. In particular, it is possible that an underestimation of the value for the year 2008 occurred, which means an overestimation made by the R-Solomon parameter.

The fact that, according to the R-Solomon parameter, foF2 variations correlate well with those of $MgII$ and $Lym-\alpha$ confirms what was found in the previous section and shown in Figures 3.10 and 3.11, namely that in the period considered by the R-Solomon parameter the foF2 observed values are well represented by synthetic values related to both $MgII$ and $Lym-\alpha$.

Hence, the R-Solomon parameter analysis suggests that $MgII$ and $Lym-\alpha$ can be considered as the best candidates to describe the variations of foF2. This result, combined with the one achieved in the previous section, suggests that $MgII$ is the best index to describe the dependence of foF2 on solar activity.

3.3.3 Considerations on the best proxy for the EUV solar radiation

The results reported in the previous sections give us the possibility to do some interesting considerations about the aforementioned problem of the research of the best proxy for the solar radiation in the EUV wavelengths.

As it was claimed in Section 3.2.1, some solar EUV irradiance models rely on the assumption that the relation between solar EUV indices and $F_{10.7}$ is invariant over different solar cycles (Chen et al., 2011a). Figure 3.12 reports the scatterplot ($EUV_{0.1-50}$ vs $F_{10.7}$) for the ascending

phases of the solar cycle 23 (black dots) and 24 (green dots). For the two distributions, a linear (red line) and a quadratic (blue curve) fit is done, with the correspondent *Adj. R-Square* parameter displayed. The main feature highlighted by Figure 3.12 is the change in the relationship passing from cycle 23 to 24. For the ascending solar cycle 23, a linear and a quadratic fit provide the same result, with the parameter *Adj. R-Square* passing from 0.99489 (linear fit) to 0.99490 (quadratic fit). For the ascending solar cycle 24, there is a clear change in the relationship, with the quadratic fit (*Adj. R-Square* = 0.99725) which is much more accurate than the linear one (*Adj. R-Square* = 0.99318).

Figure 3.13 is the same as Figure 3.12 but for ($EUV_{0.1-50}$ vs $MgII$). In this case a different pattern is observed, in particular the figure underlines how the relation between these two indices can be considered constant with the time; in fact, the *Adj. R-Square* parameter gives the same inter-cycle results for both the linear (0.99251 for ascending cycle 23 and 0.99219 for ascending cycle 24) and quadratic fit (0.99549 for ascending cycle 23 and 0.99432 for ascending cycle 24).

A comparison of the results obtained for all the four indices ($F_{10.7}$, Lym-α, $MgII$ and R; plots not shown) points out how improved results are obtained using a quadratic relation between $EUV_{0.1-50}$ and the indices, for both ascending cycles 23 and 24. The best result, in term of the *Adj. R-Square* parameter, is obtained using the index Lym-α for the ascending cycle 24 (0.99957), while the worst results are encountered using the index R.

As it was already said, the index $MgII$ is the only one that shows similar results for the ascending cycle 23 and 24, therefore providing a constant relation with the EUV radiation in the wavelengths 0.1-50 nm.
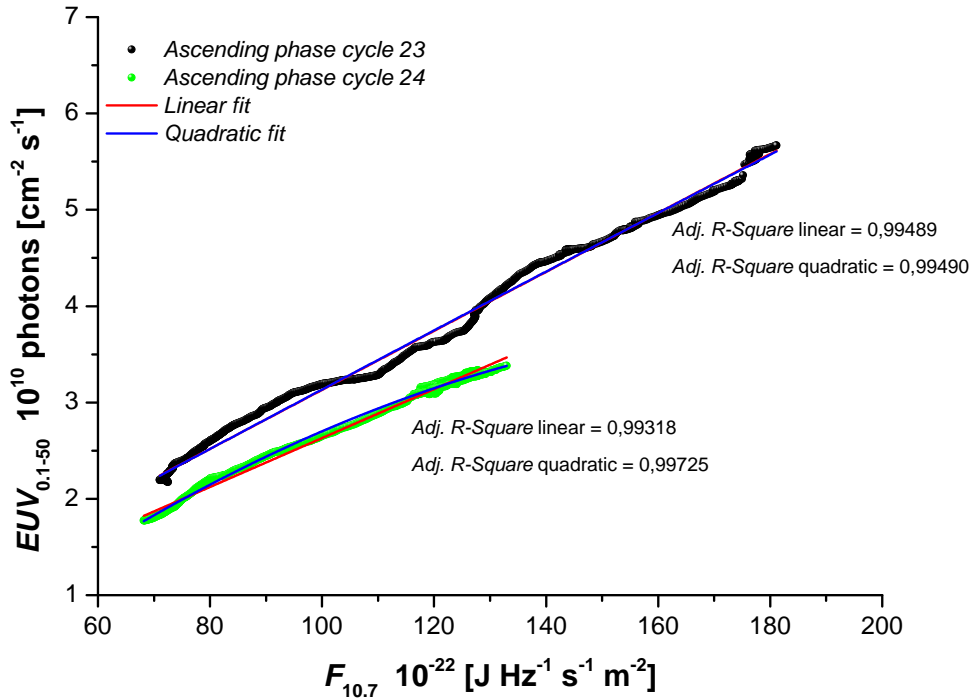

Figure 3.12: Scatterplot ($EUV_{0.1-50}$ vs $F_{10.7}$) for the ascending cycle 23 (black dots) and 24 (green dots). For every distribution a linear and a quadratic fit are displayed with a red line and a blue curve respectively. The value of the *Adj. R-Square* parameter is reported for every fit.
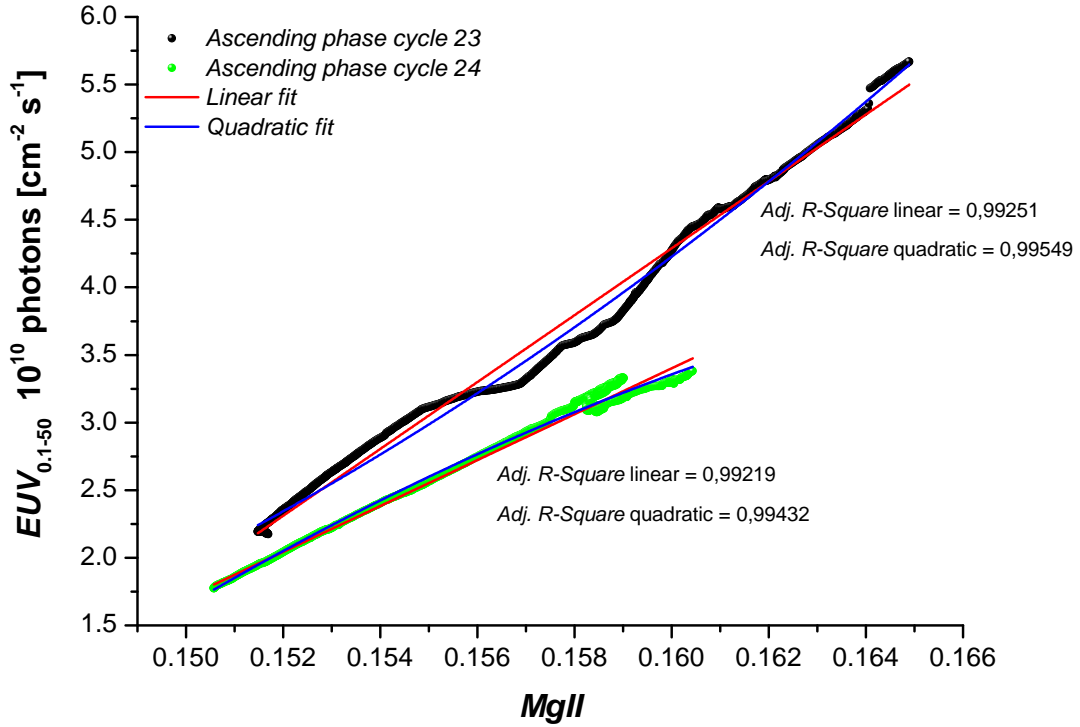
Figure 3.13: Same as Figure 3.12 for the relation ($EUV_{0.1-50}$ vs $MgII$).

Additional information can be retrieved from the R-Solomon parameter values reported in Table 3.6. In this case, it emerges that the index $F_{10.7}$ provides a poor agreement (-0.028) with the index $EUV_{0.1-50}$ (-0.123), while Lym-α, $MgII$ and R provides better results (-0.071, -0.058 and -0.056, respectively).

Considering both the R-Solomon parameter indications and the inter-cycle constant behavior, it is possible to say that, besides being the best index to represent the foF2 variability, $MgII$ can be also considered a good solar proxy for the radiation in the EUV band. Contrariwise, accordingly to Chen et al. (2011a) and Solomon et al. (2013), $F_{10.7}$ should not be considered for this purpose, in particular when low solar activity levels occur.

However, it is intention of the author to underline once again how the solar EUV data are frequently re-calibrated to correct possible instrument degradation, so the reported results have to be considered only qualitative; moreover, the available dataset is quite short ($\sim$20 years), covering only one complete solar cycle (solar cycle 23) and partially the current solar cycle 24. Further studies and a longer dataset are necessary to accurately assess and find the best proxy for the solar EUV radiation.

3.4 Brief outline of additional analyses carried out

In this section, additional analyses carried out during the Ph.D. work, linked to the main study of the relations (foF2 vs $Index$) and to the research of the best index for the foF2 variations, will be reported.

In detail, the following issues will be briefly discussed: (1) the possibility to use a system of

analytical relations to describe the foF2 variations; (2) the analysis of the relationships foF2 (01 LT) vs *Index* and foF2 (19 LT) vs *Index*; (3) the analysis of the relationships NmF2 (12 LT) vs *Index* and hmF2 (12 LT) vs *Index*; (4) the influence of the geomagnetic activity, with an example of a synthetic dataset obtained using a two-variable fit, linear in the geomagnetic activity and quadratic in the solar activity.

3.4.1   Systems of analytical relations

As it was reported in Section 3.3.1 and confirmed by the mean absolute deviation values listed in Table 3.5, considering the whole period 1976-2013, the index $MgII$ provides the best synthetic dataset for foF2 at local noon. However, the goodness of a synthetic dataset is strictly linked to the level of solar activity: $F_{10.7}$ works properly for mid and high solar activity, while $MgII$, Lym-α and R show good results in particular for low solar activity. Therefore, attempts have been done using systems of analytical relations that require the "switch" of the relation for a definite level of solar activity.

Here it is discussed the case of a system composed of an analytical quadratic relation for the index $F_{10.7}$ for high solar activity ($F_{10.7} \geq 120 \cdot 10^{-22}$ [J s^{-1} Hz^{-1} m^{-2}]) and for the index Lym-α for low solar activity ($F_{10.7} < 120 \cdot 10^{-22}$ [J s^{-1} Hz^{-1} m^{-2}]). The analytical formulas used are:

$$fo\text{F2} \cong 1.16 + 0.07(F_{10.7}) - 1.17 \cdot 10^{-4}(F_{10.7})^2 \text{ for } F_{10.7} \geq 120 \cdot 10^{-22}[\text{J s}^{-1}\text{Hz}^{-1}\text{m}^{-2}]; \quad (3.3\text{a})$$

$$fo\text{F2} \cong -10.55 + 5.68(Lym\text{-}\alpha) - 0.32(Lym\text{-}\alpha)^2 \text{ for } F_{10.7} < 120 \cdot 10^{-22}[\text{J s}^{-1}\text{Hz}^{-1}\text{m}^{-2}]. \quad (3.3\text{b})$$

The synthetic foF2 dataset obtained using this system is plotted and compared with observed values in Figure 3.14. In the figure only the first smoothed value of the month is displayed, in order to emphasize the main problem faced using a system of equations, that is the clear discontinuity for solar activity levels near the "switch" point $F_{10.7} = 120 \cdot 10^{-22}$ [J s^{-1} Hz^{-1} m^{-2}] (green circles). The discontinuity in the passage from relation (3.3a) to relation (3.3b) (and vice versa) can appear either as a superimposition of the synthetic datasets provided by the two relations (first green circle on the left) or as holes for some ranges of solar activity.

Owing to these issues characterizing the switch point, there is not an improvement of the accuracy of the synthetic dataset with respect to the ones obtained using a single quadratic analytical relation. However, it is important to underline that, when choosing a solar index for an ionospheric model, the level of solar activity has to be taken into account by virtue of the fact that some indices could be not indicated for some ranges, such as $F_{10.7}$ for low solar activity.

3.4.2   *fo*F2 (at 01 LT and 19 LT) vs *Index*

In previous sections, attention has been paid to the analysis of relations (foF2 vs *Index*), considering the parameter foF2 at local noon. As it was mentioned, this is the choice that gives the most reliable results for two main reasons: (1) usually the daily solar activity index value refers to data registered at local noon; (2) the 12 LT is the hour of the day usually considered in long-term trend studies of the ionospheric parameters.

Nevertheless, during the Ph.D. work, analyses have been carried out also for the relations foF2 (01 LT) vs *Index* and foF2 (19 LT) vs *Index*. Both 01 LT and 19 LT have been chosen considering the continuity of validated values available for the Rome ionosonde, and with the
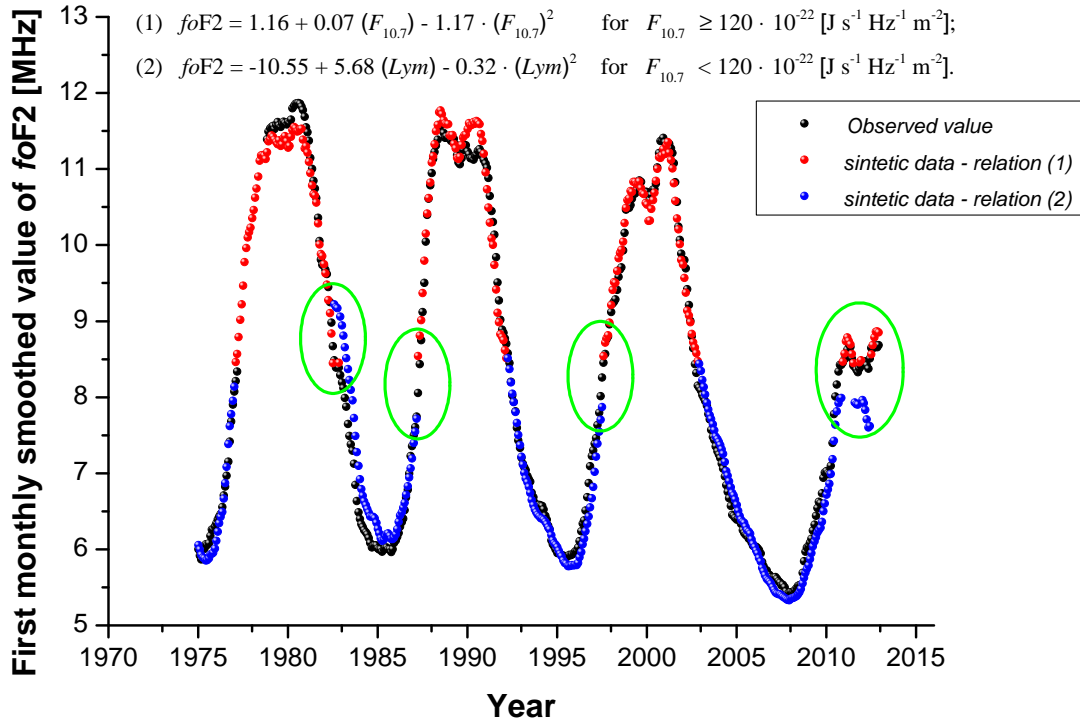
Figure 3.14: Synthetic and observed *fo*F2 datasets for the period January 1976-December 2013. The synthetic dataset has been obtained using the relation for the index $F_{10.7}$ (equation (3.3a); red dots) for high solar activity ($F_{10.7} \geq 120 \cdot 10^{-22}$ [J s^{-1} Hz^{-1} m^{-2}]) and for the index Lym-α (equation (3.3b); blue dots) for low solar activity ($F_{10.7} < 120 \cdot 10^{-22}$ [J s^{-1} Hz^{-1} m^{-2}]). Only the first smoothed value of the month is plotted. Green circles emphasize the discontinuity characterizing the passage from equation (3.3a) to equation (3.3b) and vice versa.

aim to describe the nighttime ionosphere (01 LT) and the sunset hour (19 LT) that is interested by very particular and variable ionospheric conditions, owing to the solar terminator passage[2]. Therefore, it is interesting to briefly report the results obtained.

Figure 3.15 shows the scatterplots *fo*F2 (01 LT) vs $F_{10.7}$ and *fo*F2 (19 LT) vs $F_{10.7}$, with the correspondent linear (red line) and quadratic (blue curve) fit. The first smoothed value of each month is plotted, with values for the last three minima emphasized. Comparing Figure 3.15 with the plot for *fo*F2 at local noon (left panel of Figure 3.7), the loss of linearity for the last minimum is more pronounced, in particular at 19 LT. A linear fit provides clear overestimations considering the last minimum, with a quadratic fit providing better results but again with a slightly overestimation. Furthermore, it is very interesting to observe how the saturation effect is less pronounced for both 01 and 19 LT than at 12 LT, while no differences are observed about the hysteresis effect at mid solar activity.

The same analyses carried out for other indices (plots not reported) show that: (1) the deviation from linearity is more pronounced at 01 LT and 19 LT than at 12 LT; (2) a quadratic fit provides better results than a linear one for the very low solar activity of the last minimum, but slight overestimations are still obtained, in particular at 19 LT; (3) the saturation effect is

---

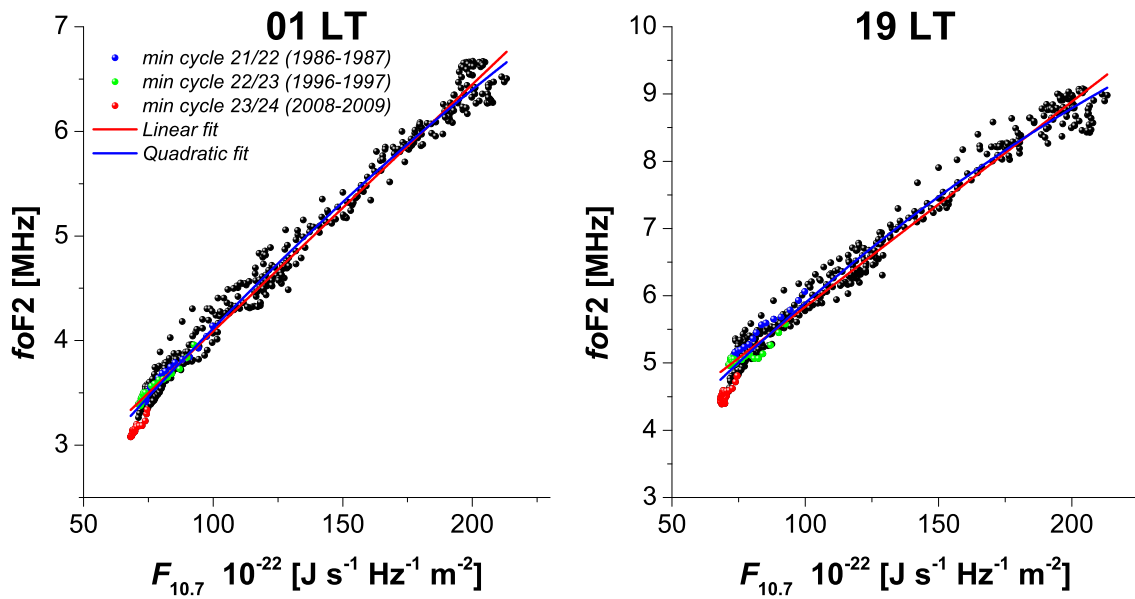[2]Similar conditions are observed for sunrise hour (06 LT).

Figure 3.15: *fo*F2 (01 LT) vs $F_{10.7}$ and *fo*F2 (19 LT) vs $F_{10.7}$. Red line and blue curve identify a linear and a quadratic fit respectively.
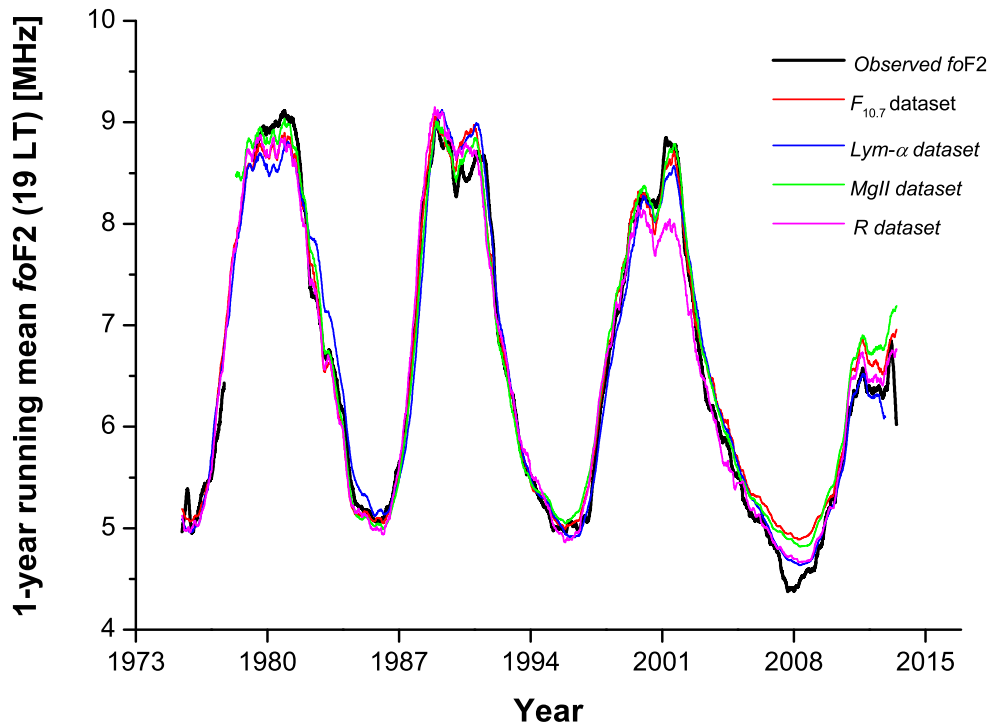

Figure 3.16: Synthetic datasets obtained using a quadratic fit for the relations (*fo*F2 (19 LT) vs *Index*) along with the corresponding observed values.

2008-2009				
Hour/Index	$F_{10.7}$	*Lym-α*	*MgII*	*R*
01:00 LT	0.253	0.056	0.197	0.087
12:00 LT	0.248	0.140	0.121	0.104
19:00 LT	0.425	0.169	0.357	0.200
Avg on three hours	0.309	0.122	0.225	0.130
1976-2013				
Hour/Index	$F_{10.7}$	*Lym-α*	*MgII*	*R*
01:00 LT	0.108	0.143	0.110	0.111
12:00 LT	0.577	0.678	0.446	0.644
19:00 LT	0.494	0.503	0.408	0.502
Avg on three hours	0.393	0.442	0.321	0.419

Table 3.7: Mean absolute deviations $\left(\sum_{i=1}^{n}|fo\mathrm{F2}_{\mathrm{syn}}-fo\mathrm{F2}_{\mathrm{obs}}|_i/n\right)_{\mathrm{SI}}=M_{\mathrm{SI}}$ in MHz between observed and synthetic foF2 values. Results for the last solar minimum (2008-2009) and for the complete period 1976-2013 are reported for 01, 12 and 19 LT.

less pronounced at 01 and 19 LT than at 12 LT; (4) the hysteresis effect remains unaltered at all hours; (5) using a quadratic fit, $MgII$, Lym-α and R provide the best results for low solar activity.

Figure 3.16 shows synthetic foF2 values, obtained using the same procedure described in Section 3.3.1, for every index, compared to observed values. The results show how for the last solar minimum, also using a quadratic fit, clear overestimations are obtained. Better results are obtained using Lym-α and R indices. The results obtained at 01 LT (not shown) are very similar to those shown in Figure 3.16 for 19 LT.

To quantify the differences between synthetic datasets and observed values, mean absolute deviations have been calculated. Table 3.7 reports mean absolute deviations for 01, 12 and 19 LT, for the last solar minimum (2008-2009) and the complete (1976-2013) period. Results for the validation window (July 2000-December 2013) are not reported here but they are very similar to those of the complete period. Table 3.7 shows that, considering the period 1976-2013 and the three hours analyzed, the $MgII$ index provides the best synthetic dataset to describe the variations of foF2. In this case, the poor influence of the hysteresis effect represents the most important reason behind these results. Nevertheless, for 01 and 19 LT and for the very low solar activity years of the last minimum, a better choice can be done, using either Lym-α or R. However, as it was previously pointed out, the use of a system of analytical relations is not recommended and $MgII$ provides, in author's opinion, the best choice. Nevertheless, attention must be paid when using $MgII$ for very low solar activity for 19 LT, when relevant deviations from observed values are observed. It is at the same time confirmed and emphasized that $F_{10.7}$ is not a good choice in every case and alternative indices should be considered.

3.4.3 Relationships (*Nm*F2 vs *Index*) and (*hm*F2 vs *Index*)

foF2 represents the main ionospheric parameter and the study of its dependence on the main ionospheric controller, the solar activity, is of primary importance. Nevertheless, during the Ph.D. work, short analyses on the relations (*Nm*F2 vs *Index*) and (*hm*F2 vs *Index*) have been

carried out, even though they do not represent the focus of the Ph.D. project.

As reported in Sections 1.1.2 and 1.3, NmF2 can be calculated from foF2 using the plasma frequency relation NmF2 $[\text{m}^{-3}] = 1.24 \cdot 10^{10} \ (fo$F2 $[\text{MHz}])^2$. For the parameter hmF2, it is possible to use values given as output by ionogram inversions, which are however available only for short periods, or those calculated by using analytical formulations. The dataset available for NmF2 for the Rome station is the same as for foF2, with data from January 1976 to December 2013. For hmF2, the use of analytical formulations is necessary because, to study the relations (hmF2 vs $Index$), a long dataset is essential. Thanks to its very easy formulation, the Shimazaki analytical formula, that needs as input the parameters foF2 and MUF(3000)F2, gives the possibility to have for hmF2 the same long and continuous dataset available for foF2 and NmF2. The results that are shown refer only to ionospheric parameters recorded at Rome at local noon.

Figures 3.17 and 3.18 show the relations of NmF2 (at 12 LT) as a function of the indices $F_{10.7}$ (Figure 3.17) and $MgII$ (Figure 3.18); as usual, only the first smoothed value of each month is plotted and, as for the plot of foF2, blue, green and red dots refer to the min 21/22, 22/23 and 23/24 respectively. Red line and blue curve are a linear and a quadratic fit of the scatterplot.
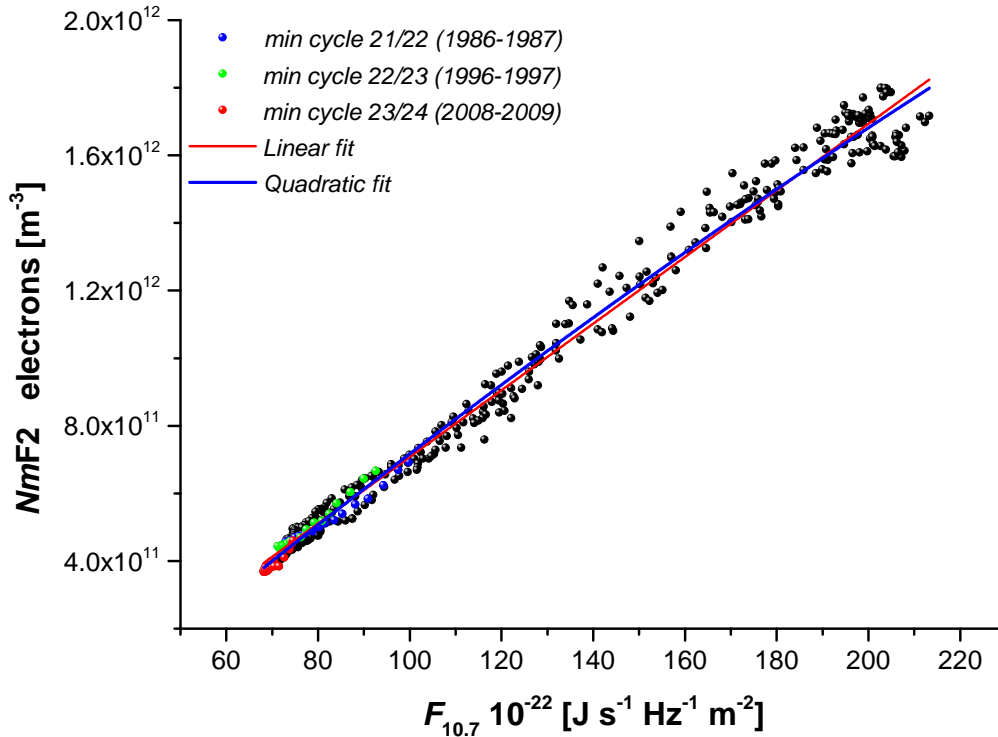

Figure 3.17: Scatter plot (NmF2 (12 LT) vs $F_{10.7}$). Blue, green and red dots represent values for minima of solar cycles 21/22, 22/23 and 23/24 respectively. The linear and quadratic fit of the whole dataset are highlighted by the red line and blue curve respectively. For both foF2 and $F_{10.7}$ only the first smoothed (1-year running mean) value of each month is considered.

The most important feature highlighted by the figures is that for NmF2 there are not clear differences between a linear and a quadratic fit, contrariwise to the results for foF2. As an
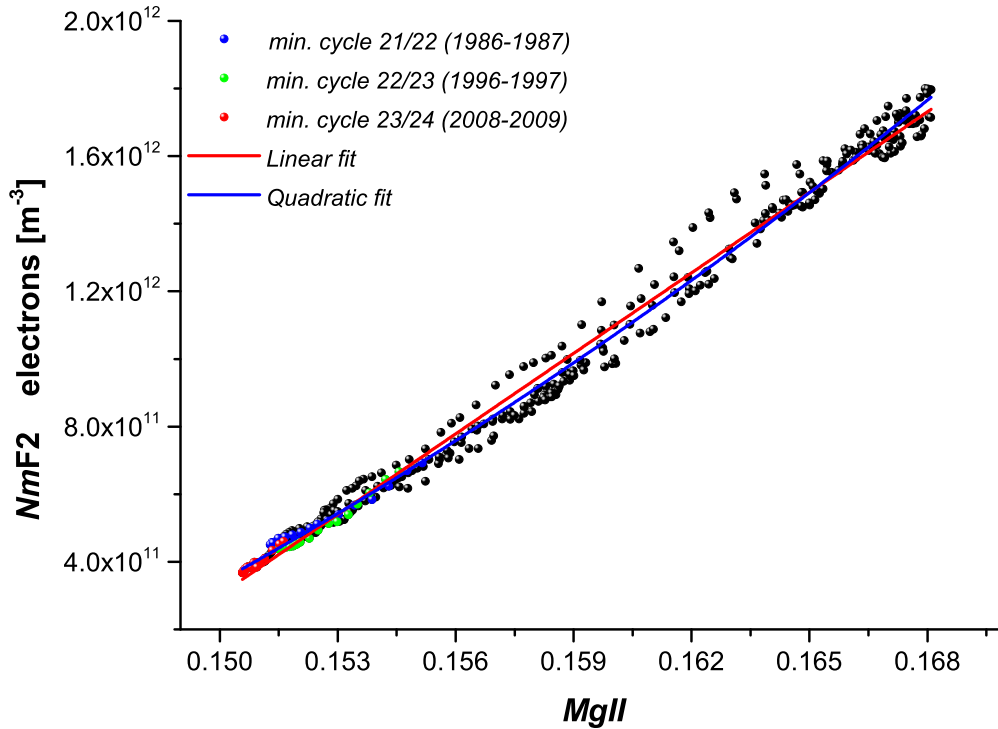
Figure 3.18: Same as Figure 3.17 for (NmF2 (12 LT) vs $MgII$).

example, for the index $F_{10.7}$ the value of the *Adj. R-Square* parameter is 0.98935 for a linear fit and 0.98987 for a quadratic fit, and for the index $MgII$ is 0.99029 (linear fit) and 0.99216 (quadratic fit). Therefore, the use of a linear relation (NmF2 vs *Index*) can be still considered a good choice and no clear improvements are obtained using a polynomial relation.

The analysis of the relations (foF2 vs *Index*) revealed that a quadratic fit results the best one because it is able to correctly describe the values for high solar activity (saturation effect) and for the very low solar activity of the last solar minimum. Using the parameter NmF2, both effects are no more visible. This is obviously due to the quadratic relation between foF2 and NmF2. These results give use the possibility to claim that by considering the relation (foF2 vs *Index*), the remaining saturation effect and values for very low solar activity can be considered both second order effects.

Using the Shimazaki analytical formulation for the parameter hmF2, plots like the one shown in Figure 3.19 between hmF2 and R have been obtained.

The use of analytical formulations for hmF2 has the advantage to provide, in an easy way, values for very long periods. Nevertheless, a loss of accuracy can be relevant. As a consequence, a wide spread of the scatter plot is obtained, which makes extremely difficult to obtain reliable analytical relations. However, Figure 3.19 shows how (1) also for hmF2 the values for the last solar minimum are particularly lower than those of previous minima and (2) for high solar activity no saturation effect is visible. The first feature will be deeply examined in the Chapter 5, when an inter-minima comparison for the main ionospheric parameters will be carried out, while the second feature is not a surprising result because the saturation is a characteristic of the ionospheric parameter foF2.
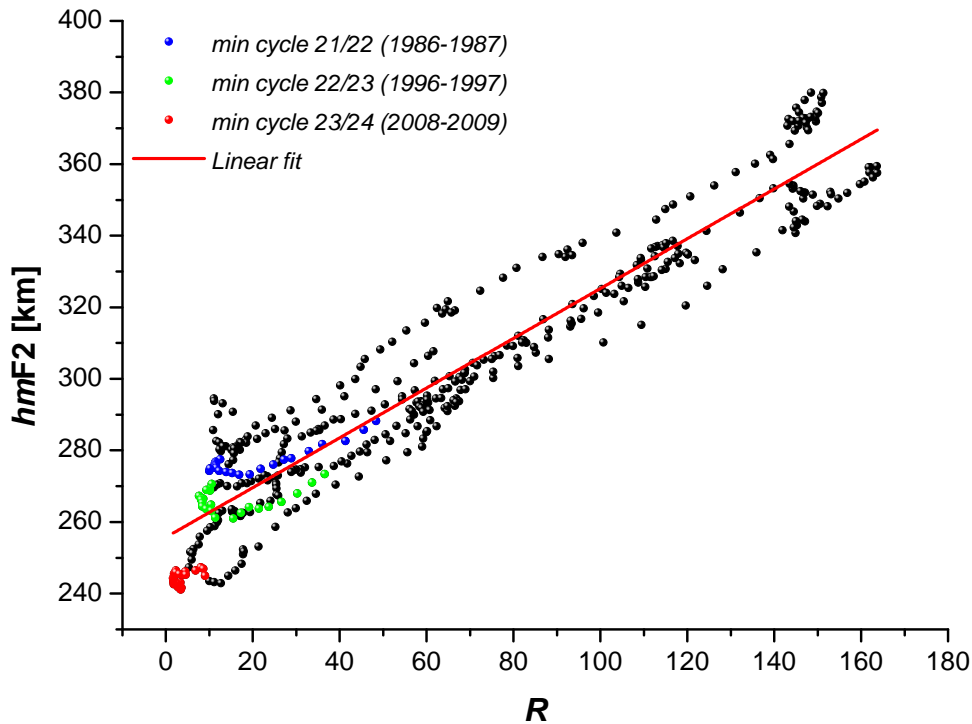
Figure 3.19: Scatter plot (hmF2 (12 LT) vs R). Blue, green and red dots represent values for minima of solar cycles 21/22, 22/23 and 23/24 respectively. The linear fit of the whole dataset is highlighted by the red line. For both parameters, only the first smoothed value of each month is considered. For hmF2, the Shimazaki analytical formulation has been used.

3.4.4   Geomagnetic activity influence

The solar activity represents the main driver of the ionosphere and it strongly affects the variability of the corresponding parameters. Nevertheless, under particular conditions and for short period analyses, the geomagnetic activity should be also taken into account. In particular, the ionospheric parameters can show very different behaviors under disturbed geomagnetic conditions than for quiet conditions.

In this work, the primary aim is the study of the foF2 parameter dependence on solar activity. As a first approach, the geomagnetic activity has not been considered, because using a 1-year running mean all the short-period geomagnetic disturbances (such as those related to geomagnetic storms) are completely eliminated. However, some attempts using a two-variable regression and calculating the correspondent synthetic dataset have been carried out. In particular, a comparison with the synthetic dataset obtained with the simple quadratic fit between (foF2 vs *Index*) will be shown. A priori, a coincidence of the two synthetic datasets it is expected.

Figure 3.20 shows the dependence of foF2 (at 12 LT in Rome) on solar activity (solar index $F_{10.7}$), displayed by blue dots in the YZ projection plane, and on geomagnetic activity (geomagnetic index Ap), displayed by green dots in ZX projection plane. Daily values of the Ap index have been provided by the *World Data Center for Geomagnetism-Kyoto* and downloaded at website http://wdc.kugi.kyoto-u.ac.jp/kp/.

To understand how the geomagnetic activity can be considered influent in comparison to the solar activity, two different synthetic datasets have been calculated and compared to the observed values of foF2 at local noon. The first synthetic dataset is the same previously calculated using a quadratic relation (foF2 vs $Index$); the second one has been obtained using a regression with two variables (the solar $Index$ and the geomagnetic index Ap), by considering a quadratic dependence on the solar index and a linear dependence on the geomagnetic index Ap. The relation can be then simply expressed by:

$$fo\text{F2}(I, Ap) = C_0 + C_1 I + C_2 I^2 + C_3 Ap, \tag{3.4}$$

where I represents the solar activity index, Ap is the geomagnetic index, C_0, C_1, C_2 and C_3 are constant values.

The results obtained are shown in Figure 3.21 using the index $F_{10.7}$. It is clear how there are not differences in the two synthetic datasets. Therefore, it is possible to claim that, using a 1-year running mean when studying the dependence of the parameter foF2 on solar activity, the geomagnetic activity can be considered irrelevant.

The analyses carried out using other solar activity indices confirm the results obtained for $F_{10.7}$, that is using a two-variable regression an improvement of the synthetic dataset is never obtained.

However, it is important to underline that the situation is completely different when monthly average or median values are used and, in these cases, the geomagnetic activity can affect foF2 as much as the solar activity. At the same time, an alternative approach to explain the long-term ionospheric trends has been proposed and developed by Danilov and Mikhailov (1999, 2001), Mikhailov and Marin (2000, 2001), Mikhailov (2002, 2006), Mikhailov and de la Morena (2003). We are talking about the so-called geomagnetic control concept, which explains the main morphological features of the ionospheric trends in the F2 and E regions by natural variations of solar and geomagnetic activity in the framework of contemporary ionospheric storm mechanisms (Mikhailov, 2006). In the geomagnetic control concept, usually very long-time running means (11-year or more) are applied to observe periodic variations in the geomagnetic activity that can be linked with long-term trends characterizing the ionospheric parameters foF2 and hmF2.

A deep analysis of the geomagnetic activity control of the foF2 variability lies outside the purpose of the present work. Anyhow, it is important to underline once again that using a 1-year running mean for the foF2 time series, the geomagnetic activity can be considered irrelevant if compared with the solar activity, which is the main driver to which we are interested in.

3.5 Conclusions

The study of the relations between ionospheric characteristics and solar activity indices is of primary importance to improve ionospheric models. In this chapter five different widely used solar indices ($F_{10.7}$, $MgII$, Lym-α, R and $EUV_{0.1-50}$) have been considered and, relying on a long, continuous and very reliable dataset of foF2 values recorded at the ionospheric station of Rome between January 1976 and December 2013 at local noon, it was shown that, in order to properly approximate the relations (foF2 vs $Index$), a quadratic polynomial is better than a linear fit. In fact, the use of linear relations, widely utilized as input for both several ionospheric models and trend analyses, can cause a significant overestimation of observed data, mainly because of the saturation effect at high solar activity and the unusual low solar activities like
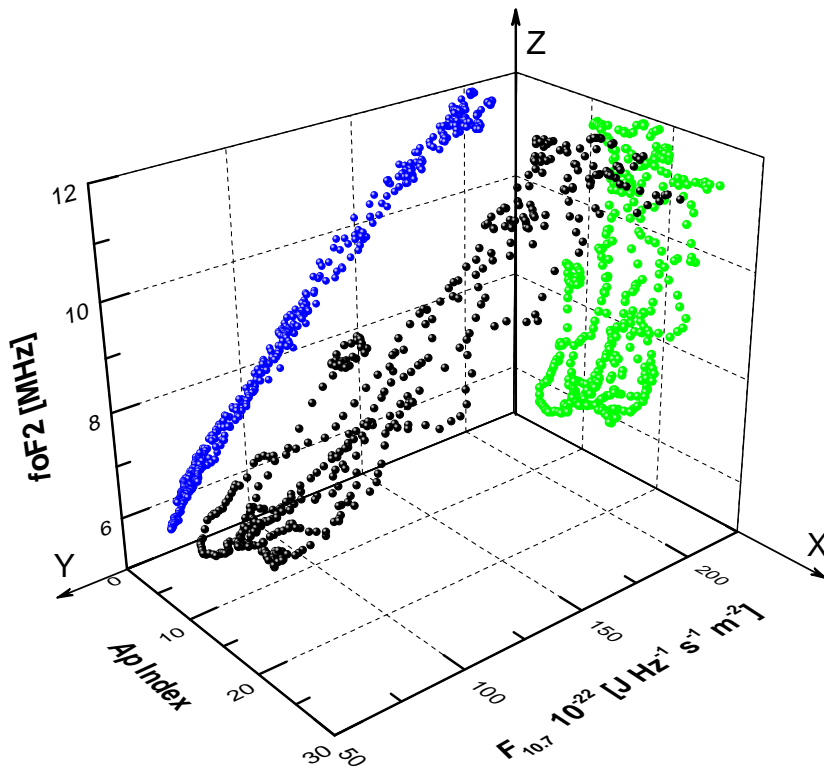
Figure 3.20: 3-D scatter plot of the *fo*F2 dependence on solar activity (index $F_{10.7}$) and geomagnetic activity (index Ap). Blue dots represent the (*fo*F2 vs $F_{10.7}$) scatterplot, green dots represent the (*fo*F2 vs Ap) scatterplot. Only the first smoothed value (1-year running mean) of each month is displayed for all parameters.

the one that characterized the solar cycle 23/24.

Once a quadratic polynomial has proved to be the best one to approximate the relations (*fo*F2 vs *Index*), as a second step it was then shown that (*fo*F2 vs $MgII$) is the best relation to model the dependence of *fo*F2 on the solar activity. The main reasons of this outcome are: (1) a good sensibility of $MgII$ to the variations of *fo*F2 for low solar activity; (2) a reduced saturation effect characterizing $MgII$ at high solar activity; (3) a very slight hysteresis effect characterizing $MgII$ for medium solar activity; (4) the observed inter-cycle constancy in the relationship between *fo*F2 and $MgII$.

With regard to the other solar indices, the study showed that: (1) at medium solar activity Lym-α and R are significantly affected by the hysteresis effect, and then it is important to pay particular attention when using analytical relations between *fo*F2 and these two indices; (2) $F_{10.7}$ cannot properly follow the variations of *fo*F2 for the very anomalous minimum of solar cycle 23/24. In fact, for this solar minimum, synthetic *fo*F2 values calculated using $F_{10.7}$ considerably overestimate the observed ones. It is then recommended to use $F_{10.7}$ for low solar activity with special care. In particular, a threshold of $82 \cdot 10^{-22}$ [J Hz^{-1} s^{-1} m^{-2}] below which *fo*F2 variations are no longer suitably reproduced was identified.

The knowledge of an accurate relation between *fo*F2 and the solar activity is basic for the improvement of every ionospheric model and for the study of ionospheric parameters trends. The good correspondence found using a quadratic fit has been directly tested on the *Simplified*
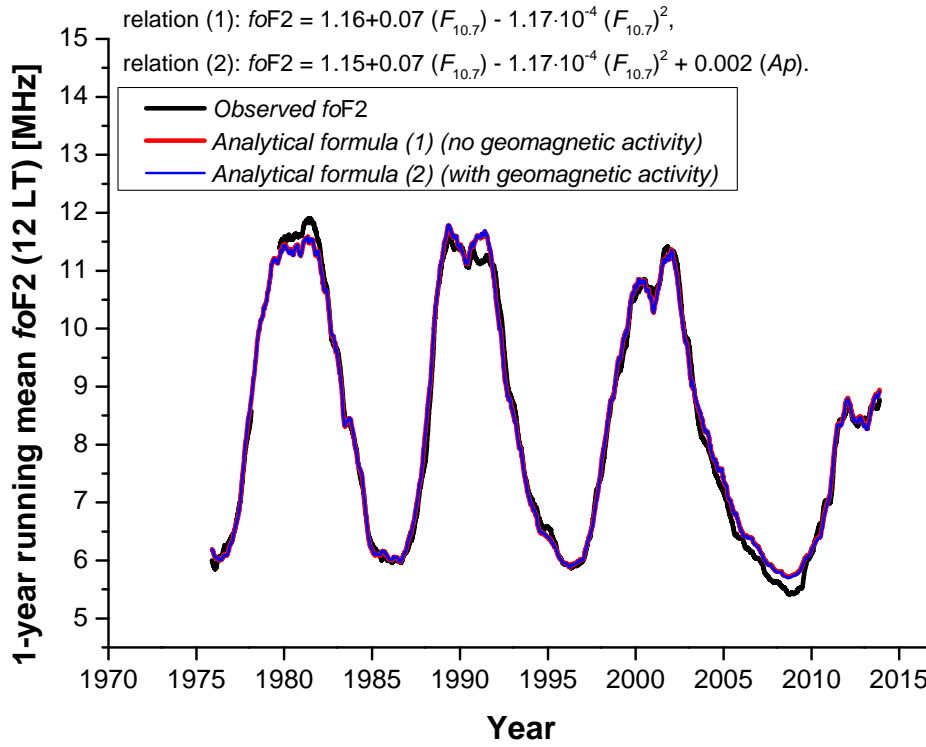
Figure 3.21: Comparison between observed (black curve) and synthetic values of foF2. Synthetic values are calculated by considering only the solar activity ($F_{10.7}$ index; red curve) and both the solar activity and the geomagnetic activity ($F_{10.7}$ and Ap indices; blue curve). The fitting relations are also displayed.

Ionospheric Regional Model (Zolesi et al. (1993); SIRM), and a brief outline of preliminary results obtained is reported in Chapter 4.

Furthermore, it is intention of the author to consider the quadratic relation (foF2 vs $MgII$) found for the Rome station to investigate whether the corresponding long-term trend of residuals ΔfoF2 $= (fo$F2$_{\text{observed}} - fo$F2$_{\text{synthetic}})$ presents some signature due to the greenhouse effect.

Chapter 4

Updating the *SIRM* model: an outline

Introduction

The study of the ionosphere, together with other geophysical disciplines like meteorology, oceanography and geomagnetism, plays an important role in basic and applied sciences. The cold plasma environment, forming the ionosphere and enveloping the Earth, represents the main controller for terrestrial and Earth-space radio systems altering radio communications in HF range, interrupting trans-ionospheric commands, controls and communication systems, compromising global positioning networks, and inducing damaging currents in land-based power grids and transcontinental pipelines (Zolesi and Cander, 1998). Therefore, variations in the ionosphere have a prominent impact on numerous daily activities on Earth and for this reason ionospheric modeling and short-time and long-time forecast are of primary importance.

The development of ionospheric models represents a very interesting challenge because the parameters that characterize the ionospheric structure and dynamics are subject to spatial and temporal variations that can be either periodic or irregular. Moreover, changes that take place into the ionosphere are different at different heights because of varying relative ionization production, loss and transport influences; additionally, ionospheric characteristics, used for the electron-density height profile reconstruction for a given location, experience systematic daily, seasonal and solar cycle changes (Tsagouri et al., 2005). Furthermore, the ionospheric behaviors show a clear dependence on latitude, with a climatological mid-latitude ionosphere being easier to characterize compared to the equatorial, low-latitude and polar ionosphere.

Since its discovery, many models of the Earth's ionosphere, based on different physical approaches, on various mathematical techniques and describing different parameters, have been developed. In general, ionospheric models can be divided in three main groups (Zolesi and Cander, 2014):

- Theoretical, parameterised, and empirical models that define the ionospheric electron density profile and also the profile parameters in terms of the ionospheric characteristics at every point on the globe;

- Assimilation models for a full 3-D electron density profile;

- Empirical and physical models or methods for 2-D global, regional, and local mapping of the ionospheric parameters for both long-term prediction and nowcasting in the field of radio propagation and navigation.

Currently, the most widely used models are the International Reference Ionosphere (IRI) (Bilitza et al., 1990; Bilitza, 2001; Bilitza and Reinisch, 2008; Bilitza et al., 2014) and the NeQuick2 model (Nava et al., 2008). As already reported in Section 2.2, the IRI model is an international project sponsored by the Committee on Space Research (COSPAR) and the International Union of Radio Science (URSI), based on an extensive database and able to capture much of the repeatable characteristics of the ionosphere such as the electron density, the electron content, the electron temperature and the ion composition, as a function of height, location, and local time for quiet and storm-time periods (Araujo-Pradere et al., 2011, 2013; Zakharenkova et al., 2013). IRI is an empirical model representing the reference model for the ionospheric community.

The NeQuick2 model represents the second version of NeQuick (Hochegger et al., 2000; Radicella and Leitinger, 2001), an empirical ionospheric model being widely used for the estimation of vertical electron density profiles and related parameters. Moreover, it is a quick-run model particularly tailored for trans-ionospheric applications that allows calculation of the electron concentration at any given location in the ionosphere, and thus the Total Electron Content (TEC) along any ground-to-satellite ray path by means of numerical integration (Zolesi and Cander, 2014). The model was developed at the Aeronomy and Radiopropagation Laboratory of the Abdus Salam International Centre for Theoretical Physics (ICTP; Trieste, Italy) and at the Institute for Geophysics, Astrophysics and Meteorology of the University of Graz (Austria), and it has been adopted by the International Telecommunication Union (ITU) for TEC modeling (ITU, 2003). NeQuick2 uses a sum of five semi-Epstein layers for the bottom side ionosphere up to the F2-layer peak and a sum of six semi-Epstein layers to describe the topside ionosphere (Rawer, 1982). Its outputs have been validated by several workers who reported a very good agreement with measurements at middle latitudes and improved performances while assimilating measurements (Jodogne et al., 2005; Bidaine and Warnant, 2010). Both IRI and NeQuick2 are global models to describe the climatological features of the ionosphere all around the world.

During the last decades, there has been a trend to focus on regional models, rather than global, because of their capability to produce a more accurate ionospheric representation over particular areas, which gives better results for both telecommunications and geophysical modeling (Brown et al., 1991; Rawer, 1991; Zolesi and Cander, 2014). At the same time, *Single Station Models* (*SSMs*) have been introduced for both long-term prediction and short-term forecasting. These models, based on an accurate study of the most important ionospheric parameters at a single ionosonde station for which a long history of observations is available, can be considered the extreme limit of the regional models which in their immediate vicinity represent the most accurate option (Zolesi and Cander, 2014).

Regarding regional models, numerous techniques based on different spatial and temporal fitting algorithms have been proposed for the European sector (Dvinskikh, 1988; Singer and Dvinskikh, 1991; Zolesi et al., 1993; Reinisch et al., 1993; Mikhailov et al., 1996; De Franceschi and De Santis, 1994; Bradley et al., 1994). The development of regional techniques for the description of median and real-time specifications arose (1) from the request to improve the performances for specific areas, (2) in response to the availability of denser network of stations and (3) to simplify the complex ionospheric morphology over a restricted area.

By introducing the *Simplified Ionospheric Regional Model* (*SIRM*), Zolesi et al. (1993) addressed the question of how to model the ionosphere in areas with a sparse network of vertical incidence ionosondes and how to use data from inhomogeneous periods. In this modeling, the monthly median behaviors of foF2, MUF(3000)F2, h'F, foF1, and foE over Europe (10°W-30°E

in longitude, 30°N-60°N in latitude) were expressed as functions of the geographic coordinates, of the local (or universal) time, and of the 12-month running mean of the monthly mean sunspot number R_{12} (Zolesi et al., 1993, 1996). The procedure was based on the assumption that at constant local time there are no longitude changes of the ionospheric characteristics and that their diurnal and seasonal variations can be well represented by a Fourier expansion with a relatively small number of numerical coefficients (Zolesi et al., 1996). The main aim of the model is to treat the simple problem of modeling the key ionospheric characteristics of vertical incidence in a restricted area, and to demonstrate how well the model fits the measured data. For this purpose, a limited region in Europe is considered where the spatial resolution of the F-layer maximum electron density measurements may be sufficiently high in comparison to the typical horizontal scale sizes of dynamical phenomena. Moreover, such a mid-latitude area is not interested by the complex physical processes occurring at high and low latitude. Because of the limited longitudinal range covered (about 30°), large "point-to-point" variability in the monthly median behavior of the ionospheric parameters should not be expected as a function of geographic longitude for the selected area (Khachikyan et al., 1989), and only the model dependence on the geographic latitude can be taken into account (Zolesi et al., 2004).

The SIRM model was developed under the Co-operation in the field of Scientific and Technical Research (COST) Action 238 Prediction and Retrospective Ionospheric Modeling over Europe (PRIME, Bradley, 1995) and improved and tested under the COST Action 251 Improved quality of service in Ionospheric Telecommunication Systems planning and operation (IITS Hanbaba, 1999). The aforementioned Fourier coefficients are calculated from the analysis of the hourly monthly median values of the ionospheric characteristics measured at some mid-latitude stations over the European region and collected under the COST Actions. For every different month, there are 12 couples of Fourier coefficients showing, as a first approximation, a linear dependence on solar activity and on geographic latitude. The COST251 testing procedure, that consisted in comparing measurements of all hourly median data available from a given set of ionospheric stations and the predicted values by different models, showed that the overall root mean square (RMS) error from SIRM was slightly smaller than the RMS error for the ITU recommended model (ITU-R, 1994; Levy et al., 1998). This validation test proved that SIRM performances are satisfactory for the description of median ionospheric conditions at mid latitudes. Furthermore, SIRM also provides an efficient and user-friendly software program with a very simple mathematical formulation of the complex ionospheric media and reduced number of numerical coefficients involved (Tsagouri et al., 2005).

The simplicity of the SIRM model led to the introduction of a real-time updating method of SIRM, with the assimilation of autoscaled ionospheric characteristics observed by four European digisondes, in order to enable SIRM method to capture the instant distribution of ionospheric characteristics during ionospheric disturbances.

The *SIRM UPdating* (*SIRMUP*, Zolesi et al., 2004) method is based on the idea that real-time foF2 and $M(3000)$F2[1] at one location can be determined with SIRM by using an effective sunspot number R_{eff}, instead of the 12-month smoothed sunspot number R_{12}. The method of determining R_{eff} was introduced and described in details by Houminer et al. (1993).

In light of the results reported in Chapter 3 regarding the relationships (*fo*F2 vs *Solar Index*), it is interesting to discuss briefly how and whether the SIRM model can be accordingly improved. Therefore, in the present chapter the preliminary results obtained through a partial updating of the SIRM model and by developing a specific model for the Rome ionosonde will be displayed and discussed. In Section 4.1, the mathematical description of the SIRM

---

[1]$M(3000)\text{F2} = MUF(3000)\text{F2}/fo\text{F2}.$

model, in its original form, and its performances for low and high solar activity levels, are reported. In Section 4.2 a modified version of the SIRM model according to the results obtained in Chapter 3, the *SIRMPol* (*Simplified Ionospheric Regional Model Polynomial*) model, and the corresponding preliminary results are discussed. In Section 4.3, a very simple Single-Station Model for the Rome station, named *SSM-R*, is introduced and corresponding results are compared with ionosonde values, SIRM and SIRMPol outputs. Conclusions and guidelines for a future complete implementation of the SIRM model are reported in Section 4.4.

4.1   The *SIRM* model

The SIRM is a regional long-term prediction model developed by Zolesi et al. (1993) to predict the key standard vertical incidence ionospheric characteristics (*fo*F2, *MUF*(3000)F2, *h*'F, *fo*F1 and *fo*E) over a restricted area of the Europe. The European area was chosen because the spatial resolution of the maximum electron density measurements was sufficiently high in comparison to the typical horizontal scale size of ionospheric dynamic phenomena (Zolesi and Cander, 2014). The first version of the SIRM model provided a description of the aforementioned ionospheric parameters in term of monthly median values.

The database used to develop the model was collected by the Centre National d'Etudes des Telecommunications (CNET) in Lannion (France) and by the Word Data Center-A (Boulder, Colorado), and it consisted of monthly median values of the ionospheric parameters available for several years, recorded by the European vertical incident ionospheric stations listed in Table 4.1 and mapped in Figure 4.1.

Station Name	Geog. Lat.	Geog. Lon.	Dataset available
Uppsala	59.8°N	17.6°E	1967-1976
De Bilt	52.1°N	5.1°E	1968-1976
Lannion	48.6°N	3.5°W	1971-1984
Poitiers	46.5°N	0.3°E	1964-1984
Grocka	44.8°N	20.5°E	1964-1985
Rome	41.8°N	12.5°E	1957-1987
Gibilmanna	38.0°N	14.0°E	1976-1979 and 1984-1987

Table 4.1: Geographic latitude, longitude and dataset available for the European stations used for the development of the SIRM model.

Considering the seven stations of Table 4.1, the SIRM spans an area of 40° in longitude (10°W to 30°E) and 30° in latitude (30° to 60°N). Given the limited longitudinal range, it is expected that, at the middle latitudes considered by the SIRM, the large variability of the ionospheric characteristics should not be longitudinal-dependent. Therefore, only model dependence on geographical latitude is taken into account.

In this section, the SIRM procedure used to produce monthly median values of the ionospheric characteristics is reported.

Dominici and Zolesi (1987) found that monthly median values of the ionospheric characteristics at Rome station vary linearly with the sunspot number (monthly mean or median values) or its 12-month running mean R_{12}. Therefore, the first step of the procedure is a linear regression of the monthly median values for a given ionospheric characteristic $\theta_{h,m}$, taken at local (or universal) time, against the solar index R_{12}:

Figure 4.1: Ionospheric stations used to develop the SIRM model.

$$\theta_{\mathrm{h,m}} = \alpha_{\mathrm{h,m}}(R_{12}) + \beta_{\mathrm{h,m}}. \tag{4.1}$$

$\alpha_{\mathrm{h,m}}$ and $\beta_{\mathrm{h,m}}$ are two matrices of 288 coefficients (24 hours x 12 months), one for each hour of the day, h, and for each month of the year, m. Using equation (4.1), it is considered that the solar cycle variation of the monthly median values θ can be fully described at any ionospheric station, for each month and hour, by only two levels of solar activity and the straight line joining them (McNamara, 1991). Therefore, the simple linear regression analysis is considered as the best prediction of the observed data at every single station. Two established values of solar activity, $R_{12} = 0$ and $R_{12} = 100$, are chosen and used to describe low and high solar activity levels, respectively. By applying equation (4.1) to the data base available for the two preselected R_{12} values, two sets of synthetic monthly median values for the ionospheric characteristic θ are obtained for every considered station.

The second step is a Fourier analysis of the synthetic datasets obtained at the end of the first step:

$$\theta_{\mathrm{h,m}} = A_0 + \sum_{n}^{l} A_{\mathrm{n}} \sin\left(\frac{2\pi nt}{T} + Y_{\mathrm{n}}\right), \tag{4.2}$$

where n is the harmonic number, $T = 288$ hours corresponds to a fundamental period of a "virtual year" with a fixed level of R_{12}, t is the time in hours for which $t = 1$ corresponds to 00:00 LT of January and $t = 288$ to 23:00 LT of December. It is clear that considering the coefficients A_0, A_{n} and Y_{n}, with $n = 1, 2, ..., l = 144$, the Fourier synthesis repeats the θ values that are obtained from equation (4.1) by considering the two original matrices $\alpha_{\mathrm{h,m}}$ and $\beta_{\mathrm{h,m}}$. Zolesi et al. (1993, 1996) have shown that only 12 dominant Fourier coefficients are

sufficient to reproduce the main features of the diurnal, seasonal and solar cycle behavior of the mid-latitude ionosphere under quite conditions, which indeed leads to a significant reduction of the numerical calculation involved. Using this technique for every station, Zolesi et al. (1993) found a good agreement between the results of the Fourier synthesis and the results of a simple linear regression. In this way, it is possible to reproduce the temporal variations of the key ionospheric characteristics at each ionospheric station and, considering this evidence, the Fourier coefficients A_n and Y_n in equation (4.2) can be considered, as a first approximation, linearly related to R_{12}:

$$A_n = a_n(R_{12}) + b_n, \quad Y_n = c_n(R_{12}) + d_n. \tag{4.3}$$

Relations (4.3) are applied to the database of the seven ionospheric stations considered, using a local time (LT) format and taking into account the differences between LT and the local standard time through the phases Y_n. Zolesi et al. (1993) found that the results for the coefficients A_n and Y_n used in the evaluation of foF2, $M(3000)$F2 and h'F, corresponding to $R_{12} = 0$ and $R_{12} = 100$, show a linear variation with the geographic latitude; this confirms the validity of the concept that the coefficients a_n, b_n, c_n and d_n, can be regarded as a linear function of the geographic latitude in a restricted area. Therefore, the spatial distribution of the selected ionospheric characteristics can be expressed as:

$$\begin{aligned} A_n &= (a_n^1 \phi + a_n^2)R_{12} + a_n^3 \phi + a_n^4, \\ Y_n &= (b_n^1 \phi + b_n^2)R_{12} + b_n^3 \phi + b_n^4. \end{aligned} \tag{4.4}$$

The numerical coefficients a_n^j and b_n^j, with $j = 1, 2, 3, 4$, can be easily calculated by a linear regression of the Fourier coefficients of every ionospheric station versus their latitudes (Zolesi et al., 1990, 1991).

The SIRM model is completely described by equations (4.1)-(4.4). To fix the key points, the characteristics of the model are here summarized:

- It is based on linear regressions between monthly median values $\theta_{h,m}$ and R_{12};

- It sets two solar activity levels: $R_{12} = 0$ (low solar activity) and $R_{12} = 100$ (high solar activity). Other levels of solar activity are considered by a linear interpolation between these two bounds;

- Linear regressions are considered between the Fourier coefficients A_n and Y_n and the R_{12} index;

- Linear regressions are considered between the Fourier coefficients A_n and Y_n and the latitude ϕ;

- No variations in longitude are considered.

As it was mentioned, it is important to underline how the total representation involves only 100 numerical coefficients for each ionospheric characteristic and therefore yields considerable economy in data storage and computation as compared with global representations such as for instance that of CCIR which makes use of the Jones-Gallet technique (Jones and Gallet, 1962), on which the IRI model is based.

Preliminary results show that the SIRM model outputs match the input data used in their generation with a standard deviation of about 0.5 MHz (Zolesi et al., 1990). The reliability of the SIRM outputs have been also tested making comparisons with station measurements

not used when generating the SIRM coefficients. For high solar activity, typical differences of around 0.7 MHz or less have been observed (Zolesi et al., 1991, 1993).

Figure 4.2 shows the comparison between SIRM monthly median values for foF2 and $M(3000)$F2 parameters and the ionosonde values for Dourbes station (50.1°N, 17.6°E; Belgium), for January 1982 (monthly mean sunspot number $R = 100$) and June 1982 ($R = 110$). The results show a good agreement between ionosonde data and SIRM outputs for the parameter foF2, in particular for the summer month of June, while more pronounced discrepancies are observed for the winter month of January, in particular during daytime hours when model underestimations are observed. For the parameter $M(3000)$F2 a very good agreement is obtained.
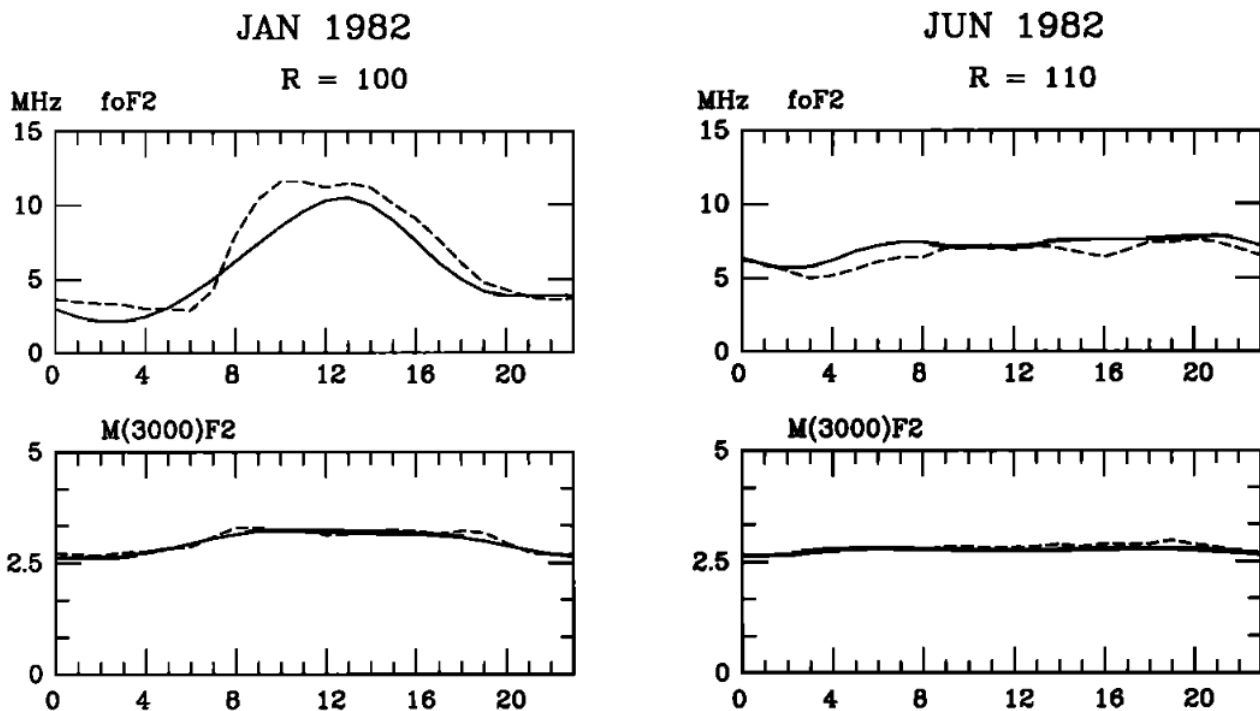

Figure 4.2: Hourly median values for the ionospheric parameters foF2 and $M(3000)$F2, measured at Dourbes station (dashed line) and calculated with the SIRM model (solid line) for January and June 1982, when monthly mean sunspot number $R = 100$ and 110 were registered respectively (modified from Zolesi et al. (1993)).

Zolesi et al. (1996) have tested the SIRM performances to several inhomogeneous periods of ionospheric datasets from a sparse network of ionospheric stations in mid-latitude areas such as northeastern North America, southeastern South America, northeast Asia, and southeast Australia.

The results show that the agreement between model and observed data for foF2 and $M(3000)$F2 is quite remarkable when taking into account simple assumptions, that is, no longitudinal-dependent variations, linear variation of the model coefficients with the geographic latitude, and their reduced number.

SIRM performances have been also tested in the Antarctic region (80°S to 60°S in latitude, 110°E to 165°E in longitude) by De Franceschi and Zolesi (1998). Using data from only three stations, namely Casey (66.3°S, 110.5°E), Terre Adelie (66.7°S, 140.0°E) and Scott Base (77.9°S, 166.8°E), covering inhomogeneous periods of observations with several gaps, an average

difference of 0.4 MHz has been obtained between SIRM and ionosonde *fo*F2 values for the mid solar activity months of December 1993 ($R_{12} = 40$) and January 1994 ($R_{12} = 37$), by considering the Terra Nova Bay ionospheric station (74.7°S, 164.1°E) as the test-station. Therefore, as expected, poor results are obtained when the model is used in a complex ionospheric region and where the availability of continuous data and dense area of ionosondes are inadequate.

However, it is expected that for mid-latitude areas with a dense ionosondes network and continuous, long and reliable datasets, such as the European region, SIRM outputs provide very good agreements with observed data. In fact, due to its good results in the European area, economy in computation and quick response, the SIRM model and its real-time version SIRMUP, have been used in the European projects *DIAS* (*DIgital upper Atmosphere Server*; http://www.iono.noa.gr/DIAS/) and *ESPAS* (*Near-Earth Data Infrastructure for e-Science*; http://www.espas-fp7.eu/) to produce *fo*F2 and $M(3000)$F2 maps.

As reported in Chapter 2, the last solar minimum has shown an unprecedented prolonged and low solar activity, providing a perfect natural window to study the ionospheric plasma response and the reliability of ionospheric models for such particular conditions. Therefore, thanks to a very long, continuous and reliable dataset available for the Rome station, it is very interesting to compare the SIRM outputs with the Rome ionosonde monthly median values, limiting the study to the main ionospheric parameter *fo*F2.

Figures 4.3 and 4.4 report the comparison of hourly monthly median values calculated by SIRM (red dashed line) and measured by the ionosonde (black solid line), for Rome, for the years 2008 and 2009, which represent the deepest phase of the last solar minimum.
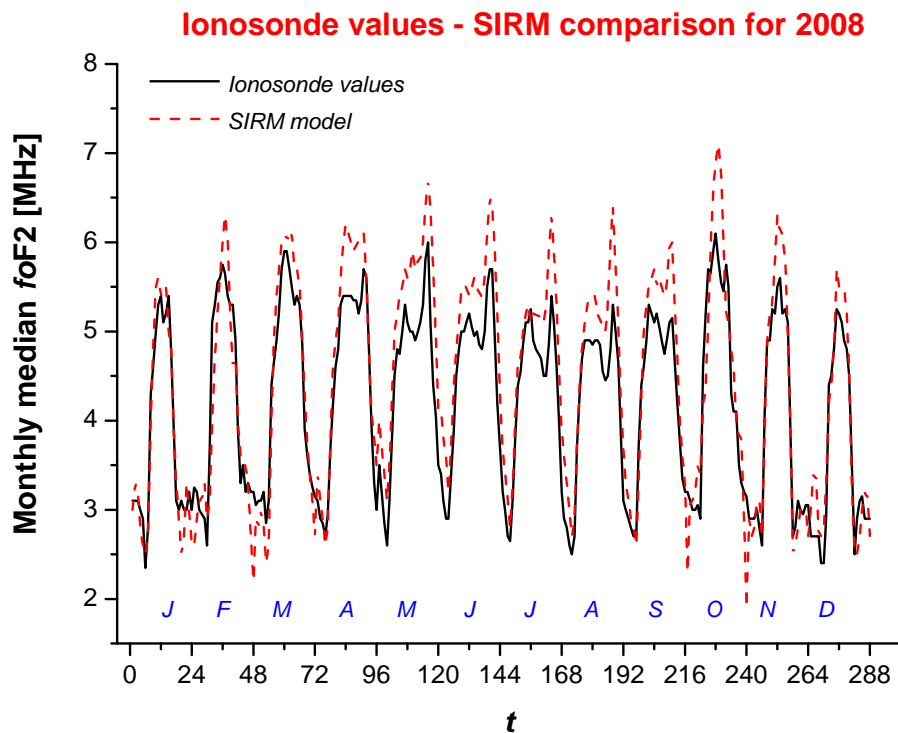

Figure 4.3: Hourly monthly median *fo*F2 values for the Rome station as measured by the ionosonde (black line) and calculated by the SIRM model (red dashed line) for the whole year 2008. The x scale spans from $t = 0$ (00:00 LT of January 2008) to $t = 288$ (23:00 LT of December 2008). The capital letters in blue identify the months from January (J) to December (D).
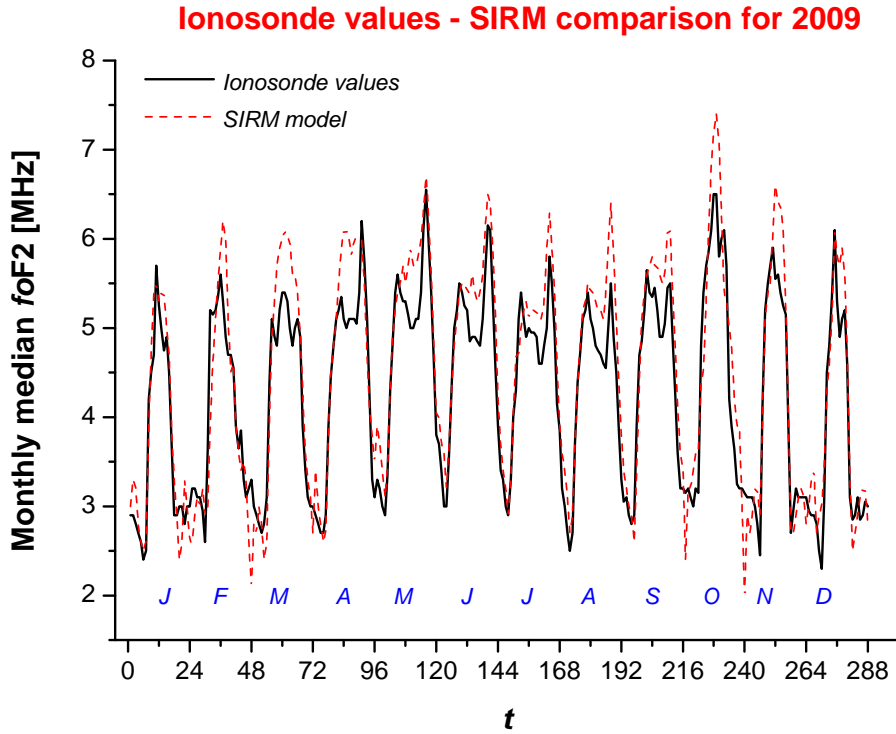
Figure 4.4: Same as Figure 4.3 for the year 2009.

SIRM outputs provide good agreement with ionosonde data for both 2008 and 2009, using as input observed values for the solar index R_{12}. To quantify the SIRM performance, the same mean deviation introduced in Section 3.3.1 has been calculated, using the formula:

$$\Big(\sum_{i=1}^{n} \big| fo\mathrm{F2}_{\mathrm{SIRM}} - fo\mathrm{F2}_{\mathrm{obs}} \big|_i / n \Big)_{\mathrm{Model}} = M_{\mathrm{Model}},$$

where $fo\mathrm{F2}_{\mathrm{SIRM}}$ and $fo\mathrm{F2}_{\mathrm{obs}}$ are monthly median $fo\mathrm{F2}$ values from SIRM and ionosonde, respectively. The mean deviation values are 0.47 MHz and 0.43 MHz for the whole 2008 and 2009 respectively, confirming the good results provided by SIRM.

These results are not surprising because, as mentioned, it is expected that SIRM model provides good correspondences with ionosonde data in mid-latitude areas with a dense ionosondes network. Furthermore, (1) Rome ionosonde data are used as input in the SIRM model and (2), as shown in Table 4.2, the R_{12} values for the years 2008 and 2009 are very low and close to the value $R_{12} = 0$ that is one of the two levels of solar activity set in the model.

However, Figures 4.3 and 4.4 also show the following features: (1) the SIRM model tends to overestimate the daily peak $fo\mathrm{F2}$ value, in particular for the 2008; (2) for both years, the SIRM model clearly overestimates $fo\mathrm{F2}$ values around midday (10-14 LT) in October; (3) night-time values are well described by the SIRM model during summer and spring months, while more pronounced gaps characterize winter and autumn months (in particular January, February, September and October).

As it will be deeply discussed in Chapter 5 and as it was partially reported in Section 2.2, the ionospheric plasma is well modeled for the last solar minimum when observed values are used as input for the solar activity indices. In the case here reported, observed R_{12} values have been used, therefore good results are not surprising.

Month	2008	2009	1958
January	4.2	1.8	199.0
February	3.6	1.9	200.9
March	3.3	2.0	201.3
April	3.4	2.2	196.8
May	3.5	2.3	191.4
June	3.3	2.7	186.8
July	2.8	3.6	185.2
August	2.7	4.8	184.9
September	2.3	6.2	183.8
October	1.8	7.1	182.2
November	1.7	7.6	180.7
December	1.7	8.3	180.5

Table 4.2: R_{12} for the years 2008, 2009 and 1958.

Nevertheless, as it was explained in Chapter 3, for mid and very high solar activity levels the hysteresis and saturation effects become important, in particular when (foF2 vs *Index*) relationships are considered using mean or median values, such as in the SIRM model. In particular, it was shown how the saturation can be considered a second order effect that, using linear regressions for (foF2 vs R_{12}) relationships, can lead to pronounced model overestimations. Figure 4.5 shows a comparison between foF2 SIRM outputs and ionosonde values for the Rome station, for the 1958, a year of very high solar activity (maximum of solar cycle 19). Table 4.2 reports the monthly R_{12} values for the considered year.

Contrary to years 2008 and 2009, the year 1958 is included in the input dataset used by SIRM to produce the correspondent outputs, therefore very good results should be expected. This year has been chosen to test SIRM outputs because for all months the R_{12} value is markedly over the saturation level[2], therefore it is expected that using the linear regression (4.1) pronounced overestimations could occur. The mean deviation between SIRM and ionosonde values for the whole year 1958 is 1.04 MHz that is more than 50% higher than the results obtained for the years 2008 and 2009. Furthermore, Figure 4.5 shows that during daytime hours for February, March, October, and December, SIRM overestimations as high as 3-4 MHz can be obtained. As it was already said, the simple formulation of the SIRM model makes it easy to be used for interfacing with other regional or global models. The model can be also used as a suitable tool to study the basic physical processes controlling the behaviors of the F region of the Earth's ionosphere and to provide a quick forecast of the ionospheric conditions. For these reasons and in light of the overestimation obtained for high solar activity levels, it is interesting to test the results of a very simple, and only partial, updating of the SIRM model, named SIRMPol, implemented using part of the results reported in Chapter 3.

4.2   The *SIRMPol* model

The analysis of the (foF2 vs *Index*) relationships carried out in Chapter 3 revealed information that can be useful to improve the reliability of ionospheric models. In particular, it was shown

---

[2]For relationships (foF2 vs R_{12}), saturated foF2 values have been observed usually for $R_{12} > 150$.
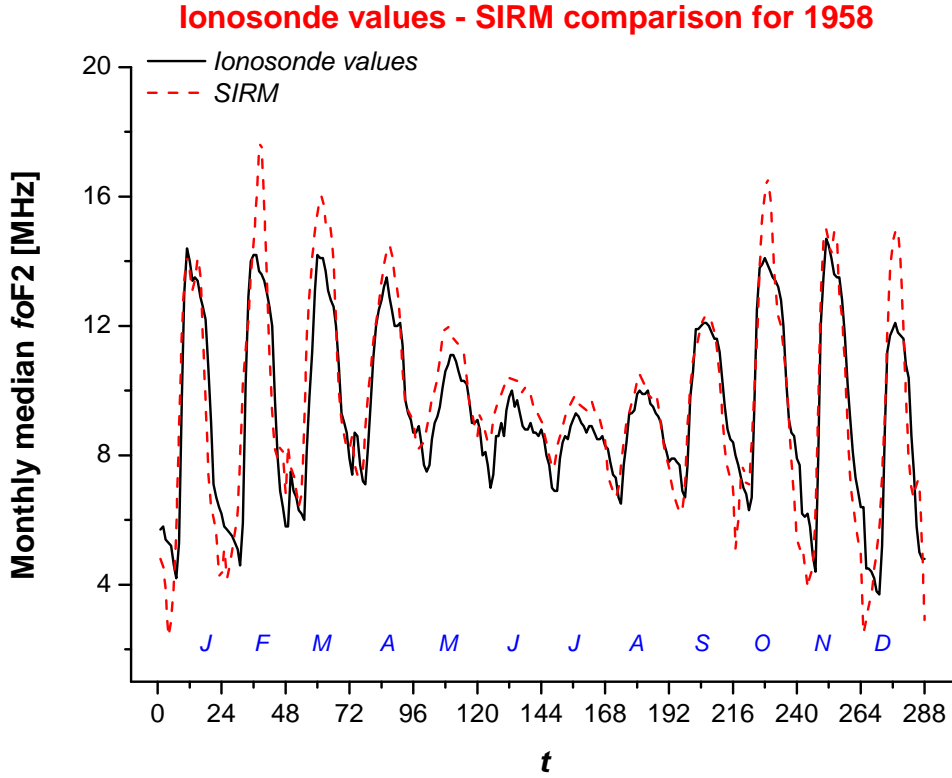
Figure 4.5: Same as Figure 4.3 for the year 1958.

that: (1) the relationships (*fo*F2 vs *Index*) can be well described with a quadratic polynomial regression for the mid-latitude station of Rome and for *fo*F2 values measured at local noon; (2) using linear fitting relations significant overestimations of observed data can be obtained, mainly due to the saturation effect at high solar activity and the unusual low solar activity during the minimum 23/24. As it was mentioned in Section 4.1, the SIRM model is based on linear regressions between monthly median values of the ionospheric characteristics and R_{12} index (equation (4.1)), and in Chapter 3 it has been clearly shown that this is not the best choice, considering *fo*F2 values recorded at local noon. Moreover, the results reported in Section 3.4 about *fo*F2 values recorded at 01 and 19 LT indicate that a more pronounced loss of linearity can occur for very low solar activity levels.

The updating of the SIRM model, named *SIRMPol* (*Simplified Ionospheric Regional Model Polynomial*), is based on very simple changes that are summarized in the following points:

1. The dataset for Rome station has been updated, spanning now from January 1957 to December 2007;

2. Second order polynomial regressions are used for the relationships (*fo*F2 vs R_{12}):

$$fo\text{F2}_{\text{h,m}} = \hat{\alpha}_{\text{h,m}}(R_{12})^2 + \hat{\beta}_{\text{h,m}}(R_{12}) + \hat{\gamma}_{\text{h,m}}, \qquad (4.5)$$

where the coefficients $\hat{\alpha}_{\text{h,m}}$, $\hat{\beta}_{\text{h,m}}$ and $\hat{\gamma}_{\text{h,m}}$ are calculated with the regressions;

3. 9 synthetic *fo*F2 datasets are constructed by setting 9 possible solar activity levels: $R_{12} = 0, 25, 50, 75, 100, 125, 150, 175, 200$;

4. The best fit (linear or polynomial) is chosen for the relationships between the Fourier coefficients A_n and Y_n and the solar index R_{12}.

Before showing the results of the SIRMPol, it is interesting to discuss, clarify and justify briefly the changes done.

As a first consideration, it is worth noting that, owing to a lack of data, it has not been possible to consider the aforementioned changes for the other six ionosondes used to develop the SIRM model. Furthermore, it was not possible to reuse the "old" data for these stations. Consequently, the SIRMPol model takes in input only Rome data and provides a description, in terms of monthly median values, of the *fo*F2 parameter for the only Rome station. Therefore, the updating here proposed has to be considered a partial/local updating of the SIRM model and can be considered a particular case of a Single-Station Model (see Section 4.3). However, it is important to underline that the main aim behind the development of the SIRMPol is to obtain useful information to draft a list of guidelines for a future accurate and complete updating of the SIRM model, also considering other ionospheric stations for which reliable datasets are available.

The choice of second order polynomial regressions (equation (4.5)) should improve the reliability of the output for high solar activity levels, and for the very low solar activity levels of the last solar minimum, according to what it was described in Chapter 3. Nevertheless, the study shown in Chapter 3 has been based on relations between smoothed (1-year running mean) values for both *fo*F2 and solar activity indices. Furthermore, the study was carried out considering *fo*F2 at local noon. As it was mentioned, SIRM and SIRMPol use monthly median values of *fo*F2 and the 12-month smoothed monthly mean sunspot number, consequently some differences with respect to the conclusions of Chapter 3 are expected.

Figure 4.6 reports examples of (*fo*F2 vs R_{12}) relationships for the Rome dataset (1957-2007) for the months of January and May at 01 and 12 LT. Red lines and blue curves identify a linear and a polynomial (2° order) regression of the dataset. Red dots represent values of the last solar minimum (years 2008 and 2009) that are not included in the fits. The figure shows how the saturation effect presents both a seasonal and an hourly dependence, being more pronounced at 12 LT in May. Furthermore, it is observed how the low values for the last solar minimum can be well predicted using a second order regression only for May; for January a linear fit seems to provide better results.

To implement the SIRMPol model, 9 levels of solar activity have been considered from $R_{12} = 0$ to $R_{12} = 200$, with a step of $R_{12} = 25$. This change should provide a better correspondence for levels of solar activity between the anchor points of the SIRM model ($R_{12} = 0$ and $R_{12} = 100$) and for high solar activity levels. Furthermore, considering 9 values of R_{12}, it has been observed how the relations between Fourier coefficients A_n (and Y_n) and R_{12} are no more linear, as they are in the SIRM model.

This is clearly shown in Figure 4.7, where the relationships (A_{13} vs R_{12}) (black squares) and (Y_{13} vs R_{12}) (blue squares) are displayed. It is noticeable how the linear regressions calculated on the base of the only two values $R_{12} = 0$ and $R_{12} = 100$ (red lines), as it is done in the SIRM model, are inadequate. In general, it has been obtained that, for all the Fourier coefficients, polynomial (2° or 3° order) regressions provide the best choice to represent the relationships between Fourier coefficients and R_{12}, as indicated by green curves in Figure 4.7.

As well as for the SIRM model, it is confirmed that 12 Fourier coefficients are enough to describe correctly the chosen ionospheric parameter. A test extending the series to 16 Fourier coefficients has not improved significantly the performances of SIRMPol.

Figures 4.8 and 4.9 display the comparison of monthly median *fo*F2 values for the Rome
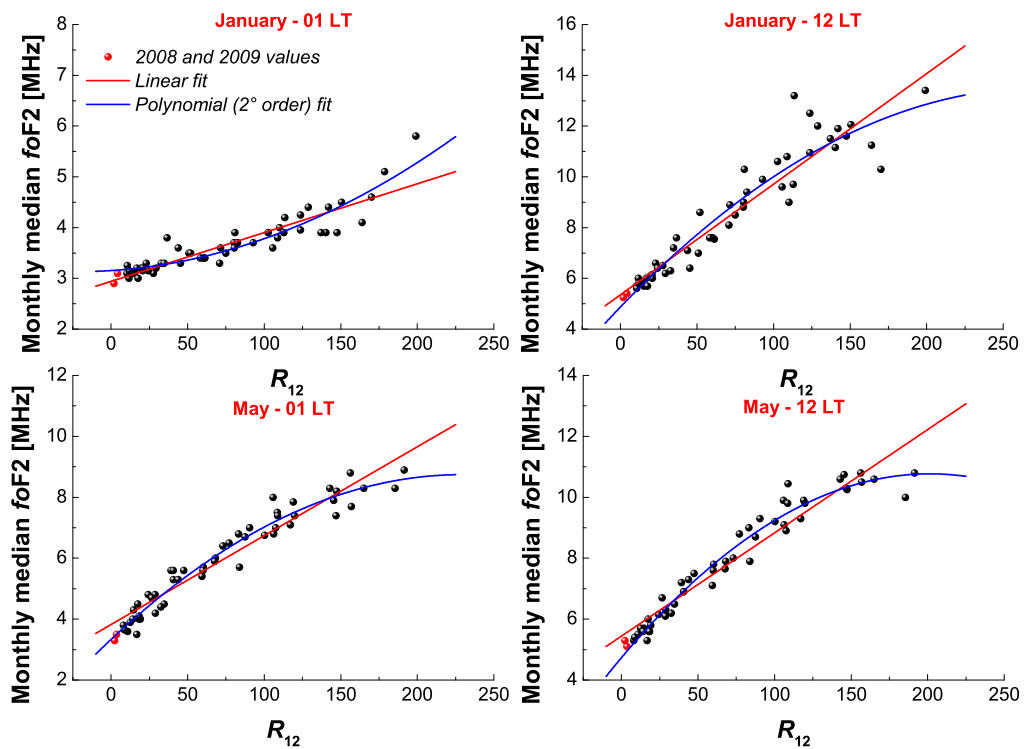
Figure 4.6: Monthly median *fo*F2 vs R_{12} at 01 and 12 LT, for January and May, for the Rome dataset (1957-2007). The red line and the blue curve represent respectively the linear and the 2° order polynomial regression. Red dots represent values for the years 2008 and 2009.
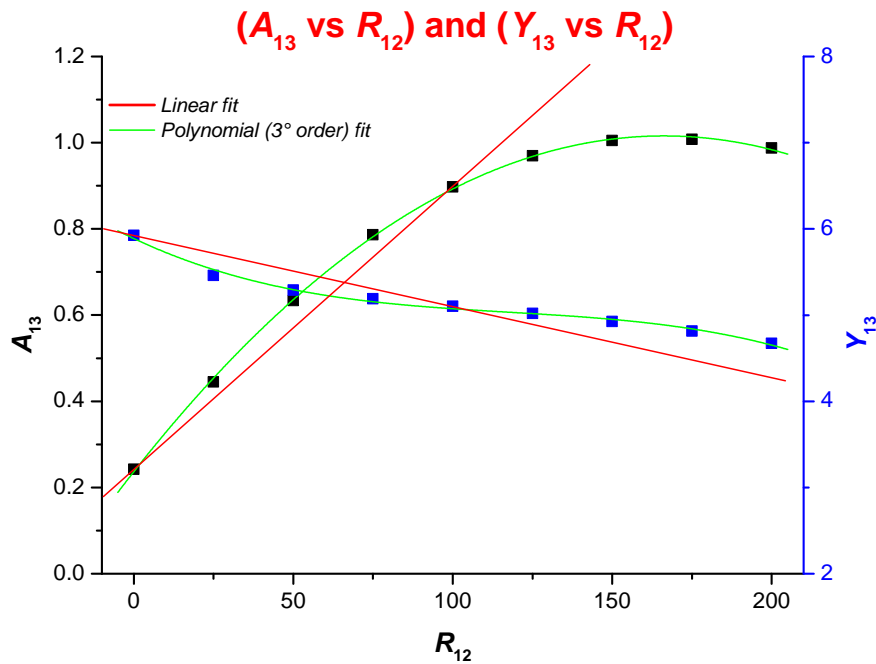

Figure 4.7: (A_{13} vs R_{12}) (black squares) and (Y_{13} vs R_{12}) (blue squares) plots. Red lines represent linear regressions between the two points $R_{12} = 0$ and $R_{12} = 100$; green curves represent third-order polynomial regressions.

station, as measured by the ionosonde (black line), and calculated by SIRM (red dashed line) and SIRMPol (blue line) for the year 2008 and 2009, respectively. It is appreciable how, in some cases, the SIRMPol provides a slight better agreement with ionosonde data than the SIRM model. In particular, the SIRM tendency to overestimate ionosonde values around midday from April to November (feature more pronounced for 2008) appears substantially reduced. Similarly, the SIRM underestimations observed during nighttime hours in January-March and September-November periods result to be reduced as well. Mean deviation M_{Model} values for the whole 2008 and 2009 reveal a slight improvement using SIRMPol, passing from 0.47 MHz (SIRM) to 0.37 MHz (SIRMPol) for the 2008 and from 0.43 MHz (SIRM) to 0.35 MHz (SIRMPol) for the 2009. As already shown in Figure 4.6, it is important to underline that using monthly median values for foF2 and 12-month running mean for the sunspot number, the loss of linearity depends on the month and the hour of the day considered. Therefore, further analyses and considerations are necessary before updating definitely the model, to understand whether a second order regression can be actually considered better than a linear one to catch the variability of the ionospheric plasma for low solar activity.
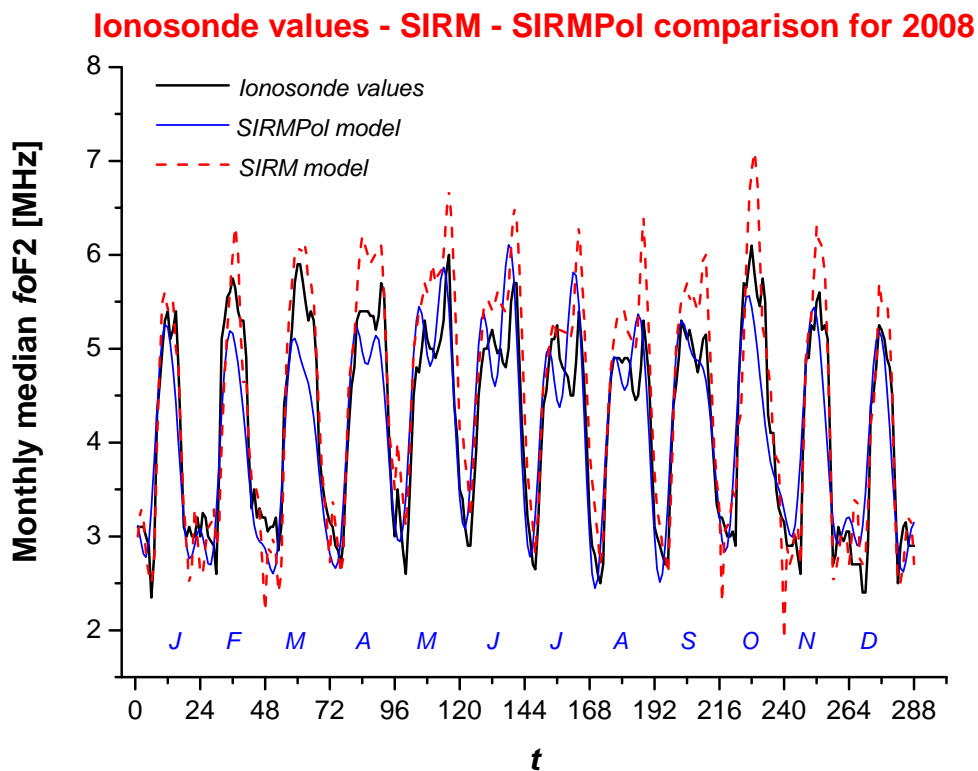

Figure 4.8: Comparison of monthly median foF2 values for the Rome station as measured by the ionosonde (black line), and calculated by SIRM (red dashed line) and SIRMPol (blue line), for the whole 2008. t parameter is the same defined in Figure 4.3.

Figure 4.6 also shows how the saturation effect for high solar activity remains an important issue to be considered for a good implementation of the model. Accordingly with the results of Chapter 3, a second order polynomial regression is useful to reduce the overestimations that can occur using a linear regression for high solar activity. In order to briefly discuss this issue, a comparison between ionosonde data, and SIRM and SIRMPol outputs has been carried out for
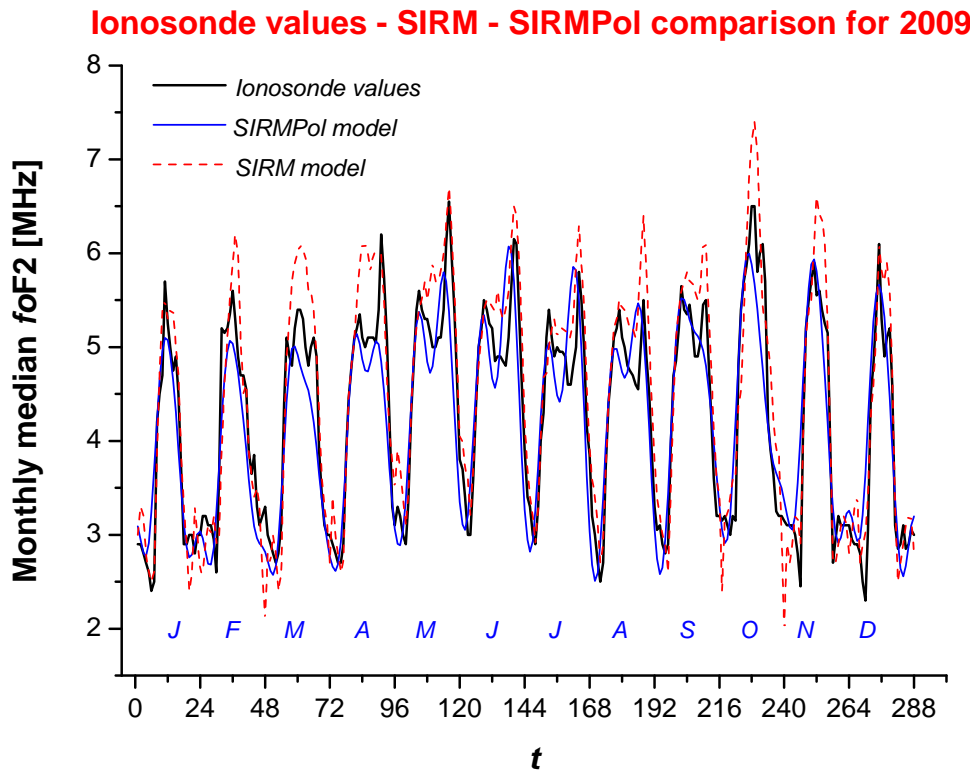
Figure 4.9: Same as Figure 4.8 for the year 2009.

1958, a year of high solar activity, and the corresponding results are displayed in Figure 4.10 (in Table 4.2 the corresponding R_{12} values are listed).

Considering the whole year, mean deviations from ionosonde data of 1.04 and 0.81 MHz have been obtained for SIRM and SIRMPol, respectively. The slight difference of 0.23 MHz, for the whole 1958, increases to 0.32 MHz (1.04 and 0.72 MHz for SIRM and SIRMPol respectively) for the time range 10-15 LT, when the saturation effect is more pronounced during all the year. However, the comparison of mean deviations calculated for the whole 1958 give only a partial view of the improvement done by substituting linear regressions with second order polynomial ones. This is because the saturation effect strongly depends on the solar activity level, month and hour considered. In particular, it is expected that SIRMPol provides sizeable improvements only when the saturation effect is clearly observed. As an example, Figure 4.11 reports the relationships (foF2 vs R_{12}) for the month of March at 12 LT (left) and 15 LT (right) for the Rome dataset 1957-2007. The orange triangles emphasize the value recorded for the year 1958. The figure suggests that, using SIRM (which is based on linear regressions), important overestimations should be obtained, while less pronounced gaps are expected using SIRMPol (which is based on second order polynomial regressions). The comparison between ionosonde data, SIRM and SIRMPol outputs for March 1958 is displayed in Figure 4.12. For the considered month, the value of R_{12} (201.3) is the highest registered during the whole period 1957-2007. It is obtained that SIRM provides relevant overestimations during daytime hours (06-17 LT), while better agreements are obtained using SIRMPol. Focusing our attention on the two hours displayed in Figure 4.11 (12 and 15 LT), a relevant improvement is obtained: at 12 LT the deviations for SIRM and SIRMPol are +1.90 MHz and -0.77 MHz, respectively;

at 15 LT, +2.20 MHz (SIRM) and -0.99 MHz (SIRMPol). Therefore, when a pronounced saturation effect occurs, improvement of more than 1 MHz can be obtained using a second order polynomial regression instead of a linear one.
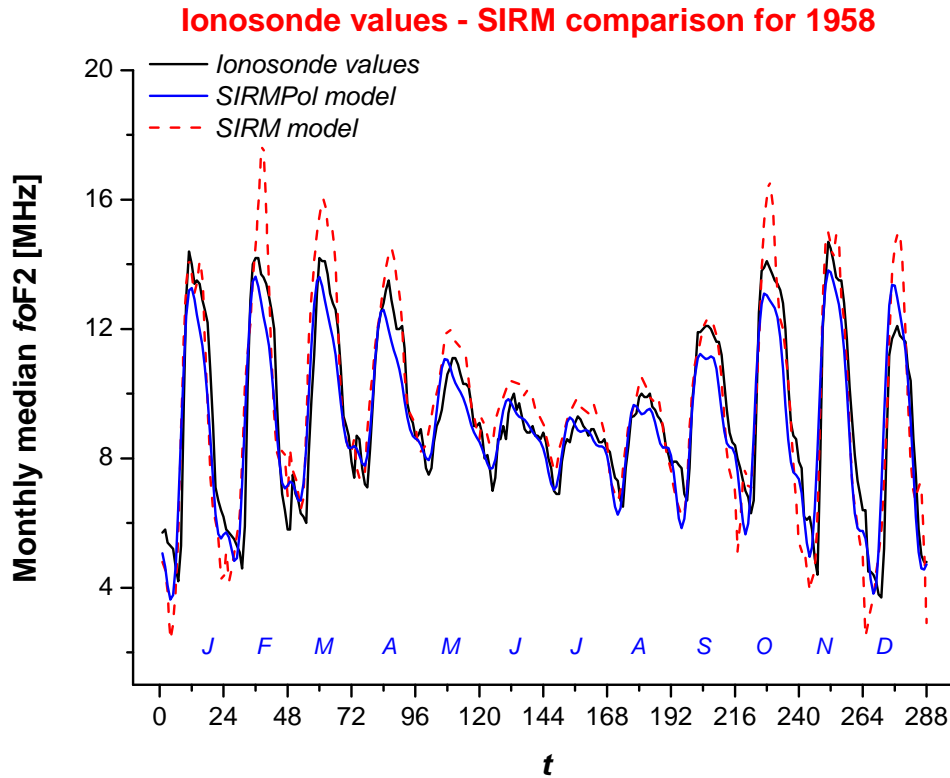

Figure 4.10: Same as Figure 4.8 for the year 1958.

Comparing mean deviations obtained for 2008, 2009 and 1958 it is possible to claim that both SIRM and SIRMPol provide better results for the low solar activity of the last solar minimum than for very high solar activity levels. In future, further studies about this issue should be carried out to improve the reliability of the model.

In this section, it has been shown how introducing very simple changes to the basic procedure of the SIRM model gives better results. In particular, (1) the use of second order polynomial regressions for the relationships (foF2 vs R_{12}) can lead to a consistent reduction of the overestimations obtained using linear regressions, especially for months and hours characterized by a significant saturation effect; (2) polynomial fits (A_n (or Y_n) vs R_{12}) instead of linear ones can provide more reliable foF2 outputs. Nevertheless, the SIRMPol model represents only a partial updating of the SIRM model, because it provides output only for the Rome location and for the parameter foF2. As it will be described in the next section, it is possible to obtain a better description of vertical incidence ionospheric parameters for a single station without considering the Fourier analysis given by equation (4.2). In fact, without a network of ionosondes, to link Fourier coefficients with latitude is no more necessary and the procedure can be considered redundant.

However, as it was previously highlighted, the main aim of the development of the SIRMPol model is to obtain a compendium of guidelines for a future complete and accurate updating of the SIRM model. A summary of these guidelines will be reported at the end of the chapter.
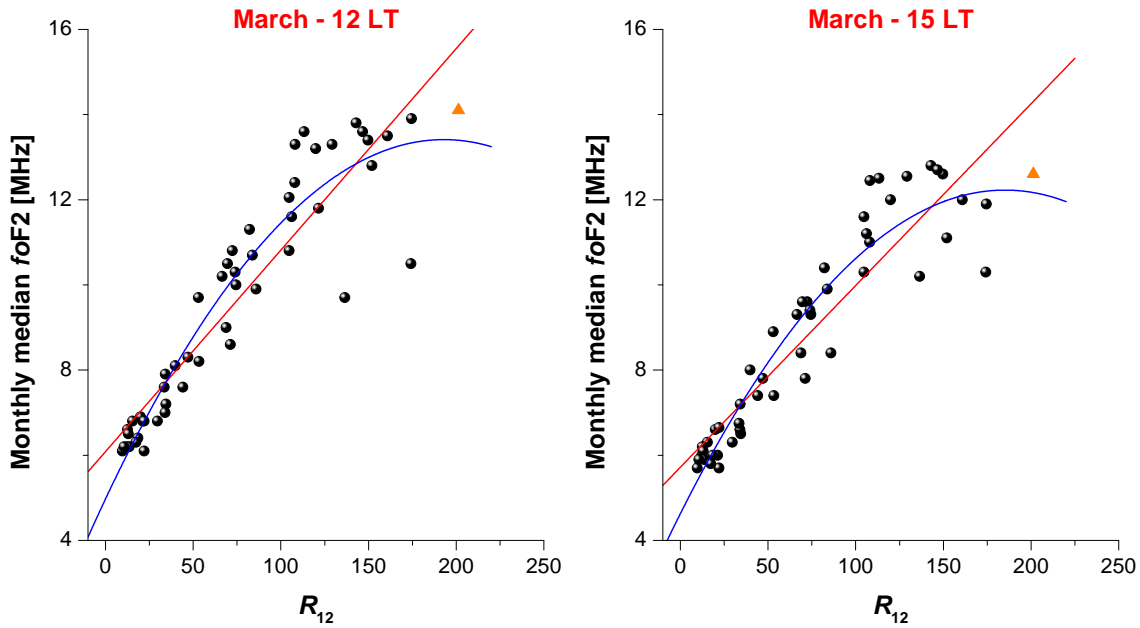
Figure 4.11: (*fo*F2 vs R_{12}) for Rome dataset (January 1957-December 2007) for the month of March at 12 LT (left) and 15 LT (right). Red lines and blue curves represent linear and 2° order polynomial regressions of the data. Orange triangles identify values for the year 1958.

4.3 A Single-Station Model for Rome ionosonde: the *SSM-R* model

When a long, continuous and reliable dataset is available for an ionosonde, the best description and forecasting of the main ionospheric parameters can be obtained with a local Single-Station Model (SSM).

These kind of ionospheric models are in fact based on an accurate study of the ionospheric parameters, such as *fo*F2 and $MUF(3000)$F2, at a single ionosonde station. Linear or polynomial regressions are used to fit the relationships (*fo*F2 vs *Index*) for every hour and month of the year, and usually monthly median or mean values are used for both *fo*F2 and *Index*.

SSMs represent the typical home-made methods produced, either from theory or from measurements, by many ionospheric prediction services for both long-term prediction and short-term forecasting. These models may be considered the extreme limit of the regional models, which in their immediate vicinity should be the most accurate option (Zolesi and Cander, 2014).

This type of models are useful for many reasons: (1) because of their accuracy, they provide very important information for local and medium distance telecommunications; (2) they can be easily interfaced with other regional and global models; (3) they are used to fill data gaps at active stations; (4) they produce new screen points for the mapping of ionospheric characteristics; (5) they are widely used in HF communications to estimate ionospheric conditions at the midpoint of a radio link, evaluating the $MUF(3000)$F2 parameter. As an example of application, SSMs have been used by the ionospheric prediction service provided by the French CNET (Centre National d'Études des Télécommunications) (Sizun, 2005).

A very long, continuous and reliable dataset (manually validated values) is available, with
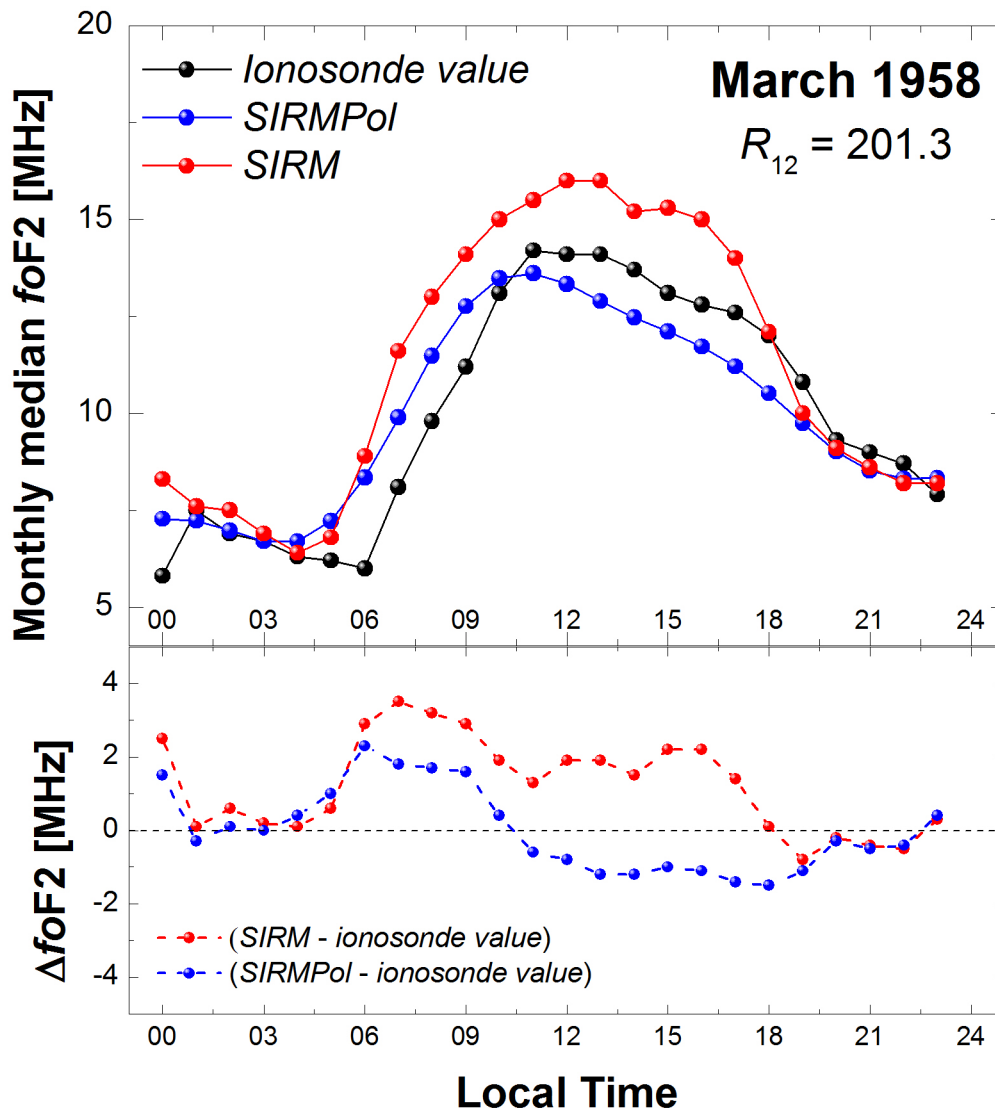
Figure 4.12: (Top) Comparison between monthly median *fo*F2 values measured by the ionosonde (black), and calculated by SIRM (red) and SIRMPol (blue) for the month of March 1958. The correspondent value of R_{12} is also displayed. (Bottom) Point-to-point differences SIRM-Ionosonde (red) and SIRMPol-Ionosonde (blue).

monthly median values starting from January 1957[3], for the Rome ionosonde. Therefore, it is interesting to use this dataset to obtain a local **S**ingle-**S**tation **M**odel for **R**ome, called *SSM-R*, and to compare its outputs with SIRM and SIRMPol ones for low and high solar activity levels.

The SSM-R model uses simple second order polynomial regressions for the relationships between an ionospheric parameter and the solar activity index:

$$\theta_{\mathrm{h,m}} = \hat{\alpha}_{\mathrm{h,m}}(R_{12})^2 + \hat{\beta}_{\mathrm{h,m}}(R_{12}) + \hat{\gamma}_{\mathrm{h,m}}. \tag{4.6}$$

R_{12} will be used as the solar activity index, although the very good results shown in Chapter 3 for $MgII$; this is because R_{12} is the index characterized by the longest dataset. $F_{10.7}$, for which a comparable dataset to that of R_{12} is available, has not been considered by virtue of the poor results shown in Chapter 3 for low solar activity. Focusing our attention on the *fo*F2 parameter, the equation (4.6) turns into equation (4.5). To develop the SSM-R model, equation (4.5) has been applied to the Rome dataset from January 1957 to December 2007.

From the application of second order polynomial regressions on the (*fo*F2 vs R_{12}) relationships, three matrices of 24 x 12 coefficients, namely $\hat{\alpha}_{\mathrm{h,m}}$, $\hat{\beta}_{\mathrm{h,m}}$ and $\hat{\gamma}_{\mathrm{h,m}}$, are obtained. Therefore, for every hour of a specific month, three coefficients are available and the correspondent $fo\mathrm{F2}_{\mathrm{h,m}}$ value is calculated simply introducing in equation (4.5) the observed R_{12} for the chosen month. Xenos (2002), by considering third-order polynomial regressions for six mid-latitude European ionosondes, found that the coefficients of the cubic term are significant in only 4-5% of cases, accordingly with the results previously reported in Section 3.2.1. Solé (1998) considered also a geomagnetic dependence and introduced a SSM based on a second degree multiregression between *fo*F2, the monthly ionospheric index T (Turner, 1968) and the monthly geomagnetic index Ap:

$$fo\mathrm{F2}_{\mathrm{h,m}} = a_{\mathrm{h,m}}(T)^2 + b_{\mathrm{h,m}}(T) + c_{\mathrm{h,m}} + d_{\mathrm{h,m}}(Ap)^2 + e_{\mathrm{h,m}}(Ap),$$

where $a_{\mathrm{h,m}}$, $b_{\mathrm{h,m}}$, $c_{\mathrm{h,m}}$, $d_{\mathrm{h,m}}$ and $e_{\mathrm{h,m}}$ are empirical coefficients that are determined by assimilating ionosonde data. Nevertheless, the main interest here is in the solar activity dependence; on the other hand, as it was shown in Section 3.4.4, no improvements are expected considering a first order dependence of *fo*F2 on Ap for the mid-latitude station of Rome.

The results obtained with the *SSM-R* model for the years 2008 (low solar activity), 2009 (low solar activity), and 1958 (high solar activity) are displayed in Figures 4.13, 4.14 and 4.15.

It is clearly observed how SSM-R provides a strong improvement of the performances for all the three years considered. With regard to the daily peak *fo*F2 values of 2008 and 2009, the SSM-R model provides a better agreement with ionosonde data than the SIRM model. In particular, the improvements are significant for both years in October and November. For the same years, the pronounced gaps characterizing the SIRM model during nighttime hours in winter and autumn have been strongly reduced by the SSM-R model.

In Section 4.1 it was shown that the SIRM model provides a better agreement with ionosonde data for the low solar activity of the last solar minimum (years 2008 and 2009) than for high solar activity (year 1958). In particular, pronounced overestimations, as high as 3-4 MHz, have been obtained during daytime hours of 1958 in February, March and October. The outputs of the SSM-R model substantial improve the ionospheric representation for the 1958: (1) the SIRM overestimation characterizing the aforementioned months is severely reduced by the SSM-R model; (2) the agreement with ionosonde data from May to August is strongly enhanced by the SSM-R model.

---

[3]Monthly median values for Rome are available also before 1957, starting from 1949. However, for the period 1949-1957 numerous lacks of data are present.

To quantify the improvement made by the SSM-R model in comparison with SIRM and SIRMPol models, Table 4.3 summarizes the corresponding mean deviations for 2008, 2009 and 1958. The yearly mean $\bar{R}_{12}$ values are also displayed for every year to underline the solar activity level.
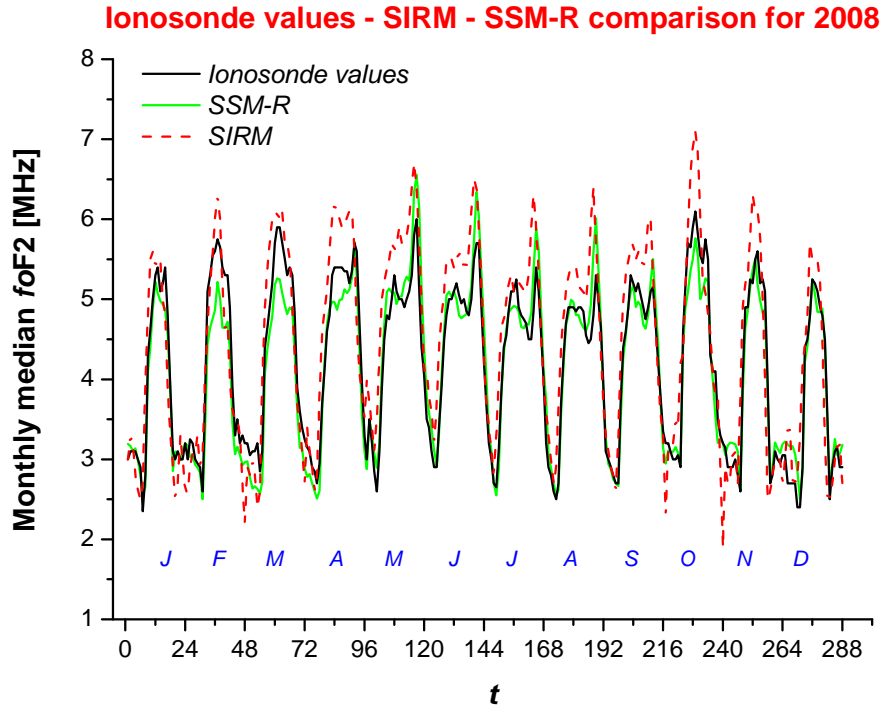

Figure 4.13: Comparison between monthly median *fo*F2 values as measured by the ionosonde (black line), and calculated by SIRM (red dashed line) and SSM-R (green line) for the whole year 2008. The t parameter is the same defined in Figure 4.3. Capital letters identify months from January (J) to December (D).

Table 4.3 shows that the mean deviation values decrease of 50% passing from SIRM to SSM-R. All models show a better agreement with ionosonde data for low solar activity (2008 and 2009) than for high solar activity (1958), for which a doubling of the deviations is observed. The SIRMPol model provides halfway results between SIRM and SSM-R performances for all the three years considered.

Year	$\bar{R}_{12}$	M_{Model} **SIRM**	M_{Model} **SIRMPol**	M_{Model} **SSM-R**
2008	3	0.47	0.37	0.23
2009	4	0.43	0.36	0.21
1958	189	1.04	0.81	0.45

Table 4.3: Mean absolute deviations $(\sum_{i=1}^{n}|fo\text{F2}_{\text{SIRM}} - fo\text{F2}_{\text{obs}}|_i /n)_{\text{Model}} = M_{\text{Model}}$ for SIRM, SIRMPol and SSM-R models for 2008, 2009 and 1958. The values are expressed in MHz. The yearly mean $\bar{R}_{12}$ is also reported.

Therefore, the SSM-R provides a very accurate description of the monthly mean features of the parameter *fo*F2 at the mid-latitude station of Rome. It is worth noting that the used
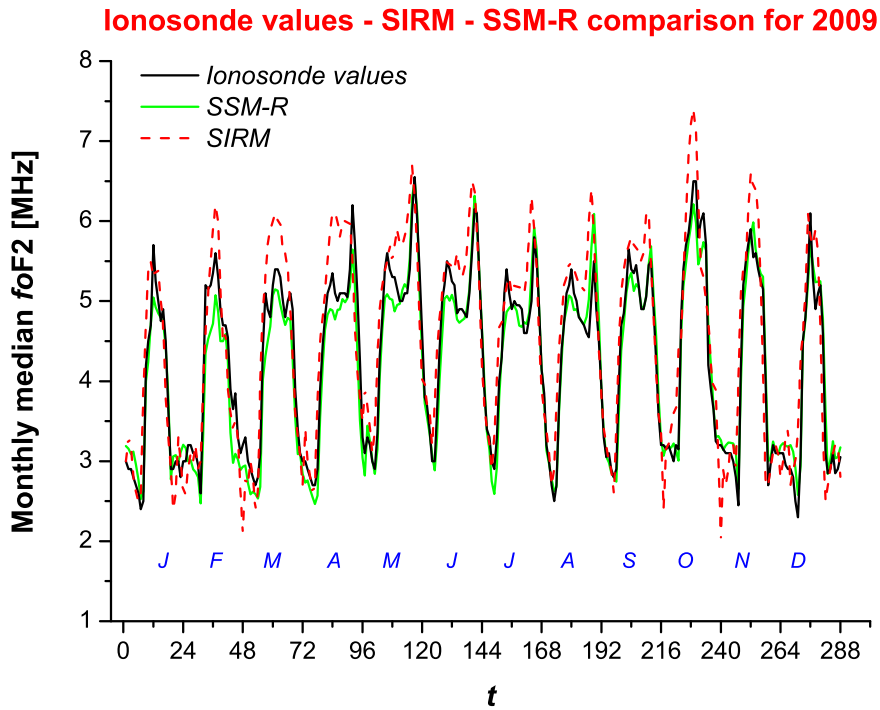
Ionosonde values - SIRM - SSM-R comparison for 2009

Figure 4.14: Same as Figure 4.12 for the year 2009.

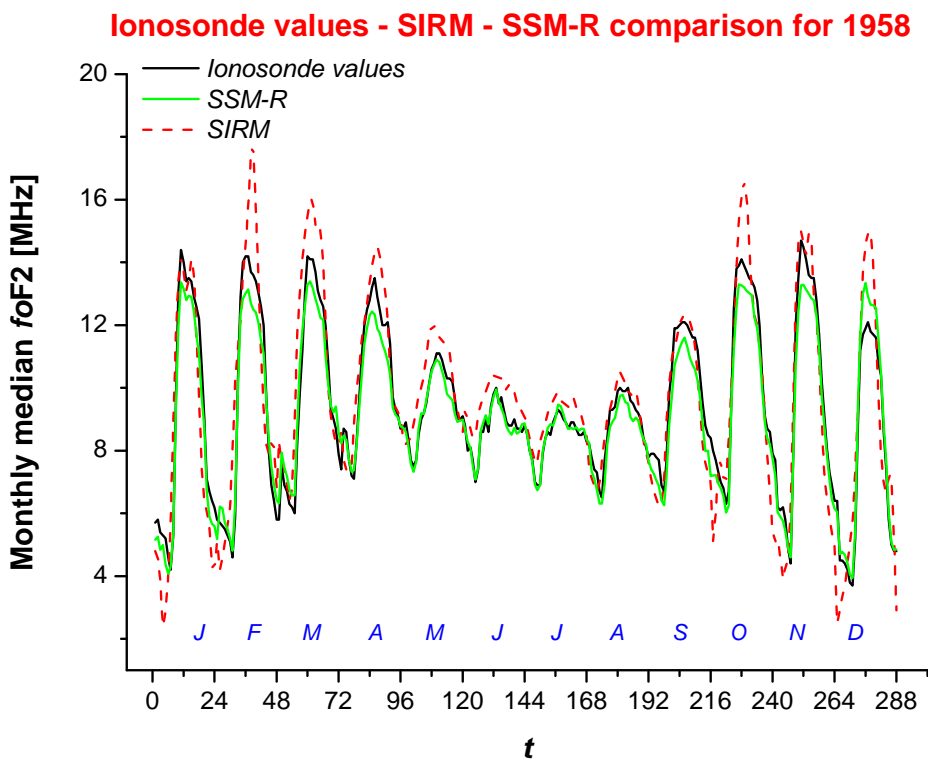**Ionosonde values - SIRM - SSM-R comparison for 1958**

Figure 4.15: Same as Figure 4.12 for the year 1958.

dataset is very long and continuous providing as a consequence very reliable analytical relations. Furthermore, the forecasting power of the SSM-R model is proved by the very good agreement for 2008 and 2009 that were not included in the regressions. Nevertheless, it is important to underline that a good forecast of the ionospheric parameters strongly depends on reliable forecasted values of the index R_{12}.

4.4   Conclusions

In this chapter the *fo*F2 outputs given by three models, namely SIRM, SIRMPol and SIRM-Rome have been compared with ionosonde data, for the mid-latitude station of Rome, for low solar activity (years 2008 and 2009) and high solar activity (year 1958).

The SIRM model provides for a quiet ionosphere a description and forecasting of the hourly monthly median vertical incidence ionospheric parameters. The SIRM model is a regional model characterized by a very simple procedure that (1) provides a quick response than global models such as IRI or NeQuick and (2) gives the possibility to interface it easily with other models. For these reasons, it has been widely used for the description and forecast of ionospheric parameters in the mid-latitude European area.

Nevertheless, SIRM is based on linear regressions between monthly median *fo*F2 values and the R_{12} index, that cannot be considered the best fitting relations.

The SIRMPol model provides a partial updating of the SIRM model. The main changes introduced in the SIRMPol are: (1) updating of the Rome ionosonde dataset (from 1957-1987 to 1957-2007); (2) use of second order polynomial regressions for the relations (*fo*F2 vs R_{12}); (3) use of 9 levels of solar activity instead of 2; (4) use of polynomial relations to fit the relations (A_n vs R_{12}) and (Y_n vs R_{12}) (which is a consequence of point (3)). The outputs of the SIRMPol model for low and high solar activity show a slight improvement with respect to the SIRM model. However, the SIRMPol model represents a local implementation of the SIRM model, which is suitable when an ionosondes network is available. For an accurate local description of ionospheric parameters, SSMs are preferable.

The local SSM-R model represents the best choice to describe and forecast the ionospheric parameters for the Rome station. The agreement with ionosonde data is optimal for both low and high solar activity, with a mean deviations reduction of $\sim$50% with respect to the SIRM model.

Better results are obtained for low solar activity than for high solar activity for all the three models. In fact, the corresponding mean deviations show an increase of $\sim$50% passing from low solar activity to high solar activity.

A complete updating of SIRM lies outside the objectives of the Ph.D. work here described. Anyhow, the analyses carried out to develop the SIRMPol and SSM-R models allow us to summarize the following guidelines that should be considered for a future complete updating of the SIRM model:

1. Besides those listed in Table 4.1, additional ionosondes have to be considered over the European area;

2. The model should be based on a "switch-case" between linear and 2° order polynomial regressions for the relationships (*fo*F2 vs R_{12}), and the choice between the two should be based on a deep statistical analysis of both the saturation effect occurrence and the loss of linearity for the last solar minimum;

3. Polynomial relations have to be used for the (A_n vs R_{12}) and (Y_n vs R_{12}) relationships;

4. The model, which is based on the Fourier analysis to link data from several ionosondes, should be supported and integrated with SSMs, elaborated for every ionosonde included in the network.

Furthermore, in the next years, it will be possible to analyze the characteristics of other solar activity indices (such as $MgII$ and EUV), when a longer dataset will be available for them. By considering $MgII$ and EUV instead of R_{12} should give better results for mid solar activity, due to a reduction of the hysteresis effect. Moreover, a future development of the SIRM model will concern both its applicability to high- and low-latitude regions, where more complex ionospheric behaviors in time and space are well known, and its use as a reference ionospheric model for regional short-term predictions.

Chapter 5

Analysis of the recent solar minima at mid and low latitudes and comparison with *IRI-2012* performances

Introduction

The solar EUV irradiance (10-120 nm) represents the main ionization source of the ionospheric F2 layer (e.g., Chen et al., 2012; Tobiska, 1996), and significantly affects the variability of ionospheric parameters such as the critical frequency of the F2 layer (foF2), and the corresponding maximum of electron density (NmF2) and height (hmF2). Therefore, as previously shown in Figure 1.2, it is expected that the time variation of these parameters follows almost identically the variations of the solar activity.

In recent years, there has been an increasing interest in the study of the ionospheric plasma response to extreme solar activity conditions, that is for periods of maximum or minimum solar activity.

As reported in Chapter 2, the last solar minimum (minimum 23/24 with a deep phase in years 2008-2009) has been characterized by an unprecedented low and prolonged solar activity, providing a unique natural window to study the ionosphere under extreme conditions of solar activity. At the same time, it is particularly interesting to evaluate the differences encountered in the pattern of the main ionospheric parameters, comparing the last minimum with the previous ones. Moreover, since the ionosphere is significantly latitudinal-dependent, it is important to compare results obtained at mid latitudes with those recorded at low latitudes.

In Section 1.2 has been described how some particular ionospheric effects strongly depend on solar activity level. In particular, strictly linked to the solar activity level, two typical ionospheric anomalies can be analyzed to detect the anomalous conditions characterizing the last solar minimum: the winter anomaly and the semi-annual anomaly (Chen and Liu, 2010; Dominici, 1971; Ezquer et al., 2014; Liu et al., 2012; Rishbeth and Setty, 1961; Rishbeth and Garriot, 1969; Rishbeth et al., 2000; Torr and Torr, 1973; Yonezawa and Arima, 1959; Yonezawa, 1967, 1971). As already described in Chapter 1, the winter anomaly consists of lower local noon NmF2 values recorded in summer than in winter. It has been proposed that this anomaly is related to changes in the neutral composition of the atmosphere, generated by a heating of the summer hemisphere which gives rise to a convection of lighter neutral elements towards the winter hemisphere, which causes changes in the ratio of [O]/[N2] in both hemispheres (Johnson, 1964; Rishbeth and Setty, 1961; Torr and Torr, 1973). This anomaly tends to disappear for low

solar activity at low latitudes (e.g., Ezquer et al., 2014). The semi-annual anomaly is characterized by NmF2 values that are greater around equinoxes (April and October) than at solstices (June and December). This anomaly is more visible at low latitudes (e.g., Ezquer et al., 2014; Rishbeth and Garriot, 1969), and the corresponding amplitude is larger for high solar activity (Ma et al., 2003). Several mechanisms have been proposed to explain this anomaly. Yonezawa (1971) proposed that it is related with the variation of the upper atmosphere temperature. Torr and Torr (1973) suggested that it is due to semi-annual variations of neutral densities associated with the geomagnetic and auroral activity. Mayr and Mahajan (1971) showed that the anomaly requires significant variation in the neutral composition at lower height. Ma et al. (2003) suggested that the semi-annual variation of the diurnal tide in the lower thermosphere induces the semi-annual variation of the amplitude of the equatorial electrojet, thus causing the semi-annual anomaly at low latitudes.

However, it is worth noting that the winter anomaly and the semi-annual anomaly are strongly influenced by solar activity variations and therefore they represent good indicators of the overall solar activity level. Therefore, it is interesting to evaluate the observed response of these two anomalies to the very low solar activity occurred during the last minimum at both low and mid latitudes.

Furthermore, the last solar minimum was characterized by a very long duration. In fact, the last minimum began around March 2006 and many predictions of the start and size of solar cycle 24 were given thereafter and corrected many times (Pesnell, 2008). The minimum actually happened in the middle of 2009 and thus more than 2 years after the earliest prediction (Zakharenkova et al., 2013).

The problem linked with the predictability of this minimum has been already discussed in Section 2.2 and shown in Figure 2.7 where monthly median values for three different updates of the Ionospheric Index IG12 (Liu et al., 1983) were plotted for the recent solar cycles. With a focus on the deeper part of the last minimum (years 2008-2009), the figure shows how this minimum was expected well before and with a level of solar activity higher than the measured one. Considering that ionospheric models strongly depend on input parameters, such as geomagnetic and solar activity indices, it is very interesting to test the reliability of ionospheric models during the last solar minimum, for both mid- and low-latitude ionosphere, and compare the results with the previous minima.

Among the numerous global models, the *International Reference Ionosphere* (*IRI*) (e.g., Bilitza, 2001; Bilitza and Reinisch, 2008; Bilitza et al., 1990, 2014) is the best-known and most widely used empirical model for the description of the ionosphere. IRI results depend on several input parameters, like the solar activity and magnetic indices, and the use of uncertain predicted values of them can lead to significant discrepancies in the model outcome (Zakharenkova et al., 2013). The aforementioned IG12 index represents one of the parameters used as input by the model, therefore it was expected that IRI had some problems in representing the ionosphere during the minimum 23/24, also because there were no previous data recorded under similar conditions for IRI modeling (Bilitza et al., 2012).

In this chapter, an analysis of the recent solar minima and the investigation of the IRI model reliability, at mid- and low-latitude stations is carried out. The study is based on data from four ionospheric stations: Rome (41.8°N, 12.5°E, geomagnetic latitude 41.7°N, Italy), Gibilmanna (37.9°N, 14.0°E, geomagnetic latitude 37.6°N, Italy), São José dos Campos (23.1°S, 314.5°E, geomagnetic latitude 19.8°S, Brazil), and Tucumán (26.9°S, 294.6°E, geomagnetic latitude 17.2°S, Argentina). Rome and Gibilmanna are descriptive of the mid-latitude ionosphere, while São José dos Campos and Tucumán represent low-latitude stations located in an ionosp-

herically critical position, being close to the south crest of the *Equatorial Ionization Anomaly*, representing one of the most relevant and dynamically complex ionospheric phenomena.

The analysis is focused on the electron density peak NmF2 and the height hmF2 at which it is reached. The particularity of the ionospheric behaviors during the last solar minimum is emphasized by an inter-minima comparison for both parameters. Moreover, the reliability of the output given by the last version of the IRI model, namely IRI-2012 (Bilitza et al., 2014), is tested for both parameters, by comparing it with the one recorded by the ionosonde. Using data from the four aforementioned ionosondes, a comparison between results obtained at mid and low latitudes, for both the inter-minima comparison and the IRI-2012 reliability, can be carried out.

Section 5.1 is dedicated to a description of the dataset used for the four ionosondes and to the analyses carried out to discuss (1) the most relevant differences between the last minimum and the previous ones concerning NmF2 and hmF2 patterns, (2) the differences between results obtained at mid and low latitudes and (3) the reliability of IRI-2012 for both mid and low latitudes, for both parameters considering low solar activity periods. Section 5.2 reports the comparison between the last solar minimum features of NmF2 and hmF2, and those characterizing the previous minima. Section 5.2.1 and Section 5.2.2 are dedicated to compare results obtained at mid-latitude and low-latitude stations, respectively. Particular emphasis is given to the winter and semi-annual anomalies visibility, used as indicators of the solar activity level for both latitudes. Section 5.3 is devoted to the comparison between ionosonde data and IRI-2012 outputs for NmF2 and hmF2. Section 5.3.1 introduces briefly the main characteristics of the IRI model and some results, complementary to what already reported in Section 2.2 and Figure 2.8. As for the results of Section 5.2, also the results related to the comparison between the output of IRI-2012 and that from the ionosonde are reported separately for the mid-latitude stations of Rome and Gibilmanna (Section 5.3.2) and for the low-latitude stations of São José dos Campos and Tucumán (Section 5.3.3). Conclusions are the subject of Section 5.4.

5.1 Datasets and analysis

5.1.1 Data Sources

The study is based on data from four ionospheric stations: Rome (41.8°N, 12.5°E, geomagnetic latitude 41.7°N, Italy), Gibilmanna (37.9°N, 14.0°E, geomagnetic latitude 37.6°N, Italy), São José dos Campos (23.1°S, 314.5°E, geomagnetic latitude 19.8°S, Brazil), and Tucumán (26.9°S, 294.6°E, geomagnetic latitude 17.2°S, Argentina). Rome (hereafter RM) and Gibilmanna (GL) are descriptive of the mid-latitude ionosphere, while São José dos Campos (SJ) and Tucumán (TU) represent low-latitude stations located in an ionospherically critical position, being close to the south crest of the *Equatorial Ionization Anomaly* (*EIA*). Figure 5.1 shows the location of the four aforementioned ionosondes, along with the constant main field inclination isolines (red for positive inclination, blue for negative inclination) and the geographic latitude and longitude. Bands embracing low-latitude/equatorial regions (yellow dashed lines, within ±30° geographic latitude), mid-latitude regions (blue dashed lines, between ±30° and ±60° geographic latitude) and polar regions (> 60° geographic latitude) are also indicated. Moreover, the north and south crests of the EIA are displayed with black dashed lines.

RM, GL and TU stations are all equipped with an *AIS-INGV* (*Advanced Ionospheric Sounder-INGV*) ionosonde (Zuccheretti et al., 2003); SJ station is equipped with a *CADI* (*Canadian Advanced Digital Ionosonde*) ionosonde (MacDougall et al., 1997).
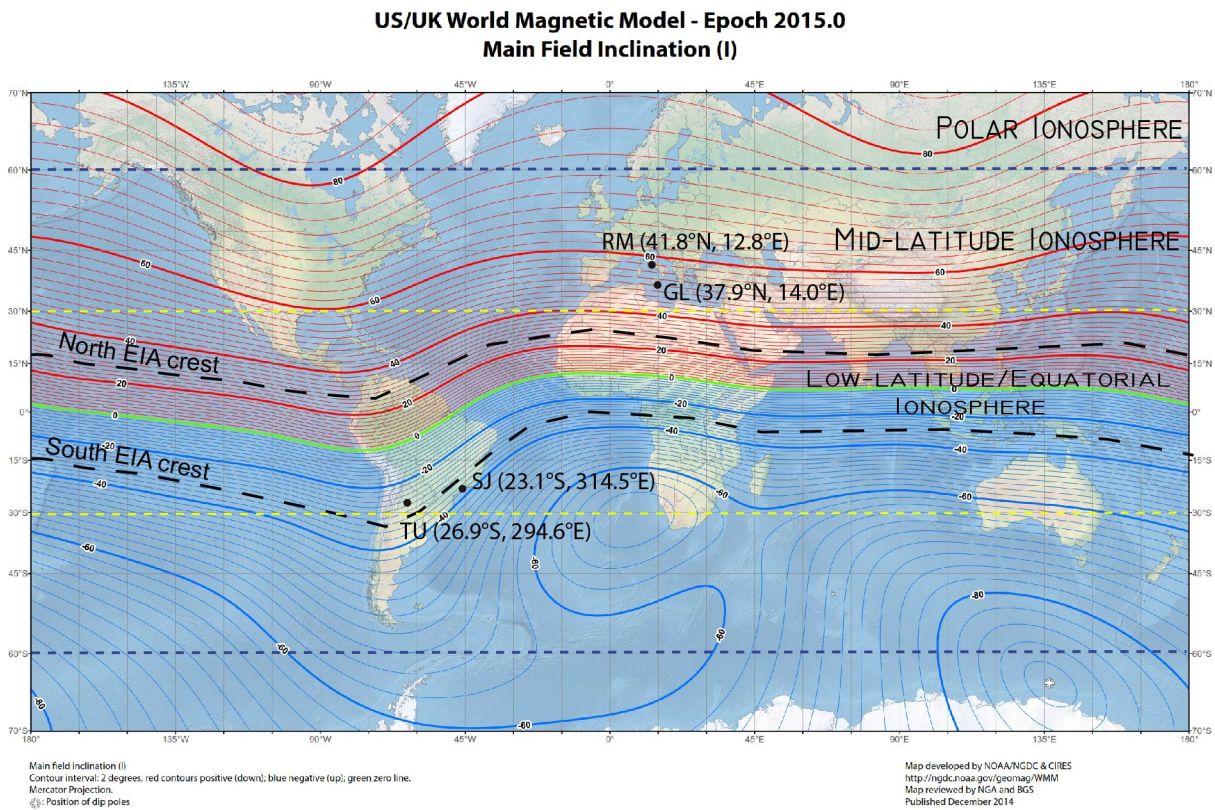
Figure 5.1: Location of the four ionosondes, along with constant main field inclination isolines (red for positive inclination, blue for negative inclination). The geographic latitude and longitude are indicated. The black dashed lines represent the north and south crests of the EIA, to emphasize the position of SJ and TU upon the south one. Furthermore, the three main bands in which the ionosphere can be divided are underlined: low-latitude/equatorial (within $\pm 30°$ geographic latitude), mid-latitude (between $\pm 30°$ and $\pm 60°$ geographic latitude) and polar ($> 60°$ geographic latitude).

As reported in Section 3.1, at Rome station foF2 values were all validated from traces recorded by classical ionosondes, which cannot tag the different polarization characterizing the two different modes of propagation of the electromagnetic wave. A VOS-1 chirp ionosonde produced by the Barry Research Corporation, Palo Alto, CA, USA (Barry Research Corporation, 1975) sounded from January 1976 to November 2004, and then it was replaced by an AIS-INGV ionosonde. Therefore, a very long, continuous and very reliable dataset is available, with hourly validated values of foF2 starting from January 1976, and monthly median values of foF2 starting from 1957: a period covering the last five solar cycles.

The GL station is equipped with an AIS-INGV ionosonde since November 2002. Before, the ionospheric observatory was equipped with a Digisonde 128P produced by the Center for Atmospheric Research of the University of Lowell, MA (USA) (Bibl and Reinisch, 1975). The ionograms were recorded on paper and manually scaled by specialized operators. For this station, data are available starting from April 1976, but unfortunately the dataset is discontinuous with a lack of data for many years. For our purposes, the minimum 21/22 (1986-1987) and 23/24 (2008-2009) will be representative for this station.

The ionospheric measurements at TU began in 1957, the International Geophysical Year, when an analogical ionosonde was transferred from the Navy of Argentina to the National University of Tucumán. That ionosonde stopped working in 1987 (Ezquer et al., 2014). In

August 2007, an AIS-INGV was installed at the Upper Atmosphere and Radiopropagation Research Center of the Regional Faculty of Tucumán of the National Technological University (UTN). Data for the last five minima, except for the minimum 22/23, are available for this station.

In SJ a Canadian Advanced Digital Ionosonde is operational and located at the UNIVAP (Universidade do Vale do Paraíba) since August 2000. The digital ionosonde antenna is a double delta dipole array supported by a 20 m tower, where one of the dual antennas is used for transmitting and the other one is used for receiving (Grant et al., 1995; MacDougall et al., 1997). For our purposes, data are available only for the last solar minimum.

In this chapter, the analyses are done for the parameters NmF2 and hmF2. As already described, NmF2 represents the maximum electron density of the ionospheric vertical electron density profile. It is linked to foF2 by the relation NmF2 $[\mathrm{m}^{-3}]{=}1.24 \cdot 10^{10}(fo\mathrm{F2}\ [\mathrm{MHz}])^2$. Values of NmF2 were calculated using this equation, starting from manually validated values of foF2. As for all foF2 data used in the present work, foF2 values were validated according to the International Union of Radio Science (URSI) standard (Wakai et al., 1987), and all the corresponding numerical values were considered independently of the presence of qualifying and descriptive letters. foF2 validated data were downloaded from the electronic Space Weather upper atmosphere database (eSWua; http://www.eswua.ingv.it/) (Romano et al., 2008). The parameter hmF2 has been obtained using the Shimazaki and D55 analytical formulations, defined by equations (1.26) and (1.27). As explained in Section 1.3.2, these formulations require the knowledge of the parameters foF2 and $MUF(3000)$F2 (Shimazaki) and foF2, $MUF(3000)$F2 and foE (D55); all these parameters can be directly reduced from ionograms and have been manually scaled. It is important to underline that foE is a parameter that can be obtained only during daytime hours, therefore hmF2 from D55 analytical formula is available only during daytime, while hmF2 from Shimazaki is available for all 24 hours.

The use of analytical formulations is necessary when a long dataset has to be studied, because the inversion of a consistent number of ionograms require an extremely long validation procedure. In these situations, the analytical formulations provide reliable values for hmF2 if used in opportune time ranges. For this purpose, a preliminary study has been carried out, comparing hmF2 values from Shimazaki and D55 with those obtained after performing an automatic inversion of the ionogram. In detail, a comparison has been carried out for the Rome ionosonde, for which hmF2 values from two different kind of automatic inversions, namely *ARTIST* (Galkin and Reinisch, 2008) and *Autoscala* (Pezzopane and Scotto, 2005), were available.

The corresponding results are displayed in Figure 5.2. The figure reports hourly monthly median values for the parameter hmF2, for the Rome ionosonde, calculated using data from Shimazaki (black) and D55 (red) analytical formulations, and from automatic inversion models ARTIST (green) and Autoscala (blue). The comparison has been carried out for summer, winter and equinoctial months for both 2008 and 2009. Figure 5.2 reports results for the summer months of July 2008 and 2009, and for the winter months of December 2008 and 2009. A detailed analysis of "reliability zones" for the Shimazaki and D55 is out of the scope of the present work. However, for our purpose, the key information retrieved from this analysis are: (1) the Shimazaki formula provides reliable hmF2 values during nighttime hours (19:00-06:00 LT); (2) the D55 formula gives reliable hmF2 values during daytime hours (07:00-18:00 LT), in particular for winter/autumn months; (3) the Shimazaki formulation provides strong overestimations during daytime hours, in particular for spring/summer months. By virtue of the aforementioned results, the ionosonde hmF2 values used in this part of the work has been calculated using the
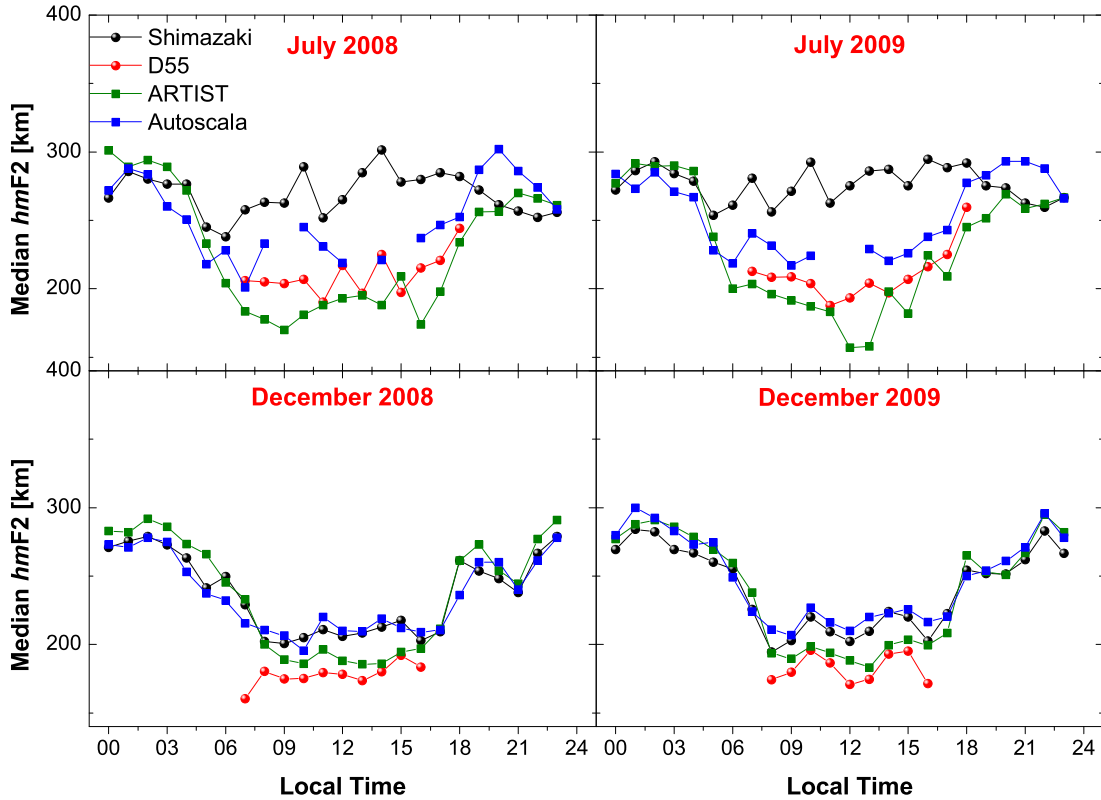
Figure 5.2: Monthly median values of hmF2 from Shimazaki (black), D55 (red), ARTIST (green) and Autoscala (blue) for the months of July 2008 and 2009 and December 2008 and 2009.

Shimazaki formula (1.26) for the nighttime range 19:00-06:00 LT and using the D55 formula (1.27) for the daytime range 07:00-18:00 LT.

Values of NmF2 and hmF2 from the IRI-2012 model were obtained using as input the latest updates for the solar and geomagnetic activity indices. In particular, since the IRI model uses the ionospheric-effective solar index IG12 to obtain NmF2 (Bilitza et al., 2012), it is important to underline that, having in mind the results and discussions reported in Section 2.2, the latest available IG12 update was used. Furthermore, after a preliminary comparison for the RM station, the International Radio Consultative Committee (CCIR) coefficients (CCIR, 1967a,b) were preferred to the Union of Radio Science (URSI) (Rush et al., 1989) ones (see Section 5.3.1 for more details).

Table 5.1 summarizes, for every station, the minima that can be analyzed for the parameters NmF2 and hmF2, considering the data available. For each minimum of solar activity, two years were chosen as representative using the following scheme: 1964-1965 (min 19/20), 1975-1976 (min 20/21), 1986-1987 (min 21/22), 1996-1997 (min 22/23), and 2008-2009 (min 23/24).

5.1.2   Analysis method

The analyses carried out can be divided in two main parts: (1) an inter-minima comparison of NmF2 and hmF2; (2) a comparison between measured NmF2 and hmF2 values and those given as output by the IRI-2012 model.

Station	Minima for which NmF2 values are available	Minima for which hmF2 values are available
Rome	19/20 - 20/21 - 21/22 - 22/23 - 23/24	21/22 - 22/23 - 23/24
Gibilmanna	21/22 - 23/24	21/22 - 23/24
Tucumán	19/20 - 20/21 - 21/22 - 23/24	23/24
São José dos Campos	23/24	23/24

Table 5.1: Minima for which NmF2 and hmF2 data are available for the four considered ionosondes.

To obtain a quantitative and reliable minimum-to-minimum difference, only the continuous hourly validated data available for the four stations have been used. Therefore, this analysis takes into account only the last three solar minima: the minimum 21/22 (years 1986-1987), the minimum 22/23 (years 1996-1997) and the minimum 23/24 (years 2008-2009) for the stations of RM, GL and TU. For the SJ ionosonde, only the last solar minimum is available for both NmF2 and hmF2, therefore is not possible the comparison between the last minimum and the previous ones. Nevertheless, the station of SJ is useful to confirm (or not) the results obtained for the last minimum at TU.

For RM, GL and TU stations, for which an inter-minima comparison is possible, seasonal median values were calculated in the following way: for each considered year, four seasons were definite considering 60 days around the March Equinox (Days of the Year (DOY) from 51 to 111), around the June Solstice (DOY 144-204), around the September Equinox (DOY 237-297), and around the December Solstice (DOY 327-022). For every season and every minimum, the hourly representative value is then calculated as a median of 120 values (60 values for every year). It is worth highlighting that the median is calculated only if at least 40 values out of 120 are available. With these choices, the comparison between different minima can be considered highly reliable, as already shown by Liu et al. (2012). It is important to underline that data for the last three solar minima are available only for the RM station. For GL and TU stations, only a comparison between the last minimum and the minimum 21/22 is possible.

Monthly median values of NmF2 will be used to analyze the winter and the semi-annual anomalies. In particular, hourly median values for April and October (equinoxes) and June and December (solstices) were considered. As shown in Table 5.1, monthly median values are available for RM for the last five minima; for TU, data of the minimum 22/23 are not available, while for GL data are available only for minima 21/22 and 23/24. The monthly median values have been calculated only if at least 15 values were available for a month.

The comparison between observed values and IRI-2012 outputs is done by considering hourly monthly median values for the two years included in each minimum. To catch the performances of IRI-2012, the relative percentage difference ($PD(\%)$ parameter) was calculated according to Bilitza et al. (2012):

$$PD(\%) = \frac{A_{\text{IRI}} - A_{\text{Iono}}}{A_{\text{Iono}}} \cdot 100, \tag{5.1}$$

where A_{IRI} and A_{Iono} are respectively monthly median values of NmF2 or hmF2 calculated by using IRI-2012 outputs and ionosonde data.

To display the results, opportune percentage relative difference maps were created. In

these maps, the $PD(\%)$ parameter is plotted with the local time on the x axis and the month on the y axis. Therefore, using a chromatic scale, it is possible to visualize easily zones of underestimation/overestimation made by the model. Furthermore, for every map a unique percentage value is calculated, that is a mean of $|PD(\%)|$ on 24-hours and two-years values, for each minimum. In this way, we have a measure of the "distance" between observed values and IRI model outputs. Comparing this value for different minima and for different latitudes, we can evaluate if there has been a real worsening of IRI performances for the last minimum and if latitudinal dependences are observed. Moreover, a possible dependence on the hour of the day is analyzed by plotting the $PD(\%)$ parameter for each available minimum, separately for daytime hours (10:00-14:00 LT) and nighttime hours (22:00-02:00 LT).

5.2 Results for inter-minima comparison

In this section, the results of the comparison between NmF2 and hmF2 values measured during the last solar minimum 23/24 (years 2008-2009) and the previous ones will be reported. As mentioned, this analysis cannot be done for the SJ station for which there are not data for the previous minima. Furthermore, for the hmF2 parameter, the comparison is possible only for the mid-latitude ionosondes of RM and GL.

As shown in Chapter 3, for Rome station a long and continuous dataset is available for the main ionospheric parameter foF2. This dataset provides the possibility to apply a 1-year running mean, emphasizing the solar activity influence on the foF2 parameter, cleaning the foF2 time series from short-time ionospheric features, like those caused by geomagnetic disturbances, ionospheric seasonal and day-to-day variations. Before to show the inter-minima comparisons carried out with the analyses described in Section 5.1.2, it is interesting to report the inter-minima comparison obtained for Rome station after the application of a 1-year running mean to the foF2 dataset. Figure 5.3 shows the 1-year running mean of foF2 registered at local noon (12:00 LT) at RM station, for the whole dataset used in the present work (January 1976-December 2013). It is highlighted the measured difference of 0.5 MHz between the absolute minimum of the last minimum and the previous one, resulting in a relevant decrease of $\sim$10%.

Figure 5.4 shows the hourly percentage differences between the foF2 absolute minima (after the application of a 1-year running mean) measured for the last solar minima. Black dots indicate the differences between minimum 23/24 and 22/23, green dots between minimum 22/23 and 21/22 and blue dots between the minimum 21/22 and 20/21. The differences are normalized to the value of the previous minimum between the two considered. The figure clearly shows how a huge decrease for all hours characterizes the passage from the minimum 22/23 to the minimum 23/24, with a mean decrease (over the 24h) of $\sim$9%. Comparing the previous minima, mean decreases of $\sim$1% (between min 21/22 and 22/23) and $\sim$0% (between min 20/21 and 21/22) appear. Furthermore, a slightly hour dependence is found with a more pronounced decrease between the last two minima in the range 15:00-19:00 LT.

These simple preliminary results underline how very particular conditions have characterized the ionospheric plasma during the last solar minimum, with foF2 values significantly lower than those recorded in previous minima.

5.2.1 Results at mid latitudes: Rome and Gibilmanna

Figures 5.5 and 5.6 show the seasonal inter-minima comparison of NmF2 for the mid-latitude stations of RM and GL, by considering the minimum of cycle 21/22 (black points), the minimum
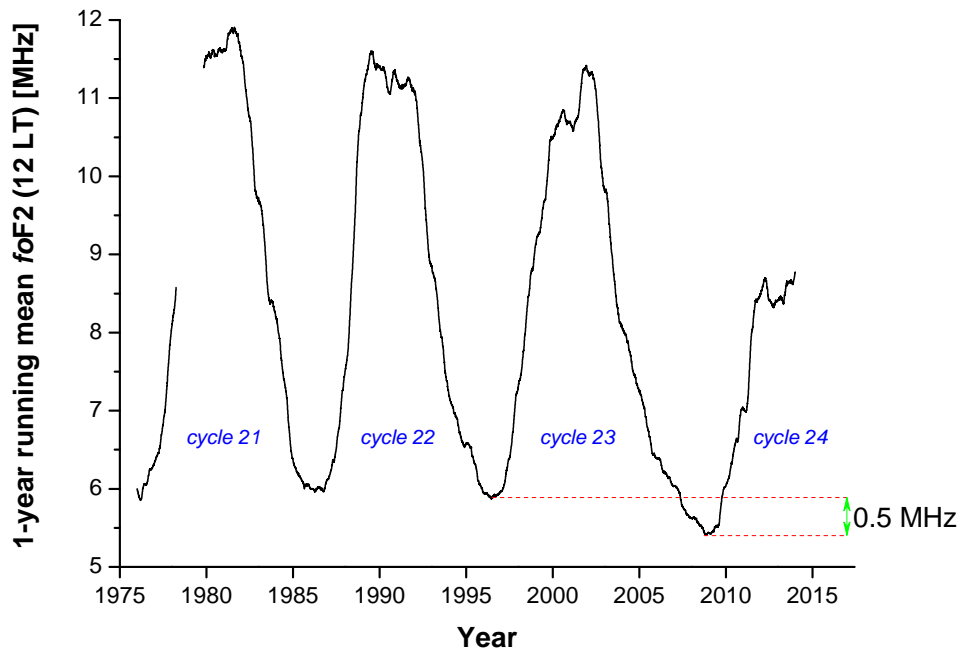
Figure 5.3: 1-year running mean of foF2 at local noon for the Rome ionosonde for the dataset January 1976-December 2013.
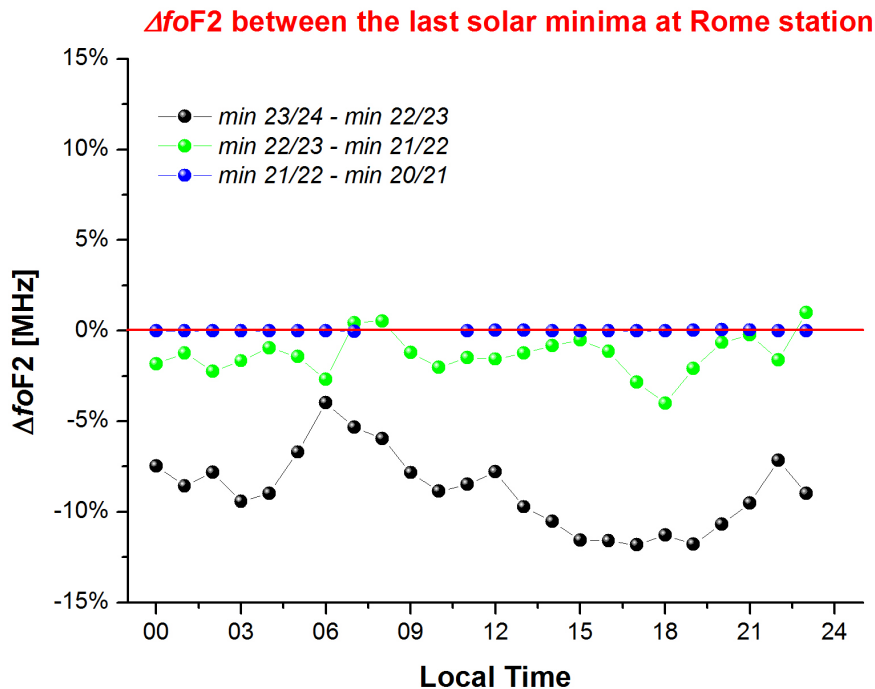

Figure 5.4: Hourly foF2 percentage differences between the last solar minima at Rome ionosonde. Black dots indicate the differences between minimum 23/24 and 22/23, green dots between minimum 22/23 and 21/22 and blue dots between the minimum 21/22 and 20/21. The red line indicates the zero value.

min 23/24-21/22 comparison	March Equinox	June Solstice	September Equinox	December Solstice	Yearly mean
Rome	-18%	-21%	-21%	-21%	-20%
Gibilmanna	-3%	-16%	-13%	-16%	-12%
Tucumán	-38%	-39%	-31%	-18%	-32%
min 23/24-22/23 comparison	**March Equinox**	**June Solstice**	**September Equinox**	**December Solstice**	**Yearly mean**
Rome	-12%	-18%	-21%	-19%	-18%

Table 5.2: Relative percentage variations averaged over 24 hours. The percentage is calculated using the relation $((NmF2_{min23/24} - NmF2_{minX})/NmF2_{minX}) \cdot 100$, where X can represent the minimum 21/22 or 22/23. The values used for $NmF2$ are the seasonal median plotted in Figures 5.5 and 5.6.

of cycle 22/23 (blue points), and the minimum of cycle 23/24 (red points).

It is possible to observe that the values measured for the last solar minimum are lower than those of the previous ones. This is true for both stations and for all the analyzed seasons. This result agrees with what was found by other authors (Ezquer et al., 2014; Lee and Reinisch, 2012; Liu et al., 2011a, 2012). On the contrary, it does not agree with what was shown by Araujo-Pradere et al. (2011) who did not find a decrease of $NmF2$ for the last minimum with respect to the minimum 22/23, for the mid-latitude station of Point Arguello (42.3°N, 239.4°E, USA).

Table 5.2 shows the seasonal relative percentage variations (averaged over 24 hours) between minima 21/22 and 23/24 (for RM, GL and TU), and between minima 22/23 and 23/24 (only for RM). The values for the relative percentages were calculated using the relation $(NmF2_{min23/24} - NmF2_{minX})/NmF2_{minX} \cdot 100$, where X can represent the minimum 21/22 or 22/23. The results for TU ionosonde are discussed and compared to RM and GL in Section 5.2.2.

For RM and GL, it is possible to perform an inter-station comparison between values during the minimum 21/22 and 23/24. Yearly mean decreases of -20% and -12% for RM and GL have been obtained, respectively. Therefore, a significant difference can be observed between the results of the two stations; however, this might be due to the lack of data characterizing GL in March and June for the last minimum, providing possible underestimated decreases.

In detail, from Table 5.2 and Figure 5.5, it is possible to observe that at RM the decrease between the minimum 21/22 and the minimum 23/24 is more pronounced than that between the minimum 22/23 and the last minimum, showing a monotone decreasing trend of $NmF2$ considering the last three solar cycles. A similar decreasing pattern can be observed for all seasons with the most pronounced decrease being observed for the June Solstice for the nighttime range 21:00-04:00 LT (mean decrease of -43% between minima 21/22 and 23/24, and -27% between minima 22/23 and 23/24). Nevertheless, considering all the seasons, the largest decreases are visible during the local sunset hours 16:00-18:00 LT (-28% between minima 21/22 and 23/24 and -24% between minima 22/23 and 23/24), while the lowest decreases occur at local sunrise hours 06:00-07:00 LT (+7% between minima 21/22 and 23/24 and -9% between minima 22/23 and 23/24).

Similar results are obtained for the GL station, as shown in Figure 5.6 and confirmed by values in Table 5.2, with percentage variations less pronounced than for RM. For March
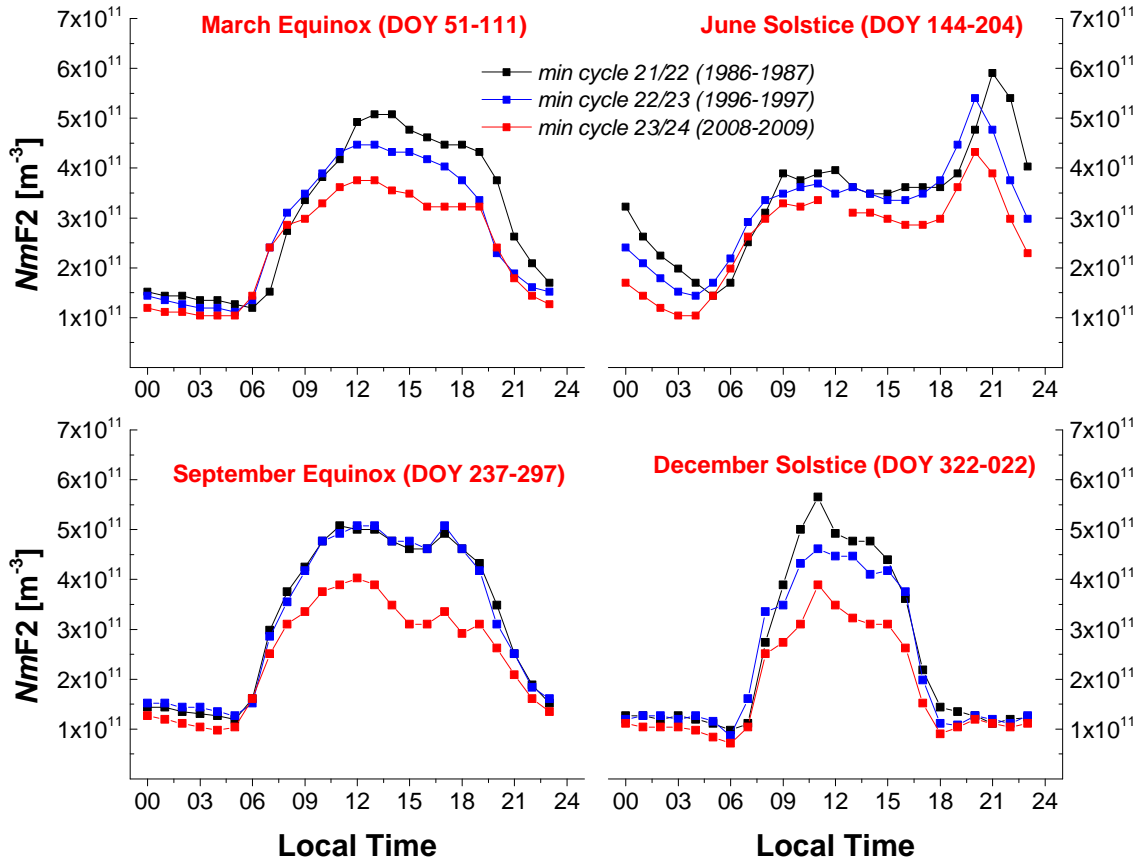
Figure 5.5: Seasonal median values of NmF2 for the minimum 21/22 (black squares), 22/23 (blue squares) and 23/24 (red squares), for RM.

Equinox, at GL is registered a mean decrease of -3% that is much lower than the one measured for RM (-18%). However, as clearly shown by Figure 5.6, this is likely due to the lack of data for GL station for the range 01:00-13:00 LT. It is worth noting that, considering daytime hours (09:00-18:00 LT), it is observed an important decrease during December Solstice between minima 21/22 and 23/24, for both RM and GL (mean decrease of -32% and -21% respectively), resulting in the most pronounced one considering all seasons. On the contrary, the lower decreases are found during nighttime hours of September Equinox and December Solstice, for both ionosondes. In particular, at GL comparable values between the minimum 21/22 and 23/24 are observed.

Using monthly median values, available also for the minima 19/20 and 20/21 for RM, it is possible to analyze two characteristic ionospheric anomalies already introduced in Section 1.2: the winter anomaly and the semi-annual anomaly. Figure 5.7 shows the monthly median values for April, June, October and December, for the years of recent minima, as recorded at RM. In order to distinguish the contribution of the solar activity to the seasonal differences shown by the NmF2 values, Table 5.3 reports the monthly mean sunspot numbers R_{12} of April, June, October and December for the last 5 solar minima.

For the mid-latitude station of RM, it is interesting to note that the winter anomaly is not visible for both years (2008 and 2009) of the minimum 23/24, while it is clearly visible during the minima 21/22, 20/21, for the year 1964 of the minimum 19/20 and for the year 1997 of the minimum 22/23, while it is barely visible for the year 1996 of the minimum 22/23. Hence,
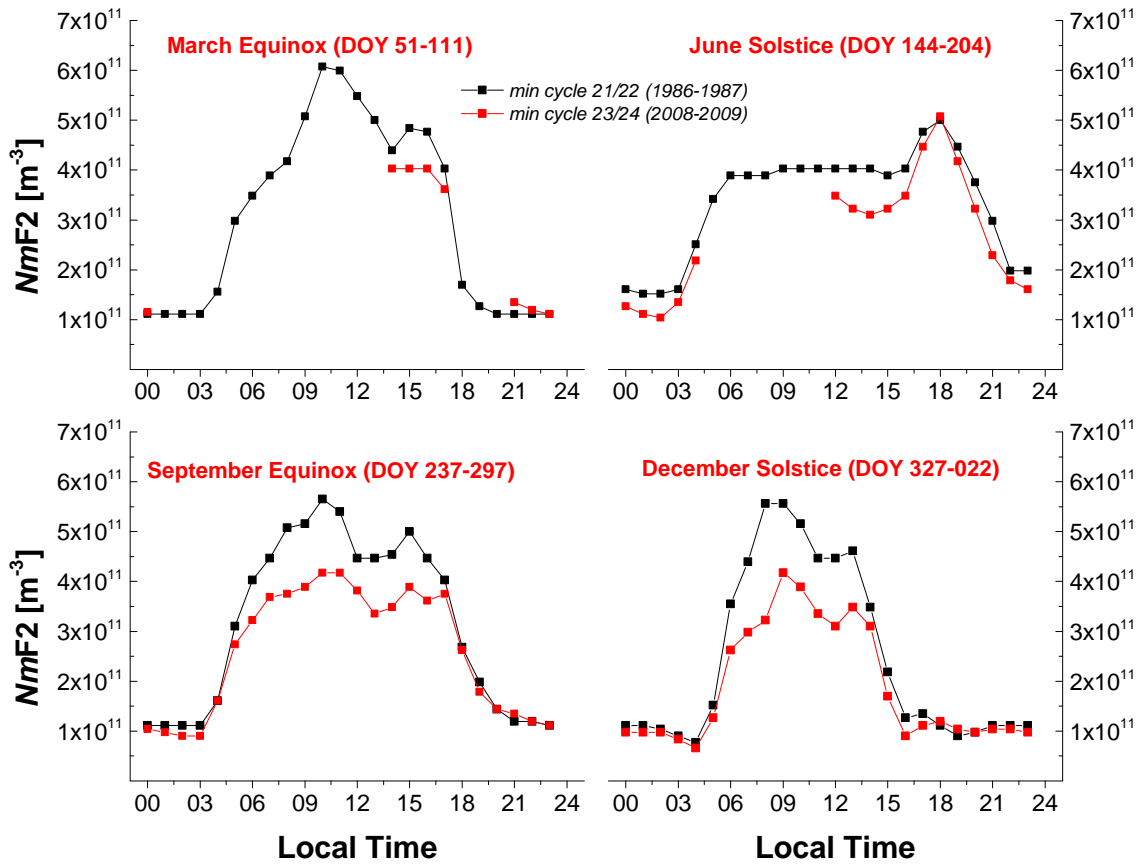
Figure 5.6: Same as Figure 5.5 but for GL.

remembering the monotone behaviour of the NmF2 values for the last three solar minima and the clear visibility of the winter anomaly for high solar activity years reported in Figure 2.5, it is confirmed that at mid latitudes the winter anomaly tends to disappear as the solar activity decreases. The fact that this anomaly is not visible at all for the two years of the last minimum proves the particular response of the ionospheric plasma to the last anomalous solar minimum. The same phenomenon is recorded at GL (plot not shown).

Another ionospheric feature that can be analyzed from Figure 5.7 is the semi-annual anomaly. Concerning RM (and GL), this anomaly is clear for October, and less obvious for April, anyhow its amplitude tends to decrease for the last solar minimum. However, it is not a typical mid-latitude anomaly, being more visible at low latitudes.

For the height hmF2 of the electron density peak, for RM and GL it is possible to perform an inter-minima comparison, using the values provided by the Shimazaki and D55 analytical formulations. As previously anticipated, using Shimazaki for the range (19:00-06:00 LT) and the D55 for the range (07:00-18:00 LT), indicative hmF2 values can be obtained. The results obtained are shown in Figures 5.8 and 5.9 respectively, with seasonal and yearly averaged minimum-to-minimum differences reported in Table 5.4.

It is observed how the hmF2 values measured during the last solar minimum result lower than the previous ones for both stations, as for NmF2. Seasonal averages reported in Table 5.4 show how for RM and GL a similar pattern can be observed, with particularly low inter-minima differences during March Equinox and very pronounced differences for December Solstice, com-
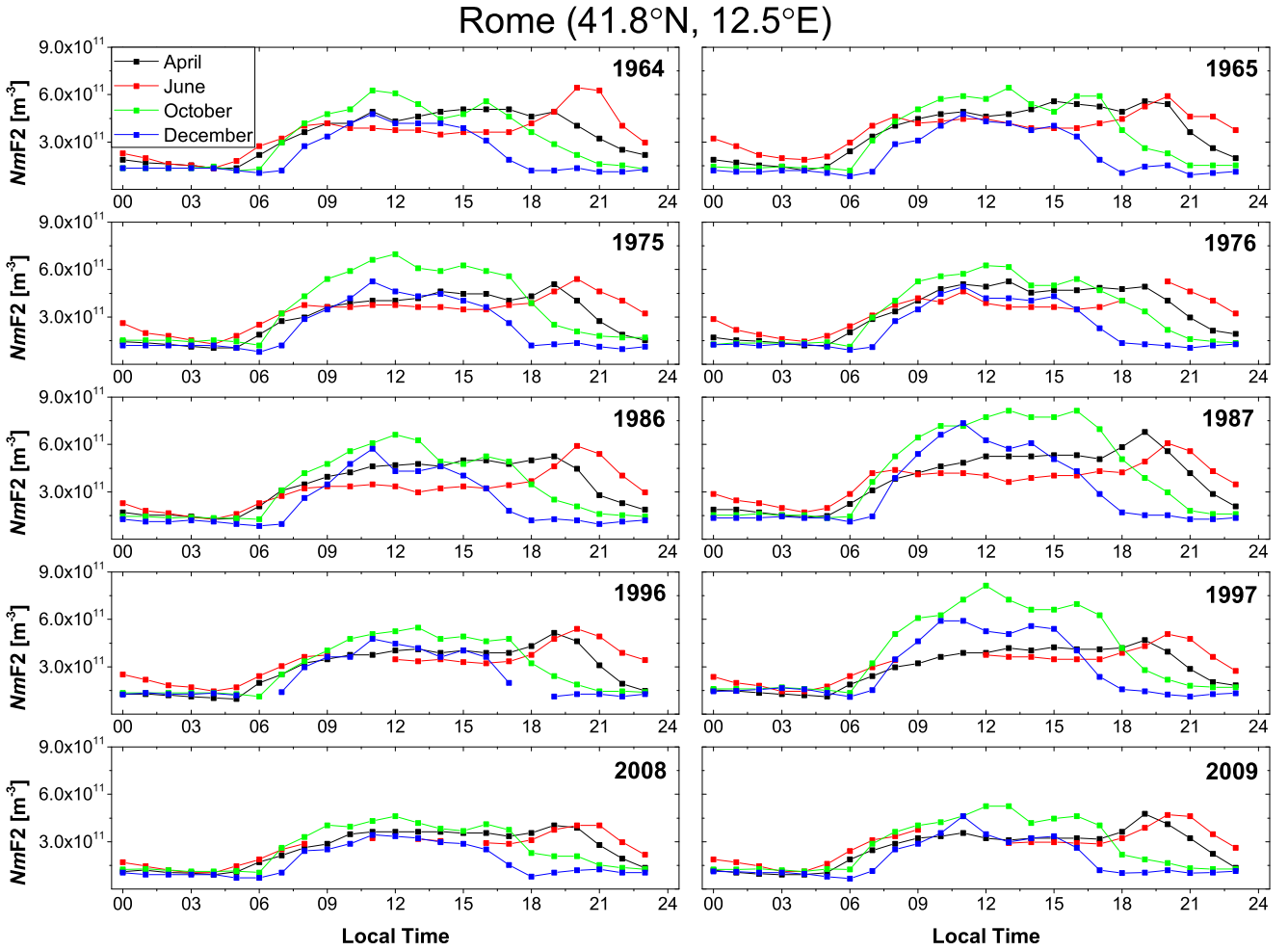
Figure 5.7: Hourly monthly median *Nm*F2 values for April (black squares), June (red squares), October (green squares) and December (blue squares), for the solar activity minima 19/20, 20/21, 21/22, 22/23, and 23/24, for RM.

Year	April	June	October	December
1964	12.9	13.5	9.2	22.1
1965	10.2	23.3	29.1	24.7
1975	7.7	16.7	13.6	11.6
1976	27.3	17.9	29.7	22.3
1986	22.4	0.6	40.1	5.1
1987	46.0	18.8	63.4	29.1
1996	6.8	16.5	0.7	14.0
1997	23.0	20.8	32.8	55.5
2008	3.6	5.2	4.2	1.0
2009	1.2	6.3	7.7	16.3

Table 5.3: Monthly mean sunspot numbers R_{12} of April, June, October and December for the years of the last 5 solar minima.

min 23/24-21/22 comparison	March Equinox	June Solstice	September Equinox	December Solstice	Yearly mean
Rome	-11%	-11%	-13%	-14%	-12%
Gibilmanna	-3%	-8%	-10%	-12%	-8%

min 23/24-22/23 comparison	March Equinox	June Solstice	September Equinox	December Solstice	Yearly mean
Rome	-9%	-9%	-11%	-10%	-10%

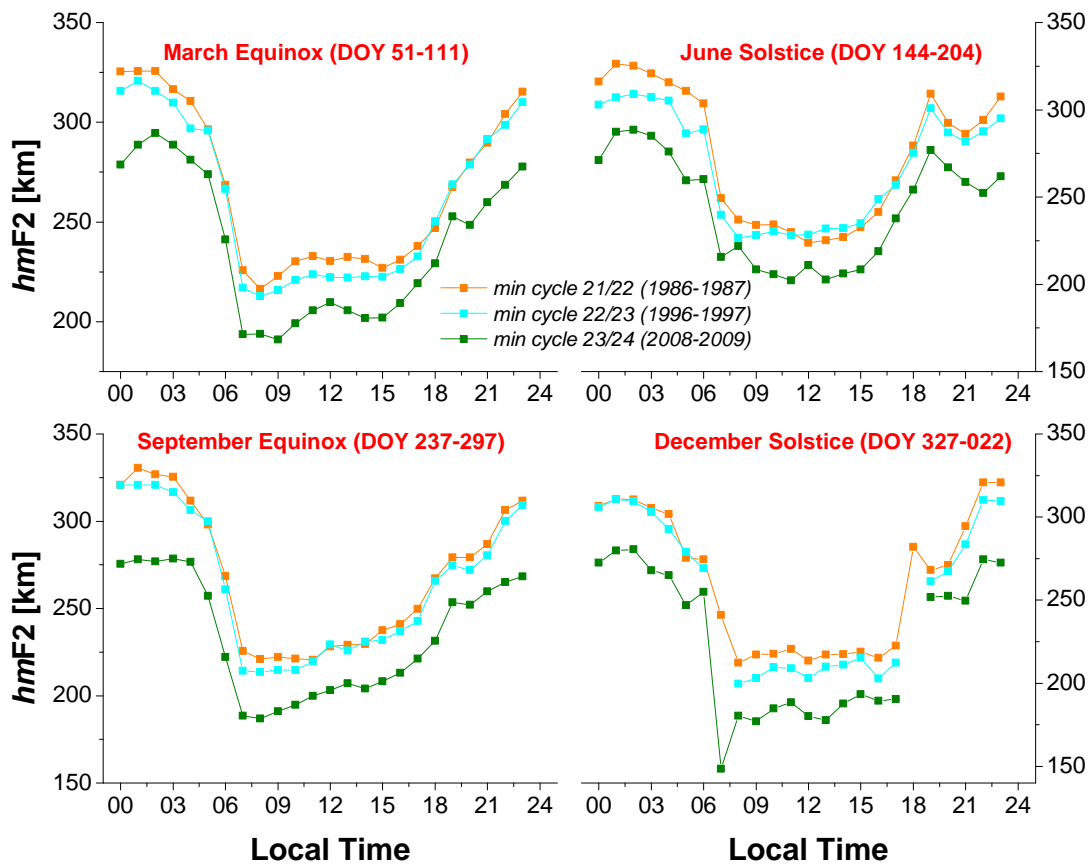**Table 5.4:** Same as Table 5.3 but for hmF2.

Figure 5.8: Seasonal median values of hmF2 for the minima 21/22 (orange squares), 22/23 (cyan squares) and 23/24 (dark green squares), for RM.
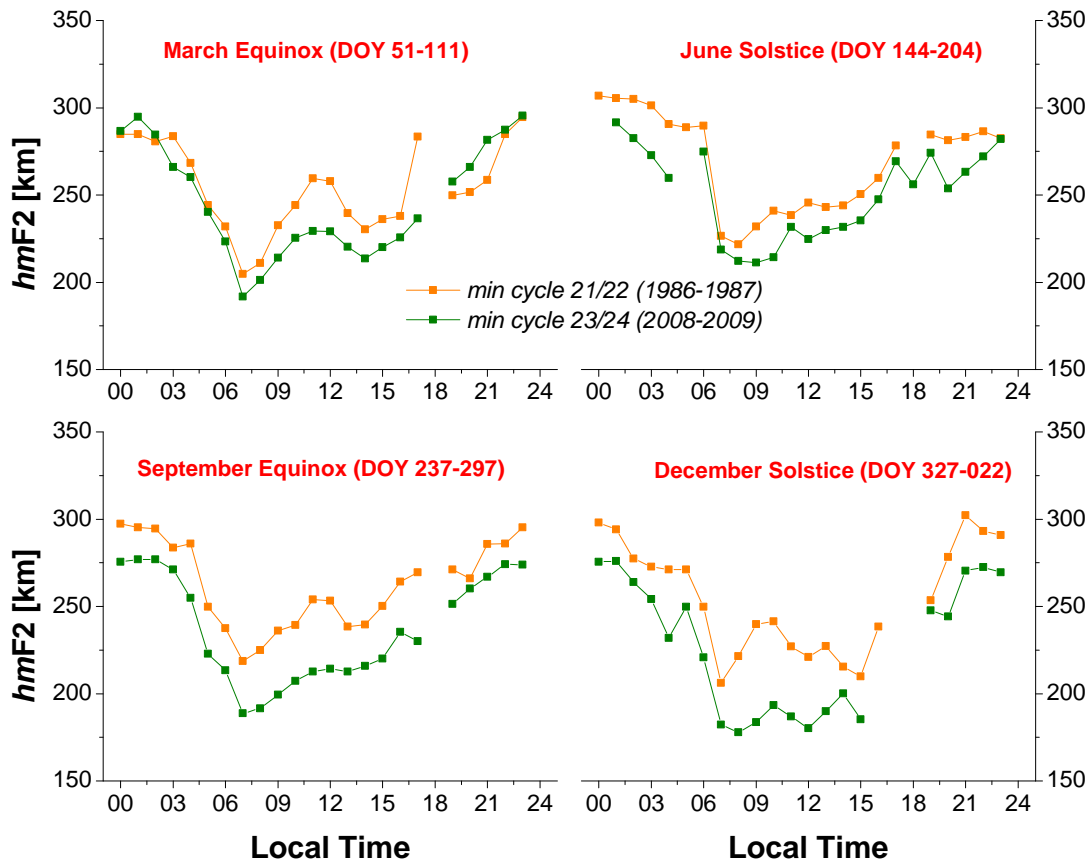
Figure 5.9: Same as Figure 5.8 but for GL.

paring values recorded during the minima 23/24 and 21/22. As for the parameter $NmF2$, the decrease appears more pronounced at RM than at GL, in particular during March Equinox. For RM, a comparison of $hmF2$ values for the last two solar minima reveals how the decrease is quite constant during all year, and slightly less pronounced (yearly mean -10%) than that between minima 21/22 and 23/24 (yearly mean -12%).

A detailed overview of Figures 5.8 and 5.9 reveals interesting features. For RM, contrariwise to what obtained for $NmF2$, it appears how the lower values for the last solar minimum, in comparison to the previous ones, are obtained for both daytime and nighttime hours, with constant decreases of ∼-11/-12%. Slightly enhanced decreases are however obtained during daytime hours in the range 07:00-14:00 LT during December Solstice, when an average decrease of ∼-18% is observed from min 21/22 to min 23/24.
For GL, there is a less decrease during March Equinox, in particular during nighttime hours in the range 19:00-05:00 LT when similar $hmF2$ values are found for the min 23/24 and 21/22. Contrariwise, quite pronounced decreases appear during September Equinox and December Solstice, in particular, during daytime hours in the range 08:00-15:00 LT, for which peak decreases of ∼-16% and ∼-23% are obtained at 11:00 LT for September Equinox and at 09:00 LT during December Solstice.

The results of this section for $NmF2$ and $hmF2$ confirm the particular conditions of the ionosphere in conjunction with the last solar minimum at mid latitudes. A clear decrease for both parameters is measured at RM and GL, with slightly more pronounced decreases at RM.

Moreover, it is very important to underline that the winter and semi-annual anomalies tend to disappear as the solar activity decreases. Furthermore, the typical mid-latitude phenomenon of the winter anomaly is completely absent only during the last solar minimum, which emphasizes once more the particularity of this solar activity window.

5.2.2   Results at low latitudes: Tucumán and São José dos Campos

As shown in Figure 5.1, TU and SJ are two very close stations, located near the southern crest of the *Equatorial Ionization Anomaly* (*EIA*) (e.g., Lyon and Thomas, 1963; MacDougall, 1969; Balan and Iyer, 1983; Batista and Abdu, 2004; Abdu et al., 2008), also called *Appleton anomaly* (Appleton, 1946).

At low latitudes and along the geomagnetic equator, the ionosphere shows a significant variability due to the EIA, linked to the equatorial fountain effect (Martyn, 1955; Duncan, 1960; MacDougall, 1969; Balan and Iyer, 1983; Batista and Abdu, 2004; Abdu et al., 2008). As described by Abdu et al. (2008), during the day the development of the EIA is generated by the E-region dynamo zonal electric field, linked to the *Equatorial Electrojet* (*EEJ*), which gives rise to an $\mathbf{E} \times \mathbf{B}$ plasma vertical drift leading to the aforementioned plasma fountain effect. As discussed by Martyn (1955) and Duncan (1960), ionization is uplifted over the magnetic equator and diffuses down the geomagnetic lines of force, under pressure gradient and gravity forces (Stening, 1992), modifying the electron density concentrations at low latitudes where the F-region plasma increases, thus forming electron density crests on both sides (north and south) of the magnetic equator (at about $\pm 15 - 18°$ geomagnetic latitude) (Lyon and Thomas, 1963). Consequently, the scenario of the equatorial and low latitude ionospheric F-region is the following: F-region is uplifted at the magnetic equator, which causes a decrease of the density peak, while the F-region density peak increases at the crests of the anomaly (Batista and Abdu, 2004). Owing to these particular conditions, the equatorial and low-latitude ionosphere show a strong spatio-temporal variability making its modeling particularly difficult. Figure 5.10, modified from Lin et al. (2007), reports the *Total Electron Content* (*TEC*) variations between 400 and 450 km in 2h segments, with latitude, longitude and hour of the day, as imaged by the FORMOSAT-3/COSMIC satellite. For our purposes, it is important to notice the increase of the TEC upon the two crests of the EIA in the South American sector, in particular between 10:00-18:00 LT.

The results for the inter-minima comparison for TU station for the electron density peak NmF2 will be reported and compared to the ones obtained at mid latitudes for RM and GL.

A comparison between NmF2 values measured during the min 21/22 and 23/24 is in fact possible for RM, GL and TU. From this point of view, it is clearly visible from Table 5.2 that the decrease is much more pronounced at low latitudes (yearly mean decrease of -32% for TU) than at mid latitudes (-20% and -12% at RM and GL, respectively).

In the seasonal patterns visible in Figure 5.11 and quantified in Table 5.2, it is possible to observe that the most prominent decreases are measured for March Equinox, June Solstice and September Equinox (mean decrease of -38%, -39% and -31% respectively), while the decrease for the December Solstice is substantially lower (-18%). It is then clear that the decrease for the low-latitude station of TU is larger than that observed at the mid-latitude stations of RM and GL.

An hourly NmF2 based analysis shows for TU a clear pattern, with more pronounced decreases during nighttime hours (21:00-06:00 LT) than for daytime hours (07:00-20:00 LT), for all the seasons. Averaging over the aforementioned time intervals (21:00-06:00 LT and
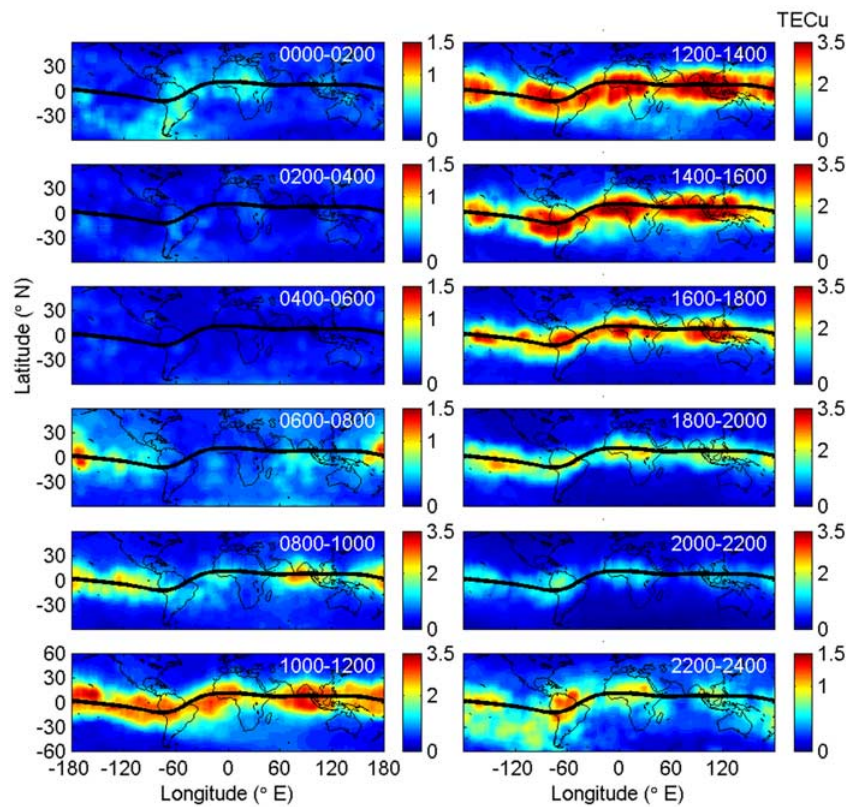
Figure 5.10: Temporal variations of the longitudinal structure of the integrated total electron content between 400 and 450 km in 2h segments measured by the FORMOSAT-3/COSMIC satellite (modified from Lin et al. (2007)).
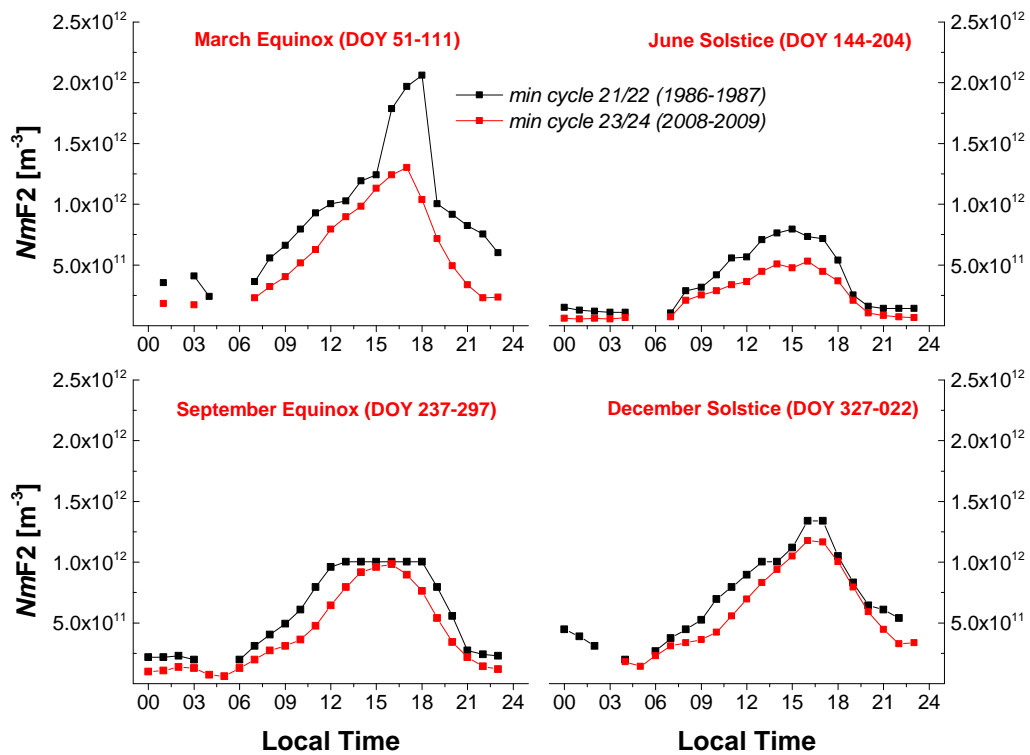

Figure 5.11: Same as Figure 5.5 but for TU.

07:00-20:00 LT), percentage decreases of -45%/-33%, -51%/-32%, -41%/-26% and -22%/-17%
are obtained for March Equinox, June Solstice, September Equinox and December Solstice,
respectively.

Using monthly median values, available for TU also for the minima 19/20 and 20/21, it is
possible to analyze the winter and the semi-annual anomalies. Figure 5.12 shows the monthly
median values for April, June, October and December, for the years of the recent minima, as
recorded at TU. Figure 5.7 has shown how at RM the winter anomaly was not visible only for
the years 2008 and 2009 of the last solar minimum. For TU, Figure 5.12 shows that the situation
is quite different, with the winter anomaly which is never visible. However, as mentioned, the
anomaly is less visible at low latitudes and in particular in the south hemisphere, so this is
not an unexpected result. On the contrary, the semi-annual anomaly is a typical low-latitude
phenomenon. Figure 5.12 reveals that at TU the semi-annual anomaly is clearly visible for
minima 19/20 and 20/21, while it is not clearly visible for the year 1986 and for the last
minimum. In fact, in 2008 and 2009 similar values for October and December are observed at
local noon, in support of an extremely quiet ionosphere observed during the last solar minimum.
For the SJ ionosonde, an inter-minima comparison for NmF2 is not possible. Nevertheless, data
for the last solar minimum are available and can provide useful information about the visibility
of the winter and semi-annual anomalies. Figure 5.13 shows the hourly monthly median values
of NmF2 measured at SJ during April, June, October and December 2008 and 2009. The
results confirm what previously reported for TU, showing that both the winter anomaly and in
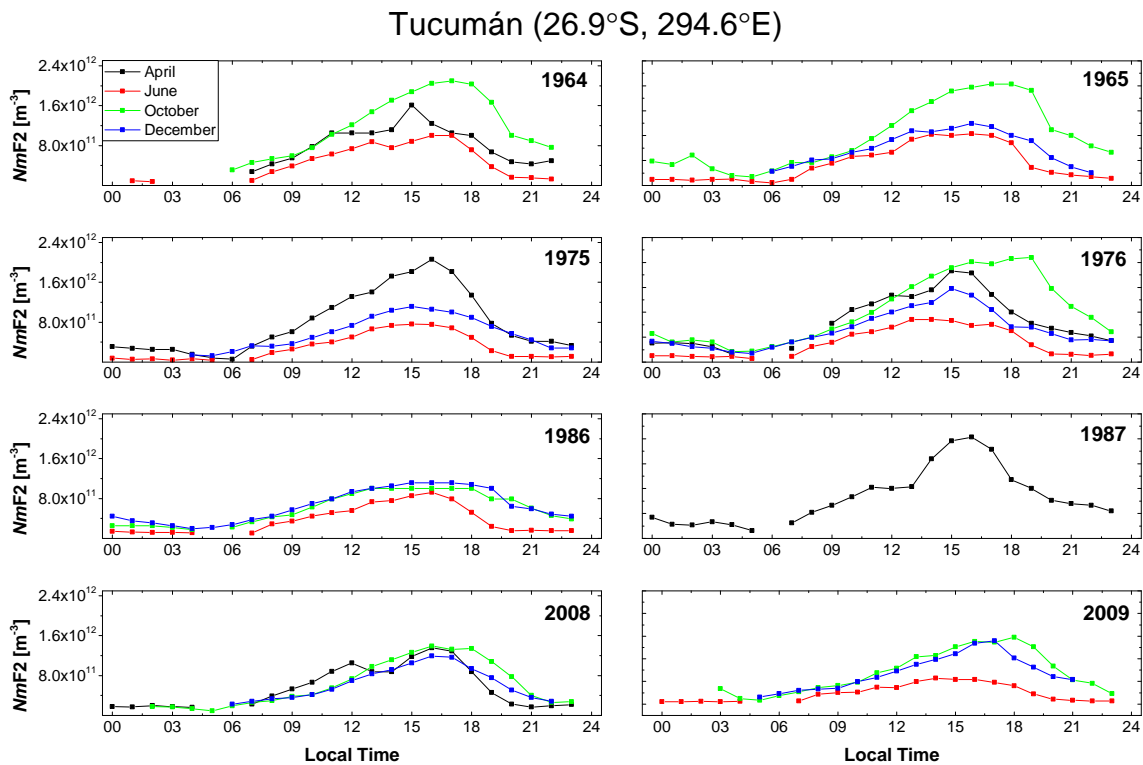particular the semi-annual anomaly are not visible for the years 2008 and 2009.

Figure 5.12: Hourly monthly median NmF2 values for April (black squares), June (red squares),
October (green squares) and December (blue squares), for the solar activity minima 19/20, 20/21,
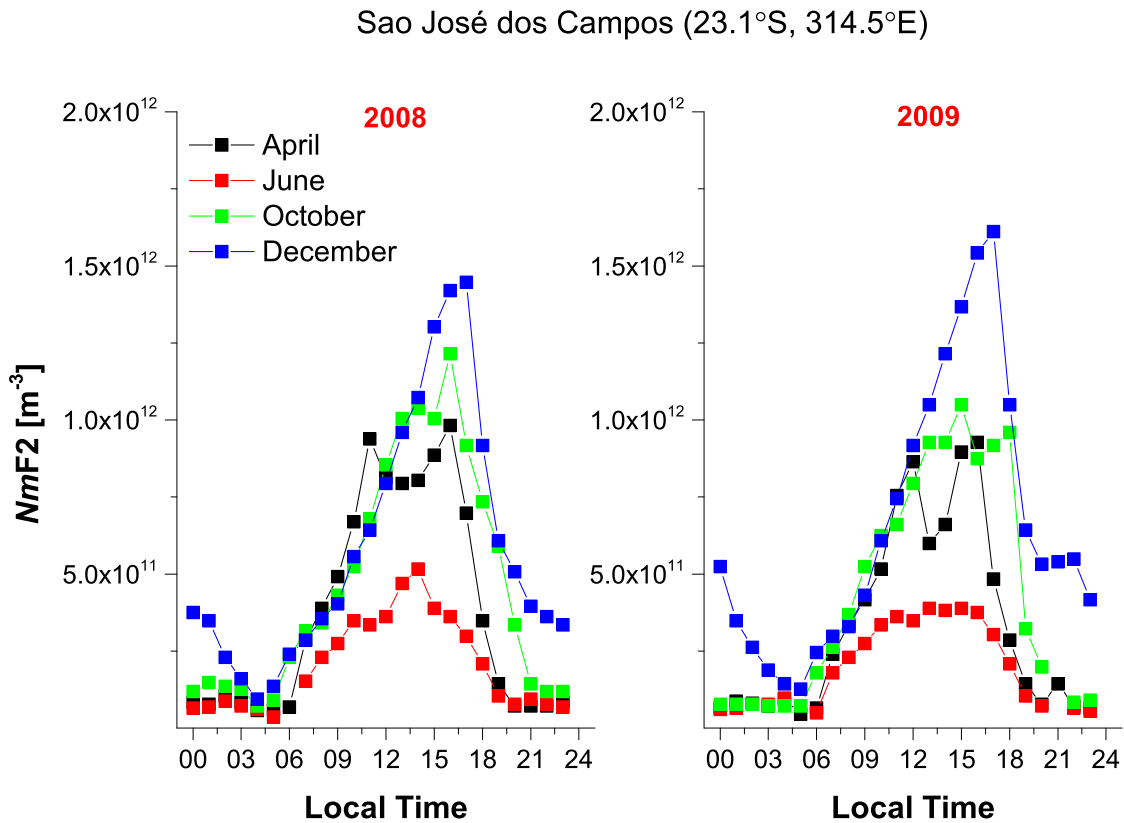21/22 and 23/24, for TU.

Figure 5.13: Hourly monthly median *Nm*F2 values for April (black squares), June (red squares), October (green squares) and December (blue squares), for the solar activity minimum 23/24, for SJ.

Comparing the results obtained at mid latitudes (RM and GL) with those at low latitudes (TU), in accordance with the study by Liu et al. (2011a), it is confirmed that the more pronounced decreases of *Nm*F2 for the last solar minimum are found at latitudes of the EIA's crests. Furthermore, the lower electron density values observed for the last solar minimum at RM, GL and TU agree with other studies that found the same pattern for ionosonde at different latitudes (Solomon et al., 2013; Ezquer et al., 2014; Lee and Reinisch, 2012; Liu et al., 2011a, 2012; Araujo-Pradere et al., 2011, etc.).

Regarding the observed *hm*F2 pattern at mid latitudes, the decreases observed for the last minimum agree with the results reported by Araujo-Pradere et al. (2013), who measured a considerable decrease of *hm*F2 passing from min 22/23 to min 23/24 at the mid-latitude stations of Millston Hill (lat. 42.6°N, lon. 288.5°E) and Grahamstown (lat. 33.3°S, lon. 26.5°E); they agree also with the results by Lee and Reinisch (2012), who found for the last solar minimum a decrease of the daily peak *hm*F2 value, for the equatorial station of Jicamarca (lat. 12.0°S, lon. 283.1°E), with more pronounced differences in winter (as high as ∼40 km).

5.3 Comparison with *IRI-2012*

5.3.1 The International Reference Ionosphere model: a brief review

Among the numerous ionospheric models, the *International Reference Ionosphere* (*IRI*) (e.g., Bilitza, 2001; Bilitza and Reinisch, 2008; Bilitza et al., 1990, 2014) is the best-known and most

widely used empirical model for the description of the ionosphere. It is an international project sponsored by the Committee on Space Research (COSPAR) and the International Union of Radio Science (URSI), based on an extensive database and able to capture much of the repeatable characteristics of the ionosphere for quiet and storm-time periods, such as the electron density, the electron content, the electron temperature and the ion composition, as a function of height, location, and local time (e.g., Araujo-Pradere et al., 2011, 2013; Zakharenkova et al., 2013).

IRI development has benefitted greatly from the synergism between COSPAR and URSI which are represented about evenly in the IRI Working Group and during annual IRI Workshops. The goals and intent of the IRI project are summarized in its COSPAR/URSI Terms of Reference as follows (Bilitza et al., 2014):

> The Task Group was established to develop and improve a standard model of the ionospheric plasma parameters. The model should be primarily based on experimental evidence using all available ground and space data sources; theoretical considerations can be helpful in bridging data gaps and for internal consistency checks. Where discrepancies exist between different data sources, the IRI team should promote critical discussion to establish the reliability of the different databases. IRI should be updated as new data become available and as old data sources are fully evaluated and exploited. IRI is a joint working group of COSPAR and URSI. COSPAR's prime interest is in a general description of the ionosphere as part of the terrestrial environment for the evaluation of environmental effects on spacecraft and experiments in space. URSI's prime interest is in the electron density part of IRI for defining the background ionosphere for radiowave propagation studies and applications.

The IRI Working Group has grown over the years to a team of now 58 experts providing a balanced representation both in terms of global presence as well as concerning the coverage of the different ground and space techniques used to acquire ionospheric data. Other ingredients for the IRI success story include the annual IRI meetings where improvements and additions to the model are discussed and decided (http://irimodel.org/docs/iri_workshops.html), the publication of a selection of the papers from these workshops in dedicated issues of Advances in Space Research (http://irimodel.org/docs/asr_list.html), and from early on open source availability of the IRI Fortran code, first on punched tape and cards, then on 9-track magnetic tapes, then on floppy disks, then on CDs, and finally through a web interface which gives the user the possibility to obtain a direct online computation (Bilitza et al., 2014).

As an empirical model, IRI has the advantage that it does not depend on the evolving theoretical understanding of the processes that shape the ionospheric plasma. Nevertheless, a possible disadvantage of empirical models is the strong dependence on the underlying database. Regions and time periods not well covered by the database will result in a diminished reliability of the model in these space and time areas. As an example, conditions during the most recent solar minimum in 2008/2009 were very different from earlier minima. The last minimum was lower and more extended than earlier minima and consequently it should be expected that IRI, being built with the data from earlier minima, overestimates the plasma densities during this minimum.

As discussed in Section 2.2, IRI outputs severely depend on input parameters, like the solar activity and magnetic indices, and the use of uncertain predicted values of them can lead to significant discrepancies in the model output (Zakharenkova et al., 2013). Figures 2.7 and 2.8

have shown how, using predicted values for the ionospheric index IG12, considerable $foF2$ (or $NmF2$) overestimations are obtained at RM station for the year 2009 of the last minimum. Similar results are obtained for the 2008 (plot not shown). Nevertheless, using observed IG12 values as input for the IRI model, a good agreement with ionosonde data is obtained, underlining the problems encountered by ionospheric models to provide good predictions for the minimum 23/24.
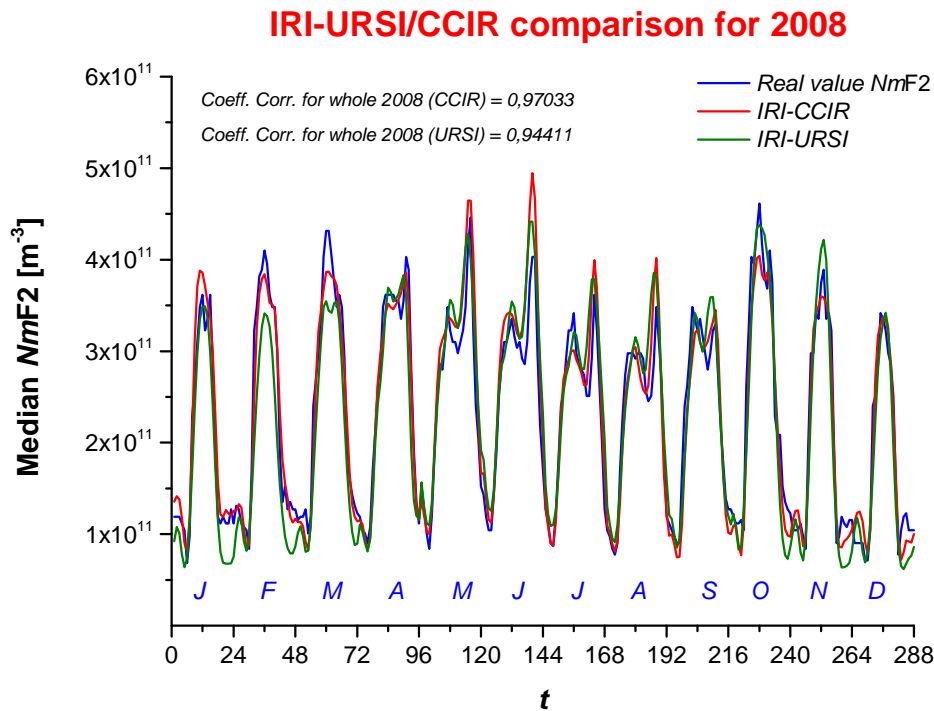

Figure 5.14: Comparison between IRI-2012 CCIR and URSI outputs and observed hourly monthly median values for RM for the year 2008. The blue curve represents the observed values, the red curve represents the IRI outputs using the CCIR set of coefficients, and the green curve represents the IRI outputs using the URSI set of coefficients. The x scale spans from $t = 0$ (00:00 UT of January 2008) to $t = 288$ (23:00 UT of December 2008). The capital letters identify the months from January (J) to December (D).

The IRI model offers two options for the mapping of $NmF2$ and $foF2$: the CCIR (CCIR, 1967a,b) model and the URSI model (Rush et al., 1989). A preliminary study has been carried out for RM, in order to choose the most reliable set of coefficients between CCIR and URSI ones. Figure 5.14 reports a comparison between hourly monthly median $NmF2$ values recorded by the ionosonde of Rome (blue line), and those calculated by IRI-2012 using CCIR coefficients (red line) and by IRI-2012 using URSI coefficients (green line), for the whole year 2008. The correlation coefficients, displayed in Figure 5.14, reveal that the CCIR coefficients provide a slightly better agreement with ionosonde data than the URSI coefficients. A detailed analysis shows that a considerable improvement is obtained using CCIR coefficients in particular during nighttime hours of winter/autumn season. This effect is clearly visible from November to March. Considering daytime hours, slightly better results with CCIR coefficients are obtained in February, while for the other months CCIR and URSI provide comparable results. However, this result is not surprising because the CCIR coefficients are recommended for locations on

the continents, whereas URSI coefficients are recommended for the ocean areas (Rush et al., 1989).

By virtue of the aforementioned preliminary results, the CCIR coefficients and observed values for all the indices used as input have been used to run the IRI model. Furthermore, the last version of the model, namely IRI-2012 (Bilitza et al., 2014), has been used to compare its output with the ionosonde one.

5.3.2   Results at mid latitudes: Rome and Gibilmanna

As previously reported, to display the results of the comparison between NmF2 and hmF2 values from ionosonde and IRI, opportune percentage relative difference maps were created. In these maps, the $PD(\%)$ parameter defined by equation (5.1) is plotted, with the local time on the x axis and the month on the y axis. In this way, thanks to the chromatic scale, it is possible to visualize easily zones of underestimation/overestimation made by the model. The solar minima that can be analyzed are the same discussed in Section 5.2 and listed in Table 5.1.

Figure 5.15 reports the relative percentage difference maps for RM (first and second row) and GL (third row) for all the available minima, for NmF2. The total mean percentage distances (mean over 24 hours and over the 2 years of every minimum) for NmF2 are reported in Table 5.5 for all the available minima and for all the stations.

In general, Figure 5.15 and Table 5.5 reveal that good correspondences between observed values and IRI outputs are found for the recent minima at both mid-latitude stations of RM and GL, confirming what was shown by both Zakharenkova et al. (2013) and Bilitza et al. (2012). In fact, percentage differences within ±20% characterize most of the periods analyzed for RM. Slightly larger differences can be observed at GL station during nighttime hours (19:00-04:00 LT) of the minimum 21/22. A very important result is that at mid latitudes there is not a clear loss of accuracy of the IRI model for the last minimum in comparison to the previous ones. For RM, the IRI output is similar to those of the last five solar minima, as it is shown in Table 5.5, with an average distance of ∼11%.

Unexpectedly, for GL better results are obtained for the last minimum than for the minimum 21/22. Therefore, it is not observed an IRI overestimation for the last particular solar minimum, with the model providing results for NmF2 that are comparable with the previous "climatological" minima.

In general, no clear seasonal patterns can be inferred from Figure 5.15 for both stations, meanwhile it is possible to observe for both RM and GL stations a slight tendency of the IRI model to underestimate during sunrise hours (05:00-08:00 LT) and to overestimate during sunset hours (17:00-19:00 LT) for the last minimum. By doing a comparison with the results of Section 5.2, it is worth noting that the underestimation made by IRI for sunrise hours corresponds to the hours where the lower decreases are observed in the inter-minima comparison. Likewise, the tendency of IRI to overestimate at sunset hours coincides to the more pronounced decreases in inter-minima comparison. However, for all the minima studied and for both stations, it is observed that the hours for which the more pronounced differences between IRI and ionosonde values are found are those of sunrise and sunset, with percentage differences as high as ±20%; on the contrary, hours around midday are usually well described by IRI, with percentage differences usually within ±10%.

A possible general and recurring dependence on the hours of the day characterizing the IRI model can be well revealed by plotting the parameter $PD(\%)$, separately for daytime hours (10:00-14:00 LT) and nighttime hours (22:00-02:00 LT) for the available minima. Figure 5.16,
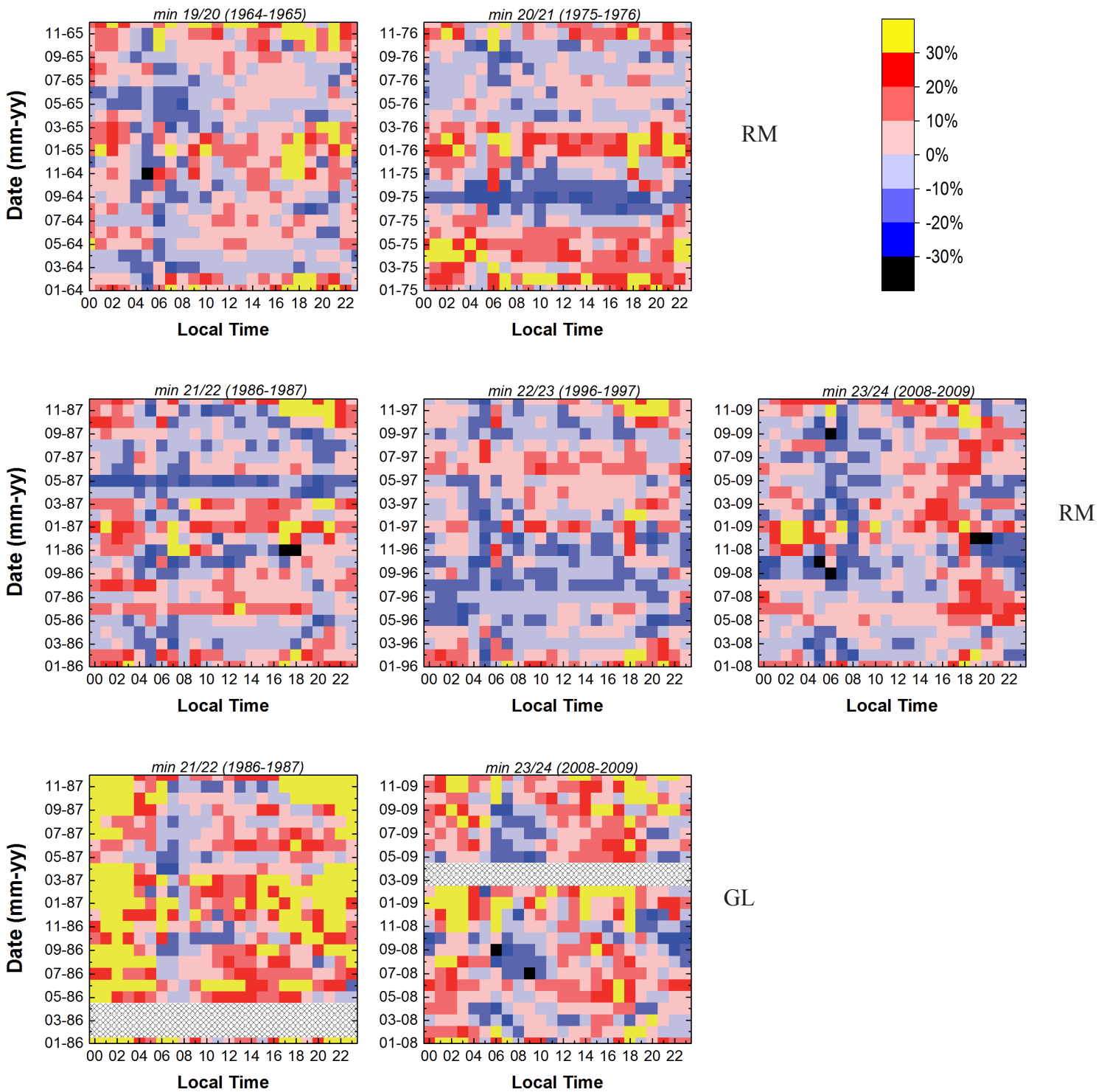
Figure 5.15: Relative percentage difference maps for NmF2, according to equation (5.1), for RM (first and second row) and GL (third row), for all the solar minima analyzed. Grey areas refer to lack of measured values. The chromatic scale is the same for all maps.

showing plots of $PD(\%)$ for NmF2 for the available minima, for RM and GL, and for the two aforementioned time ranges, helps us to make a comparison between IRI and observations for daytime and nighttime hours. For RM, the IRI model does not show particular features, with equivalent zones of overestimation and underestimation, with the $PD(\%)$ values always within the range $\pm30\%$. For nighttime hours, a slightly more pronounced overestimation made by IRI is visible, in particular for minima 19/20, 20/21 and 21/22. This result is quite in accordance with the outcomes shown by Bilitza et al. (2012). Surprisingly, the situation is quite different for GL, where a steady and significant overestimation made by IRI is observed for both daytime and nighttime hours and for the two displayed minima 21/22 and 23/24. Moreover, for the min 23/24 the overestimation is the same for daytime and nighttime hours ($PD(\%)$ within the range $\pm55\%$), meanwhile for the min 21/22 the overestimation is more pronounced during nighttime hours, with $PD(\%)$ parameter as high as $+90\%$.

Station	Min 19/20	Min 20/21	Min 21/22	Min 22/23	Min 23/24
Rome	11%	12%	11%	10%	11%
Gibilmanna	–	–	25%	–	15%
Tucumán	20%	25%	21%	–	29%
São José dos Campos	–	–	–	–	31%

Table 5.5: Mean percentage distance ($|\overline{PD}(\%)|$) of NmF2 between measured values and IRI outputs for the recent minima. The distances are averaged over the 24 hours and the two years included in each minimum.
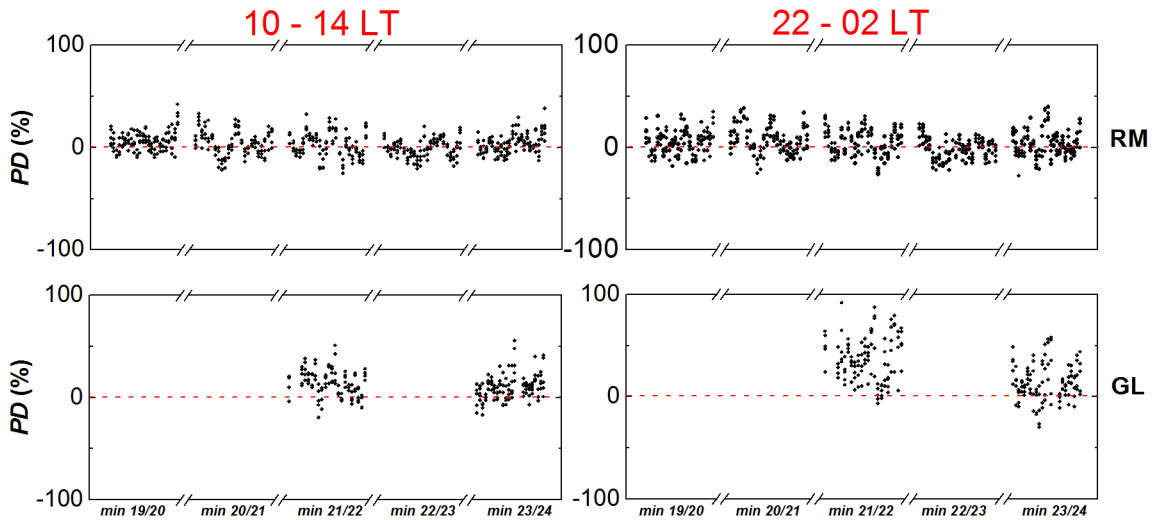

Figure 5.16: Relative percentage differences according to equation (5.1), for NmF2, for recent solar minima, for RM (first row) and GL (second row). Panels on the left refer to daytime hours (10:00-14:00 LT), while panels on the right refer to nighttime hours (22:00-02:00 LT). The red dashed horizontal line identifies the zero.

An interesting feature that emerged during the comparison between IRI outputs and ionosonde values for RM and GL, regards a typical mid-latitude phenomenon called meridian

depression (Dominici, 1971). The meridian depression is a peculiarity for which the daily absolute maximum of NmF2 is observed at hours close to the local sunset. It has been also called *Mid latitude Summer Evening Anomaly* (*MSEA*), defined by the mathematical condition NmF2(at 12:00 LT)$/Nm$F2(at 21:00-22:00 LT)> 1 (Klimenko et al., 2015a). The meridian depression (or MSEA), can be easily visualized as an impulsive increase of the electron density during the sunset hours, starting around 17:00 LT, peaking around 19:00 LT (corresponding to the daily peak value with electron density as high as $\sim 7 \cdot 10^{11}$ [m^{-3}]) and then quickly decreasing to climatological levels around 22:00 LT. The main possible mechanisms involved in the meridian depression development are: (1) the prolonged Solar UV and EUV photoionization in the summer hemisphere due to a later sunset, (2) the upward plasma transport along the geomagnetic field lines due to thermospheric winds, maximal near midnight, together with the later sunset and (3) the variations in the ratio [O]/[N2], that increases from noon to midnight, owing to the heating in the auroral zone due to energetic particle precipitation, Joule heating and global thermospheric circulation (Dudeney and Piggott, 1978; Jee et al., 2009; He et al., 2009; Liu et al., 2010; Chen et al., 2011b; Karpachev et al., 2011; Klimenko et al., 2015b).

It has been observed that this phenomenon is visible at RM and GL stations from April to September for mid and low solar activity. An analysis of data for the high solar activity years 1990-1991 (max of the cycle 22) and 2001-2002 (max of the cycle 23) has shown that the meridian depression is less clear and concerns a shorter period from June to August. These results agree with the findings of Klimenko et al. (2015a), for the mid-latitude ionosondes of Irkutsk (52.3°N, 104.3°E; Russia) and Kaliningrad (54.5°N, 20.2°E; Russia), and Zakharenkova et al. (2013) for the Juliusrush ionosonde (54.6°N, 13.4°E; Germany). However, due to the longitudinal gradients of the [O]/[N2] ratio, consistent longitudinal-dependent variations in the meridian depression magnitude can occur.

Figure 5.17 reports the comparison between hourly monthly median values of NmF2 as recorded by the ionosonde (black dots) and calculated by IRI (green dots) for the RM station. Four different months, April, June, August and September of the minimum year 1987 are displayed.

The figure shows that the meridian depression is clearly visible for all the months displayed and that the IRI model provides a clear underestimation of it. This feature is visible also for GL and for all the minima studied, with different magnitudes, being particularly pronounced for the year 1987. In particular, from Figure 5.17 it is possible to observe that for June and August the IRI model slightly underestimates the peak around 21:00 LT, but the meridian depression is present in the IRI daily pattern; on the contrary, for April and September, the IRI daily pattern does not take into account any meridian depression, providing sizeable underestimations. This feature appears at both RM and GL stations and for all the minima studied.

Figure 5.18 reports the relative percentage difference maps for RM (first row) and GL (second row) for all the available minima for hmF2. The total mean percentage distances are reported in Table 5.6 for all the available minima and for all the stations. It is important to underline that, as previously discussed, hmF2 observed values are those calculated through the Shimazaki formulation and the D55 formulation for nighttime hours (19:00-06:00 LT) and daytime hours (07:00-18:00 LT), respectively. Therefore, the hmF2 analysis has to be considered only qualitative because it represents a comparison between three different models.

A general overview of the maps in Figure 5.18 reveals three main results: (1) the IRI model overestimates the hmF2 parameter; (2) a worsening in IRI performances is observed for the last minimum in comparison to the previous ones; (3) comparable results are obtained for RM and GL for all the minima. The IRI model provides slight overestimations for the min 21/22
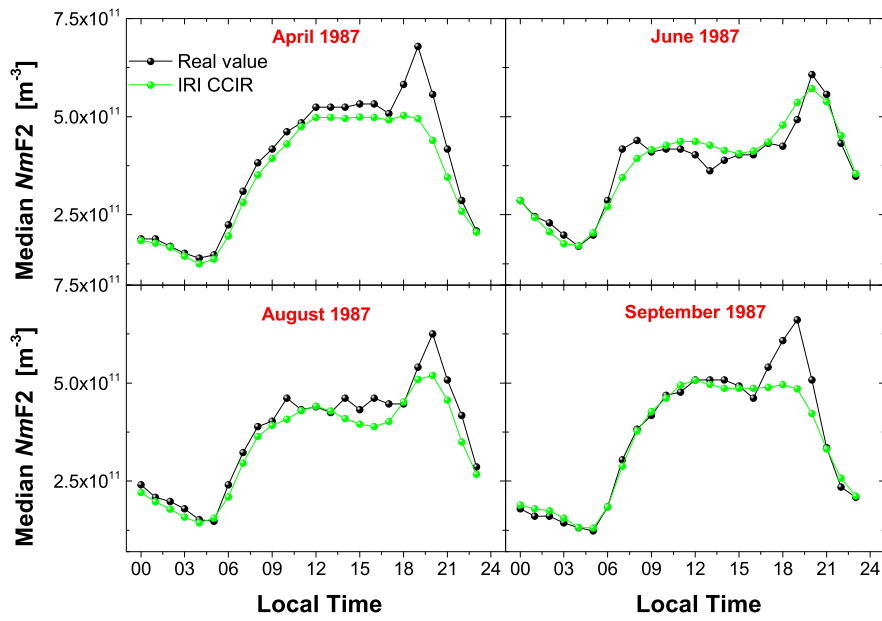
Figure 5.17: Hourly monthly median values of NmF2 obtained for RM as measured by the ionosonde (black dots) and calculated by IRI (green dots). April, June, August and September of the minimum year 1987 are displayed.
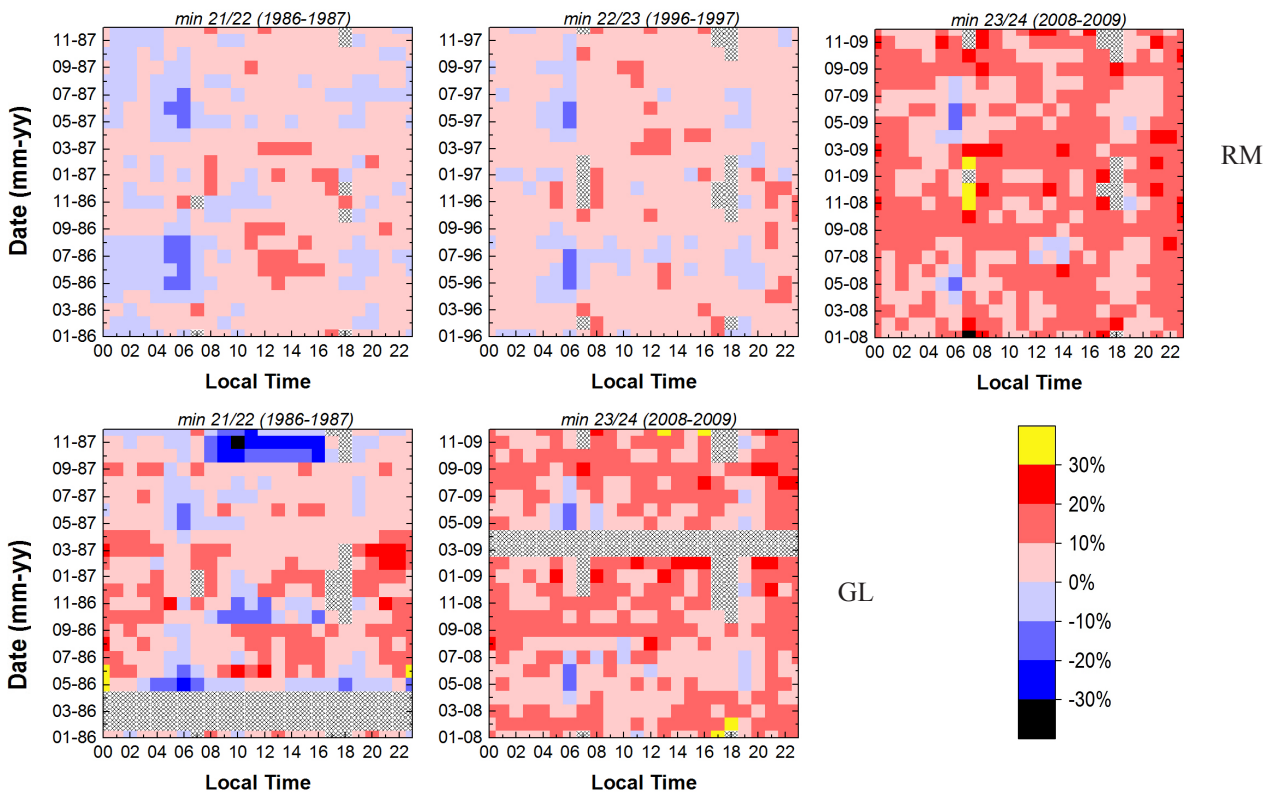

Figure 5.18: Relative percentage difference maps, according to equation (5.1), for RM (first row) and GL (second row), for all the solar minima analyzed, for the height hmF2 of the electron density peak. Grey areas refer to lack of measured values. The chromatic scale is the same for all maps.

Station	Min 21/22	Min 22/23	Min 23/24
Rome	5%	5%	13%
Gibilmanna	8%	–	11%
Tucumán	–	–	11%
São José dos Campos	–	–	17%

Table 5.6: Mean percentage distance ($|\overline{PD}(\%)|$) of hmF2 between measured values and IRI outputs for the recent minima. The distances are averaged over the 24 hours and the two years included in each minimum.

and 22/23 but with very low differences usually within ±10% and with total mean percentage distances of 5% for RM (min 21/22 and 22/23) and 8% for GL (min 21/22). The worsening of the IRI performances for the last minimum is underlined by the mean distances in Table 5.6 that increase to 13% for RM and to 11% for GL.

Similarly to what obtained for NmF2, no clear seasonal dependences are detectable. In order to catch possible variations in IRI performances between daytime and nighttime hours (10:00-14:00 LT and 22:00-02:00 LT), Figure 5.19 shows plots of the $PD(\%)$ parameter for hmF2, for daytime and nighttime hours range, separately. The panels in Figure 5.19 confirm that IRI overestimates the hmF2 values for both stations, for all minima and for both daytime and nighttime hours. Only for GL, during daytime hours for the minimum 21/22, IRI underestimations as high as -30% are visible.
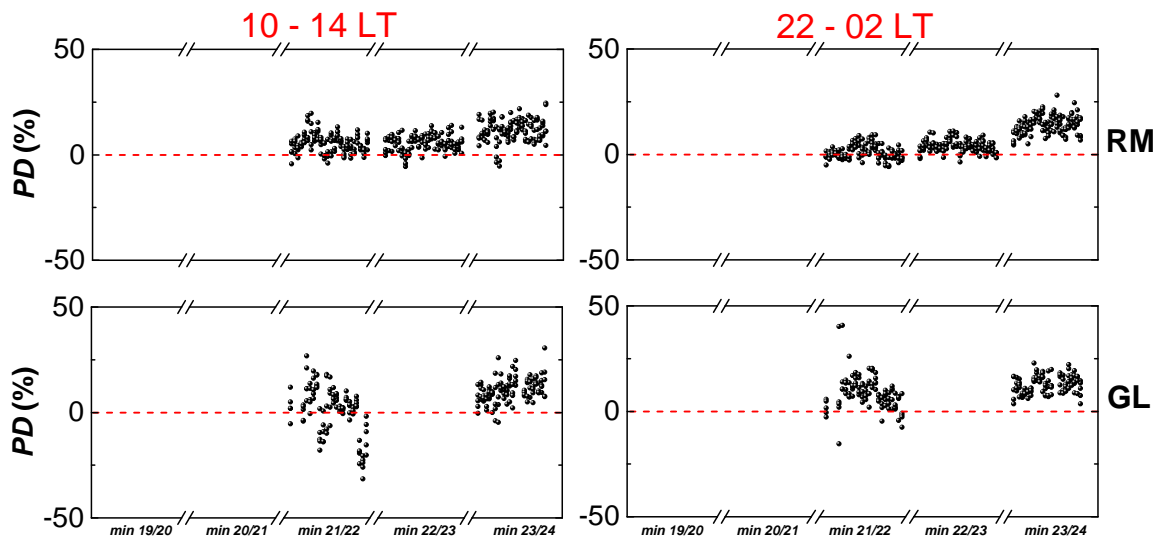

Figure 5.19: Same as Figure 5.16 for hmF2.

5.3.3 Results at low latitudes: Tucumán and São José dos Campos

Figure 5.20 displays the relative percentage difference maps for NmF2, for the stations of TU and SJ. The most important result, clearly visible comparing Figure 5.20 with Figure 5.15, and confirmed by the mean percentage distances of Table 5.5, is that IRI works better at mid latitudes (RM and GL) than at low latitudes (TU). This effect is particularly visible for the
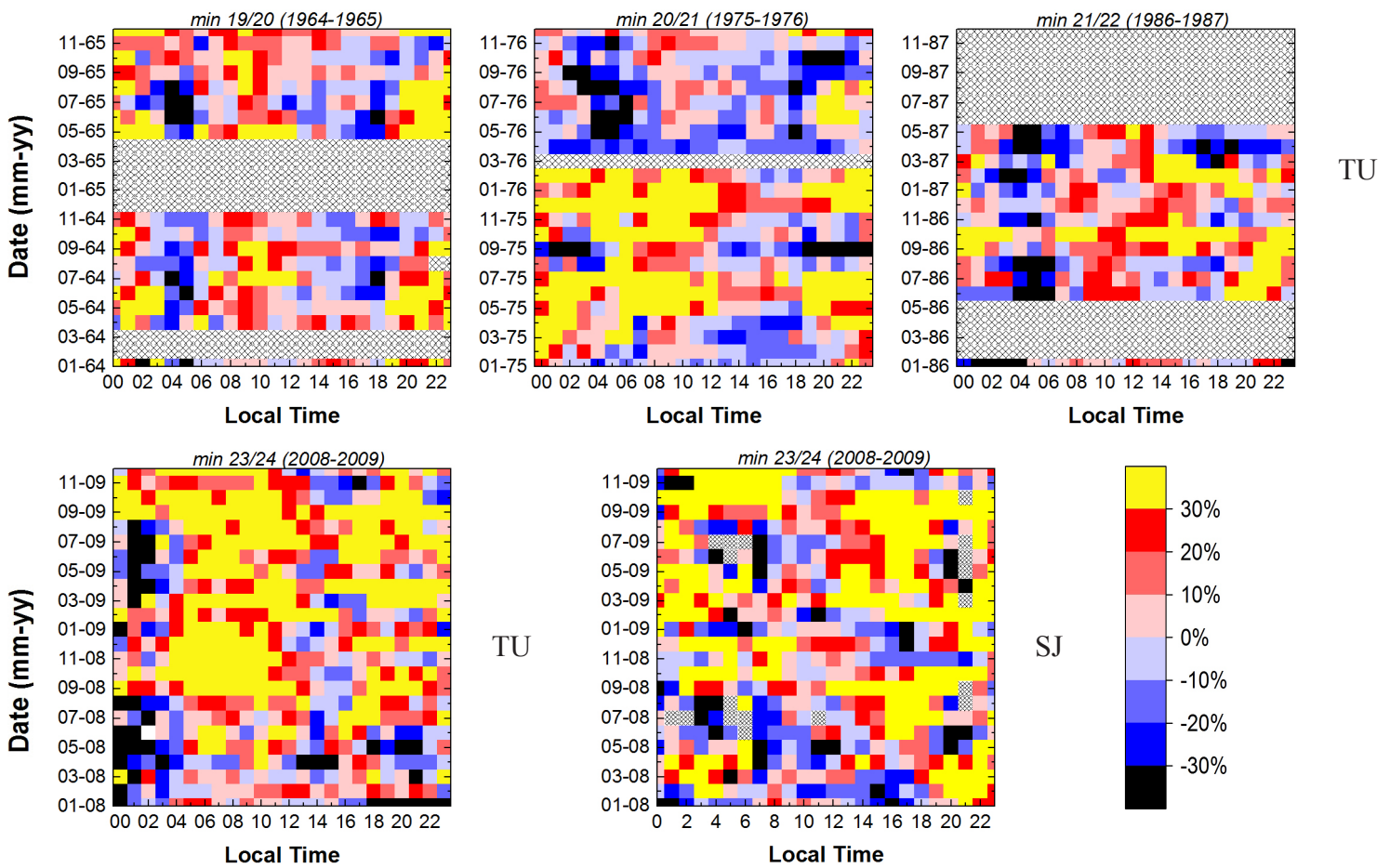
Figure 5.20: Relative percentage difference maps for NmF2, according to equation (5.1), for TU and SJ, for all the solar minima analyzed. Grey areas refer to lack of measured values. The chromatic scale is the same for all maps.

minimum 23/24, with total mean percentage distances of 29% and 31% observed for TU and SJ respectively, meanwhile lower values of 15% and 11% are observed at GL and RM. Moreover, comparing values of Table 5.5 for RM and TU, for which numerous minima are available, it is confirmed that the worsening of IRI performances, passing from mid to low latitudes, is observed also for the previous minima. The lower accuracy found at low latitudes than at mid latitudes agrees with the results of Bilitza et al. (2012), Lee and Reinisch (2012) and Adebesin et al. (2014).

In Section 5.3.2 it has been underlined that for RM, concerning NmF2, the IRI model works approximately in the same way for the last five solar minima, while for GL better results are obtained for the last minimum than for the minimum 21/22. A slightly different result is obtained for TU: a higher total mean percentage distance is observed for the last solar minimum (29%) than for the previous ones. Anyhow, this worsening (4% with respect to the minimum 20/21), is not so significant and might not be due to the particularity of the last solar minimum. Focusing the attention on the last minimum, maps in Figure 5.20 for TU and SJ exhibit an IRI tendency to overestimate the observed NmF2 values. This effect is particularly accentuated for both stations from September 2008 to the end of 2009. Zones of sizeable underestimation can be detected at TU during nighttime hours (00:00-03:00 LT) from January 2008 to August 2008

and from March 2009 to August 2009.

Figure 5.21 displays the $PD(\%)$ parameter for TU and SJ, for the available minima, for NmF2, for daytime hours (10:00-14:00 LT) and nighttime hours (22:00-02:00 LT). It is observed that for TU, the IRI model substantially overestimates the measured values of NmF2 for all the analyzed minima and for both daytime and nighttime hours. It is confirmed that at low latitudes IRI provides less reliable results than at mid latitudes. For the last solar minimum, the general IRI tendency to overestimate measured values observed at TU is confirmed, with comparable magnitudes, for SJ. These results are in accordance with what was found by Bilitza et al. (2012) for daytime hours by considering data recorded at the station of Cachoeira Paulista (22.7°S, 45.0°W, Brazil) that, similarly to TU and SJ, is located close to the south crest of the EIA and for which IRI overestimations over 50% have been reported.
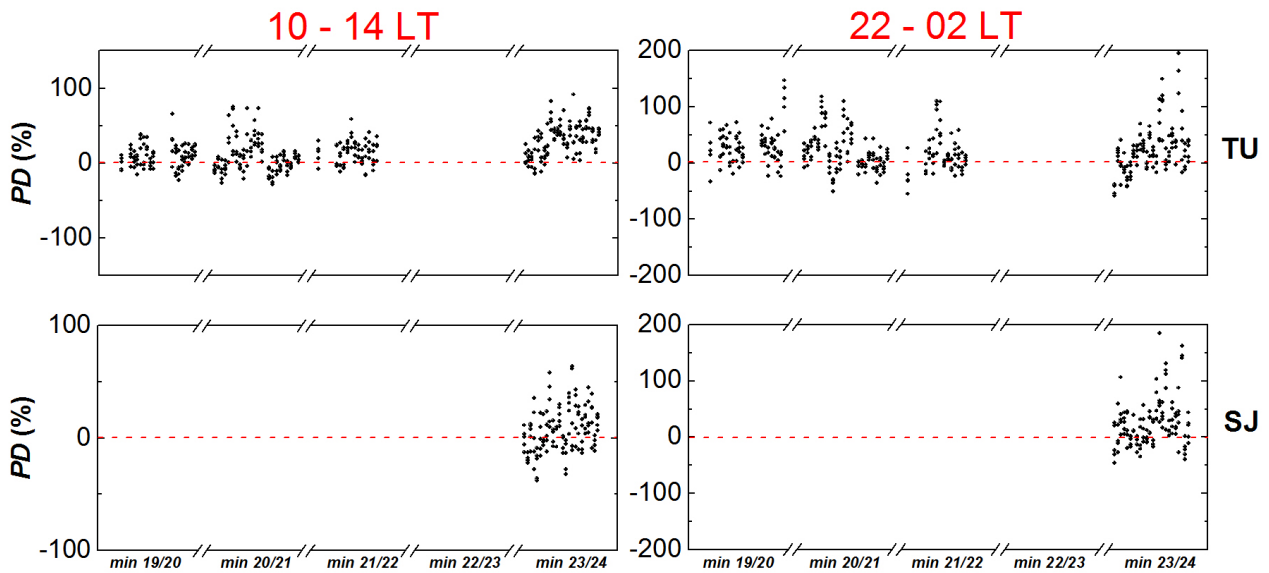

Figure 5.21: Same as Figure 5.16 for TU and SJ.

Figure 5.22 reports the relative percentage difference maps for TU and SJ for hmF2 and for the last solar minimum, that is the only one for which data are available. The mean percentage distances are displayed in Table 5.6. Contrary to what previously obtained for NmF2, the results for hmF2 show that it is not clearly visible a worsening in IRI performances at low latitudes in comparison to mid latitudes. In fact, comparable results are obtained at TU (mean distance of 11%), RM (13%) and GL (11%) for the last minimum. Slightly enhanced differences (mean distance of 17%) are found at SJ. The overestimation revealed at mid latitudes is confirmed during all day at TU and during nighttime hours at SJ. On the contrary, during daytime hours (09:00-18:00 LT) clear underestimations are observed at SJ. This pattern is confirmed by the daytime and nighttime plots of the $PD(\%)$ parameter for hmF2 for TU and SJ, displayed in Figure 5.23. The figure shows that at SJ in the range 10:00-14:00 LT the $PD(\%)$ parameter is usually between 0 and -25%. An opposite pattern appears in the other three panels of Figure 5.23, underlining the IRI tendency to overestimate the measured values in the range 10:00-14:00 LT at TU, and in the range 22:00-02:00 LT, at both stations.
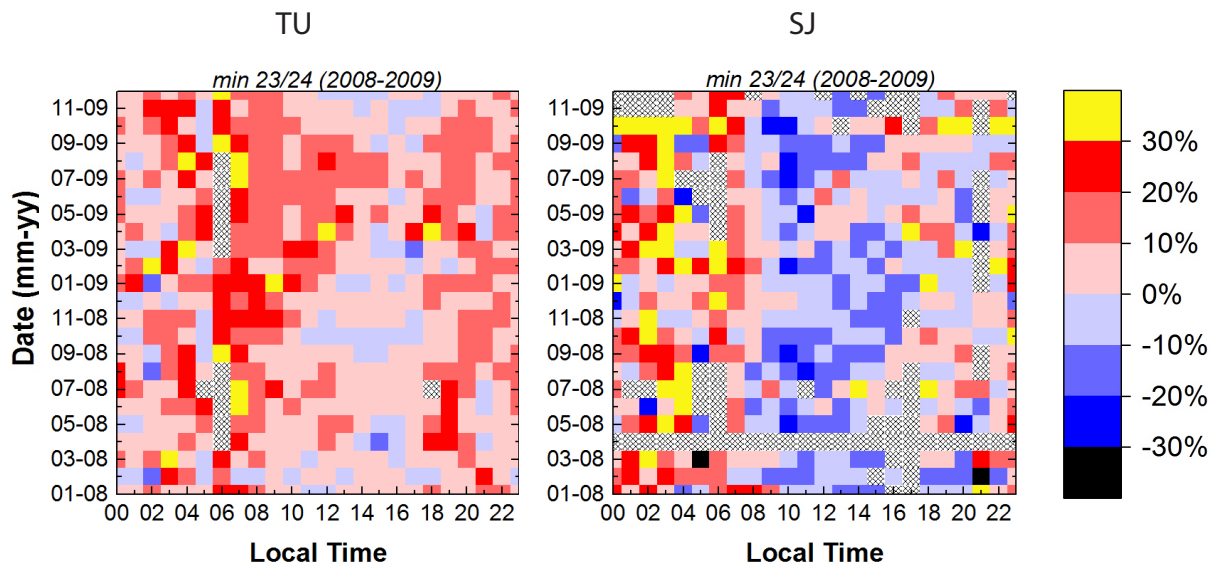
Figure 5.22: Relative percentage difference maps for hmF2, according to equation (5.1), for TU and SJ, for the last minimum. Grey areas refer to lack of measured values. The chromatic scale is the same for the two maps.

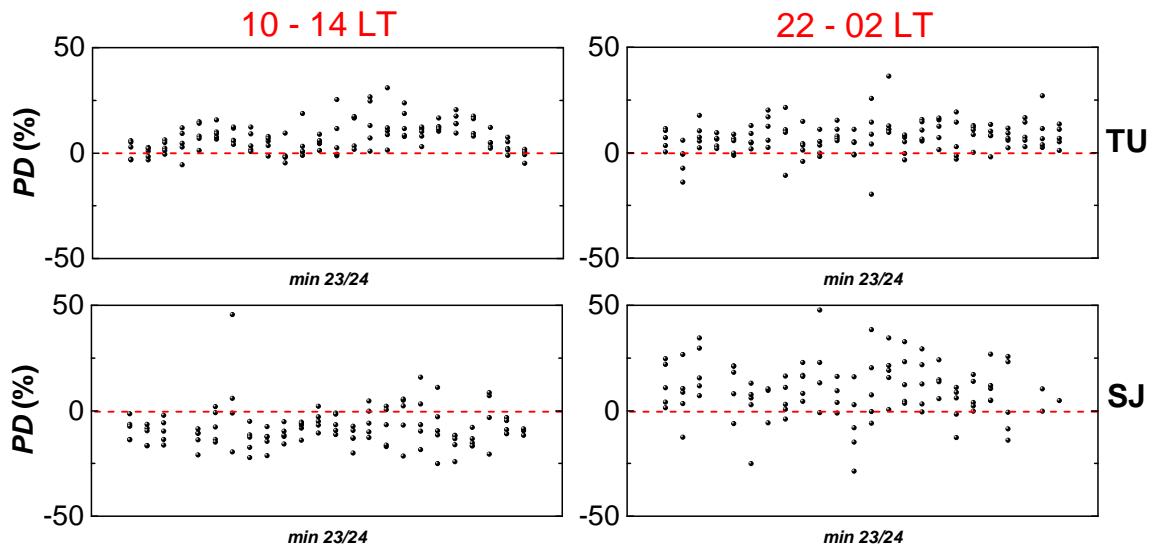**Figure 5.23:** Relative percentage differences for hmF2 according to equation (5.1), for the last solar minimum, for TU (first row) and SJ (second row). Panels on the left refer to daytime hours (10:00-14:00 LT), while panels on the right refer to nighttime hours (22:00-02:00 LT). The red dashed horizontal line identifies the zero.

5.4 Conclusions

There is no doubt that the last minimum of solar activity has shown unprecedented features, providing a unique opportunity to study the response of the ionospheric plasma under an extremely low and prolonged solar activity. Furthermore, it represents a very interesting period to test the reliability of ionospheric models for such particularly conditions.

This chapter was focused on (1) a comparison between the last minimum and the previous ones and (2) on the reliability evaluation for the parameters NmF2 and hmF2 of the IRI model, the most important ionospheric global model, for both mid and low latitudes.

A decrease of the parameter NmF2 appears for the last minimum in comparison to the previous ones for the three stations of RM, GL and TU, for which an inter-minima comparison was possible. A quite clear latitudinal dependence is observed, with more pronounced decreases at low latitudes (TU) than at mid latitudes (RM and GL). An analysis based on seasonal median values reveals that at mid latitudes the decrease is more pronounced from June to December Solstices, with slightly lower decreases for the March Equinox. The hours of the day for which more significant decreases have been observed are those near the sunset (16:00-18:00 LT), with less pronounced decreases around sunrise hours (06:00-07:00 LT). On the contrary, at low latitudes the largest decrease is visible from March to September Equinox, with a more pronounced decrease during nighttime hours (21:00-06:00 LT). Moreover, it is very important to underline that at RM and GL, the winter anomaly was not recorded only for the last minimum (years 2008-2009), confirming its anomalous low level of solar activity. At TU, the semi-annual anomaly, clearly visible for the minima 19/20 and 20/21, is not perceived for the minimum 23/24. The NmF2 values measured at SJ for the last minimum confirm that the typical semi-annual anomaly was not visible near the south crest of the EIA where both TU and SJ are located.

An inter-minima comparison for the parameter hmF2 was possible for the mid-latitude stations of RM and GL, for nighttime (19:00-06:00 LT) and daytime (07:00-18:00 LT) hours, using respectively the Shimazaki and D55 analytical formulations, for which a preliminary analysis has pointed out their reliability. Accordingly to the results found for NmF2, it has been observed that the hmF2 values measured during the last solar minimum are lower than those of the previous ones, for both stations.

A comparison between IRI outputs and measured monthly median values of NmF2, for the recent solar minima, reveals that IRI does not worsen its performances for the last minimum with respect to the previous ones, at both mid and low latitudes. With regard to this, it is very important to underline that observed values for solar and geomagnetic indices have been used as input for the model. This is a key result to emphasize the IRI dependence on input data.

For low and very low solar activities, IRI provides reliable outputs at mid latitudes for both NmF2 and hmF2. The exception is represented by the typical mid-latitude phenomenon of the meridian depression, also called MSEA, clearly visible at RM and GL for all minima analyzed, from April to September. The results reported in this chapter show that IRI does not describe correctly the meridian depression, in particular in April and September.

It was shown that the IRI model shows a clear loss of reliability at low latitudes for the parameter NmF2, in particular for the last solar minimum. Instead, different IRI performances between mid and low latitudes do not characterize the parameter hmF2, for which comparable results have been obtained for the last minimum at the four considered ionospheric stations. Contrariwise to what obtained for NmF2, for hmF2 it is observed a worsening of IRI performances at mid latitudes for the last minimum in comparison to the previous ones. Furthermore,

the IRI model reveals a tendency to overestimate hmF2 values during all day at both low and mid latitudes for the recent solar minima. This pattern is observed at all stations during nighttime hours, but not during daytime hours of the last solar minimum at SJ, for which IRI underestimations occur.

The results here reported suggest that IRI needs to be continuously tested, in particular at low/equatorial latitudes and near the crests of the EIA, in order to improve the reliability and capability of the model to describe and forecast the ionospheric plasma features. Furthermore, in order to improve the IRI description of the phenomenon of the meridian depression (or MSEA), an ingestion of more data from mid-latitude areas is recommended. Finally, given the significant hmF2 general overestimation made by IRI, some improvements are also recommended for the calculation of this parameter made by the model.

Conclusions and future developments

This thesis concerns the analysis of the ionospheric plasma response to the last minimum of solar activity, the minimum of the cycle 23/24. This minimum has shown unprecedented characteristics, providing a unique natural window to study the most relevant ionospheric features at all latitudes using a wide range of instruments and datasets.

Two main features have characterized the minimum 23/24: (1) a delay of ∼2 years in its observation with respect to the previsions and (2) an extremely low and prolonged solar activity. Considering the duration of the solar cycle 23, it is clear that the last solar minimum has been unusual. Previous recent solar minima have occurred in 1966, 1976, 1986 and 1996, following the canonical 11-year solar cycle. The end of the solar cycle 23 was expected in 2006, but in 2007 every indicator of solar activity (such as sunspots or solar fluxes) continued to drop, as they did through all the 2008 and 2009. Considering the sunspots number, the onset of a constant increase, that ratified the start of solar cycle 24, could be established in December 2009, with more than 2 years of delay than it was expected. In fact, the onset of the cycle 24 has been announced more times: in 2007, the solar cycle 24 Prediction Panel anticipated that the solar minimum would occur in March 2008 (±6 months), but the date was then corrected to August 2008 and later to December 2008. As mentioned, the end of the cycle 23 has been detected one year later.

In addition to the aforementioned delay in its occurrence, the last minimum has been characterized by an extremely low and prolonged solar activity. Section 2.1 reports some of the characteristics observed during the last minimum as described by numerous studies (Emmert et al., 2010; Heelis et al., 2009; Russell et al., 2010; Chen et al., 2011a), which provided a general picture of the very interesting particularities that typified the minimum. Furthermore, these particularities characterized a period than spans from 2006 to the end of the minimum at the end of 2009, providing a very long interval of extremely low solar activity.

The pattern observed during the last solar minimum is unprecedented in the space age, with solar wind and interplanetary conditions that have never seen before.

The solar radiation in the EUV wavelength range (0.1-120 nm) represents the main ionization source for the Earth's atmospheric high layers and it is the main responsible for the formation of the ionosphere. Therefore, the solar activity represents the main cause of the observed variability of the most important ionospheric parameters. Given this strong coupling, it is very interesting to analyze the ionospheric plasma response to the very low and prolonged input of solar flux registered during the deep phase of the last solar minimum (years 2008-2009) and compare it with the ones of the previous minima.

This work analyzes in detail the behaviors of the ionospheric parameters foF2, NmF2 and hmF2, by exploiting data recorded at four ground-based ionosondes located at mid and low latitudes: Rome (41.8°N, 12.5°E, geomagnetic latitude 41.7°N, Italy), Gibilmanna (37.9°N, 14.0°E, geomagnetic latitude 37.6°N, Italy), São José dos Campos (23.1°S, 314.5°E, geomagnetic latitude 19.8°S, Brazil), and Tucumán (26.9°S, 294.6°E, geomagnetic latitude 17.2°S,

Argentina).

The study has been divided in two main parts: (1) an analysis of the relations (foF2 vs *Solar Index*) (hereafter (foF2 vs *Index*)) for the long and continuous dataset recorded at Rome, and a subsequent partial updating of the *Simplified Ionospheric Regional Model* (*SIRM*); (2) a comparison between the last minimum and the previous ones and a comparison between measured values and *IRI-2012* model outputs, for NmF2 and hmF2, for the recent minima and for all the stations.

The first part of the work has been based on the long and continuous dataset of Rome to study the relations between the main ionospheric parameter, foF2, and five widely used solar activity indices, namely $F_{10.7}$, Lym-α, $MgII$, the sunspots number R and the solar irradiance in the EUV band 0.1-50 nm ($EUV_{0.1-50}$). For this part of the work, three main goals have been identified:

1. To observe if the a priori supposed linear relation is kept or there have been changes due to the particular features of the last minimum;

2. To find the best fit and index to describe the foF2 variations;

3. To perform a partial updating of the SIRM model based on the results obtained at points 1. and 2.

The relationships between ionospheric parameters and solar activity indices represent a main field of study in the ionospheric research, in particular because they are essential for every ionospheric model. During the last solar minimum, as shown by Chen et al. (2011a), clear changes characterized the relationship between the EUV radiation, measured by the SOHO/SEM instrument, and the widely used solar index $F_{10.7}$, questioning the widely used linear and constant relation between them. The extremely long, continuous and very reliable dataset recorded at Rome for foF2 from January 1976 to December 2013, gave us the possibility to reveal possible changes in the (foF2 vs *Index*) relationships, considering only the solar activity influence, and by applying a 1-year running mean to both parameters. The results reported in Chapter 3 show that, in order to describe properly the (foF2 vs *Index*) relationships, a quadratic polynomial is the best choice. The use of linear relations can lead to significant overestimations of observed data, mainly because of the saturation effect occurring at high solar activity and the unusual low solar activities registered during the last minimum. Considering that a linear relation is still a good choice to describe the observed data for the previous minima, we can say without doubt that the last minimum has caused a change in the (foF2 vs *Index*) relationships.

Using quadratic polynomial relations, a comparison of opportune synthetic datasets gave us the possibility to find the best index to describe the variations of the foF2 parameter at local noon in Rome. The results have shown that the $MgII$ index can be considered the best one for four main reasons: (1) a good sensibility to the variations of foF2 for low solar activity; (2) a reduced saturation effect at high solar activity; (3) a very slight hysteresis effect for medium solar activity; (4) the observed inter-cycle constancy in the relationship with foF2.

Moreover, a key finding in this first part of the work regards the index $F_{10.7}$ that represents a widely input parameter for ionospheric models. It has been shown that $F_{10.7}$ cannot properly follow the variations of foF2 for the very low solar activity levels of the last minimum, with synthetic foF2 values calculated using $F_{10.7}$ that considerably overestimate the observed ones. Consequently, for $F_{10.7}$ it was identified a threshold value of $82 \cdot 10^{-22}$ [J Hz^{-1} s^{-1} m^{-2}] below which foF2 variations are no more suitably reproduced.

The efficiency of the results achieved in Chapter 3 were then tested by using them to perform an updating (called *SIRMPol*) of the SIRM model, developed by Zolesi et al. (1993), and to develop a single station model for Rome (*SSM-R*).

In Chapter 4, the foF2 output given by SIRM has been compared with ionosonde data and with that of the SIRMPol and SSM-R. The comparison has been carried out for the mid-latitude station of Rome, for both low solar activity (years 2008 and 2009) and high solar activity (year 1957). Results for the SIRMPol model shows that for both low and high solar activity a slight improvement with respect to SIRM is obtained. However, SIRMPol represents only a local updating of the SIRM model, which is much more performing when an ionosondes network is available. This is why for an accurate local description of ionospheric parameters, *Single Station Models* (*SSMs*) are preferable, in particular when a very long dataset is available, as it is the case for Rome. Therefore, by applying a second order polynomial fit to the relationships between monthly median values of foF2 and R_{12}, the SSM-R has been developed, and this model turned out to be the best one to describe and forecast the ionospheric parameters for the Rome station.

Anyhow, the analyses carried out to perform a local updating of SIRM have shown how a substantial improvement of the model is possible, especially using a wide network of ionosondes. With regard to this, very useful guidelines have been compiled for a future complete updating of the SIRM model:

i. Besides the seven stations used in SIRM (listed in Table 4.1), additional ionosondes have to be considered over the European area;

ii. The model should be based on a "switch-case" between linear and 2° order polynomial regressions for the relationships (foF2 vs R_{12}), and the choice between the two should be based on a deep statistical analysis of both the saturation effect occurrence and the loss of linearity for the last solar minimum;

iii. Polynomial relations have to be used for the (A_n vs R_{12}) and (Y_n vs R_{12}) relationships;

iv. The model, which is based on the Fourier analysis to link data from several ionosondes, should be supported and integrated with updated SSMs, elaborated for every ionosonde included in the network.

The second part of the work, described in Chapter 5, has been based on available NmF2 and hmF2 data from two mid-latitude stations (Rome and Gibilmanna) and two low-latitude stations (São José dos Campos and Tucumán), for the recent solar minima. It is worth noting that the stations of São José dos Campos and Tucumán are located in a very critical ionospheric area, being close to the south crest of the *Equatorial Ionization Anomaly* (*EIA*) that represents one of the most prominent ionospheric phenomena.
For this part of the project, two main goals have been identified:

1. To evaluate the main behaviors of the ionosphere for the last solar minimum, making a comparison with previous minima, using the NmF2 and hmF2 parameters for all stations;

2. To make a comparison between observed values and the output of the last version of the IRI (*International Reference Ionosphere*) model, namely *IRI-2012* (hereafter IRI), for the recent solar minima, for NmF2 and hmF2 and for all stations.

It is important to underline that, using data from mid- and low-latitude ionosondes, it is possible to detect latitudinal-dependent behaviors for both the inter-minima comparison and IRI performances.

The inter-minima comparison for the parameter NmF2 revealed lower values for the last minimum than for the previous ones, for the three stations of Rome, Gibilmanna and Tucumán, for which this analysis was possible. The results showed also a latitudinal dependence, with a more pronounced decrease observed at low latitudes than at mid latitudes.

The particularity of the last solar minimum, with respect to the previous ones, has been underlined using hourly NmF2 monthly median values recorded in April, June, October and December, to study the occurrence of the *winter* and *semi-annual anomalies*. As described in Chapter 1, the visibility of both anomalies is directly proportional to the level of solar activity. The winter and semi-annual anomalies are phenomena that typically characterize the mid- and low-latitude ionosphere, respectively. The winter anomaly consists in higher NmF2 midday values during winter months (such as December for the North hemisphere) than during summer months (such as June for the North hemisphere); the semi-annual anomaly is instead observed when NmF2 midday values are higher during equinox months (such as April and October) than during solstice months (such as June and December). The results reveal that: a) at the mid-latitude stations of Rome and Gibilmanna the winter anomaly was not recorded only for the last minimum; b) at the low-latitude station of Tucumán, the semi-annual anomaly, clearly visible for the minima 19/20 and 20/21, is not perceived for the minimum 23/24. The latter is confirmed also by the NmF2 values measured at São José dos Campos for the last minimum. Therefore, both the analyses of the winter and semi-annual anomalies confirm the particularly low solar activity level characterizing the deep phase of the last solar minimum. An inter-minima comparison has been carried out at mid latitudes (Rome and Gibilmanna) also for the parameter hmF2, using the Shimazaki and D55 formulae for nighttime (19:00-06:00 LT) and daytime (07:00-18:00 LT) hours respectively. The results show that for both stations the hmF2 values measured during the last solar minimum are lower than those measured in the previous ones, in accord with the results obtained for the parameter NmF2.

The IRI model represents the reference model for the ionospheric community and it is the most widely used empirical global model for the description and forecast of the main ionospheric parameters. The model is periodically updated, with implementations based on information provided by numerous studies that analyze the reliability of the model at different solar and geomagnetic activity levels, latitudes, etc.

A comparison between outputs of the last available version of IRI, namely IRI-2012, and measured values for the recent solar minima reveals for NmF2 that, at both mid and low latitudes, the model does not worsen its performances for the last minimum. It is worth noting that this is true only if observed values of solar and geomagnetic indices are used as input. In fact it has been clearly shown in Section 2.2 that using forecasted values of these indices gives rise to a huge overestimation of the NmF2 measured values for the last solar minimum.

Considering the NmF2 parameter, a clear latitudinal dependence of the IRI output is observed, with a clear loss of reliability at low latitudes, in particular for the last solar minimum.

Differences in IRI performances between mid and low latitudes are not found for the parameter hmF2, for which comparable results have been obtained for the last minimum at the four stations. Nevertheless, for hmF2 it is observed a worsening in IRI performances at mid latitudes for the last minimum with respect to the previous ones. The results for hmF2 clearly show a tendency of the model to overestimate measured values during all day at both low and mid latitudes for the recent solar minima. This pattern is observed at all stations during night-

time hours, but not during daytime hours of the last solar minimum at São José dos Campos, for which IRI underestimations occur. This difference can be due to the strong latitudinal and longitudinal variations characterizing the ionospheric pattern in the South American sector, due to the particular configuration of the magnetic equator.

However, it is possible to claim that for low and very low solar activities, IRI provides reliable outputs at mid latitudes for both NmF2 and hmF2. The only exception is represented by the mid-latitude phenomenon of the *meridian depression* (or *Mid latitude Summer Evening Anomaly* (*MSEA*)), clearly visible for all minima analyzed at Rome and Gibilmanna from April to September. The analyses of Chapter 5 clearly show the IRI inability to describe appropriately the meridian depression, in particular in April and September.

The results obtained in this study open the door to exciting future developments. Specifically, from the results of the first part of the work, two possible developments that can be pursued are:

I. A complete implementation of the SIRM model, based on the guidelines described in Chapter 4;

II. An application of the relationships obtained in Chapter 3 to look for possible ionospheric signatures of greenhouse gases increase.

As already explained, a complete implementation of the SIRM model can be carried out, using a wide network of ionosondes over the European region, simply extending to all stations the same procedure applied to the Rome ionosonde to develop the SIRMPol model. Furthermore, the new model should be interfaced with opportune updated SSMs developed for every station. It is worth noting that in the next years, it will be possible to analyze the characteristics of other solar activity indices (such as $MgII$ and EUV), when a longer dataset will be available for them. As an example, by considering $MgII$ and EUV indices instead of R_{12}, better results should be expected for mid solar activity, due to a reduction of the hysteresis effect. Moreover, a future development of the SIRM model will concern both its applicability to high- and low-latitude regions, where more complex ionospheric behaviors in time and space are well known, and its use as a reference ionospheric model for regional short-term predictions.

The second possible development is very intriguing and is linked to a recent field of research about the effect that the greenhouse gases increase may have on the ionospheric plasma.

Long-term trend investigations in the upper atmosphere and ionosphere began with pioneering studies by Roble and Dickinson (1989); Rishbeth (1990) and Rishbeth and Roble (1992). Roble and Dickinson (1989) first suggested that there would be long-term changes of the ionospheric E and F-region peak densities in response to cooling and contraction of the mesosphere and the thermosphere, due to changes in greenhouse gas concentrations. Rishbeth (1990) concluded that long-term cooling in the upper atmosphere would lower the E and F2-region peak heights. Rishbeth and Roble (1992) investigated the global change in the ionosphere using the NCAR Thermosphere-Ionosphere General Circulation Model (TIGCM) (Roble et al., 1988) by doubling CO_2 and CH_4 concentrations, and they found that hmF2 dropped on average by about 15 km, while the change of NmF2 was minimal. In general, the aforementioned studies predicted a lowering of hmF2 of about -10 to -20 km and a reduction of the critical frequency foF2 of about -0.2 to -0.5 MHz for a doubling of the greenhouses CO_2 (Mielich and Bremer, 2013). Following these theoretical and modeling studies, ground-based ionosonde data have been widely analyzed trying to detect long-term trends in the ionosphere (e.g., Bremer, 1992; Ulich and Turunen, 1997; Bremer, 1998; Upadhyay and Mahajan, 1998; Danilov and Mikhailov,

1999; Mikhailov and Marin, 2000, 2001; Clilverd et al., 2003; Danilov, 2003) and, in the last years, a significant number of studies focused on the possible link of ionospheric trends with the middle and upper atmosphere cooling due to an increase of greenhouse gases (e.g., Danilov, 2012; Laštovička et al., 2012; Laštovička, 2013; Danilov and Konstantinova, 2015; Danilov, 2015; Scott and Stamper, 2015; Upadhyay and Mahajan, 1998; Hall and Cannon, 2002; Bremer et al., 2012; Mielich and Bremer, 2013; Qian et al., 2014; Cnossen and Franzke, 2014; Roininen et al., 2015). Nevertheless, the results were often inconsistent and sometimes controversial (Laštovička, 2013).

Causes of long-term trends of the ionosphere can be natural or anthropogenic (Rishbeth, 1997). Consequently, in order to emphasize possible anthropogenic causes of long-term trends of parameters such as foF2 or hmF2, the key point is the elimination of the solar and geomagnetic activity-induced parts. For this purpose, different methods have been used as well as different regression methodologies (e.g., Bremer, 1992; Ulich, 2000; Alfonsi et al., 2002; de Adler et al., 2002; Mikhailov, 2002; Danilov, 2002, 2003; Yue et al., 2006; Qian et al., 2008). In most of the published studies, the solar sunspot number R has been used as proxy of the solar EUV radiation (Mielich and Bremer, 2013), while Ulich et al. (2006) found slightly less noisy results by using $F_{10.7}$ instead of R. This to highlight that, since the influence of the solar activity causes marked variations of the ionospheric parameters, it is necessary to use the optimum solar activity index and the best analytical relation to derive reliable ionospheric long-term trends.
With regard to this, the results obtained in the present work suggest that both indices R and $F_{10.7}$ do not represent the best choice to describe the relationships (foF2 vs $Index$). Therefore, it could be very interesting to consider the second order polynomial relation (foF2 vs $MgII$) found for the Rome station (at local midday) to investigate whether the corresponding long-term trend of residuals $\Delta fo\text{F2} = (fo\text{F2}_{\text{observed}} - fo\text{F2}_{\text{synthetic}})$ presents some signature related to the greenhouse effect.

The second part of the present work has underlined the very particular conditions of the ionosphere for the last solar minimum in comparison to the previous ones, for both low and mid latitudes. Specifically, the comparison between ionosonde values of NmF2 and hmF2 and those calculated by IRI suggests that IRI needs to be continuously tested, in particular at low/equatorial latitudes and near the crests of the EIA, in order to improve the reliability and capability of the model to describe and forecast the ionospheric plasma features in these complex regions. Nevertheless, an improvement of the accuracy of the model is required also at mid latitudes, in particular concerning the meridian depression (or MSEA), for which a greater assimilation of data from mid-latitude ionosondes becomes necessary for IRI. Moreover, because of the hmF2 overestimations made by IRI for the last solar minimum, some improvements concerning the analytical relations used by IRI to calculate this parameter are also requested.
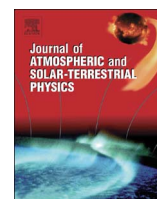
*fo*F2 vs solar indices for the Rome station: Looking for the best general relation which is able to describe the anomalous minimum between cycles 23 and 24

L. Perna [a,b,*], M. Pezzopane [b]

[a] Università di Bologna "Alma Mater Studiorum", Viale Berti Pichat 6/2, 40126 Bologna, Italy
[b] Istituto Nazionale di Geofisica e Vulcanologia, Via di Vigna Murata 605, 00143 Roma, Italy

ABSTRACT

Analyses of the dependence of the F2 layer critical frequency, *fo*F2, on five widely used solar activity indices ($F_{10.7}$, *Lym-α*, *MgII*, *R* and $EUV_{0.1-50}$) are carried out considering noon values manually validated at the ionospheric station of Rome (41.8°N, 12.5°E, Italy) between January 1976 and December 2013, a period of time covering the last three solar cycles and including the prolonged and anomalous minimum of solar cycle 23/24 (years 2008–2009). After applying a 1-year running mean to both *fo*F2 and solar activity indices time series, a second order polynomial fitting proves to perform better than a linear one, and this is specifically due to the very low solar activity of the last solar minimum and to the remaining saturation effect characterizing the high solar activity. A comparison between observed and synthetic *fo*F2 values, the latter calculated by using the analytical relations found for every index, and some considerations made on the *R* parameter introduced by Solomon et al. (2013), suggest that *MgII* is the best index to describe the dependence of *fo*F2 on the solar activity. Three main reasons justify this result: (1) the good sensibility of *MgII* to the variations of *fo*F2 for low solar activity; (2) the reduced saturation effect characterizing *MgII* at high solar activity; (3) the poor influence of the hysteresis effect characterizing *MgII* at medium solar activity. On the other hand, the $F_{10.7}$ index, widely used as input parameter for numerous ionospheric models, does not represent properly the last minimum; specifically, it is not able to describe the variations of *fo*F2 under a solar activity level of $F_{10.7}=82 \cdot 10^{-22}$ [J Hz^{-1} s^{-1} m^{-2}].

© 2016 Elsevier Ltd. All rights reserved.

1. Introduction

The terrestrial ionosphere is produced by the ionization of the neutral atmosphere caused by the solar radiation, and it is then expected to follow the Sun's behavior (e.g., Araujo-Pradere et al., 2011; Hargraves, 1995; Liu et al., 2006, 2011b; Solomon et al., 2010, 2013). The study of the relations between the main ionospheric characteristics and the indices of solar activity has recently increased because of the more accurate measurements of solar radiation in the ionospherically crucial Ultra Violet (UV, 120–400 nm) and Extreme Ultra Violet (EUV, 0.1–120 nm) bands.

Ionospheric trends have become a main subject of research since the beginning of nineties when they gained importance in the context of the global climatic change (Roble and Dickinson, 1989; Roble, 1995; Rishbeth, 1990; Rishbeth and Roble, 1992). Since then, a significant number of studies focussed on

ionospheric trends and on their possible link with the middle and upper atmosphere cooling due to an increase of greenhouse gases (e.g., Ulich and Turunen, 1997; Danilov., 2012; Laštovička et al., 2012; Laštovička, 2013; Danilov and Konstantinova, 2015; Danilov, 2015; Scott and Stamper, 2015; Upadhyay and Mahajan, 1998; Hall and Cannon, 2002; Bremer et al., 2012; Mielich and Bremer, 2013; Qian et al., 2014; Cnossen and Franzke, 2014; Roininen et al., 2015).

The solar activity variations represent the most influent cause of the ionospheric characteristics observed variability. This is clearly shown by Fig. 1 where the 1-year running means of the solar radio flux at 10.7 cm ($F_{10.7}$), and of the F2 layer critical frequency (*fo*F2) observed at local noon at the ionospheric station of Rome (41.8°N, 12.5°E, Italy), are plotted for the time period from January 1976 to December 2013.

The analysis of relations (*fo*F2 vs *Solar Index*) is essential for two main reasons: (1) every ionospheric model is based on these relations; (2) possible signatures of the greenhouse effect on the ionosphere can be found only after an accurate cleaning of the ionospheric characteristic time series from solar activity (in particular) and geomagnetic dependences. As a consequence, the

NmF2 trends at low and mid latitudes for the recent solar minima and comparison with IRI-2012 model

L. Perna [a,b,*], M. Pezzopane [b], R. Ezquer [c,d,f], M. Cabrera [c,e], J.A. Baskaradas [g]

[a] Università di Bologna "Alma Mater Studiorum", Viale Berti Pichat 6/2, 40126 Bologna, Italy
[b] Istituto Nazionale di Geofisica e Vulcanologia, Via di Vigna Murata 605, Roma 00143, Italy
[c] CIASUR, Facultad Regional Tucumán, Universidad Tecnológica Nacional, Tucumán, Argentina
[d] Laboratorio de Ionósfera, Dto. De Fisica, FACET, Universidad Nacional de Tucumán, Indipendencia 1800, 4000 S.M. Tucumán, Argentina
[e] Laboratorio de Telecomunicaciones, FACET, Universidad Nacional de Tucumán, Indipendencia 1800, 4000 S.M. Tucumán, Argentina
[f] CONICET, Buenos Aires, Argentina
[g] SAP, School of Electrical and Electronics Engineering, SASTRA University, Thirumalaisamudram, Thanjavur, Tamil Nadu 613401, India

Abstract

The ionospheric electron density peak ($NmF2$) is analyzed for the recent minima of solar activity for two mid-latitude stations, Rome (41.8°N, 12.5°E, geomagnetic latitude 41.7°N, Italy) and Gibilmanna (37.9°N, 14.0°E, geomagnetic latitude 37.6°N, Italy), and for the low-latitude station of Tucumán (26.9°S, 294.6°E, geomagnetic latitude 17.2°S, Argentina), located in the south ridge of the equatorial ionization anomaly. An inter-minima comparison reveals that from an ionospheric point of view the last minimum of solar activity (minimum 23/24) was peculiar, with values of $NmF2$ lower than those recorded during the previous minima for all the stations and all the hours of the day. A more pronounced decrease is observed at Tucumán than at Rome and Gibilmanna. The study of the winter and semi-annual anomaly shows that at mid-latitude stations the winter anomaly is not visible only for the years 2008 and 2009, which represent the deeper part of the prolonged and anomalous last solar minimum. The same is for the semi-annual anomaly. A comparison with the version 2012 of the International Reference Ionosphere model (IRI) is also carried out. The results reveal that for low solar activity the model works better at mid latitudes than at low latitudes, confirming the problems of IRI in correctly representing the low-latitude ionosphere. Nevertheless, using as input updated values of the solar and geomagnetic indices, no loss of accuracy is detected in the IRI performances for the last solar minimum with respect to the previous ones, both at mid and low latitudes.
© 2016 COSPAR. Published by Elsevier Ltd. All rights reserved.

Keywords: Ionosphere; Ionospheric electron density peak; IRI model; Solar minimum; Solar cycle

1. Introduction

The ionosphere is produced by the ionization of the neutral atmosphere caused by the solar radiation and it is then expected to follow the Sun's behavior (e.g., Araujo-Pradere et al., 2011; Hargreaves, 1992; Liu et al., 2006, 2011; Solomon et al., 2010, 2013). The solar Extreme Ultra Violet irradiance (10–120 nm) represents the main ionization source of the ionospheric F2 layer (e.g., Chen et al., 2012; Tobiska, 1996), and significantly affects the variability of ionospheric parameters such as the critical frequency of the F2 layer ($foF2$), and the corresponding maximum of electron density ($NmF2$) and height ($hmF2$).

The time variation of $NmF2$ is expected to follow almost identically the variations of the solar activity, owing to the

Acknowledgements

Heartfelt thanks go to all the people that have been, directly or indirectly, part of this 3-year route. I will thank everyone of them in their more comfortable language.

Ringrazio Ale con tutto l'amore che ho. Lei ha rappresentato e rappresenta un *"dolce rifugio"* in ogni momento della mia vita. La ringrazio per l'aiuto, il supporto, la pazienza, la sopportazione, l'incoraggiamento e l'amore che ha sempre saputo darmi nei momenti buoni e meno buoni. Senza il suo supporto e la sua adorabile presenza non sarei riuscito a portare a termine questo percorso e non avrei avuto nemmeno le palle per iniziarlo...tutto sarebbe stato maledettamente più difficile. Grazie amore!

Un grande grazie ai miei genitori Emanuele e Rocchina. Grazie per i sacrifici che avete fatto sin dall'inizio del mio percorso di studi e grazie per tutte quelle rinunce che avete fatto negli anni e che ancora continuate a fare. Non ci saranno mai parole adeguate o traguardi importanti che potranno ridarvi tutto quello che avete fatto per me. Grazie per l'opportunità che mi avete dato e per il vostro costante supporto anche nei momenti più difficili. Questo traguardo è stato possibile solo grazie a voi e ai vostri sacrifici.

Grazie mille a Giuseppe e Giorgia. Grazie per l'affetto fraterno, per il sostegno e l'aiuto nei momenti più difficili. So che ci sarete sempre per me e io, quando vorrete, sarò sempre lì per voi.

Grazie a Roberto, Roberta e Marco. Grazie per l'ospitalità e la gentilezza che avete sempre avuto nei miei confronti. Per me siete come una seconda famiglia e non dimenticherò mai tutte le accortezze e le attenzioni che avete verso di me. Questo traguardo è stato possibile anche grazie a voi.

Grazie a Vincenzo. Grazie per la fraterna amicizia e per la preziosa presenza nei momenti critici attraversati in tutti questi anni universitari e post universitari. Senza i consigli, le pacche sulle spalle e i sorrisi che ti tirano su il morale non è semplice affrontare e superare immuni le difficoltà. Grazie per tutto questo.

Grazie a Michael Pezzopane, insostituibile guida durante questi ultimi 5 anni. Grazie per i saggi consigli, per i suggerimenti e per la presenza costante e rassicurante in ogni situazione. Grazie per la pazienza e la cordialità mostrata durante tutto questo percorso anche in risposta alle mie mancanze e assenze mai troppo giustificate. Grazie per avermi fatto crescere come studente, ricercatore e come persona. Non potevo sperare in una persona migliore da seguire e da cui imparare. Grazie per i sacrifici e per la costante attenzione dedicata al lavoro durante tutti questi anni. Grazie per essere stato un relatore, una guida, un insegnante, un amico.

Sincera gratitudine va al dipartimento di *Fisica e Astronomia* dell'Università di Bologna per avermi dato l'opportunità di sviluppare il progetto di dottorato descritto in questa tesi. Un ringraziamento a tutti i docenti che hanno tenuto i corsi di dottorato tra Bologna e Roma, fornendomi conoscenze assai utili per la mia crescita professionale. Un ringraziamento particolare va al mio supervisore Prof. Michele Dragoni per la gentilezza e competenza mostrata in tutti questi tre anni nel chiarire ogni dubbio di qualsiasi natura.

Un ringraziamento va a tutti i membri dell'Unità Funzionale di *Fisica dell'alta atmosfera* dell'Istituto Nazionale di Geofisica e Vulcanologia. Grazie per aver messo a mia disposizione le strutture, gli strumenti e i dati necessari allo sviluppo di questo progetto di dottorato. Grazie a tutti i ricercatori che con i loro preziosi consigli hanno fornito un input per il miglioramento della qualità finale del lavoro. Nutro per ciascuno di loro profonda stima perchè essere ricercatore nel nostro paese è una missione impossibile e quasi sempre i sacrifici, il lavoro, gli studi, il tempo negato agli affetti e alla vita non vengono riconosciuti con la meritata riconoscenza. Li ringrazio perchè è stato per me un piacere ed un onore lavorare dietro e accanto a loro, perchè in quelle stanze viene condotta una ricerca di altissimo livello anche da chi ancora lavora in una situazione di instabilità spinto solo ed esclusivamente dalla passione per quello che fa. Auguro a voi il meglio per il vostro futuro. In particolare vorrei ringraziare Enrico Zuccheretti e Marco Pietrella per la disponibilità mostrata durante i nostri incontri e le nostre chiacchierate.

A very sincere thank to Prof. Paulo Roberto Fagundes and to the IP&D department of the UNIVAP. Thanks for the opportunity you gave me to stay in São José, providing me the instrumentations and resources I needed to improve the quality of my work. Thanks to Prof. Fagundes to have been a constant reference during my stay in Brazil and for all the suggestions and advices. It has been a wonderful life experience that has made me grow professionally and temperamentally.

A very big thank you to all the guys, Valdir, Marcio, Caius, Venkatesh, Virginia, Eduardo-Laura-Luna, Brunno, Alan, Prof. Rocha Fernandes, Prof. Abalde, Irapuan, Marcelo, Angela, Oli, Alexandre, Flavia, Alexandre José, Arian, Antonio, Will, Victor, Pamela, Thays, Fredson V., Fredson C., Maukers, Diego, Vilson, Luis, Laurita. Thank you to have teached me the lightness, the smile and that the work can exist also without stress.

Un sincero ringraziamento ai colleghi che hanno condiviso con me questa esperienza. Grazie ad Andrea, Davide, Grazia, Ines, Marco, Marcello e Pablo. Grazie per i sorrisi, per i consulti scientifico-burocratici, grazie per i momenti passati insieme a Bologna e Roma. Grazie per aver reso quei periodi leggeri e spensierati, grazie per il sostegno e l'aiuto durante i mesi di lavoro per consegnare le infinite tesine dei corsi e grazie per avermi aiutato ad affrontare tutto con il sorriso e con qualche pensiero in meno in testa. Vi auguro tutto il meglio dalla vita e per il vostro futuro, perchè siete delle persone fantastiche ma anche dei brillanti ricercatori (a tal riguardo direi che non mi sono affatto *"ricreso"*). Sono sicuro che raggiungerete tutti i vostri obiettivi nella vostra carriera. Ancora grazie.

Ultimi ma non ultimi, grazie a Tito e Rufo. Perchè spesso la sola cosa che desideri e di cui hai bisogno è di svuotare la mente guardando nei vostri occhi innamorati e fedeli e lasciarsi sommergere dalle vostre coccole. Grazie!

E infine un ringraziamento alla strada, a tutto il percorso che mi sono lasciato alle spalle e che guardo adesso con un filo di nostalgia. Grazie a tutti coloro che ci sono sempre stati, che hanno corso con me, che si sono fermati ad attendere che passasse la bufera insieme a me, che mi hanno aiutato, che mi hanno soccorso, che mi hanno teso una mano per rialzarmi, che mi hanno spinto quando ho avuto delle esitazioni, che mi hanno sorretto per superare ostacoli che pensavo insormontabili, che ci hanno messo l'amore, la passione, la gioia, che ci hanno messo la faccia, la testa...ma soprattutto il cuore. Ma grazie anche a chi non c'ha messo proprio nulla.

Tutti coloro che incontriamo lungo un viaggio ci lasciano qualcosa, a volte è un insegnamento, a volte sono delle domande, a volte delle cicatrici...ma siamo fatti di tutto questo e io sono fatto di tutto questo...quindi a voi tutti ancora, Grazie!

Bibliography

Abdu, M.A., Brum, C.G.M., Batista, I.S., Sobral, J.H.A., de Paula, E.R., Souza, J.R, 2008. Solar flux effects on equatorial ionization anomaly and total electron content over Brazil: observational results versus IRI representations. Adv. Space Res. 42, 617-625, doi:10.1016/j.asr.2007.09.043.

Adebesin, B.O., Adekoya, B.J., Ikubanni, S.O., Adebiyi, S.J., Adebesin, O.A., Joshua, B.W., Olonade, K.O., 2014. Ionospheric foF2 morphology and response of F2 layer height over Jicamarca during different solar epochs and comparison with IRI-2012 model. J. Earth Syst. Sci. 123, 4, 751-765, doi: 10.1007/s12040-014-0435-y.

Alfonsi, L., de Franceschi, G., Perrone, L., Materassi, M., 2002. Long-term trends of the critical frequency of the F2 layer at northern and southern high latitude regions. Phys. Chem. Earth 27, 607-612.

Appleton, E.V., 1946. Two anomalies in the ionosphere. Nature 157, 691.

Araujo-Pradere, E.A., Redmon, R., Fedrizzi, M., Viereck, R., Fuller-Rowell, T.J., 2011. Some Characteristics of the Ionospheric Behavior During the Solar Cycle 23-24 Minimum. Sol. Phys. 274, 439-456, doi:10.1007/s11207-011 9728-3.

Araujo-Pradere, E.A., Buresova, D., Fuller-Rowell, D.J., Fuller-Rowell, T.J., 2013. Initial results of the evaluation of IRI hmF2 performance for minima 22-23 and 23-24. Adv. Space Res. 51(4), 630-638, doi:10.1016/j.asr.2012.02.010.

Balan, N., Iyer, K.N., 1983. Equatorial anomaly in ionospheric electron content and its relation to dynamo currents. J. Geophys. Res. 88(A12), 10259-10262.

Barry Research Corporation, 1975. VOS-1A User Manual. Palo Alto, California, USA.

Batista, I.S., Abdu, M.A., 2004. Ionospheric variability at Brazilian low and equatorial latitudes: comparison between observations and IRI model. Adv. Space Res. 34(9), 1894-1900, doi:10.1016/j.asr.2004.04.012.

Bibl, K., Reinisch, B.W., 1975. Digisonde 128P, an Advanced Ionospheric Digital Sounder. University of Lowell Research Foundation.

Bidaine, B., Warnant, R., 2010. Assessment of the NeQuick model at mid-latitudes using GNSS TEC and ionosonde data. Adv. Space Res. 45(9), 1122-1128, doi:10.1016/j.asr.2009.10.010.

Bilitza, D., Rawer, K., Bossy, L., Kutiev, I., Oyama, K.-I., Leitinger, R., Kazimirovsky, E., 1990. International Reference Ionosphere 1990. NSSDC 90-22, Greenbelt, Maryl., 53, 160, doi:10.1017/CBO9781107415324.004.

Bilitza, D., 2001. International Reference Ionosphere 2000. Radio Sci. 36, 261-275, doi:10.1029/2000RS002432.

Bilitza, D., Reinisch, B.W., 2008. International Reference Ionosphere 2007: Improvements and new parameters. Adv. Space Res. 42(7), 599-609, http://dx.doi.org/10.1016/j.asr.2007.07.048.

Bilitza, D., Brown, S., Wang, M.Y., Souza, J.R., Roddy, P., 2012. Measurements and IRI model predictions during the recent solar minimum. J. Atm. Sol. Terr. Phys. 86, 99-106, http://dx.doi.org/10.1016/j.jastp.2012.06.010.

Bilitza, D., Altadill, D., Zhang, Y., Mertens, C., Truhlik, V., Richards, P., McKinnell, L.-A., Reinisch, B., 2014. The International Reference Ionosphere 2012 - a model of international collaboration. J. Sp. Weath. Sp. Clim. 4, A07, doi:10.1051/swsc/2014004.

Bradley, P.A., Cander, L.R., Dick, M., Jodogne, J.C., Kouris, S.S., Leitinger, R., Singer, W., Xenos, T.D., Zolesi, B., 1994. The December 1993 new mapping meeting, in Numerical Mapping and Modelling and their Applications to PRIME, Proceedings of the PRIME COST 238 Workshop, pp. 169-179, Eindhoven Univ. of Technol., Eindhoven, Netherlands.

Bradley, P.A., 1995. PRIME (prediction regional ionospheric modelling over Europe). COST Action 238 Final Report. Commission of the European Communities, Brussels.

Bremer, J., 1992. Ionospheric trends in mid-latitudes as a possible indicator of the atmospheric greenhouse effect, J. Atm. Terr. Phys. 54, 1505-1511.

Bremer, J., 1998. Trends in the ionospheric E and F regions over Europe, Ann. Geophys. 16, 986-996.

Bremer, J., Damboldt, T., Mielich, J., Suessmann, P., 2012. Comparing long-term trends in the ionospheric F2-region with two different methods. J. Atm. Sol. Terr. Phys. 77, 174-185, doi:10.1016/j.jastp.2011.12.017.

Brown, L.D., Daniell, R.E., Fox, M.W., Klobuchar, J.A., Doherty, P.H., 1991. Evaluation of six ionospheric models as predictors of total electron content. Rad. Sci. 26(4), 1007-1015, doi:10.1029/91RS00513.

Cebula, R.P., Deland, M.T., Hilsenrath, E., 1998. NOAA 11 solar backscattered ultraviolet, model 2 (SBUV/2) instrument solar spectral irradiance measurements in 1989-1994 1. Observations and long-term calibration. J. Geophys. Res. 103, D13, 16235-16250.

Chen, Y., Liu, L., 2010. Further study on the solar activity variation of daytime NmF2. J. Geophys. Res. 115, A12337, doi:10.1029/2010JA015847.

Chen, Y., Liu, L., Wan, W., 2011a. Does the F10.7 index correctly describe solar EUV flux during the deep solar minimum of 2007-2009? J. Geophys. Res. 116, A04304, doi:10.1029/2010JA016301.

Chen, C.H., Huba, J.D., Saito, A., 2011b. Theoretical study of the ionospheric Weddell Sea Anomaly using SAMI2. J. Geophys. Res. 116, A04305, http://dx.doi.org/10.1029/2010JA015573.

Chen, Y., Liu, L., Wan, W., 2012. The discrepancy in solar EUV-proxy correlations on solar cycle and solar rotation timescales and its manifestation in the ionosphere. J. Geophys. Res. Sp. Phys. 117, A3, doi:10.1029/2011JA017224.

Clilverd, M.A., Ulich, T., Jarvis, M.J., 2003. Residual solar cycle influence on trends in ionospheric F2-layer peak height. J. Geophys. Res. 108(A12), 1450, doi:10.1029/2003JA009838.

Cnossen, I., Franzke, C., 2014. The role of the Sun in long-term change in the F2 peak ionosphere: New insights from EEMD and numerical modeling. J. Geophys. Res. Sp. Phys. 119, 10, 8610-8623, doi:10.1002/2014JA020048.

Covington, A.E., Medd, W.J., 1954. Variations of the daily level of the 10.7-centimetre solar emission. J. Radio Astron. Soc. Can. 48, 136.

Danilov, A.D., Mikhailov, A.V., 1999. Long-Term Trends in the Parameters of the F2 Region: A New Approach. Geomagnetism and aeronomy c/c of geomagnetizm i aeronomiia 39(4), 473-479.

Danilov, A.D., Mikhailov, A.V., 2001. F2-layer parameters long-term trends at the Argentine Islands and Port Stanley stations. Ann. Geophys. 19, 3, 341-349.

Danilov, A.D., 2002. The method of determination of the long-term trends in the F2 region independent of geomagnetic activity. Ann. Geophys. 20, 511-521, doi:10.5194/angeo-20-511-2002.

Danilov, A.D., 2003. Long-term trends of foF2 independent of geomagnetic activity. Ann. Geophys. 21, 1167-1176, doi:10.5194/angeo-21-1167-2003.

Danilov, A.D., 2012. Long-Term Trends in the Upper Atmosphere and Ionosphere (a Review). Geomag. Aeron. 52(3), 271-291.

Danilov, A.D., Konstantinova, A.V., 2015. Variations in foF2 Trends with Season and Local Time. Geomag. Aeron. 55(1), 51-58.

Danilov, A.D., 2015. Seasonal and diurnal variations in foF2 trends. J. Geophys. Res. Sp. Phys. 120, 5, 3868-3882, doi:10.1002/2014JA020971.

de Adler, N.O., Elias, A.G., Heredia, T., 2002. Long-term trend in the ionospheric F2 layer peak height at a southern low latitude station. Phys. Chem. Earth 27, 613-615.

De Franceschi, G., De Santis, A., 1994. PASHA: regional long-term predictions of ionospheric parameters by ASHA. Ann. Geophys. 37(2), doi: 10.4401/ag-4228.

De Franceschi, G., Zolesi, B., 1998. Regional Ionospheric mapping and modelling over Antarctica. Ann. Geophys. 41(5-6), doi: 10.4401/ag-3821.

Didkovsky, L., Judge, D., Wieman, S., McMullin, D., 2009. Minima of Solar Cycles 22/23 and 23/24 as Seen in SOHO/CELIAS/SEM Absolute Solar EUV Flux. Arxiv Prepr. arXiv0911.0870 6.

Dominici, P., 1971. Radiopropagazione Ionosferica. Annali di Geofisica 24, pp. 157.

Dominici, P., Zolesi, B., 1987. A model for the normal ionosphere over Rome. II Nuovo Cimento 10C, 191-208.

Dudeney, J.R., 1974. A simple empirical method for estimating the height and semi thickness of the F2-layer at the Argentine Islands, Graham Land. Scientific Reports 88 , British Antarctic Survey, Cambridge, U.K.

Dudeney, J.R., Piggott, W.R., 1978. Antarctic ionospheric research, in Upper Atmosphere Research in Antarctica. Antarct. Res. Ser. AGU 29, 200-235.

Duncan, R.A, 1960. The equatorial F-region of the ionosphere. J. Atm. Terr. Phys. 18, 89-100.

Dvinskikh, N.I., 1988. Expansion of ionospheric characteristics fields in empirical orthogonal functions. Adv. Sp. Res. 8(4), 179-187, doi:10.1016/0273-1177(88)90238-4.

Eddy, J.A., 1976. The Maunder minimum. Science 192, 1189, doi:10.1126/science.192.4245.1189.

Eddy, J.A., 1981. Climate and the role of the Sun. In Climate and History: Studies in Interdisciplinary History, edited by R.I. Rotberg and T.K. Rabb, pp. 145, Princeton Univ. Press, Princeton, N. J.

Elias, A.G., Barbas, B.F.D.H., Shibasaki, K., Souza, J.R., 2014. Effect of solar cycle 23 in foF2 trend estimation. Earth Planets Sp. 66, 111, doi:10.1186/1880-5981-66-111.

Emmert, J.T., Lean, J.L., Picone, J.M., 2010. Record-low thermospheric density during the 2008 solar minimum. Geophys. Res. Lett. 37(12), doi:10.1029/2010GL043671.

Ezquer, R.G., López, J.L., Scidá, L.A., Cabrera, M.A., Zolesi, B., Bianchi, C., Pezzopane, M., Zuccheretti, E., Mosert, M., 2014. Behaviour of ionospheric magnitudes of F2 region over Tucumán during a deep solar minimum and comparison with the IRI-2012 model predictions. J. Atm. Sol. Terr. Phys. 107, 89-98, dx.doi.org/10.1016/j.jastp.2013.11.010.

Floyd, L., Tobiska, W.K., Cebula, R.P., 2002. Solar uv irradiance its variation and its relevance to the earth. Adv. Sp. Res. 29, 1427-1440, doi:10.1016/S0273-1177(02)00202-8.

Floyd, L., Newmark, J., Cook, J., Herring, L., McMullin, D., 2005. Solar EUV and UV spectral irradiances and solar indices. J. Atm. Sol. Terr. Phys. 67, 3-15, doi:10.1016/j.jastp.2004.07.013.

Galkin, I.A., Reinisch, B.W., 2008. The new ARTIST 5 for all digisondes. Ionosonde Network Advisory Group Bulletin 69(8).

Gillmor, C.S., 1976. The history of the term 'ionosphere'. Nature 262, 347-348.

Grant, I.F., MacDougall, J.W., Ruohoniemi, J.M., Bristow, W.A., Sofko, G.J., Koehler, J.A., Danskin, D., Andre, D., 1995. Comparison of plasma flow velocities determined by the ionosonde Doppler drift technique, SuperDARN radars, and patch motion. Radio Sci. 30, 1537-1549, doi:10.1029/95RS00831.

Hall, C.M., Cannon, P.S., 2002. Trends in foF2 above Tromsø. Geophys. Res. Lett. 29(23), doi:10.1029/2002GL016259.

Hanbaba, R., 1999. Improved quality of service in ionospheric telecommunication systems planning and operation. COSTAction 251 Final Report, Space Research Centre, Warsaw, pp. 102-103.

Hargreaves, J.K., 1995. The Solar-terrestrial Environment: An Introduction to Geospace. Cambridge University Press, pp. 420.

He, M., Liu, L., Wan, W., Ning, B., Zhao, B., Wen, J., Yue, X., 2009. A study of the Weddell Sea Anomaly observed by FORMOSAT-3/COSMIC. J. Geophys. Res. 114, A12309, http://dx.doi.org/10.1029/2009JA014175.

Heelis, R.A., Coley, W.R., Burrell, A.G., Hairston, M.R., Earle, G.D., Perdue, M.D., Power, R.A., Harmon, L.L., Holt, B.J., Lippincott, C.R., 2009. Behavior of the O+/H+ transition height during the extreme solar minimum of 2008. Geophys. Res. Lett. 36, L00C03, doi:10.1029/2009GL038652.

Hochegger, G., Nava, B., Radicella, S., Leitinger, R., 2000. A family of ionospheric models for different uses. Phys. Chem. Earth, Part C: Solar, Terrestrial and Planetary Science 25(4), 307-310, doi:10.1016/S1464-1917(00)00022-2.

Houminer, Z., Bennett, J.A., Dyson, P.L., 1993. Real-time ionospheric model updating. Journal of Electrical and Electronics Engineering, Australia, IE Australia & IREE Australia 13(2), 99-104.

International Radio Consultative Committee (CCIR), 1967a. Atlas of Ionospheric Characteristics. Report 340, International Telecommunication Union, Geneva.

International Radio Consultative Committee (CCIR), 1967b. Atlas of Ionospheric Characteristics. Report 340-2 (and later suppl.), International Telecommunication Union, Geneva.

ITU-R, 1994. HF Propagation Prediction Method. Recommendation ITU-R P. 533. International Telecommunication Union, Geneva.

ITU, 2003. Ionospheric propagation data and prediction methods required for the design of satellite services and systems, Recommendation, Geneva, pp. 531-537.

Jee, G., Burns, A.G., Kim, Y.-H., Wang, W., 2009. Seasonal and solar activity variations of the Weddell Sea Anomaly observed in the TOPEX total electron content measurements. J. Geophys. Res. 114, A04307, http://dx.doi.org/10.1029/2008JA013801.

Jodogne, J.C., Nebdi, H., Warnant, R., 2005. GPS TEC and ITEC from digisonde data compared with NEQUICK model. Adv. Radio Sci. 2(11), 269-273, doi:10.5194/ars-2-269-2004.

Johnson, F.S., 1964. Composition changes in the upper atmosphere. In: Electron Density Distributions in the ionosphere and Exosphere, (Eds.), Thrane, E., North Holland, Amsterdam, 81-84.

Jones, W.B., Gallet, R.M., 1962. Representation of diurnal and geographical variations of ionospheric data by numerical methods. Telecommun. J. 29, 129-149.

Judge, D.L., McMullin, D.R., Ogawa, H.S., Hovestadt, D., Klecker, B., Hilchenbach, M., Möbius, E., Canfield, L.R., Vest, R.E., Watts, R., Tarrio, C., Kühne, M., Wurz, P., 1998. First solar EUV irradiances obtained from SOHO by the CELIAS/SEM. Chapter of the book Solar Electromagnetic Radiation Study for Solar Cycle 22: Proceedings of the SOLERS22 Workshop held at the National Solar Observatory, Sacramento Peak, Sunspot, New Mexico, U.S.A., June 17-21, 1996, Springer Netherlands, pp. 161-173, doi:10.1007/978-94-011-5000-212.

Kane, R.P., 1992. Sunspots, solar radio noise, solar EUV and ionospheric foF2. J. Atm. Terr. Phys. 54, 463-466.

Karpachev, A.T., Gasilov, N.A., Karpachev, O.A., 2011. Morphology and causes of the Weddell Sea Anomaly. Geomag. Aeron. 51 (6), 828-840.

Khachikyan, G.Y.A., Pogoreltsev, A.I., Drobzheva, Y.A.V., 1989. Characteristics of the longitudinal variations of foF2 at middle latitudes in the northern hemisphere: Dependence on local time and season. Geomagn. Aeron., Engl. Transl. 29(4), 437-440.

Klimenko, M.V., Klimenko, V.V., Ratovsky, K.G., Zakharenkova, I.E., Yasyukevich, Yu.V., Korenkova, N.A., Cherniak, I.V., Mylnikova, A.A., 2015a. Mid-latitude Summer Evening Anomaly (MSEA) in F2 layer electron density and Total Electron Content at solar minimum. Adv. Sp. Res. 56(9), 1951-1960, http://dx.doi.org/10.1016/j.asr.2015.07.019.

Klimenko, M.V., Klimenko, V.V., Karpachev, A.T., et al., 2015b. Spatial features of Weddell Sea and Yakutsk Anomalies in foF2 diurnal variations during high solar activity periods: Interkosmos-19 satellite and ground-based ionosonde observations, IRI reproduction and GSM TIP model simulation. Adv. Sp. Res. 55 (8), 2020-2032, http://dx.doi.org/10.1016/j.asr.2014.12.032.

Kouris, S.S., Bradley, P.A., Dominici, P., 1998. Letter to the Editor: Solar-cycle variation of the daily foF2 and M(3000)F2. Ann. Geophys. 16, 1039-1042, doi:10.5194/angeo-16-1039-1998.

Laštovička, J, Mikhailov, A.V., Ulich, T., Bremer, J., Elias, A.G., Ortiz de Adler, N., Jara, V., Abarca del Rio, R., Foppiano, A.J., Ovalle, E., Danilov, A.D., 2006. Long-term trends in foF2: A comparison of various methods. Ann. Geophys. 68, 1854-1870, doi:10.1016/j.jastp.2006.02.009.

Laštovička, J., Solomon, S.C., Qian, L., 2012. Trends in the Neutral and Ionized Upper Atmosphere. Sp. Sci. Rev. 168, 113-145, doi:10.1007/s11214-011-9799-3.

Laštovička, J., 2013. Trends in the upper atmosphere and ionosphere: Recent progress. J. Geophys. Res. Sp. Phys. 118, 3924-3935, doi:10.1002/jgra.50341.

Lee, C.C., Reinisch, B.W., 2012. Variations in equatorial F2-layer parameters and comparison with IRI-2007 during a deep solar minimum. J. Atmos. Sol. Terr. Phys. 74, 217-223, http://dx.doi.org/10.1016/j.jastp.2011.11.002.

Levy, M.F., Dick, M.I., Spalla, P., Scotto, C., Kutiev, I., Muhtarov, P., 1998. Results of COST 251 testing of mappings and models. COST251TD(98)021.

Lin, C.H., Hsiao, C.C., Liu, J.Y., Liu, C.H., 2007. Longitudinal structure of the equatorial ionosphere: Time evolution of the four-peaked EIA structure. J. Geophys. Res. 112, A12305, doi:10.1029/2007JA012455.

Liu, R.Y., Smith, P.A., King, J.W., 1983. A new solar index which leads to improved foF2 prediction using the CCIR Atlas. Telecommun. J. 50, 8, 408-414.

Liu, J.Y., Chen, V.I., Lin, J.S., 2003. Statistical investigation of the saturation effect in the ionospheric foF2 versus sunspot, solar radio noise, and solar EUV radiation. J. Geophys. Res. Sp. Phys. 108, A2, doi:10.1029/2001JA007543.

Liu, L., Chen, Y., Le, H., 2006. Solar activity variations of the ionospheric peak electron density. J. Geophys. Res. Sp. Phys. 113, 1-13, doi:10.1029/2008JA013114.

Liu, H., Thampi, S.V., Yamamoto, M., 2010. Phase reversal of the diurnal cycle in the midlatitude ionosphere. J. Geophys. Res. 115, A01305, http://dx.doi.org/10.1029/2009JA014689.

Liu, L., Chen, Y., Le, H., Kurkin, V.I., Polekh, N.M., Lee, C.-C., 2011a. The ionosphere under extremely prolonged low solar activity. J. Geophys. Res. 116, A04320, doi:10.1029/2010JA016296.

Liu, L., Wan, W., Chen, Y., Le, H., 2011b. Solar activity effects of the ionosphere: A brief review. Chinese Sci. Bull. 56, 1202-1211, doi:10.1007/s11434-010-4226-9.

Liu L., Wan, W., Chen, Y., Le, H., Zhao, B., 2012. Recent progresses on ionospheric climatology investigations. Chin. J. Space Sci. 32(5), 665-680.

Lühr, H., Xiong, C., 2010. IRI-2007 model overestimates electron density during the 23/24 solar minimum. Geophys. Res. Lett. 37, L23101, doi:10.1029/2010GL045430.

Lyon, A.J., Thomas, L., 1963. The F2-region equatorial anomaly in the African, American and East Asian sectors during sunspot maximum. J. Atm. Terr. Phys. 25, 373-386.

Ma, R., Xu, J., Liao, H., 2003. The features and a possible mechanism of semiannual variation in the peak electron density of the low latitude F2 layer. J. Atm. Sol. Terr. Phys. 65, 47-57, http://dx.doi.org/10.1016/S1364-6826(02)00192-X.

Ma, R., Xu, J., Wang, W., Yuan, W., 2009. Seasonal and latitudinal differences of the saturation effect between ionospheric NmF2 and solar activity indices. J. Geophys. Res. 114, A10303, doi:10.1029/2009JA014353.

MacDougall, J.W., 1969. The equatorial ionospheric anomaly and the equatorial electrojet. Rad. Sci. 4(9), 805-810.

MacDougall, J.W., Halland, G.E., Hayashi, K., 1997. F-region gravity waves in the central polar cap. J. Geophys. Res. 102, 14 513-14 530.

MacPherson, B., Gonzalez, S.A., Bailey, G.J., Moffett, R.J., Sulzer, M.P., 1998. The effects of meridional neutral winds on the O+/H+ transition altitude over Arecibo. J. Geophys. Res. Sp. Phys. 103, A12, 29183-29198, doi:10.1029/98JA02660.

Martyn, D.F, 1955. The Physics of the Ionosphere. Physical Society, London, pp. 254.

Mayr, H.G., Mahajan, K.K., 1971. Seasonal variation in the F2 region. J. Geophys. Res. 76(4), 1017-1027.

McNamara, L., 1991. The Ionosphere: Communications, Surveillance and Direction Finding. Krieger, Nalabar, Fla., pp. 237.

Mielich, J., Bremer, J., 2013. Long-term trends in the ionospheric F2 region with different solar activity indices. Ann. Geophys. 31, 291-303, doi:10.5194/angeo-31-291-2013.

Mikhailov, A.V., Mikhailov, V.V., 1995. Solar cycle variations of annual mean noon foF2. Adv. Sp. Res. 15, 79-82.

Mikhailov, A.V., Mikhailov, V.V., Skoblin, M.G., 1996. Monthly median foF2 and M(3000)F2 ionospheric model over Europe. Ann. Geophys. 39(4), 791-805, http://hdl.handle.net/2122/1707.

Mikhailov, A.V., Marin, D., 2000. Geomagnetic control of the foF2 long-term trends. Ann. Geophys. 18, 6, 653-665.

Mikhailov, A.V., Marin, D., 2001. An interpretation of the foF2 and hmF2 long-term trends in the framework of the geomagnetic control concept. Ann. Geophys. 19, 7, 733-748.

Mikhailov, A.V., 2002. The geomagnetic control concept of the F2-layer parameter long-term trends. Phys. Chem. Earth 27, 595-606.

Mikhailov, A.V., de la Morena, B.A., 2003. Long-term trends of foE and geomagnetic activity variations. Ann. Geophys. 21, 751-760, http://www.ann-geophys.net/21/751/2003/.

Mikhailov, A.V., 2006. Ionospheric long-term trends: can the geomagnetic control and the greenhouse hypotheses be reconciled? Ann. Geophys. 24, 2533-2541, http://www.ann-geophys.net/24/2533/2006/.

Nava, B., Coisson, P., Radicella, S.M., 2008. A new version of the NeQuick ionosphere electron density model. J. Atm. Sol. Terr. Phys. 70(15), 1856-1862, http://dx.doi.org/10.1016/j.jastp.2008.01.015.

Ouattara, F., 2012. foF2 long term trends at Ouagadougou station. British Journal of Applied Science and Tecnology 2(3), 240-253.

Pesnell, W.D., 2008. Predictions of solar cycle 24. Solar Phys. 252, 209-220, doi:10.1007/s11207-008-9252-2.

Pezzopane, M., 2004. Interpre: a Windows software for semiautomatic scaling of ionospheric parameters from ionograms. Comput. Geosci. 30, 125-130.

Pezzopane, M., Scotto, C., 2005. The INGV software for the automatic scaling of foF2 and MUF(3000)F2 from ionograms: A performance comparison with ARTIST 4.01 from Rome data. J. Atm. Sol. Terr. Phys. 67(12), 1063-1073, http://dx.doi.org/10.1016/j.jastp.2005.02.022.

Picone, J.M., Hedin, A.E., Drob, D.P., Aikin, A.C., 2002. NRLMSISE-00 empirical model of the atmosphere: Statistical comparisons and scientific issues. J. Geophys. Res. 107, 1-16, doi:10.1029/2002JA009430.

Qian, L., Solomon, S.C., Roble, R.G., Kane, T.J., 2008. Model simulations of global change in the ionosphere. Geophys. Res. Lett. 35, L07811, doi:10.1029/2007GL033156.

Qian, L., Solomon, S.C., Roble, R.G., 2014. Secular changes in the thermosphere and ionosphere between two quiet Sun periods. J. Geophys. Res. Sp. Phys. 119, 2255-2262, doi:10.1002/2013JA019438.

Radicella, S.M., Leitinger, R., 2001. The evolution of the DGR approach to model electron density profiles. Adv. Sp. Res. 27(1), 35-40, doi:10.1016/S0273-1177(00)0013-1.

Ratcliffe, J.A., 1959. The Magneto-ionic Theory and its applications to the ionosphere. Cambridge University Press, pp. 206.

Rao, M.S.J.G., Rao, R.S., 1969. The hysteresis variation in F2-layer parameters. J. Atm. Sol. Terr. Phys. 31, 1119-1125.

Rawer, K., 1982. Replacement of the present sub-peak plasma density profile by a unique expression. Adv. Sp. Res. 2(10), 183-190.

Rawer, K., 1991. Data needed for an analytical description of the electron density profile. Adv. Sp. Res. 11(10), 57-65, doi:10.1016/0273-1177(91)90322-B.

Reinisch, B.W., Huang, X., Sales, G.S., 1993. Regional ionospheric mapping. Adv. Sp. Res. 13(3), 45-48, doi:10.1016/0273-1177(93)90246-8.

Rishbeth, H., Setty, C.S.G.K., 1961.The F layer at sunrise. J. Atm. Terr. Phys. 10, 263-276.

Rishbeth, H., Garriot, O.K., 1969. Introduction to Ionospheric Physics. Academic Press Inc., New York, United States, pp. 340.

Rishbeth, H., 1990. A greenhouse effect in the ionosphere? Planet Sp. Sci. 38, 945-948.

Rishbeth, H., Roble, R.G., 1992. Cooling of the upper atmosphere by enhanced greenhouse gases. Modeling of the thermospheric and ionospheric effects. Planet Sp. Sci. 40, 1011-1026.

Rishbeth, H., 1997. Long-term changes in the ionosphere. Adv. Sp. Res. 20, 2149-2155.

Rishbeth, H., Müller-Wodarg, I.C.F., Zou, L., Fuller-Rowell, T.J., Millward, G.H., Moffett, R.J., Idenden, D.W., Aylward, A.D., 2000. Annual and semiannual variations in the ionospheric F2-layer: II. Physical discussion. Ann. Geophys. 18, 945-956.

Roble, R.G., Ridley, E.C., Richmond, A.D., Dickinson, R.E., 1988. A coupled thermosphere/ionosphere general circulation model. Geophys. Res. Lett. 15, 1325-1328.

Roble, R.G., 1995. Major greenhouse cooling (yes, cooling): the upper atmosphere response to increased CO2. Rev. Geophys. 33, 539-546.

Roble, R.G., Dickinson, R.E., 1989. How will changes in carbon dioxide and methane modify the mean structure of the mesosphere and thermosphere? Geophys. Res. Lett. 16, 1441-1444.

Roininen, L., Laine, M., Ulich, T., 2015. Time-varying ionosonde trend: Case study of Sodankylä hmF2 data 1957-2014. J. Geophys. Res. Sp. Phys. 120, 6851-6859, doi:10.1002/2015JA021176.

Romano, V., Pau, S., Pezzopane, M., Zuccheretti, E., Zolesi, B., De Franceschi, G., Locatelli, S., 2008. The electronic Space Weather upper atmosphere (eSWua) project at INGV: advancements and state of the art. Ann. Geophys. 26, 345-351, doi:10.5194/angeo-26-345-2008.

Rottman, G., Floyd, L., Viereck, R., 2004. Measurement of the solar ultraviolet irradiance. In: Pap, J.M., Fox, P., Frohlich, C., Hudson, H.S., Kuhn, J., McCormack, J., North, G., Sprigg, W., Wu, S. (Eds.), Solar Variability and its Effect on the Earth's Atmosphere and Climate System. American Geophysical Union, Washington DC, 111-125.

Rush, C.M., Fox, M., Bilitza, D., Davies, K., McNamara, L., Stewart, F.G., PoKempner, M., 1989. Ionospheric mapping-an update of foF2 coefficients. Telecommun. J. 56, 179-182.

Russell, C.T., Luhmann, J.G., Jian, L.K., 2010. How unprecedented a solar minimum? Rev. Geophys. 48, RG2004, doi:10.1029/2009RG000316.

Scott, C.J., Stamper, R., 2015. Global variation in the long-term seasonal changes observed in ionospheric F region data. Ann. Geophys. 33, 449-455, doi:10.5194/angeo-33-449-2015.

Shimazaki, T., 1955. World-wide variations in the height of the maximum electron density of the ionospheric F2 layer. J. Radio Res. Labs. Japan 2, 85-97.

Singer, W., Dvinskikh, N.I., 1991. Comparison of empirical models of ionospheric characteristics developed by means of different mapping methods. Adv. Sp. Res. 11(10), 3-6, doi:10.1016/0273-1177(91)90311-7.

Sizun, H., 2005. Radio Wave Propagation for Telecommunication Applications. Springer-Verlag Berlin, Heidelberg, pp. 414, 10.1007/b137896.

Solé, 1998. Relations between hourly monthly median values of foF2 and some geophysical indices. Their application to an ionospheric single station model. Acta Geophys. Pol. XLVI, 77-88.

Solomon, S.C., Woods, T.N., Didkovsky, L.V., Emmert, J.T., Qian, L., 2010. Anomalously low solar extreme ultraviolet irradiance and thermospheric density during solar minimum. Geophys. Res. Lett. 37, L16103, doi:10.1029/2010GL044468.

Solomon, S.C., Qian, L., Burns, A.G., 2013. The anomalous ionosphere between solar cycles 23 and 24. J. Geophys. Res. Sp. Phys. 118, 6524-6535, doi:10.1002/jgra.50561.

Stening, R.J., 1992. Modeling the low-latitude F-region, a review. J. Atm. Sol. Terr. Phys. 54, 1387-1412, doi:10.1016/0021-9169(92)90147-D.

Thuillier, G., Floyd, L., Woods, T.N., Cebula, R., Hilsenrath, E., Herse, M., Labs, D., 2004. Solar irradiance reference spectra. In: Pap, J.M., Fox, P., Frohlich, C., Hudson, H.S., Kuhn, J., McCormack, J., North, G., Sprigg, W., Wu, S. (Eds.). Solar Variability and its Effect on the Earth's Atmosphere and Climate System. American Geophysical Union, Washington, 171-194.

Titheridge, J.E., 1985. Ionogram analysis with the generalized program POLAN. United States, pp. 194.

Tobiska, W.K., 1996. Current status of solar EUV measurements and modeling. Adv. Sp. Res. 18, 3-10, doi:10.1016/0273-1177(95)00827-2.

Torr, M.R., Torr, D.G., 1973. The seasonal behavior of the F2-layer of the ionosphere. J. Atm. Terr. Phys. 35, 2237-2251.

Triskova, L., Chum, J., 1996. Hysteresis in dependence of foF2 on solar indices. Adv. Sp. Res. 18, 145-148.

Tsagouri, I., Zolesi, B., Belehaki, A., Cander, L.R., 2005. Evaluation of the performance of the real-time updated simplified ionospheric regional model for the European area. J. Atm. Sol. Terr. Phys. 67(12), 1137-1146, http://dx.doi.org/10.1016/j.jastp.2005.01.012.

Turner, J.F., 1968. The development of the ionospheric index, T, IPS Series R Report, R11.

Ulich, T., Turunen, E., 1997. Evidence for long-term cooling of the upper atmosphere in ionosonde data. Geophys. Res. Lett. 24, 1103-1106.

Ulich, T., 2000. Solar Variability and long-term trends in the ionosphere, Sodankylä Geophysical Observatory Pubblications, pp. 96.

Ulich, T., Clilverd, M.A., Jarvis, M.J., Rishbeth, H., 2006. Unravelling signs of global change in the ionosphere, in: Space Weather-Research towards applications in Europe, edited by: Lilensten, J., Astrophys. Space Library, 344, 95-105, Springer, Dordrecht, The Netherlands, 2006.

Upadhyay, H.O., Mahajan, K.K., 1998. Atmospheric greenhouse effect and ionospheric trends. Geophys. Res. Lett. 25, 3375-3378.

Viereck, R.A., Floyd, L.E., Crane, P.C., Woods, T.N., Knapp, B.G., Rottman, G., Weber, M., Puga, L.C., DeLand, and M.T., 2004. A composite Mg II index spanning from 1978 to 2003. Sp. Weath. 2, S10005, doi:10.1029/2004SW000084.

Viereck, R.A., Snow, M., DeLand, M.T., Weber, M., Puga, L., Bouwer, D., 2010. Trends in solar UV and EUV irradiance: An update to the MgII Index and a comparison of proxies and data to evaluate trends of the last 11-year solar cycle, in: Presented at 2010 Fall Meeting, AGU, San Francisco, Calif, Abstract GC21B-0877, 13-17 Dec.

Wakai, N., Ohyama, H., Koizumi, T., 1987. Manual of ionogram scaling. Ministry of posts and telecommunications, Japan.

Wieman, S.R., Didkovsky, L.V., Judge, D.L., 2014. Resolving Differences in Absolute Irradiance Measurements Between the SOHO/CELIAS/SEM and the SDO/EVE. Sol. Phys. 289(8), 285-303, doi:10.1007/978-1-4939-2038-9_18.

Woods, T., Prinz, D., Rottman, G., Al., E., 1996. Validation of the UARS solar ultraviolet irradiances: Comparison with the ATLAS 1 and 2 measurements. J. Geophys. Res. 101, 9541-9569, doi:10.1029/96JD00225.

Woods, T.N., Tobiska, W.K., Rottman, G.J., Worden, J.R., 2000. Improved solar Lyman α irradiance modeling from 1947 through 1999 based on UARS observations. J. Geophys. Res. 105, 27195, doi:10.1029/2000JA000051.

Woods, T.N., Rottman, G., 2005. XUV Photometer System (XPS): Solar Variations during the SORCE Mission. Sol. Phys. 230, 375-387.

Woods, T.N., Eparvier, F.G., Hock, R., Jones, a. R., Woodraska, D., Judge, D., Didkovsky, L., Lean, J., Mariska, J., Warren, H., McMullin, D., Chamberlin, P., Berthiaume, G., Bailey, S., Fuller-Rowell, T., Sojka, J., Tobiska, W.K., Viereck, R., 2012. Extreme Ultraviolet Variability Experiment (EVE) on the Solar Dynamics Observatory (SDO): Overview of Science Objectives, Instrument Design, Data Products, and Model Developments. Sol. Phys. 275, 115-143, doi:10.1007/s11207-009-9487-6.

Xenos, T.D., 2002. Neural-network-based prediction techniques for single station modeling and regional mapping of the foF2 and M(3000)F2 ionospheric characteristics. Nonlinear Processes in Geophysics, European Geosciences Union (EGU) 9 (5/6), pp.477-486.

Yonezawa, T.,1967. On the seasonal, non-seasonal and semi-annual variations in the peak electron density of the F2 layer at noon in the equatorial zone. J. Radio Res. Lab. 14(71), 1-25.

Yonezawa, T., 1971. The solar activity latitudinal characteristics of the seasonal, non seasonal and semi-annual variations in the peak electron densities of the F2-layer at noon and at midnight in middle and low latitudes. J. Atm. Terr. Phys 33, 889-907.

Yonezawa, T., Arima, Y., 1959. On the seasonal and non-seasonal annual variations and the semi-annual variation in the noon and midnight electron densities of the F2 layer in middle latitudes. J. Radio Res. Lab. 6(25), 293-309.

Yu, T., Wan, W., Liu, L., Zhao, B., 2004. Global scale annual and semiannual variations of daytime NmF2 in the high solar activity years. J. Atm. Sol. Terr. Phys. 66, 1691-1701, http://dx.doi.org/10.1016/j.jastp.2003.09.018.

Yue, X., Wan, W., Liu, L., Ning, B., Zhao, B., 2006. Applying artificial neural network to derive long-term foF2 trends in the Asia/Pacific sector from ionosonde observations. J. Geophys. Res. 111, A10303, doi:10.1029/2005JA011577.

Zakharenkova, I., Krankowski, A., Bilitza, D., Cherniak, Y., Shagimuratov, I., Sieradzki, R., 2013. Comparative study of foF2 measurements with IRI-2007 model predictions during extended solar minimum. Adv. Sp. Res. 51(1), 620-629, doi:10.1016/j.asr.2011.11.015.

Zolesi, B., Cander, L.R., De Franceschi, G., 1990. A simple model for a global distribution of some ionospheric characteristics in a restricted area, in Solar-Terrestrial Predictions: Proceedings of a Workshop at Leura, National Oceanic and Atmospheric Administration, Boulder, Colorado, Vol. 2, 418-427.

Zolesi, B., Cander, L.R., De Franceschi, G., 1991. Mapping of some ionospheric characteristics over a restricted area using SIRM (Simplified Ionospheric Regional Model), in Seventh International Conference on Antennas and Propagation, Vol. 333, 512-515.

Zolesi, B., Cander, L.R., De Franceschi, G., 1993. Simplified ionospheric regional model for telecommunication applications. Radio Sci. 28(4), 603-612.

Zolesi, B., Cander, L.R., De Franceschi, G., 1996. On the potential applicability of the simplified ionospheric regional model to different midlatitude areas. Rad. Sci. 31(3), 547-552, doi:10.1029/95RS03817.

Zolesi, B., Cander, L.R., 1998. Advances in regional ionospheric mapping over Europe. Ann. Geophys. 41(5-6), doi:10.4401/ag-3823.

Zolesi, B., Belehaki, A., Tsagouri, I., Cander, L.R., 2004. Real-time updating of the simplified ionospheric regional model for operational applications. Rad. Sci. 39(2), doi:10.1029/2003RS002936.

Zolesi, B., Cander, L.R., 2014. Ionospheric prediction and forecasting. Springer-Verlag Berlin Heidelberg, pp. 240, doi: 10.1007/978-3-642-38430-1.

Zuccheretti, E., Tutone, G., Sciacca, U., Bianchi, C., Arokiasamy, B.J., 2003. The new AIS-INGV digital ionosonde. Ann. Geophys. 46.